

**REMOVAL OF HEXAVALENT CHROMIUM FROM
WASTEWATER BY ADSORPTION USING
NANOMATERIALS**

A THESIS

Submitted by

PADMAVATHY K.S.

*for the award of the degree
of*

DOCTOR OF PHILOSOPHY

Under the Faculty of Engineering



**SCHOOL OF ENGINEERING
COCHIN UNIVERSITY OF SCIENCE AND TECHNOLOGY, KOCHI**

DECEMBER 2017

THESIS CERTIFICATE

This is to certify that the thesis entitled “**REMOVAL OF HEXAVALENT CHROMIUM FROM WASTEWATER BY ADSORPTION USING NANOMATERIALS**” submitted by **Padmavathy K.S.** to the Cochin University of Science and Technology, Kochi for the award of the degree of Doctor of Philosophy is a bonafide record of research work carried out by her under our supervision and guidance at School of Engineering, Cochin University of Science and Technology. The contents of this thesis, in full or in parts, have not been submitted to any other University or Institute for the award of any degree or diploma.

We further certify that the corrections and modifications suggested by the audience during the pre-synopsis seminar and recommended by the doctoral committee are incorporated in the thesis.

Prof. (Dr.) G. Madhu (*Research Guide*)
Head
Division of Chemical Engineering
School of Engineering
Cochin University of Science and Technology
Kochi-682 022, Kerala, India

Prof. (Dr.) Dipak Kumar Sahoo (*Co-Guide*)
Head
Division of Safety and Fire Engineering
School of Engineering
Cochin University of Science and Technology
Kochi-682 022, Kerala, India

Place: Kalamassery
Date: 22/12/2017

DECLARATION

I hereby declare that the work presented in the thesis entitled **“REMOVAL OF HEXAVALENT CHROMIUM FROM WASTEWATER BY ADSORPTION USING NANOMATERIALS”** is based on the original research work carried out by me under the supervision and guidance of Prof. (Dr.) G. Madhu, Division of Chemical Engineering and Prof. (Dr.) Dipak Kumar Sahoo, Division of Safety and Fire Engineering, School of Engineering, Cochin University of Science and Technology for the award of degree of Doctor of Philosophy with Cochin University of Science and Technology. I further declare that the contents of this thesis in full or in parts have not been submitted to any other University or Institute for the award of any degree or diploma.

Place: Kochi

Date: 22/12/2017

Padmavathy K.S.

Dedicated to My Parents

ACKNOWLEDEMENTS

I thank the supreme power, **Almighty** God for giving me strength and courage for completing my thesis report.

First and foremost, I place on record my sincere gratitude to Prof. (Dr.) G. Madhu, my guide for giving me a chance for doing research under his supervision and guidance. I am immensely thankful to him for all the support and encouragement he has given me throughout this work. The patience in listening me in various stages and advice given by him is gratefully acknowledged. Without his suggestions and timely guidance this work will not have been progressed further. He gave me the moral support and freedom during the writing of this thesis.

I express my heartfelt gratitude to Prof. (Dr.) Dipak Kumar Sahoo for the valuable suggestions given to me in the course of my work. I express my immense thanks to him for the timely help he rendered to me in various stages of this research work.

I wish to express my sincere thanks to all the teaching staff, non-teaching staff and students of Department of Chemical Engineering, Government Engineering College, Thissur for helping and supporting me during this research work. I thank Prof. Haseena P.V., Asst. Professor in Chemical Engineering, Government Engineering College, Thrissur, Dr. Anjana R., Asst. Professor in Chemical Engineering, Government Engineering College, Thissur and Dr. Ushakumary E. R., Associate Professor in Chemical Engineering, Government Engineering College, Kozhikode for helping me during the experimental work. I thank Dr. Rejini V.O., Head of Department of Chemical Engineering, Government Engineering College, Thrissur and Dr.

Renjanadevi B., Head of Department of Chemical Engineering, Government Engineering College, Kozhikode for supporting me. I thank all the teaching staff and office staff of School of Engineering, Cochin University of Science and Technology for the help they extended to me during my research.

The financial support (SEED money) for conducting the experimental work received from CERD (Centre for Engineering Research and Development), Government of Kerala is greatly acknowledged.

The advices and prayer of my loving mother is always a source of constant encouragement to me. I express my sincere love and thanks to my parents who are always my well-wishers. I dedicate this work to them. I thank my brother Krishnan for the support he has given to me during my research work. Last but not the least, I thank my beloved husband Suraj, daughters Niranjana and Darshana for their prayers, love and support during the course of this research work.

Padmavathy K.S.

ABSTRACT

Rapid industrialisation has led to heavy metal pollution in surface and ground water and it is causing serious ecological problem. Hence, monitoring and assessing water pollution is a very critical area of study that has considerable relevance now-a-days. Cr(VI) is a toxic heavy metal. Effluents from leather tanning and electroplating industries are the major sources of Cr(VI) pollution. Several physico-chemical methods have been found to be effective in the removal of Cr(VI) from aqueous media. Adsorption techniques hold great potential in this regard.

In the present work the removal of low concentrations of Cr(VI) from aqueous solution by adsorption using nanoadsorbents namely, nanokaolinite clay, nanomagnetite and chitosan/halloysite clay nanocomposite film has been studied. The nanoadsorbents used in the study were synthesised in the laboratory using standard methods and they were characterised by instrumental methods. Batch adsorption study was conducted to assess the effect of various parameters on adsorption. The maximum Cr(VI) removal efficiency for nanokaolinite clay was 67%. Nanomagnetite synthesised in the laboratory had higher Cr(VI) removal efficiency and adsorption capacity when compared to unmodified nanoclay. Optimisation of batch adsorption by magnetite nanoparticles using RSM was carried out and maximum removal efficiency obtained was 76.11%. To overcome the difficulties in separating the nanoadsorbents from the solution after adsorption, halloysite nanoclay was mixed with chitosan to form chitosan/halloysite clay nanocomposite films. Films of thickness 0.2 mm and diameter 6.5 mm were used in the present work. From the batch study using nanocomposite films, pH 3.0 was found to

be the optimum pH and other batch studies were conducted at this pH. Kinetic studies for Cr(VI) removal using nanocomposite films showed that the adsorption data fitted to pseudo second order kinetic model. The adsorption equilibrium data of nanocomposite films fitted to Langmuir isotherm. Thermodynamic study was carried out with chitosan/halloysite clay nanocomposite films. The negative values of Gibbs free energy change (ΔG) indicated the favorability and spontaneity of the adsorption process. Also positive value of entropy change suggested that there was increase in disorder at the solid - solution interface during the binding of metal ion onto the active site of the adsorbent. The desorption study of nanocomposite was conducted using 0.01 M NaOH. From RSM, 93.04% removal of Cr(VI) was obtained at 72.2 mg/L initial Cr(VI) concentration with 0.2 g/L of nanocomposite film added to the solution. The time of shaking was 100 minutes at pH 3.0.

Continuous fixed bed studies for Cr(VI) removal using chitosan/halloysite clay nanocomposite films showed that with increase in initial concentration, the saturation of the bed occurred early and breakthrough time was lesser. Low pH was favourable for the operation of Cr(VI) column using nanocomposite adsorbent. With increase in bed height, breakthrough curve shifted to the right and more volume of effluent could be treated. As flow rate of Cr(VI) solution was increased the saturation of bed occurred faster. Modeling of the packed bed column was performed using Thomas model, Yoon Nelson model and Adam Bohart model. The correlation between experimental and theoretical data of column operation was compared for the three models by plotting $(C_f/C_0)_{\text{experimental}}$ versus $(C_f/C_0)_{\text{theoretical}}$. From the values of correlation coefficient, Thomas model and Yoon Nelson model were

found to fit well to the experimental data. Adam Bohart correlation was fitted best to the initial part of the adsorption process except for high pH of Cr(VI) solution. Packed bed adsorption column using nanocomposite films proved to be an efficient method for treatment of water containing low concentrations of Cr(VI).

Key words: Adsorption, Nanoadsorbents, Chitosan, Halloysite nanoclay, Nanocomposite films, Packed bed Cr(VI) column.

CONTENTS

ACKNOWLEDGEMENTS	i
ABSTRACT.....	iii
TABLE OF CONTENTS	vii
LIST OF TABLES	xiii
LIST OF FIGURES	xv
ABBREVIATIONS	xxi
CHAPTER 1 INTRODUCTION.....	1
1.1 Introduction	1
1.2 Background on Chromium.....	2
1.3 Sources of Cr(VI).....	3
1.4 Adverse Effects of Cr(VI).....	4
1.5 Methods of Cr(VI) Removal	4
1.6 Adsorption.....	8
1.7 Scope of the Study	10
1.8 Objectives of the Present Work	11
1.9 Thesis Outline	12
CHAPTER 2 LITERATURE REVIEW.....	15
2.1 Introduction	15
2.2 Sources of Hexavalent Chromium in Water	16
2.3 Impacts of Cr(VI).....	18
2.4 Methods of Cr(VI) Removal	19
2.4.1 Chemical Precipitation	20
2.4.2 Ion exchange for Cr(VI) Removal	20
2.4.3 Membrane Filtration.....	21
2.4.4 Electrochemical Methods.....	22
2.4.5 Photocatalysis.....	23
2.4.6 Coagulation and Flocculation	23
2.4.7 Adsorption.....	24

2.5	Literature Review on Adsorption and Adsorbents.....	26
2.6	Mechanism of Adsorption.....	40
2.7	Factors Affecting Batch Adsorption	40
2.7.1	Effect of pH on Adsorption.....	41
2.7.2	Effect of Contact Time.....	42
2.7.3	Effect of Initial Concentration on Adsorption	43
2.7.4	Effect of Adsorbent Dosage	43
2.7.5	Effect of Agitation Speed.....	44
2.7.6	Effect of Temperature and Pressure	44
2.8	Adsorption Isotherm	45
2.8.1	Langmuir Isotherm.....	45
2.8.2	Freundlich Isotherm	47
2.8.3	Dubinin - Radushkevich (D - R) Isotherm.....	49
2.9	Adsorption Kinetics	50
2.10	Adsorption Thermodynamics.....	51
2.11	Response Surface Methodology.....	52
2.12	Desorption	54
2.13	Characterisation of Adsorbents	55
2.14	Analytical Method.....	59
2.15	Continuous Removal in Packed Bed Adsorption Column.....	60
2.15.1	Factors Affecting Breakthrough Curves	62
2.15.2	Mathematical Models of Packed Column.....	65
2.16	Summary	67
CHAPTER 3 MATERIALS AND METHODS.....		69
3.1	Introduction	69
3.2	Preparation of Cr(VI) Stock Solution	69
3.3	Preparation of Adsorbents.....	70
3.4	Analytical Method for Cr(VI) Determination.....	72

3.5	Characterisation of Adsorbents	73
3.6	Batch Experiments	75
3.6.1	Batch Experiments for Cr(VI) Removal Using Nanokaolinite Clay.....	75
3.6.2	Adsorption Using Magnetite Nanoparticles.....	76
3.6.3	Design of Experiments for Magnetite Nanoadsorbents	77
3.6.4	Effect of Various Parameters on Adsorption of Cr(VI) Using Chitosan/Halloysite Clay Nanocomposite Films.....	78
3.6.5	Kinetic Studies Using Nanocomposite films as Adsorbent	80
3.6.6	Equilibrium Studies for Cr(VI) Removal Using Chitosan/Halloysite Clay Nanocomposite Films	81
3.6.7	Thermodynamic Studies Using Nanocomposite Films.....	82
3.6.8	Desorption Studies of Nanocomposite Films.....	83
3.6.9	Response Surface Methodology for Cr(VI) Removal Using Nanocomposite Films	84
3.7	Removal of Cr(VI) in Continuous Fixed Bed Adsorption Column Using Chitosan/Halloysite Clay Nanocomposite Film as Adsorbent	84
3.7.1	Thomas Model	88
3.7.2	Yoon Nelson Model	88
3.7.3	Adam Bohart Model.....	89
3.8	Summary of the Chapter	90
CHAPTER 4 RESULTS AND DISCUSSION.....		91
4.1	Introduction	91
4.2	Batch Adsorption Study for Cr(VI) Removal Using Nanokaolinite Clay.....	92
4.2.1	Effect of Various Parameters on Cr(VI) Removal	92
4.2.2	Characterisation of Nanoclay	95
4.2.3	Scanning Electron Microscopy Equipped with Energy Dispersive X-ray Spectroscopy	95

4.2.4	X-ray Diffraction Pattern of Nanokaolinite Clay	97
4.3	Batch Adsorption Study of Cr(VI) Removal Using Nanomagnetite	98
4.3.1	Effect of pH.....	99
4.3.2	Effect of Adsorbent Dosage on Adsorption of Cr(VI).....	100
4.3.3	Effect of Initial Concentration	101
4.3.4	Effect of Time	102
4.3.5	Application of Response Surface Methodology for Cr(VI) Removal Using Magnetite Nanoadsorbents	103
4.3.6	Optimisation Using Response Surface Methodology	108
4.3.7	Combined Effect of Variables on Adsorption of Cr(VI) Using Magnetite Nanoadsorbents	109
4.3.8	Characterisation of Magnetite Nanoparticles.....	113
4.3.9	Scanning Electron Microscopy Equipped with Energy Dispersive X-ray Spectroscopy	133
4.3.10	Characterisation Using X-ray Diffraction.....	115
4.3.11	Thermogravimetric Analysis.....	116
4.4	Batch Adsorption of Cr(VI) Using Chitosan/Halloysite Clay Nanocomposite Films	117
4.4.1	Effect of pH on Adsorption.....	118
4.4.2	Effect of Adsorbent Dosage	119
4.4.3	Effect of Temperature on Adsorption of Cr(VI) Using Nanocomposite Films	120
4.4.4	Effect of Initial Concentration on Adsorption	121
4.4.5	Effect of Contact Time.....	122
4.4.6	Sorption Kinetics.....	123
4.4.7	Adsorption Isotherm Studies.....	127
4.4.8	Thermodynamics of Adsorption of Cr(VI) Using Nanocomposite Films	129
4.4.9	Desorption Studies	130

4.4.10	Response Surface Methodology for Analysis of Cr(VI) Removal Using Chitosan/Halloysite Nanoclay Nanocomposite Films	132
4.4.11	Combined Effect of Variables on Cr(VI) Removal	134
4.4.12	Characterisation of Chitosan/Halloysite Clay Nanocomposite Films	137
4.4.13	Scanning Electron Microscopy	137
4.4.14	X-ray Diffraction.....	138
4.4.15	Thermogravimetric Analysis.....	141
4.4.16	Fourier Transform Infrared Spectroscopy.....	142
4.4.17	Tensile Strength of Films and Film Thickness Measurement	144
4.5	Continuous Removal of Cr(VI) in Packed Column Using Nanocomposite Films	145
4.5.1	Effect of Initial Concentration	145
4.5.2	Effect of pH.....	147
4.5.3	Effect of Bed Height on Breakthrough Curves	149
4.5.4	Effect of Flow Rate on the Performance of Packed Column.....	151
4.6	Modeling of Packed Bed Adsorption Column	153
4.6.1	Thomas Model	153
4.6.2	Yoon Nelson Model	158
4.6.3	Adam Bohart Model.....	164
4.6.4	Comparison of Thomas Model, Yoon Nelson Model and Adam Bohart Model.....	172
4.7	Summary	179
CHAPTER 5 SUMMARY AND CONCLUSIONS.....		181
5.1	Summary	181
5.2	Conclusions of Batch Study	183
5.2.1	Limitations of Batch Study	185

5.3	Conclusions of Fixed Bed Study.....	186
5.3.1	Limitations of Fixed Bed Study	187
5.4	Scope for Future Research	188
	REFERENCES.....	189
	ANNEXURES.....	209
	LIST OF PAPERS SUBMITTED ON THE BASIS OF THIS THESIS	219
	CURRICULUM VITAE	

LIST OF TABLES

Table No	Title	Page No
Table 1.1	Physico chemical characteristics of chromium -----	3
Table 1.2	Industries and types of hexavalent chromium chemicals-----	4
Table 2.1	Comparison of Cr(VI) removal efficiency attained in different removal techniques -----	26
Table 2.2	Properties of magnetite -----	30
Table 2.3	Properties of chitosan-----	34
Table 2.4	Halloysite attributes for its application as encapsulation vessel and load bearing constituent-----	36
Table 4.1	Elemental composition of unmodified nanokaolinite from EDX-----	97
Table 4.2	Coded levels of independent variables in Box-Behnken design using nanomagnetite -----	104
Table 4.3	Design of experiments and experimental and predicted efficiency for adsorption of Cr(VI) using nanomagnetite -	105
Table 4.4	Coefficients of the model equation and t, p, (1-p) values for nanomagnetite -----	106
Table 4.5	Analysis of variance for efficiency of adsorption -----	108
Table 4.6	Elemental composition of magnetite nanoparticles -----	114
Table 4.7	d spacing and 2 θ values of synthesised magnetite nanoparticles-----	115
Table 4.8	The kinetic constants and correlation coefficients for adsorption of Cr(VI) -----	124
Table 4.9	Equilibrium parameters for adsorption of Cr(VI) on nanocomposite film -----	129
Table 4.10	Thermodynamic parameters of nanocomposite film -----	130
Table 4.11	Design of experiments for Cr(VI) removal using nanocomposite films -----	132
Table 4.12	The characteristic peaks and intergallery spacing of halloysite nanoclay powder and nanocomposite film-----	139

Table 4.13	Mathematical description of fixed bed Cr(VI) column parameters -----	153
Table 4.14	Parameters predicted by Thomas model at different initial Cr(VI) concentration, pH, bed height and flow rates -----	158
Table 4.15	Parameters predicted by Yoon Nelson model for varying initial concentration, pH, bed height and flow rate-----	162
Table 4.16	Parameters predicted by Adam Bohart model for varying initial concentration, pH, bed height and flow rate-----	172
Table 4.17	Correlation coefficients for Thomas model, Yoon Nelson model and Adam Bohart model for various experimental conditions -----	173
Table A.1	Determination of average crystallite size of halloysite nanoclay -----	210
Table A.2	Calibration data of peristaltic pump -----	211
Table A.3	Sorption kinetics-----	213
Table A.4	Adsorption isotherm -----	213
Table A.5	Thermodynamic experimental data-----	213
Table A.6	Desorption data -----	214
Table A.7	Effect of initial concentration on the performance of fixed bed column -----	214
Table A.8	Effect of pH on the performance of fixed bed column ----	215
Table A.9	Effect of bed height on the working of fixed bed column -----	216
Table A.10	Effect of flow rate on the working of fixed bed column---	217

LIST OF FIGURES

Figure	Title	Page No
Fig. 2.1	Conversion of Cr(III) to Cr(VI) -----	19
Fig. 2.2	Structure of magnetite -----	29
Fig. 2.3	Structure of chitosan -----	34
Fig. 2.4	Structure of halloysite clay mineral -----	35
Fig. 3.1	Synthesised magnetite nanoparticles -----	70
Fig. 3.2	Chitosan/halloysite nanocomposite film before and after drying -----	71
Fig. 3.3	Nanocomposite films used for adsorption -----	72
Fig. 3.4	Sample for analysing in UV spectrophotometer -----	73
Fig. 3.5	Cr(VI) solution after and before adsorption using nanocomposite films -----	79
Fig. 3.6	a) Stock solution before adsorption; b) Solution after desorption (first cycle)-----	84
Fig. 3.7	a) Schematic of the experimental set up b) Schematic of the packed bed column with proper dimensions -----	85
Fig. 3.8	Cr(VI) fixed bed column using chitosan/halloysite nanocomposite film-----	86
Fig. 4.1	Effect of pH and adsorbent dosage on adsorption efficiency and adsorption capacity of nanokaolinite clay ---	93
Fig. 4.2	Effect of initial concentration and time on percentage Cr(VI) removal and adsorption capacity of nanokaolinite clay -----	94
Fig. 4.3	SEM images of nanokaolinite clay at various magnification -----	96
Fig. 4.4	EDX of nanokaolinite clay-----	96
Fig. 4.5	XRD of nanokaolinite clay -----	98
Fig. 4.6	Effect of pH on removal efficiency of Cr(VI) and adsorption capacity of magnetite nanoparticles-----	100
Fig. 4.7	Effect of adsorbent dosage on adsorption of Cr(VI) using nanomagnetite -----	101

Fig. 4.8	Effect of initial concentration on adsorption using nanomagnetite -----	102
Fig. 4.9	Effect of time on adsorption of Cr(VI) using magnetite nanoparticles -----	103
Fig. 4.10	Predicted versus experimental Cr(VI) removal efficiency -----	107
Fig. 4.11	Optimisation plot for Cr(VI) removal using magnetite nanoparticles -----	109
Fig. 4.12	Combined effect of variables on adsorption of Cr(VI) using magnetite nanoparticles -----	112
Fig. 4.13	SEM of magnetite nanoparticles -----	113
Fig. 4.14	EDX of magnetite nanoparticles -----	114
Fig. 4.15	XRD of magnetite nanoparticles -----	116
Fig. 4.16	TGA of magnetite nanoadsorbents -----	117
Fig. 4.17	Effect of pH on the adsorption of Cr(VI) using chitosan/halloysite clay nanocomposite adsorbent -----	119
Fig. 4.18	Effect of nanocomposite film dosage on the removal efficiency and adsorption capacity of nanocomposite film ---	120
Fig. 4.19	Effect of temperature on adsorption using nanocomposite films -----	121
Fig. 4.20	Effect of initial concentration on adsorption of Cr(VI) using nanocomposite films -----	122
Fig. 4.21	Effect of time on adsorption of Cr(VI) onto chitosan/halloysite nanocomposite films -----	123
Fig. 4.22	Kinetics of adsorption of Cr(VI) using nanocomposite films-pseudo first order, pseudo second order, second order and Intra particle diffusion -----	126
Fig. 4.23	Freundlich and Langmuir isotherm of Cr(VI) adsorption using nanocomposite films -----	128
Fig. 4.24	Free energy change of adsorption of Cr(VI) using chitosan/halloysite nanoclay adsorbent versus temperature --	129
Fig. 4.25	Desorption of nanocomposite films -----	131
Fig. 4.26	Experimental versus predicted efficiency for nanocomposite films -----	133

Fig. 4.27	Optimisation of performance of chitosan/halloysite nanocomposite films for Cr(VI) removal-----	134
Fig 4.28	Surface plots for combined effect of variables using nanocomposite films-----	136
Fig 4.29	SEM of chitosan/halloysite nanocomposite films before adsorption-----	138
Fig. 4.30	XRD of halloysite nanoclay powder -----	140
Fig. 4.31	XRD of nanocomposite films before adsorption -----	140
Fig. 4.32	XRD of nanocomposite films after adsorption-----	141
Fig. 4.33	Thermogravimetric analysis of nanocomposite films-----	142
Fig. 4.34	FTIR of chitosan/halloysite nanoclay films before adsorption -----	143
Fig. 4.35	FTIR of chitosan/halloysite nanoclay nanocomposite films after adsorption -----	144
Fig 4.36	Tensile strength of nanocomposite films -----	144
Fig. 4.37	Effect of initial concentration of Cr(VI) on breakthrough curves in continuous packed bed column-----	146
Fig. 4.38	Adsorbed concentration versus time for various initial concentration in packed bed column -----	147
Fig. 4.39	Effect of pH on the breakthrough curves of Cr(VI) column-----	148
Fig 4.40	Adsorbed concentration of Cr(VI) versus time for various pH of Cr(VI) solution-----	148
Fig. 4.41	Effect of bed height on breakthrough curves-----	150
Fig. 4.42	Effect of bed height on adsorbed concentration in continuous packed bed Cr(VI) column-----	150
Fig. 4.43	Effect of flow rate on breakthrough curves-----	152
Fig. 4.44	Effect of flow rate on adsorbed concentration -----	152
Fig. 4.45	Plot for determining Thomas kinetic coefficient k_{th} (mL/min mg) and maximum solid phase concentration q_0 (mg/g) for varying initial concentration, pH, bed height and flow rate-----	155

Fig. 4.46	Comparison of experimental and theoretical breakthrough curves predicted by Thomas model for varying initial concentration, pH, bed height and flow rate-----	156
Fig. 4.47	Determination of Yoon Nelson parameters for varying initial concentration-----	159
Fig. 4.48	Determination of Yoon Nelson coefficients for varying pH -----	160
Fig. 4.49	Yoon Nelson parameters determination for varying bed height-----	161
Fig. 4.50	Determination of coefficients in the Yoon Nelson model for varying flow rate-----	162
Fig. 4.51	Comparison of experimental and theoretical breakthrough curves by Yoon Nelson model -----	164
Fig. 4.52	Determination of Adam Bohart model parameters for $C_0 = 50$ ppm, $C_0 = 70$ ppm and $C_0 = 100$ ppm-----	165
Fig. 4.53	Breakthrough curves by Adam Bohart Model for different C_0 -----	166
Fig. 4.54	Determination of Adam Bohart model parameters for pH = 4, 6.5 and 9 -----	166
Fig. 4.55	Breakthrough curves by Adam Bohart Model for varying pH -----	167
Fig. 4.56	Determination of Adam Bohart model parameters for bed height = 10 cm, 20 cm and 25 cm -----	168
Fig. 4.57	Breakthrough curves by Adam Bohart Model for bed height = 10 cm, 20 cm and 25 cm -----	169
Fig. 4.58	Determination of Adam Bohart model parameters varying flow rate -----	170
Fig. 4.59	Breakthrough curves by Adam Bohart Model for varying flow rate -----	171
Fig. 4.60	Comparison of $(C_f/C_0)_{\text{experimental}}$ and $(C_f/C_0)_{\text{theoretical}}$ by Thomas model for varying initial concentration, pH, bed height and flow rate-----	175

Fig. 4.61	Comparison of $(C_f/C_0)_{\text{experimental}}$ and $(C_f/C_0)_{\text{theoretical}}$ by Yoon Nelson model for varying initial concentration, pH, bed height and flow rate-----	177
Fig. 4.62	Comparison of $(C_f/C_0)_{\text{experimental}}$ and $(C_f/C_0)_{\text{theoretical}}$ by Adam Bohart model for varying initial concentration, pH, bed height and flow rate-----	179
Fig. A1	Standard calibration curve of UV-VIS spectrophotometer-----	209
Fig. A2	Calibration curve of peristaltic pump used in the continuous experiment -----	212

ABBREVIATIONS

A - B model	Adam Bohart model
BBD	Box Behnken Design
BDST	Bed Depth Service Time
BIS	Bureau of Indian Standards
CNT	Carbon Nanotube
COD	Chemical Oxygen Demand
DTA	Differential Thermal Analysis
D - R	Dubinin - Radushkevich
ED	Electrodialysis
EDX	Energy Dispersive X-ray Spectroscopy
EPA	Environmental Protection Agency
FTIR	Fourier Transform Infrared Spectroscopy
FWHM	Full Width at Half Maximum
HNT	Halloysite Nanotube
IR	Infrared
JCPDS	Joint Committee on Powder Diffraction Standards
MCL	Maximum Contaminant Level
MF	Microfiltration
MMT	Montmorillonite
NF	Nanofiltration
PIXE	Particle Induced X-ray Emission
PPMS	Physical Property Measurement System
RO	Reverse Osmosis

RPM	Revolutions per minute
RSM	Response Surface Methodology
SAED	Selected Area Electron Diffraction
SDWA	Safe Drinking Water Act
SEM	Scanning Electron Microscope
TEM	Transmission Electron Microscope
TGA	Thermogravimetric Analysis
UF	Ultrafiltration
USEPA	United States Environmental Protection Agency
UTM	Universal Testing Machine
UV-VIS	Ultraviolet Visible
VSM	Vibrating Sample Magnetometer
WHO	World Health Organisation
XRD	X-ray Diffraction

● Contents ●	1.1 Introduction
	1.2 Background on Chromium
	1.3 Sources of Cr(VI)
	1.4 Adverse Effects of Cr(VI)
	1.5 Methods of Cr(VI) Removal
	1.6 Adsorption
	1.7 Scope of the Study
	1.8 Objectives of the Present Work
	1.9 Thesis Outline

1.1 Introduction

Pure water is one of the key needs for human survival. Environmental degradation when pollutants without proper treatment of harmful chemicals are discharged directly or indirectly to water bodies is called the water pollution. This phenomenon affects the entire biosphere and hence it is a major global problem. Water pollution is increasing now-a-days due to rapid industrialisation. The sources of water pollutants are classified as point sources and nonpoint sources. Point source is a single identifiable source such as pollutant from a specific industry. Nonpoint source refers to diffuse contaminants that originate from many sources. The water pollution is the worldwide cause of deaths and diseases of more than 14,000 people daily.

Heavy metals are dense materials which are noted for their toxicity. Surface and ground waters are polluted with heavy metals like cadmium, chromium, copper, nickel, mercury, lead etc. produced from various industries

(Malkoc and Nuhoglu, 2006a). Heavy metals pose adverse effects on all forms of life. They bind to and interfere with the functioning of vital cellular activities in all forms of life.

1.2 Background on Chromium

Chromium is a dangerous heavy metal present in industrial wastewater. Chromium may be present in trivalent and hexavalent forms. Cr(VI) does not occur naturally and is extremely toxic even in small quantities. Cr(III) is an essential micronutrient required by human body for metabolism and it is present in many vegetables, fruits, meat, grains and yeast. Our body requires 50-200 µg of Cr(III) per day (Barnhart, 1997; Rojas *et al.*, 2005; Pandey and Mishra, 2011). Safe Drinking Water Act (SDWA) insists Environmental Protection Agency (EPA) to determine the level of contaminants in drinking water which cause no adverse health effects. Enforceable standards are set by EPA for various contaminant levels in drinking water called Maximum Contaminant Level (MCL). MCL for total chromium in drinking water set by EPA is 0.1 milligrams per litre (mg/L) or 100 parts per billion (ppb) for total chromium. As part of pollution control, the government has imposed strict legal restrictions for the discharge of Cr(VI) from industries into the receiving water bodies. Regulations made by the minister under the sections 39 and 96 of the Environment Protection Act 2002, limits the total chromium concentration in land and underground waters to a maximum of 0.05 mg/L (Jain *et al.*, 2009). The Cr(VI) concentration should be controlled in effluents before discharging to the local water bodies. As far as the environment is concerned, proper treatment methods should be implemented for limiting the discharge of Cr(VI) from industrial effluents so that it will be beneficial for the upcoming generations. Table 1.1 represents the physico chemical characteristics of chromium.

Table 1.1 Physico chemical characteristics of chromium

Property	Cr	CrCl ₃	K ₂ CrO ₄	Cr ₂ O ₃	CrO ₃
Melting Point (°C)	1857	1152	968.3	2435	196
Boiling Point (°C)	2672	1300	1000	4000	250
Solubility (g/L)	Insoluble	Slightly Soluble	790	Insoluble	624
Density (g/cm ³)	7.14	2.76	2.73	5.21	2.70

1.3 Sources of Cr(VI)

Chromium is found naturally in rocks, plants, soil, volcanic dust and animals. By products from paints, ink and plastic industries contain considerable amount of hexavalent chromium. It is also used as anti-corrosive coatings and wastewater from chrome coating sections contain Cr(VI). Effluents from tanning and electroplating industries are the major sources of hexavalent chromium pollution. Manufacture of steel, dyes, pigments, batteries, refractories, welding, catalysis and wood preservatives produce hexavalent chromium. In leather industry, chromium salts help the conversion of animal skin into durable, deterioration resistant product. Therefore, considerable amount of chromium is discharged through the effluent. Tanning of leather produces effluent containing chromium in trivalent form which is further oxidised to hexavalent form which causes serious environmental impacts (Jain *et al.*, 2009; Dalcin *et al.*, 2011). Smelting of ferro chromium ores produce Cr(VI) waste. Chromium impurity is liberated to water source during the production of Portland cement. Table 1.2 represents the sources of hexavalent chromium in industrial wastewater (Das and Mishra, 2008).

Table 1.2 Industries and types of hexavalent chromium chemicals

Industry	Types of Hexavalent Chromium Chemicals
Pigments in paints, inks and plastics	Lead chromate, zinc chromate, barium chromate, calcium chromate, potassium dichromate, sodium chromate
Anti-corrosion coatings (chrome plating, spray coatings)	Chromic trioxide (chromic acid), zinc chromate, barium chromate, calcium chromate, sodium chromate, strontium chromate
Stainless steel	Hexavalent chromium (when cast, welded, or torch cut), ammonium dichromate, potassium chromate, potassium dichromate, sodium chromate
Wood preservation	Chromium trioxide
Leather tanning	Ammonium dichromate

1.4 Adverse Effects of Cr(VI)

Chromium is an odorless and tasteless metallic element. Cr (VI) is a heavy metal which is non-biodegradable and it accumulates inside living organisms (Fu and Wang, 2011). Cr(VI) adversely affects stomach, eyes, respiratory tracts and skin. It affects stomach resulting in death. Direct contact of chromate salts with eyes can cause permanent eye damage. The mucous membrane of nasal passages is damaged due to prolonged exposure of chromium. Skin allergies and skin ulcers are results of continuous exposure to chromium. Cr(VI) is a human carcinogen. Workers in chromate production, pigment industry, plating industry are more prone to lung cancer due to Cr(VI) exposure.

1.5 Methods of Cr(VI) Removal

Various methods of Cr(VI) removal are electro dialysis, photocatalysis, ion exchange, membrane filtration, chemical precipitation, coagulation, flocculation and adsorption. Electro dialysis is a membrane process through which ions are transported from one solution to another solution through a semipermeable membrane in the presence of an electric field. Two electrodes

are present in the electrodialysis unit in which electric field is applied. The membranes are ion exchange resins that are selective in transporting positive or negative ions. High removal of Cr(VI) is accomplished in this process but it requires high capital and operating cost. Another drawback of electrodialysis is that membranes are fouled frequently.

Photocatalysis is carried out in the presence of titanium dioxide. Photocatalysis is initiated by the absorption of a photon with energy equal to or greater than the band gap of the semiconductor producing electron/hole pairs. The hole oxidizes water producing hydroxyl radicals. OH[•] radicals attack the pollutants present in the water. This method has got capability of removing trace metals. Cr(VI) is reduced to Cr(III) and is precipitated. The process is very slow compared to conventional methods and hence not used frequently (Yang and Lee, 2006).

Strong base anion exchange resin (R-N-OH) is highly efficient for Cr(VI) removal. Chromium ions are exchanged with OH⁻ ions present in the resin bed. The bed after exhaustion is regenerated by washing with a strong base like NaOH. But regeneration of ion exchange bed is a problem which is frequently encountered. Electrochemical and ion exchange process can also be combined for the removal of Cr(VI) from aqueous solutions (Dharnaik and Ghosh, 2014).

Membranes are materials that can retain minute contaminants present in aqueous solutions. Depending on the pore size, they are classified as microfiltration (MF), ultrafiltration (UF), nanofiltration (NF) and reverse osmosis (RO). Microfiltration membranes possess largest pore size and retain largest particles and microorganisms present in water. Ultrafiltration membranes possess pore size smaller than microfiltration units but larger than

nanofiltration membranes. They will retain smaller particles, bacteria and soluble macromolecules like proteins. In RO membranes filtration units, pressure more than osmotic pressure is applied across the solution side and the solvent diffuses from solution to pure solvent side. RO units can remove all the dissolved ions from the solution. RO removes mostly all the contaminants from water. Polyamide based membranes are widely used for treatment of chromium containing effluents. Nanofiltration unit separates particles in the size range between UF and RO units.

Deposits of solute on the membrane surface is a major problem encountered in the large-scale operation of this technology. Cleaning of membrane or replacement of the filters is required to increase the process efficiency. Reverse osmosis is not practical for large-scale wastewater treatment operations because of its frequent membrane fouling and higher operating costs.

Formation of separable solid substance from a solution by the addition of suitable chemicals and settling of the precipitate is called chemical precipitation (Fu and Wang, 2011). Reduction of Cr(VI) to Cr(III) followed by chemical precipitation is another commonly adopted technology for Cr(VI) removal. Ferrous sulphate and lime are commonly used for Cr(VI) removal. Ferrous ion gets oxidized to ferric and simultaneously reduces Cr(VI) to Cr(III). Lime precipitates Cr(III) to its hydroxide. But this is not used for large scale operations due to the large volume of sludge produced. Its removal efficiency is pH dependent and this method is not suitable for low concentrations of metal ion.

In coagulation, coagulant is added to the aqueous solution to destabilise the colloidal suspensions. Flocculation involves the addition of polymers that clump the destabilised particles and enhance settling. Flocculation is also

achieved by slow stirring so that particles aggregate together to larger flocs and settle subsequently by sedimentation. Numerous chemicals are required in chemical coagulation of water and large amounts of sludge is produced during the process (Tchobanoglous *et al.*, 2003).

The pollutant from wastewater is adsorbed on the surface of a suitable material by Van der Waals force or chemical bond. This process is defined as adsorption and the adsorption is called physical and chemical adsorption depending on whether Van der Waals force or chemical forces are involved. The material on which the ions are bound is called an adsorbent and the ions are called adsorbate. Different classes of adsorbents are used depending on the type of impurity present in the water. Adsorption in the presence of microorganisms as adsorbents is called biosorption. Cell walls of certain types of algae, fungi and bacteria are responsible for adsorption of toxic heavy metals in wastewater during biosorption. Proper selection of adsorbents is a key factor to improve the efficiency of adsorption.

Now-a-days nanomaterials are used as adsorbents which possess large surface area and pore size distribution. Higher removal efficiency and higher adsorption capacity are the advantages of using nanomaterials as adsorbents. When compared to conventional adsorbents, very low adsorbent dosage is required for higher removal rate. In adsorption operations, one of the difficulty associated with nanoadsorbents is the difficulty of separation of the adsorbents from the solution after adsorption. This difficulty can be resolved by crosslinking the nanoparticles with suitable polymeric matrix so that nanofiltration is not required for separation of the adsorbent from the solution and the particles will not pass with the wastewater after treatment. Polymer/nanoadsorbent composite will also improve the swelling properties, improve gel strength and reduce the production cost (Chen *et al.*, 2013).

1.6 Adsorption

During adsorption, the specific molecule gets deposited on the surface of material called the adsorbent. The molecule which gets deposited is called the adsorbate. Activated carbon, silica gel, clay, colloids, metals, nanomaterials like magnetite, maghemite, halloysite nanoclay, montmorillonite nanoclay, zeolite, carbon nanotubes, biomaterials like chitosan etc. can be used as adsorbents for removal of heavy metals from aqueous solution. Adsorption is a surface phenomenon. The process of removing the adsorbed molecules from the surface of the adsorbent is called desorption.

Adsorption is generally an exothermic process and the enthalpy change is always negative. But chemisorption can be endothermic. When the adsorbate is being adhered to the surface of the adsorbent, there will be disorder or randomness of the molecules near the surface of the adsorbent and hence the entropy change occurs during adsorption. At constant pressure, the adsorption is a spontaneous process and the free energy decreases during adsorption.

Batch adsorption process is affected by changes in the solution pH, initial solution concentration, adsorbent dosage, time of contact, agitation speed, temperature and pressure. During optimisation of batch process, the effect of these parameters are estimated to obtain maximum removal of the desired constituent. Suitable software can be used for the optimisation process. Minitab 16 is a software which has been used for the purpose in the present work. Response surface methodology is used to develop empirical relationships between a set of experimental parameters and observed results (Sadhukhan *et al.*, 2016). Both Central Composite design and Box Behnken design of response surface methodology have been used for the optimisation of batch adsorption process. Response surface methodology (RSM) consists of three steps. 1)

perform the experiments according the design of experiments given by RSM 2) developing the model equation and estimating the coefficients in the model 4) predict the response and checking the adequacy of the model.

Batch adsorption study provides the elementary information regarding the adsorption process. This process is time consuming and requires large amount of adsorbent. Batch study is applicable only for a short time and for small capacity processes. So, for large scale operations, the batch adsorption process is not effective. So continuous packed column is to be designed to perform the large-scale operations using suitable adsorbents. This can be operated for a longer period when compared to batch process and more volume of aqueous solution can be treated. Proper controlling of the adsorption process is possible in continuous fixed bed column operations. As far as economics is considered, continuous column operation is more economical when compared with the batch adsorption (Lim and Aris, 2014). The adsorbent is packed in a suitable column and the wastewater is passed through the column either in up flow or down flow mode. The solution leaving the column is analysed for the specific ions. In addition to the parameters of batch adsorption process, the packed column performance is affected by the bed height of the adsorbent and flow rate of the solution through the column. Shape of the breakthrough curve is an important factor that determines the time of operation of the fixed bed column. The column can be modeled by fitting the experimental data to suitable models like Thomas model, Yoon Nelson model, Adam Bohart model etc. Once the saturation of the bed happens, suitable eluents are selected for the regeneration of the bed. After bed regeneration, the performance of the bed improves drastically.

1.7 Scope of the Study

The main aim of wastewater engineering is to solve the issues associated with the treatment and reuse of water. The important treatment steps in wastewater from industry include preliminary treatment, primary treatment, secondary treatment and tertiary treatment. Preliminary treatment involves the coarse and suspended solids removal by screening, passing through grit chambers and equalisation chambers. Primary treatment involves the use of primary clarifiers for removal of suspended solids that are not removed during the preliminary treatment. Secondary treatment involves unit processes and is meant for treatment water by either aerobic or anaerobic methods in the presence of microorganisms.

Tertiary treatment is meant for the final treatment of wastewater which contains traces of impurities that are not removed during the secondary treatment and disinfection of water (Tchobanoglous *et al.*, 2003). Heavy metals have been used by humans from thousands of years. Cr(VI) is one such heavy metal which is to be removed from water before recycling and reuse. Presence of Cr(VI) affects all sorts of life adversely. Heavy metals in trace amounts after secondary treatment are removed during the tertiary treatment. Even though there are many tertiary treatment methods for Cr(VI) removal, adsorption is effective for removal of Cr(VI) present in low concentrations (<50 ppm). Adsorption is widely used now-a-days due to its efficiency and low cost when compared to other conventional tertiary treatment methods.

Adsorption using nanoadsorbents is a fast-growing technology due to immense capability of nanomaterials. Nanoadsorbents are highly efficient when compared to conventional adsorbents due to their small size, high surface area and pore size distribution. In this study, nanokaolinite clay and nanomagnetite have been used without any treatment, for the removal of Cr(VI) from aqueous

solution. Due to the difficulty in handling very low size nanoparticles, halloysite nanoclay was made composite with chitosan as the base material. This nanocomposite film was used in batch study for the removal of Cr(VI) from water. Further, adsorption column was fabricated and nanocomposite films were used as adsorbents to study the removal of Cr(VI) from aqueous solution.

1.8 Objectives of the Present Work

The main objective of the present work is to develop a suitable nanomaterial based adsorbent for the removal of low concentration of Cr(VI) from aqueous solution. Batch experiments were performed using nanokaolinite, nanomagnetite and chitosan/halloysite nanocomposite to analyse the effect of various parameters on Cr(VI) adsorption. Due to the operational difficulties of batch adsorption, a suitable continuous fixed bed column was to be developed for the removal of trace amounts of Cr(VI) from aqueous solution. Suitable solvent for desorption of the adsorbent was also to be determined. To achieve the objectives, the following experimental procedures were carried out:

- Synthesis of nanoadsorbents using standard methods available in the literature.
- Characterisation of the nanoadsorbents using SEM, XRD, EDX, TGA, micrometer and FTIR.
- Batch adsorption study to assess the effect of various parameters on adsorption using nanokaolinite clay, nanomagnetite and chitosan/halloysite clay nanocomposite films.

- Optimisation of performance of nanomagnetite and nanocomposite film using RSM of Minitab 16.
- Determination of adsorption kinetics of nanocomposite films.
- Estimation of isotherm parameters of nanocomposite films.
- Conduct thermodynamic study using chitosan/halloysite nanocomposite films as adsorbent.
- Establish the recovery and reuse of the nanocomposite films as adsorbent.
- Design and fabrication of fixed bed adsorption column for Cr(VI) removal using chitosan/halloysite nanocomposite films.
- Evaluation of effects of pH, initial Cr(VI) concentration, bed height and flow rate on the breakthrough performance of Cr(VI) column using nanocomposite films.
- Modeling of Cr(VI) column using Thomas model, Yoon Nelson model and Adam Bohart model.
- The objectives and methodology of this research were finalised on the basis of the gaps and leads identified from a detailed review of the pertinent literature presented in the ensuing Chapter 2.

1.9 Thesis Outline

This thesis mainly involves the comparison of percentage of hexavalent chromium removal and adsorption capacity of three adsorbents namely nanokaolinite clay, nanomagnetite and chitosan/halloysite clay nanocomposite film. Nanocomposite films possess higher adsorption efficiency and adsorption capacity than the other two adsorbents. Hence chitosan/halloysite

clay nanocomposite films were used in continuous packed bed adsorption column for Cr(VI) removal. This thesis is divided into five chapters.

In Chapter 1 introduction to the sources of various heavy metals in water has been explained. Adverse effects of hexavalent chromium and its treatment methods are clearly stated. The advantages of adsorption when compared to the other methods and the application of nanotechnology in adsorptive removal of hexavalent chromium are highlighted in this chapter. The scope and the objectives of the study have been set out.

In Chapter 2 literature review on laboratory synthesis of nanoparticles that can be used as adsorbent has been conducted. A detailed literature survey on adsorption, various adsorbents for heavy metal removal, factors affecting adsorption, kinetics, thermodynamics, isotherm and desorption study are included in this chapter. Literature review on continuous packed bed adsorption column for the removal of various heavy metals in aqueous solution is also described in this chapter.

Chapter 3 describes the various materials used and the methodology adopted in the present study for the removal of hexavalent chromium from aqueous solution by adsorption. Methods for synthesis of nanoadsorbents, batch adsorption tests performed in the work, continuous packed bed column fabrication and operation for Cr(VI) removal, models used for batch and continuous experiments, equipments used for analysis and characterisation of the nanoadsorbents are explained in this chapter.

The results obtained from the batch and continuous adsorption tests for hexavalent chromium removal are presented clearly in Chapter 4. Characterisation of adsorbents, optimisation, modeling and validation of batch results by RSM and modeling of Cr(VI) column are presented in this chapter.

The summary and conclusions of the present study are included in Chapter 5 of the thesis. This is followed by the scope for future work and the limitations of the work. List of references is included in the next section. Annexures are included after the references.

LITERATURE REVIEW

• Contents •	2.1 Introduction
	2.2 Sources of Hexavalent Chromium in Water
	2.3 Impacts of Cr(VI)
	2.4 Methods of Cr(VI) Removal
	2.5 Literature Review on Adsorption and Adsorbents
	2.6 Mechanism of Adsorption
	2.7 Factors Affecting Batch Adsorption
	2.8 Adsorption Isotherm
	2.9 Adsorption Kinetics
	2.10 Adsorption Thermodynamics
	2.11 Response Surface Methodology
	2.12 Desorption
	2.13 Characterisation of Adsorbents
	2.14 Analytical Method
	2.15 Continuous Removal in Packed Bed Adsorption Column
	2.16 Summary

2.1 Introduction

Wastewater engineering involves methods to protect public health by devising suitable methods that can commensurate with environmental, social, economic and political concerns. To achieve the goal of wastewater engineering, one should have awareness regarding the important constituents in wastewater, impact of these constituents to the environment and treatment methods for removing the toxic constituents from water (Tchobanoglous *et al.*,

2003). Manufacturing is a key requirement for the growth of the human civilization. As a result, there has been a drastic increase in the number of industries in the modern era. Industrial discharges pose adverse effects on the environment because they affect both water and air quality. Unplanned industrialisation and urbanisation are causing drastic increase in the concentration of toxic heavy metals in aqueous solution posing major threat to the surroundings and all sorts of life including fauna and flora. Heavy metals are elements that have atomic weights in the range 63.5 and 200.6 (Fu and Wang, 2011). Their specific gravity is greater than 5.0. Some heavy metals are micronutrients but are toxic in excess concentrations.

Unlike other toxic pollutants, the heavy metals are non-biodegradable and they accumulate in the live tissues and eventually become a part of the life cycle. According to WHO, cadmium, mercury, lead, arsenic, chromium, manganese, nickel, copper, cobalt, zinc, selenium, silver, arsenic, antimony and thallium are the major toxic heavy metals discharged into the water from various industries. In many geographic areas, drinking water contains Cr(III) and Cr(VI). Cr(VI) is extremely toxic and the presence of Cr(VI) in aqueous solution is a matter of concern. In the present study chromium removal is considered in detail using adsorption. Nanomaterials due to their large surface area possess high adsorption capacity. In the present work use of nanoparticles for Cr(VI) removal in both batch and continuous study is analysed in detail.

2.2 Sources of Hexavalent Chromium in Water

Chromite, an oxide of iron, magnesium, aluminium and chromium, is the only ore mineral of chromium and in nature it is found as chromite deposits. Chromium is the 22nd most abundant element in the earth's crust and it appears with silver lustrous structure. Chromium is a brittle hard metal and

its molecular weight and atomic number are respectively 51.996 and 24 respectively. It exists mostly in trivalent and hexavalent state. The major mining of chromium occurs in Africa (2400 Gg cr/year). The major consumers of chromium are Asia (1150 Gg cr/year), Europe (1140 Gg cr/year) and North America (751 Gg cr/year) and these continents are the main waste generators of chromium in the world (Johnson *et al.*, 2006).

Leather industry is one of the main sources of chromium pollution. In tanning industry for producing high quality leather that is resistant to deterioration, chromium salts play a major role. Large quantity of chromium salts are required in the leather industry. In chrome tanning only 60-80 % of applied chromium is consumed and hence the effluent from tanning industry contains considerable amount of chromium (Dalcin *et al.*, 2011). Chromium ion in tanning wastes appear as trivalent form which is less toxic, but it gets oxidised to hexavalent form which is highly toxic (Jain *et al.*, 2009).

To increase hardness and corrosion resistance, chromium salts are used in steel industry. Welding of stainless steel and other alloy steels is a source of chromium. Stainless steel contains 18% chromium. So, the wastewater from steel industry contains chromium. In electroplating industry, chromium plating is carried out for decorative purposes, anticorrosion, increase of surface hardness and ease of cleaning. Another important industry that needs chromium as a raw material is textile industry. Cr(VI) is used in textile industries as a catalyst in dyeing process and as a dye for wool. Chrome yellow obtained from chromite is a pigment used in textile industry. In wood industry chromated copper arsenate is used for protection of timber from fungi, termites and marine borers. Several chromium compounds are used as catalysts for processing hydrocarbons. For example, copper chromite is a hydrogenation catalyst. In wet cell batteries, chromic acid is used. Cooling tower blowdown, anodizing baths, rinse waters etc.

are the other main sources of Cr(VI) (Owlad *et al.*, 2009). So, the wastewater generated from all these industries contains considerable amount of chromium salts which when disposed without any treatment is a threat to the environment.

Barnhart (1997) reported on occurrences, uses and properties of chromium. This paper aimed at presenting the major sources of chromium, its properties and industrial uses of chromium. Various oxidation states in which chromium exists also has been presented in the paper.

2.3 Impacts of Cr(VI)

Chromium is a highly toxic metal eventhough it has several industrial applications. The limit of Cr(VI) is 0.1 mg/L and Cr(III) is 1 mg/L for discharge into water bodies. This is according to CONAMA (Resolution CONAMA no.397, April 3, Brazil, 2008) (Dalcin *et al.*, 2011). Of the two thermodynamically stable forms of chromium salts, Cr(VI) is extremely toxic and much more than Cr(III). Cr(III) due to its limited hydroxide solubility, is less available for biological uptake. In humans, Cr(III) is essential for glucose, fat and protein metabolism. Cr(III) is essential in mammals since it helps in glucose, protein and lipid metabolism.

Cr(VI) can diffuse as CrO_4^{2-} and HCrO_4^- through the cell membranes and is extremely toxic (Chauhan and Sankararamkrishnan, 2011). Fig. 2.1 represents the conversion of Cr(III) to Cr(VI) because of human activities (Zhitkovich, 2017). According to international agency of cancer, Cr(VI) can cause chromosomic aberration by modifying DNA transcription process. Based on the chronic effects of Cr(VI) on human it is classified as group A carcinogen by USEPA. Due to its adverse effects on all forms of life, the maximum limit of total chromium is 0.05 mg/L in drinking water as specified by World Health Organisation (WHO) and Bureau of Indian Standards (BIS).

The standards given by central pollution control board suggests the permissible limit of Cr(VI) from various industrial effluents which is discharged to various water bodies like inland surface waters, public sewers and marine coastal areas as 0.1, 2.0 and 1.0 mg/L, respectively. Consumption of water containing even minute quantities of heavy metals can lead to ill health, deformities and death. When strongly exposed to Cr(VI), human beings suffer various adverse conditions like haemorrhage, diarrhoea, vomiting nausea, epigastric pain, skin allergy, liver problems etc. Severe exposure to Cr(VI) causes cancer in lungs and digestive tracts. Continuous discharge of effluent containing chromium also affects the aquatic life including reduction in fish production (Jain *et al.*, 2009).

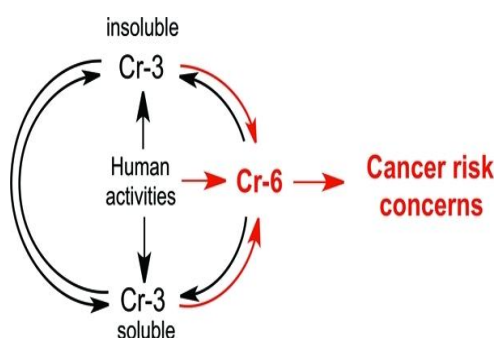


Fig. 2.1 Conversion of Cr(III) to Cr(VI)

2.4 Methods of Cr(VI) Removal

Heavy metals including chromium is a serious cause of environmental pollution when discharged to the surroundings. These are classified as priority pollutants since they affect all forms of life. To protect the people and environment these pollutants should be removed from effluent water before discharging into the water bodies. There are various methods for removal of these pollutants so that they can be maintained within the permissible limits prescribed by legislation. Several methods for removal of Cr(VI) have been

reported. Fu and Wang (2011) presented a paper on review of removal of heavy metals from water. Barakat (2011) reported regarding the new trends in removing heavy metals from industrial wastewater. The advantages and disadvantages of various methods for heavy metal removal have been discussed in detail in this literature below.

2.4.1 Chemical Precipitation

Chemical precipitation is simple and inexpensive. So, it is widely used in industries. Conventional methods include precipitation as hydroxide and sulphide (Fu and Wang, 2011). Chemical precipitation separates the contaminant by adding a suitable chemical by precipitating it out from the solution. By adding ferrous sulphate and lime, Cr(VI) can be precipitated from the solution. Maximum precipitation occurs at pH 8.7 (Mirbagheri and Hosseini, 2005). Chromium is precipitated as hydroxide during this process. The precipitates are separated by sedimentation process. Enzymatic reduction of Cr(VI) to Cr(III) followed by chemical precipitation can be used for removal of Cr(VI) from electroplating wastewater (Ahamad *et al.*, 2010).

Another method of precipitation is sulphide precipitation. This is suitable for a wide range of pH unlike hydroxide precipitation. The solubility of metal sulphide precipitate is considerably lower than that of metal hydroxide precipitate. Metal sulphide possesses better dewatering characteristics than metal hydroxide. This method must be conducted in neutral or basic medium because the precipitation of sulphide in acid medium results in the evolution of toxic H₂S gas.

2.4.2 Ion exchange for Cr(VI) Removal

Ion exchangers employ specific ion exchange resins which can be reused. Ion exchangers have high treatment capacity, high removal efficiency

and fast kinetics. Ion exchangers are classified as cationic and anionic exchangers which contain synthetic resins for exchange of specific ions. For the removal of inorganic contaminants from wastewater, synthetic resins are commonly employed. The resins are eluted to recover the ions and reused. Ion exchange method possesses high Cr(VI) removal rate, but the operating cost is very high. Also, the sludge volume is less when compared to chemical precipitation.

Rengaraj *et al.* (2001) used IRN77 and SKN1 cation exchange resins for the removal of chromium from water and wastewater. The effects of adsorbent dosage, pH and contact time on Cr(VI) removal was reported in the literature. Sahu *et al.* (2009) investigated the applicability of Indion 790 for tannery wastewater treatment for Cr(III) removal. Effect of pH and desorption of Cr(III) from the resin was studied in the above literature.

2.4.3 Membrane Filtration

This process uses membranes for removal of Cr(VI) from wastewater. The various types of membrane filtration processes are ultrafiltration, nanofiltration, reverse osmosis and electrodialysis. Ultrafiltration (UF) membranes have higher pore size. The smaller metal ions will pass through the membrane. Hence, they have less efficiency than other membrane systems. The pore size of nanofiltration (NF) membranes are lower than that of ultrafiltration membranes, but higher than that of reverse osmosis (RO). They have higher removal efficiency than UF membranes. The power consumption is less for NF when compared to RO membrane processes. RO process is highly efficient and uses a semipermeable membrane which allows the passage of pure solvent. The process is opposite to natural osmosis. The process is not popular due to large sludge generation, high capital and

operating cost and high power consumption. Hsu *et al.*, (2011) reported the removal of Cr(VI) and naphthelenesulfonate from textile wastewater by photocatalysis combining ionic exchange membrane processes. The removal of Cr(VI) has been enhanced by decreasing the solution pH. The removal of chromium from wastewater by reverse osmosis was investigated by Cimen (2015). In this investigation, comparison was made between reverse osmosis, sea water high rejection (SWHR) and high rejection brackish water membrane techniques. RO process showed high rejection of Cr(VI) when compared to the other processes.

In electrodialysis, charged membranes are used for separation of metal ions. Ion exchange cationic and anionic membranes are used in electrodialysis (ED) units. In ED, by applying electric charge, anions are made to migrate towards the anode and cations migrate towards the cathode crossing the ion exchange membranes. Nataraj *et al.* (2007) studied the removal of hexavalent chromium using ED pilot plant. ED process requires high capital and operating costs and are not used for higher capacity operations.

2.4.4 Electrochemical Methods

In electrochemical technology, electrolysis of wastewater containing higher concentration of metals is carried out. This method requires higher capital cost and its operation is expensive. So, this is not commonly used for wastewater treatment. Electrocoagulation, electrodeposition and electroflotation are the three established technologies in electrochemical methods. Sheng *et al.* (1998) analysed the treatment of saline wastewater by electrochemical method. In the experiments performed by Sheng *et al.* (1998), the influence of operating parameters, such as, pH, initial phenol

concentration, salinity, current density, temperature and addition of small amounts of H_2O_2 on the COD removal efficiency was studied.

Industrial wastewater containing Cr(VI) can be treated using Al or Fe electrodes with forced recirculation of the solution. The higher the current density, the removal rate of Cr(VI) is faster (Zongo *et al.*, 2009).

2.4.5 Photocatalysis

Photocatalysis is the acceleration of photoreaction in the presence of a catalyst. Light is absorbed by an adsorbed substrate in this process. Yang and Lee (2006) used TiO_2 for removal of Cr(VI) and humic acid. The effect of various parameters affecting the removal was studied. In the study, the Cr(VI) ions were adsorbed on the surface of TiO_2 and were reduced to Cr(III) by photooxidation.

Ruthenium dioxide coated titanium plate was used as anode and stainless steel plate as cathode for the removal of Cr(VI) from synthetic wastewater at different voltages. Ion exchange resin was placed between the electrodes. This electrochemical ion exchange cell was operated at different hydraulic retention time for analysing the efficiency of ion exchange-electrochemical process (Dharnaik and Ghosh, 2014).

2.4.6 Coagulation and Flocculation

Coagulation and flocculation are always accompanied by sedimentation. Coagulants are added to the wastewater and they destabilise the colloids by neutralising the forces that keep them apart. Wastewater treated by coagulation and flocculation produces sludge of high settling and dewatering characteristics. During flocculation, flocculants form bridges between the flocs and bind the flocs into large agglomerates which settle by sedimentation.

Disadvantage of this method is that large amount of chemicals is consumed and sludge volume is very high. Sodium Xanthogenate was grafted to polyethyleneimine and used as coagulant for removal of soluble heavy metals and insoluble substances from wastewater (Chang and Wang, 2007).

Alum is an effective coagulating agent for Cr(VI) removal from wastewater (Kotaiah and Chiranjeevh, 1998). The effect of pH and alum dose was analysed for coagulation and flocculation of Cr(VI) in the work. At optimum pH, the removal efficiency was in the range 15-28 % at different alum dosages.

2.4.7 Adsorption

When porous and discontinuity surface of a specific solid is exposed to a liquid, the specific component from the liquid will form bonds with the solid and become attached to the solid surface. This is known as adsorption. Adsorption is a separation process in which certain components of a gaseous or liquid phase are selectively transferred to the surface of a solid adsorbent. Surface energy is responsible for adsorption. In the interior surface of an adsorbent, all the bonding requirements of the atoms are filled by other atoms. But, on the surface, the atoms are not fully surrounded by other atoms and therefore adsorbates can be bonded on the surface of adsorbents. There are basically two types of adsorption, physical and chemical. Physical adsorption takes place due to the action of Van der Waals forces. There is no reaction between adsorbent and adsorbate in physical adsorption and forces present in this type are weak. In chemical adsorption there is reaction between the adsorbate and adsorbent resulting in a change in the chemical form of the adsorbate (Ruthwen, 1984). The forces of attraction between adsorbate and adsorbent are strong and they cannot be reversed.

Adsorption is a cheap and effective method for wastewater treatment. It is extremely useful for low concentrations of contaminant. Adsorption also possesses advantages like availability, profitability, ease of operation and efficiency (Demirbas, 2008). Adsorption is also a reversible process. Using proper solvents, the adsorbed contaminant can be desorbed and the adsorbent can be reused. Adsorption can be carried out for higher capacity operations in continuous column. In water treatment operations, adsorption is widely used due to its simplicity and ease of operation, less initial investment, free from or less generation of toxic substances and less production of sludge.

The adsorption is influenced by various parameters like solution pH, initial concentration, adsorbent dosage, time of contact and temperature. Various types of adsorbents are being used for treatment of wastewater. The adsorbent should have high surface area which provides large space for development of any chemical reaction and any physical activity. The solid must have relatively large pore network for the transport of molecules to the interior. Adsorbents also should be of low cost and require less time for adsorption. Polarity and functional groups of the adsorbent are the other important factors that determine the efficiency of the adsorption process.

Pan and Xing (2008) reported the adsorption mechanisms of organic chemicals on carbon nanotubes. Adsorption mechanisms were analysed by studying the effects of properties of both CNT's and organic chemicals along with environmental conditions in the literature mentioned above. Table 2.1 presents a comparison of Cr(VI) removal efficiency by different removal techniques in use.

Table 2.1 Comparison of Cr(VI) removal efficiency attained in different removal techniques

Method	Cr(VI) removal efficiency	Reference
Reverse Osmosis	>91%	Cimen, 2015
Photocatalysis combining ionic exchange membrane process	Almost complete removal	Hsu <i>et al.</i> , 2011
Electrodialysis pilot plant containing ion exchange membranes	Maximum contaminate level < 0.1 ppm for Cr(VI)	Nataraj <i>et al.</i> , 2007
Adsorption using chitosan/montmorillonite magnetic microspheres	>95%	Chen <i>et al.</i> , 2013
Biosorption of Cr(VI) by <i>Rhizopus nigricans</i>	99.2%	Bai and Abraham, 2001
Electrochemical-ion exchange process	99%	Dharnaik and Ghosh, 2014

2.5 Literature Review on Adsorption and Adsorbents

Conventional adsorbents like activated carbon, low cost agricultural waste by-products such as sugarcane bagasse, rice husk, saw dust, coconut husk, oil palm shell, neem bark etc. have been used as adsorbents for removal of heavy metals from wastewater. Waste materials like fruit wastes, coconut shell, scrap tyres, bark and other tannin rich materials, wood based materials, rice husk, petroleum waste, fertilizer waste, fly ash, sugar industry waste, blast furnace slag, chitosan and other sea food processing waste, sea weed and algae, peat moss, clay, red mud, zeolite, sediment and soil, ore minerals etc. have been effectively used for the removal of organic pollutants from wastewater (Imran *et al.*, 2012). Peat is an inexpensive and plentifully available adsorbent for removal of dissolved metals from waste streams (Brown *et al.*, 2000). Brown algae is an inexpensive substrate for biosorption of heavy metals like Cd^{2+} , Cu^{2+} , Zn^{2+} , Pd^{2+} , Cr^{3+} and Hg^{2+} (Davis *et al.*, 2003).

Modified raw Sargassum sea weed (RSW) can be used as a biosorbent for Cr(VI) removal from wastewater. Chemical modification of the biosorbent was carried out using sodium hydroxide, hydrochloric acid, calcium chloride, formaldehyde and glutaraldehyde (Yang and Chen, 2008).

Activated carbon is usually obtained from materials of high carbon content. Fresh activated carbon and waste activated carbon pre-treated with mineral acids like sulphuric acid and nitric acid at high temperature can provide higher adsorption capacity and removal efficiency than ordinary activated carbon (Ghosh, 2009). Eventhough activated carbon has high adsorption capacity, its cost is very high. Other traditional adsorbents suffer from certain drawbacks like low sorption capacity and low efficiency.

Raji and Anirudhan (1998) analysed the effect of adsorbent dose, initial sorbate concentration and pH on the adsorption of Cr(VI) by polyacrylamide-grafted saw dust. Kinetic data revealed that the adsorption process was of first order and followed Freundlich isotherm. Desorption of grafted saw dust was conducted using 0.2 M NaOH and 0.5 M NaCl.

Adsorption of Cu^{2+} and Cr^{3+} was carried out economically by batch adsorption using pumice (Pmc) and polyacrylonitrile/pumice (PAN/Pmc) composite at room temperature. The removal efficiency for the cations was 80% and 87% by Pmc and PAN/Pmc composite respectively (Yavuz *et al.*, 2008).

Natural moss and copper coated moss were used in batch experiments for the removal of Cr(III) and Cr(VI) from aqueous solutions (Lee *et al.*, 1995). The effect of parameters like pH, contact time, initial concentration, sorbent dosage and temperature were analysed in the study.

Chen and Hao (1996) presented a paper on various environmental factors affecting the microbial Cr(VI) reduction. Anaerobic chemostat fed with synthetic media containing acetate and Cr(VI) has been used to perform the batch

experiments. The various factors affecting the batch adsorption tests were analysed which include carbon concentration, acetate level, biomass concentration and type of organic compounds.

Sudha Bai and Emilia (2003) reported adsorption-desorption study of Cr(VI) using immobilized *Rhizopus nigricans*. Five polymeric matrices were used for immobilization of fungal biomass. The comparison was made for adsorption-desorption efficiency between the five matrices namely, calcium alginate, polyvinyl alcohol, polyacrylamide, polyisoprene and polysulfone. Caustic soda, sodium bicarbonate and sodium carbonate were used separately for desorption in the work.

Ayari *et al.* (2005) collected bentonite clay from Zaghouan (mideastern Tunisia) and performed characterisation using X-ray diffraction, infrared spectroscopy, TGA and DTA. Determination of cation exchange capabilities and specific and total surface area were also included in the study. The study was conducted to analyse the applicability of the clays for use as adsorbent for heavy metal removal.

Advances in nanoscience and engineering provide immense opportunities for developing efficient adsorbents for Cr(VI) removal. Nanomaterials are particles of nanoscale dimensions that are manufactured by nanotechnology. Their size comes under 100 nm (Dhermendra *et al.*, 2008). Nanoadsorbents have immense possibilities in wastewater treatment due to their unique properties of nanomaterials. Four classes of nanomaterials are being used now-a-days for water purification which include metal containing nanoparticles, carbonaceous nanomaterials, zeolites and dendrimers (Nora and Mamadou, 2005). Various methods have been developed for synthesis of nanoadsorbents. Novel properties of nanomaterials are due to their small size. Nanomaterials possess large surface area, potential for self-assembly, high specificity and high reactivity when

compared to conventional materials for water treatment processes. Nanoadsorbents possess higher efficiency and faster kinetics for removal of heavy metals from industrial wastewater. Nora and Mamadou (2005) gave an overview of opportunities and challenges of nanomaterials used for water purification.

The nanoadsorbents used for wastewater treatment should be nontoxic, possess high removal efficiency, selectivity, should be able to remove low concentration of metals, should possess ability to desorb the pollutant and should be recyclable. In addition to surface area, nanoparticles possess unique adsorption properties due to distribution of reactive surface sites and disordered surface regions (Dhermendra *et al.*, 2008). The nanoparticles should be easily separable from water after adsorption process. Due to very small size of nanoadsorbents, it is difficult for separation and there is chance for the nanoadsorbents to go along with the treated water. The nanoadsorbents should be cross linked or entrapped onto a suitable matrix to form nanocomposite so that it can be easily separated from the water after adsorption.

Numerous studies have been conducted for removal of Cr(VI) from synthetic or industrial wastewater using nanomaterials as adsorbents. Magnetite nanoparticle is easily separated from water due to its magnetic properties. Structure of magnetite is shown in Fig. 2.2.



Fig. 2.2 Structure of magnetite

The most common method of synthesis of magnetite nanoparticles in the laboratory is sol gel method (Lemine *et al.*, 2012). Magnetite nanoparticles can be synthesised using ferric chloride tetrahydrate and ferric chloride hexahydrate as the starting raw materials. Awwad and Salem (2012) synthesised magnetite nanoparticles from the raw materials mentioned above using carob leaf extract. The synthesised nanoparticles were characterised by SEM, TGA, FTIR and XRD. Properties of magnetite is shown in the Table 2.2 (Klein and Hurlbut, 1985).

Table 2.2 Properties of magnetite

Property	Characteristics
Colour	Black gray with brownish tint in reflected sun
Crystal habit	Octahedral
Fracture	Uneven
Tenacity	Brittle
Luster	metallic
Streak	black
Diaphaneity	Opaque
Specific gravity	5.17-5.18
Solubility	Dissolves slowly in hydrochloric acid

Microwave irradiation method was used for the synthesis of maghemite nanoparticles for the adsorption of Cu^{2+} , Zn^{2+} and Pb^{2+} from wastewater. The effects of contact time, initial concentration and pH on adsorption of Cu(II), Zn(II) and Ni(II) were investigated by conducting batch adsorption experiments. The results indicated that the synthesised maghemite nanoadsorbents had high potential for adsorption (Roy and Bhattacharya, 2012).

Nanoscale zerovalent iron has considerable potential in remediation of Cr(VI) and Pb(II) ions from aqueous solution (Ponder *et al.*, 2000). Fe_3O_4 , Mn_3O_4 and MnFe_2O_4 nanoadsorbents were synthesised by microwave assisted

hydrothermal synthesis technique and used for adsorption of arsenic III and V from wastewater (Parsons *et al.*, 2009). Adsorption experiments were conducted in the pH range of 2-6. Results of the above work indicated that the adsorption was largely pH independent for MnFe_2O_4 . For Mn_3O_4 , even though there was a slight pH dependence, the maximum adsorption capacity was between pH 4-5. For Fe_3O_4 the dependence of adsorption on pH was highest and removal increased from pH 2-6.

Zhou *et al.* (2009) used chitosan coated magnetic nanoparticles modified with α -ketoglutaric acid for removal of Cu^{2+} from water. The effect of pH, contact time, initial Cu^{2+} concentration and adsorbent dose were analysed, and the results proved that nanoadsorbents possessed considerable potential for removal of Cu^{2+} from aqueous solution.

Wassana *et al.* (2007) compared adsorption removal efficiency of conventional resin based sorbents (GT-73), activated carbon, nanoporous silica (SAMMS) with dimercapto succinic acid functionalised super paramagnetic Fe_3O_4 for the removal of heavy metals like Hg, Ag, Pb, Cd and Tl. Nanoparticles possessed high removal efficiency in least contact time when compared to the adsorbents mentioned above. The adsorption capacity of GMSA- Fe_3O_4 was 30-fold higher than that of GT-73.

Investigation was conducted on use of nanoporous aluminosilicate monoliths for adsorption of organic dyes from aqueous solution (Sherif *et al.*, 2011). Study was conducted to assess the effect of initial concentration, temperature and Si/Al ratio on adsorption capacity of fabricated nanoadsorbents. A study on adsorption of Arsenic(V) on Fe_3O_4 nanoparticle coated born nitride nanotubes was conducted at pH of 6.9 and at room temperature of 25 °C. The equilibrium data of Arsenic(V) adsorption was

fitted with Langmuir, Freundlich and D-R isotherm models (Rongzhi *et al.*, 2011). Adsorption of arsenate from aqueous solution was studied by conducting batch tests using α and δ manganese dioxide nanoadsorbents in Mandeep *et al.* (2010). In the above work manganese pentahydrate was used for synthesis of nanoadsorbents.

Waste iron oxide tailings were used for synthesis of magnetite nanoparticles (Giri *et al.*, 2011). Ferric iron was recovered from waste iron oxide tailings by acid leaching and precipitation. In the paper the synthesised nanoparticles were used for removal of dyes from aqueous solutions by adsorption.

Magnetite nanoparticles were synthesised and the effect of rapid mixing devices on the properties of magnetite nanoparticles was reported by Li *et al.* (2012). Comparison between pumice and polyacrylonitrile/pumice composite for the removal of Cr^{3+} and Cu^{2+} from water has been reported by Mustafa *et al.* (2008). The comparison of adsorption properties was made by conducting batch adsorption tests at room temperature.

Coprecipitation method was used for synthesis of maghemite nanoparticles from iron solution and was used for Cr(VI) adsorption from aqueous solutions (Wenjun *et al.*, 2013). In the study it was reported that the adsorption followed pseudo second order kinetics. The equilibrium adsorption data was fitted to Langmuir and Freundlich models. pH affected the adsorption and optimum pH was observed to be 4.0 corresponding to maximum Cr(VI) removal.

Yuan *et al.* (2009) used diatomite supported and unsupported magnetite nanoparticles for the removal of Cr(VI) from synthetic wastewater. Magnetite nanoparticles were synthesised using ferric chloride tetrahydrate and ferric chloride hexahydrate. The results of batch experiments showed that the adsorption was highly pH dependent. The kinetic model fitted to pseudo

second order kinetics. Langmuir equation was best fitted to the equilibrium data in the above work.

Lingyun *et al.* (2011) reported the synthesis of mesoporous magnetite on a large scale from ferric nitrate and ethylene glycol. The characterisation of synthesised particles using TEM showed that the mesoporous magnetite was formed by loose aggregation of nanoparticles with diameter of 6 nm.

Superparamagnetic, monodisperse, highly crystalline magnetite nanoparticles were synthesised in liquid polyols by Cai and Wan (2007). The characterisation was conducted using XRD, TEM, TGA, SAED and FTIR. The magnetic property of synthesised particles was studied using PPMS. Sarkar *et al.* (2012) reported on synthesis, characterisation and applications of polymer supported metal and metal oxide nanoparticles.

Chitosan is a naturally occurring polysaccharide material. Several studies have been conducted using chitosan and chitosan composites for wastewater treatment. The product of deacetylation of chitin results in the formation of chitosan. Chitosan is primarily composed $\beta(1 \rightarrow 4)$ linked 2-amino 2-deoxy D-glucopyranose units. Chitosan possesses excellent adsorption capacity. It also possess high hydrophilicity, large number of surface hydroxyl group and amino group. Chitosan is biocompatible, biodegradable and less toxic. Chitosan is immunological, antibacterial and wound healing. Chitosan is mainly obtained from crustacean shells of prawn, crab, shrimp or lobster. It has got wide applications in the sorption of heavy metals from industrial wastewater due to its flexible structure and its ability to link metal ions because of its high concentration of amine functional groups. The adsorption capacity of chitosan depends on its deacetylation degree, porosity, crystallinity and affinity for water (Miretzky and Cirelli, 2009). Structure of chitosan is represented in Fig. 2.3.

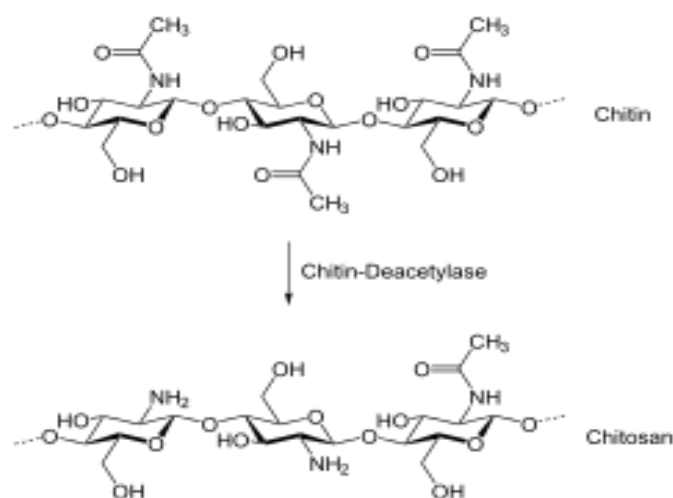


Fig. 2.3 Structure of chitosan

One of the key issues associated with chitosan based adsorbent is its solubility in acidic media. But it is insoluble in alkaline media. So cross linked chitosan has been used in several cases to prevent the dissolution of chitosan in acid medium (Cho *et al.*, 2012). Properties of chitosan is shown in Table 2.3.

Table 2.3 Properties of chitosan

Physiochemical	Biological
Cationic polyamine	Biocompatible
High charge density at pH <6	Biodegradable
Form gel with polyanions	Nontoxic
Forms salts with organic and inorganic acids	Haemostatic
Linear	Bacteriostatic
Wide range of molecular weight	Anticholesterolemic
Chelate certain transition metals	Spermicidal
Reactive amino/hydroxyl groups	Anticancerogenic

Bhatnagar and Sillanpaa (2009) reported the applications of chitin and chitosan derivatives for the removal of metal cations and anions, radionuclides, dyes, phenolic compounds, different types of anions and miscellaneous pollutants from wastewater. Batch studies were analysed for studying the various adsorption

mechanisms. The study showed that chitosan based adsorbent possesses high potential for detoxifying water and wastewater.

Babel and Kurniavans (2003) conducted a review on various low-cost adsorbents having high adsorption capacity like chitosan, zeolites, waste slurry and lignin for adsorption of heavy metals from wastewater. The heavy metals under study were mercury, lead and hexavalent chromium. The study showed that these adsorbents possess high adsorption capacity for heavy metal removal.

Novel chitosan-g-poly acrylic acid/attapulgite (CTS-g-PAA/APT) composites were prepared for use as adsorbents for removal of Cu(II) ions from aqueous solution (Wang *et al.*, 2009). Kinetic studies and equilibrium studies were conducted in the work besides analysing the effect of various parameters on adsorption efficiency.

Halloysite clay is a naturally occurring clay mineral and has similar composition as kaolin. It is a two-layered aluminosilicate ($\text{Al}_2\text{Si}_2\text{O}_5(\text{OH})_4 \cdot 2\text{H}_2\text{O}$) with a predominantly hollow nontubular structure and is a naturally available clay mineral. The structure of halloysite clay mineral is shown in Fig. 2.4.



Fig. 2.4 Structure of halloysite clay mineral

The outer surface of halloysite nanoclay has a structure like silicon dioxide while the inner surface is like that of aluminium oxide. Halloysite nanoclay is cheap and abundantly available and as a result they have got wide applications in wastewater treatment. Due to their size they will not form stable suspension in water even though they are hydrophilic (Cavallaro *et al.*, 2013; Pasbakhsh *et al.*, 2013). Besides their small size they possess remarkable properties such as biodegradability, large aspect ratio and high surface area to volume ratio. Negative SiO_2 is present outermost and positive Al_2O_3 is present in the inner lumen structure of halloysite and therefore it possess high adsorption capacity for most of the anions and cations (Zhao *et al.*, 2013). Halloysite nanoclay have found applications in polymer reinforcement and drug delivery due to their properties. HNT/chitosan hydrogels are proved to be good adsorbents for removing ammonium ions from aqueous solutions (Zheng and Wang, 2009). Properties of halloysite nanoclay is shown in Table 2.4.

Table 2.4 Halloysite attributes for its application as encapsulation vessel and load bearing constituent (De Silva *et al.*, 2013)

Use	As additives to polymers	As carriers and templates
Desirable Properties	Tubular	Tubular
	Good dispersion in polymers	Chemical Inertness/ biocompatibility
	Strong binding with polymers	Easy availability of OH groups
	High aspect ratio	Easy availability of OH groups
		Negatively charged at appropriate pH or (one) positively charged surface
Large volume in lumen		

Clays can be intercalated into polymeric network (Chen *et al.*, 2013). Polymer/clay composite possesses remarkable properties for being used as adsorbent for wastewater treatment. The properties of the composite include swelling properties, gel strength, low synthesis cost.

Chen *et al.* (2013) synthesised chitosan/montmorillonite magnetic microspheres and used for removal of Cr(VI) from synthetic wastewater. Effect of MMT weight %, initial Cr(VI) concentration, contact time, adsorbent dosage, temperature and pH on adsorption capacity were investigated. The adsorption was favourable at low pH. Equilibrium and kinetic studies were conducted using chitosan/MMT adsorbent. Adsorption data was fitted to pseudo second order kinetic equation and isotherm was described by Langmuir isotherm. Chitosan/clay/magnetite composite was synthesised for adsorption of Cu(II) and As(V) (Cho *et al.*, 2012). Cross linked chitosan and nanomagnetite were entrapped on heulandite to prepare a composite adsorbent. In the study, optimum mass ratio of the composite was determined. Kinetic and equilibrium studies were conducted for Cu(II) and As(V) removal using the prepared adsorbent. For the adsorption of methylene blue, the prepared chitosan/clay composite was used (Auta and Hameed, 2014).

CeO₂, TiO₂ and Fe₃O₄ nanoparticles were synthesised for the removal of lead from water (Sonia *et al.*, 2011). The toxicity of nanoparticles before and after adsorption were also assessed in the report. When nanoparticles of same size were compared, the best adsorption capacity was obtained for CeO₂. Iron oxide nanomaterials were synthesised using precipitation method (Steven *et al.*, 2012) and the synthesised particles were used for arsenic adsorption from water. In the study, batch experiments were conducted to determine the optimum pH of binding using a solution of constant initial concentration using 10 mg of nanoparticles. The optimum pH of binding was found to be 6.0.

Casareigo *et al.* (2009) synthesised chitosan/clay films by dispersion of chitosan in clay micro/nanoparticles. The changes in film properties with change in clay and chitosan concentrations were reported in the paper.

Chitosan/montmorillonite (CTS/MMT) nanocomposites were used for adsorption of Congo red (Wang and Wang, 2007). In the study a comparison was made between adsorption capacities of CTS, MMT and CTS/MMT in the molar ratio of 5:1. The results showed that the adsorption capacity was maximum for the nanocomposite than individual CTS and MMT. Miretzky and Cirelli (2009) conducted a review on Hg(II) removal using chitosan and chitosan derivatives. Guibal (2004) reported on interactions of metal ions with chitosan based sorbents. This is extremely useful in the use of chitosan for decontamination of effluents. The study shows that chitosan is very effective in wastewater treatment and its adsorption properties can be improved by surface modification.

Adsorption of Cr(VI) using chemically modified crosslinked chitosan was reported by Rojas *et al.* (2005). The influence of various parameters like pH, particle size, adsorbent weight, concentration and oxidation state of the metal on adsorption was studied by conducting batch tests. The optimum pH for adsorption was found to be 4.0. Equilibrium studies were also conducted in the above study.

Tirtom *et al.* (2012) conducted a comparative study of adsorption of Ni(II) and Cd(II) from aqueous solution using epichlorohydrin crosslinked chitosan/clay composite beads as adsorbent. Batch adsorption experiments were conducted to study the influence of pH, temperature, initial concentration and contact time on adsorption capacity. Desorption studies in the above study were also conducted using 0.01 M EDTA and 0.1 M HNO₃ at 25 °C. Kyzas *et al.* (2009) reported the

results of equilibrium and kinetic studies of Cu and Cr(VI) adsorption using chitosan derivatives. Chitosan was grafted and crosslinked with poly acrylamide and poly acrylic acid in the work and used for adsorption experiments. The results were compared with adsorption using chitosan.

Organic-inorganic hybrid of chitosan/organoclay bionanocomposites were used as adsorbents for Cr(VI) uptake (Pandey and Mishra, 2011). Optimum pH for adsorption was found to be 3.0 and all other batch studies including equilibrium and kinetic studies were conducted at this pH. Chitosan/clay films were prepared by dispersing clay particles in the film matrix and characterised by Casariego *et al.* (2009). The influences of various concentrations of clay and chitosan in the film was studied by analysing the tensile properties, water solubility, elongation etc in the study.

Wang *et al.* (2005) reported the synthesis and characterisation of biopolymer/ chitosan/montmorillonite nanocomposites. Nigerian kaolinite clay was used for simultaneous adsorption of Ni(II) and Mn(II) ions from aqueous solution (Dawodu and Akpomie, 2014). Factors affecting the adsorption of Mn(II) ions using polyvinyl alcohol/chitosan dry blend as adsorbent was presented (Abdeen *et al.*, 2015). Optimum pH for adsorption for Mn(II) removal was seen to be 6.0. De Silva *et al.* (2013) prepared chitosan/halloysite composite membranes and conducted the physico-chemical characterisation of the synthesised membranes. The films were prepared in the above study with different weight percentages of clay.

Optimisation, kinetics and thermodynamic studies of Cr(VI) adsorption on chitosan was conducted (Aydin and Aksoy, 2009). Effect of parameters like pH, adsorbent dosage and initial Cr(VI) concentration was studied on adsorption capacity. Equilibrium data was best fitted to Langmuir isotherm.

Nesic *et al.* (2012) reported the preparation of chitosan/montmorillonite membranes in various weight ratio and used as adsorbent for Bezactiv orange dye from wastewater.

2.6 Mechanism of Adsorption

The two common mechanisms of adsorption are physical adsorption and chemisorption. Physical adsorption is due to the presence of Van der Waals force of attraction. In physical adsorption, the individuality of adsorbent and adsorbate are preserved. Physical adsorption occurs at low temperature and adsorption decreases with increase in the temperature. It possesses low heat of adsorption and is reversible. In this type multimolecular layer is formed on the surface of the adsorbent.

Chemisorption takes place at high temperatures and is irreversible. Chemical bond forces hold the adsorbent and the adsorbate. Here sharing of electrons take place or the adsorbate molecules are broken to atoms or radicals during adsorption process. Unlike physical adsorption this is highly specific. This type of adsorption requires activation energy. In this type of adsorption monomolecular layer of adsorbate is commonly formed on the surface of the adsorbent. Kralik (2014) conducted a literature review on adsorption, chemisorption and catalysis. The work has been presented on adsorption giving special thrust to modeling. Analysis methods for the solution after chemisorption, isotherm and kinetics were reviewed detailed in the work. Maclver and Tobin (1960) reported the physical adsorption on the surface of adsorbent containing chemisorbed gas.

2.7 Factors Affecting Batch Adsorption

The factors that affect the batch adsorption are pH, contact time, initial concentration, adsorbent dosage, agitation speed, temperature and pressure. As

discussed in the section above, nature of the adsorbent is also an important factor that determines the adsorption efficiency and capacity. Numerous works have been done to study the effect of these parameters on the efficiency of adsorption. Batch experiments are conducted commonly in the laboratory in temperature controlled incubated shaker. The shaker contains an oscillating board and there are provisions for placing the beakers with the solution containing adsorbent and adsorbate. Batch tests have been conducted to study the influence of the factors that affect adsorption.

2.7.1 Effect of pH on Adsorption

Batch adsorption is governed by the pH of the solution. The adsorption capacity is influenced by the solution pH. The functional groups on the surface of the adsorbent is an important parameter that governs the adsorption of heavy metals. This parameter changes the charge on the adsorbent surface. The extent of dissociation of functional groups on the active sites of the adsorbent, degree of ionization, structural changes and conversion of the adsorbate are governed by the pH of the solution (Chen *et al.*, 2013; Auta and Hameed, 2014). Rai *et al.* (2016) reported the removal of Cr(VI) from aqueous solution using activated carbon prepared from mango kernel activated using H_3PO_4 . Batch experiments were conducted to study the effect of pH, carbon dosage, Cr(VI) concentration, rate of agitation, time and temperature. The results indicated that low pH was favourable for adsorption. At low pH Cr(VI) exists as negatively charged hydrogen chromate whereas at higher pH Cr(VI) exists as chromate and hydroxyl ions. Higher removal at low pH is due to strong electrostatic attraction between positively charged surface groups and negatively charged hydrogen chromate. At high pH there is competitive adsorption between chromate and hydroxyl radicals.

Ajmal *et al.* (2003) conducted batch adsorption studies using untreated and phosphate treated rice husk for adsorption of Ni(II), Zn(II), Cd(II) and Cr(VI). The effect of contact time, temperature, concentration, adsorbent dose and pH were analysed by conducting batch adsorption tests. Acidic pH of 2.0 was obtained as optimum pH for biosorption of Cr(VI) onto *Rhizopus Nigricans* (Bai and Abraham, 2001).

2.7.2 Effect of Contact Time

In batch adsorption processes, time of contact between the adsorbent and the adsorbate solution is an important parameter. Equilibrium time of adsorption is very much useful for the economics of the process. The adsorption efficiency first increases in most of the cases with increase in contact time. After a certain time, there will be no change in the adsorption efficiency. This means that adsorption has reached equilibrium. The amount of adsorbent at equilibrium is the maximum adsorption capacity.

Rai *et al.* (2016) reported that the removal of Cr(VI) using activated carbon prepared from mango kernel activated with H_3PO_4 first increased steeply up to 50 minutes, thereafter it was reduced and reached a constant value. At equilibrium, the rate of adsorption and desorption were equal. Further increase in contact time did not show any increase in adsorption rate.

Zhou *et al.* (2009) depicted that the removal of Cu^{2+} by chitosan coated magnetic nanoparticles modified with α -ketoglutaric acid showed a two-stage behaviour. Uptake of the heavy metal was high initially up to 180 minutes. As time progressed the removal decreased and finally equilibrium was attained. Initially due to low surface coverage, the metal ions occupied the active sites more rapidly. As time elapsed, due to increase in surface coverage, the

percentage removal decreased. Finally, the adsorbent was saturated at equilibrium and no removal took place with increase in the contact time.

2.7.3 Effect of Initial Concentration on Adsorption

Initial concentration is an important parameter affecting the adsorption efficiency. With increase in initial concentration the driving force for adsorption increases. The active sites are fixed, even though there is change in initial concentration. The driving force and fixed active sites act as opposing factors that determine the removal efficiency. With increase in initial adsorbate concentration, percentage removal of Cu^{2+} decreased since the active sites were not changing with initial concentration. The adsorbent used in the work by Zhou *et al.* (2009) was chitosan coated magnetic nanoparticles coated with α -ketoglutaric acid.

Chen *et al.* (2013) reported that when initial concentration of Cr(VI) solution was increased from 6-60 ppm, the adsorption capacity of CTS/50% MMT- Fe_3O_4 magnetic microspheres also increased from 9.97-38 mg/g. Auta and Hameed (2014) showed an increase in methylene blue (MB) uptake for increase in initial concentration when modified ball clay-chitosan (MBC-CH) was used as the adsorbent.

2.7.4 Effect of Adsorbent Dosage

When the adsorbent dosage increases, the adsorption efficiency also increases since there is increase in the active sites. After a certain dosage the increase in the removal is not significant if there is no change in the shaking speed. According to the paper presented by Pandey and Mishra (2011) initially the Cr(VI) removal increased with adsorbent dose. At the adsorbent dosage of 50 mg, maximum removal was attained and further significant change in the

removal was not observed. Organic-inorganic hybrid of chitosan/organoclay bionanocomposites was the adsorbent used in the work.

Wang and Chen (2006) presented a review on the use of *Saccharomyces cerevisiae* for the biosorption of heavy metals from wastewater. The metal binding capacities of different metals on the surface of the bioadsorbent were compared. The study showed that the removal efficiency showed considerable dependence on the initial biomass concentration.

2.7.5 Effect of Agitation Speed

Agitation speed increases the removal efficiency of adsorption. A comparison was made between agitation using laboratory shaker, mechanical agitator, magnetic stirrer and agitation by mixing with gas bubbles for 4-chlorophenol adsorption onto granular activated carbon (Krzysztof and Swiatkowski, 2015). Mechanical and magnetic stirrers possessed more adsorption efficiency than a laboratory shaker at the same shaking speed.

Ihsanullah *et al.* (2016) used surface modified activated carbon and carbon nanotubes for Cr(VI) removal from aqueous solutions. Batch experiments were conducted to study the effect of adsorbent dosage, pH, agitation speed and contact time on the removal efficiency of Cr(VI). Maximum removal efficiency was obtained at 200 rpm.

2.7.6 Effect of Temperature and Pressure

Adsorption decreases with increase in temperature generally and pressure has marked influence on the adsorption of gases. For gases, adsorption increases with pressure and decrease in pressure causes desorption.

Vashchenko *et al.* (1993) reported the effect of pressure and temperature on the adsorption equilibrium of hydrogen and neon using zeolite

NaA as the adsorbent. Optimum conditions for separation of a binary mixture of hydrogen and neon was determined in the study. At low temperature hydrogen adsorption was predominant and as pressure increased, the adsorption of hydrogen and neon increased if pressure was more than 10 kPa.

2.8 Adsorption Isotherm

The retention or release of a substance from an aqueous solution to a solid phase at constant temperature and pH is described best by adsorption isotherm. When the concentration of adsorbate in the bulk solution is in a dynamic balance with the interface concentration between solution and adsorbent, then it is called adsorption equilibrium. Adsorption equilibrium is defined as the ratio of the amount of adsorbate in the adsorbent to that in the bulk solution. Mathematical correlations are used to model adsorption isotherm of a system. A study on modeling of adsorption isotherm systems was reported in Foo and Hameed (2010). By conducting isotherm study of a system, mechanism of adsorption can be explained. Isotherm study gives an insight into the surface properties and the degree of affinity of the adsorbents. Langmuir model, Freundlich model and D-R model are commonly used to describe the adsorption of solids from aqueous solution to the specific adsorbent.

2.8.1 Langmuir Isotherm

This model was developed by Irving Langmuir in 1916 for adsorption. This is a two-parameter model and this is applicable for describing the equilibrium data for many adsorbent-adsorbate systems. According to Langmuir's postulate when an adsorbent has certain sites to which certain specific adsorbate can stick, it can be either by physisorption or by chemisorption. According to Langmuir's theory the adsorbate molecules that are bound to the adsorbent will not exceed one molecule in thickness.

Langmuir postulated his theory for monomolecular layer of adsorption. According to his theory, the surface on which adsorption takes place should be homogeneous. All the adsorbent sites are equivalent. The site possesses only monolayer coverage. According to Langmuir's theory, the interaction between adsorbed molecules adjacent to each other is considered negligible. Each adsorbent molecule possesses constant enthalpy and constant sorption activation energy. A dimensionless separation factor R_L is defined by Langmuir. It indicates whether the adsorption is favourable or not. Value of $R_L < 1$ indicates that adsorption is favourable and $R_L > 1$ indicates unfavourable adsorption. It is calculated using the equation given below.

$$R_L = \frac{1}{1 + bC_0} \quad (2.1)$$

where b is the Langmuir constant in L/mg and C_0 is the initial adsorbate concentration in mg/L (Pandey and Mishra, 2011).

Numerous studies have been conducted previously for fitting the data of adsorption to Langmuir model. In Yuan *et al.* (2009), adsorption of Cr(VI) on diatomite supported/unsupported magnetite nanoparticles followed Langmuir model. The adsorption coefficients computed using Langmuir equation showed that the equilibrium data fitted well with the model. The binding of arsenic (III) and arsenic (V) on the surface of iron oxide nanomaterials followed Langmuir isotherm model (Steven *et al.*, 2012). This indicated that the adsorption was monolayer on the surface of iron oxide nanomaterials. The adsorption of Cu(II) and As(V) on chitosan/clay/magnetite composite was favourable according to Langmuir model as described in Cho *et al.* (2012). Equilibrium data from batch studies for sorption of cadmium from aqueous solution using pre-treated rice husk as the

adsorbent fitted more to Langmuir Model than Freundlich isotherm model (Kumar and Bandyopadhyay, 2006).

The adsorption of basic dye Astrazon Blue FGRL onto sepiolite, fly ash and apricot stone activated carbon was reported by Karagozoglu *et al.* (2007). The batch studies were performed by varying the initial concentration, adsorbent dose and temperature. The equilibrium data was then fitted to the Langmuir model. Langmuir isotherm provided the best correlation for Cr(VI) adsorption onto hazelnut shell activated carbon (Koby, 2004).

2.8.2 Freundlich Isotherm

Freundlich adsorption isotherm describes the relationship between the concentration of the solute in the adsorbent surface to that in the liquid. This was developed in 1909 by Herbert Freundlich. In this model the concept of monolayer adsorption is not required. This model describes multilayer adsorption over a heterogeneous surface (Foo and Hameed, 2010). According to Freundlich model, the amount adsorbed is the total of solute adsorbed on all active sites. Each active site possesses bond energy and the sites having stronger bond energy are occupied first by the solute according to this model. Freundlich model is applicable for organic compounds and adsorption on activated carbon. The slope of $\ln q_e$ vs $\ln C_e$ is a measure of the adsorption intensity, where C_e represents the equilibrium concentration of the solution in ppm, q_e is the adsorption capacity in mg/g at equilibrium. When the slope is considerably less than unity, then it is an indication of chemisorption. When the slope is steeper than unity, it means cooperative adsorption. One of the limitations of Freundlich isotherm is that it does not approach Henry's law at low concentrations (Zhou *et al.*, 2009).

The adsorption of methylene blue on activated carbon prepared from bamboo dust, coconut shell, ground nut shell, rice husk and straw were modeled by Freundlich and Langmuir isotherm (Kannan and Sundaram, 2001). Linear relations were obtained at 95% confidence level with R^2 values close to unity in the above study. Comparative study was conducted using the different adsorbents for removal of methylene blue.

A comparative study was conducted by Mukherjee *et al.* (2007) for adsorption of phenol from water environment using activated carbon, bagasse ash and wood charcoal. For all the three adsorbents, Freundlich model fitted well with the equilibrium data. Isotherm studies were conducted in the above work for constant initial adsorbate concentration with varying adsorbent dosage and for constant adsorbent dosage with varying initial adsorbate concentration. K_f and $1/n$ values were obtained. K_f indicates adsorption capacity and n , the intensity of adsorbent and these two are called Freundlich constants. Higher K_f indicates that the adsorption is more favourable.

Equilibrium isotherm data for adsorption of arsenic on iron oxide coated cement was analysed using Langmuir, Freundlich, Dubinin - Radushkevich (D - R) and Toth and Temkin isotherm models (Kundu and Gupta, 2006). In the work equilibrium of arsenic(III and V) was examined at 288, 298 and 308 K. Six error analysis methods were adopted for determining the best fit of isotherm data. The methods used in the study of arsenic removal were linear coefficient of determination, sum of the squares of errors, sum of absolute errors, the average relative error, the hybrid fractional error function and Marquardt's percent standard deviation in the study for arsenic removal. The error values indicated that the adsorption of As(III and V) fitted best to Freundlich model at all the temperatures in the study.

2.8.3 Dubinin - Radushkevich (D - R) Isotherm

D - R model is used to overcome the limitation of Langmuir and Freundlich models. Physical and chemical characteristics of adsorption are not explained by Langmuir and Freundlich models. This model can explain the physical and chemical properties of adsorption by determining the mean free energy (E) per molecule of adsorbate. The mean free energy E is defined as the energy required for removing a molecule in the sorption space to infinity and is computed using the equation,

$$E = \frac{1}{\sqrt{2B_{DR}}} \quad (2.2)$$

where B_{DR} is the isotherm constant. It is related to adsorption energy. D-R Isotherm is given by

$$q_e = q_m \exp(-B_{DR} (RT \ln(1 + \frac{1}{C_e}))^2) \quad (2.3)$$

$$\ln q_e = \ln q_m - B_{DR} e^2 \quad (2.4)$$

$$e = RT \ln(1 + \frac{1}{C_e}) \quad (2.5)$$

where q_e represents the adsorption capacity at equilibrium in mg/g, C_e is the equilibrium concentration in ppm, q_m represents the maximum adsorption capacity in mg/g. Inyinbor *et al.* (2016) fitted the equilibrium adsorption data of Rhodamine B dye onto Raphia Hookerie fruit epicarp to isotherm models namely, Langmuir, Freundlich, D - R and Temkin models. The adsorption energy (E) obtained was 6.11 kJ/mole indicating that physisorption was the adsorption mechanism. Freundlich adsorption was best fitted to the experimental data

indicating that the adsorption was multilayer and not to a uniform site. Monolayer adsorption also played an important role in the adsorption of Rhodamine B dye using *Raphia Hookeri* fruit epicarp adsorbent.

2.9 Adsorption Kinetics

The study of rates of chemical process and the factors that govern the attainment of equilibrium in a specified time is given by the chemical kinetics. For testing the controlling mechanism of adsorption three models are commonly used, namely, Lagergren pseudo first order, second order, pseudo second order and intraparticle diffusion model. The pseudo first order kinetics are mostly applicable for the initial stage of adsorption process. In the final stages this may not be applicable for most of the adsorption processes. If the adsorption follows pseudo second order kinetics, then the mechanism is chemisorption. Chemisorption involves the exchange of electrons between the adsorbent and the adsorbate. While using pseudo second order kinetics the errors generated from experiments are minimized. Pseudo second order rate expression is widely used for the adsorption of pollutants from aqueous solution (Ho, 2006). When the intra particle diffusion controls the overall rate, then the kinetics can be expressed in terms of intra particle diffusion model. Adsorption of a solute on the surface of an adsorbent is divided into the following steps. In the first step, called the external diffusion, the solute is transferred from the bulk solution to the boundary film surrounding the adsorbent. Then the solute is transported through the film to the surface of the adsorbent. This is termed as film diffusion. In the third step called pore diffusion, the solute from the adsorbent surface diffuses to the active sites of the adsorbent. In the fourth step the adsorbent interacts with the active site of the adsorbent. The slowest step determines the overall rate of the process.

Largitte and Pasquier (2016) reported the use of activated carbon from coconut shell for the adsorptive removal of lead from aqueous solution. Ten kinetic models were tested to analyse the adsorption. The kinetic data of adsorption fitted best to Elovich model. Linear and nonlinear regression analysis was carried out for representing the kinetics of adsorption of methylene blue using activated carbon as adsorbent (Vasanth Kumar, 2006). In the study the adsorption of methylene blue was represented by pseudo first order and pseudo second order kinetics. For verifying the kinetics of adsorption, non-linear model was more appropriate than linear model.

Gordon *et al.* (1987) reported the kinetics of adsorption of dye stuffs using intraparticle diffusion model. Sorption kinetics of Cr(VI) to the surface of chitosan/organoclay bio nanocomposites was analysed by pseudo second and second order rate equations (Pandey and Mishra, 2011). The kinetic data of adsorption fitted more to pseudo second order kinetic model.

Azizian (2004) explored theoretically the kinetics of adsorption of a solute from a solution to the surface of the adsorbent. The results indicated that at high initial concentration, the kinetics followed a pseudo first order model and at low initial concentration of the solute, a pseudo second order model.

2.10 Adsorption Thermodynamics

Thermodynamic studies help to understand about the adsorption equilibrium. The isotherm studies form the basis of thermodynamic calculations. Thermodynamic analysis is used to determine the mechanism of adsorption. It helps to determine the adsorption equilibrium constant (K), Gibbs free energy change (ΔG), enthalpy change (ΔH) and entropy change (ΔS). The positive values of ΔG indicate that the reaction is not thermodynamically feasible. The negative values of ΔG indicate the thermodynamic spontaneity and favourability

of the process. The positive values of ΔH is a representation of endothermic process and vice versa. Positive values of ΔS indicate increased disorder at the adsorbent-adsorbate solution interface during the fixation of adsorbate to the active site of the adsorbent (Cho *et al.*, 2012).

The enthalpy of adsorption and adsorption equilibrium constant for the adsorption of methylene blue on activated carbon were studied (Ghasemi and Asadpour, 2007). The effect of various parameters like temperature and ionic strength on the adsorption thermodynamics were investigated in the study.

Chowdhury *et al.* (2011) used Arrhenius and Eyring equations to determine the activation energy, enthalpy, entropy and free energy of the adsorption of malachite green using chemically modified rice husk as adsorbent. The results of the thermodynamic study indicated that the adsorption of malachite green to the surface of chemically modified rice husk was spontaneous and endothermic in nature.

2.11 Response Surface Methodology

Response surface methodology is a collection of statistical and mathematical models that are helpful in modeling any engineering problems (Aslan and Cebeci, 2007). For optimisation of three or more variables, RSM is an efficient tool. The first step in RSM is to design a set of experiments by specifying the process parameters that affect the system. Experiments are performed according to the experimental runs suggested by RSM. Then the model equation is developed by RSM. Then optimum values of process parameters that maximizes or minimizes the response are determined in the third and final step.

Box-Behnken design demands only limited number of experimental runs for the optimisation of a process. Model equation is developed in the

Box-Behnken design which relates the variable of interest which is to be optimised with the various parameters that affect the process. Response surface methodology gives the interaction between various variables that affect a process and gives the shape of the response surface. Contour and surface plots of RSM, give the pictorial representation of the interaction between various parameters that affects a process.

Biosorption of cadmium by *Saccharomyces cerevisiae* was optimised using central composite design of RSM (Ghorbani *et al.*, 2008). Twenty experimental runs were performed by varying three variables namely, pH, initial cadmium ion concentration and *Saccharomyces cerevisiae* dosage. A second order polynomial equation was developed by RSM to fit the experimental data in the work.

Box-Behnken design of RSM was used to optimise the processing parameters and nanoclay content in the preparation of nanocomposites using polypropylene (PP)/high density poly-ethylene (PE) blend and nanokaolinite clay (Anjana *et al.*, 2014).

Aslan and Cebeci (2007) applied Box-Behnken design for modeling some Turkish coals. The bond work index, grinding time and ball diameter of the mill were the variables under the study. The optimal operating point for maximum biodegradability of pulp and paper industry wastewater by electrochemical pre-treatment was determined using RSM (Soloman *et al.*, 2009).

Waste tea activated carbon (WTAC) was produced under optimised conditions of activation temperature, activation time and chemical impregnation ratio (IR) with percentage removal and percentage yield as targeted responses under RSM. WTAC was used for adsorptive removal of both anionic and cationic dyes from aqueous solutions. Optimised activation

temperature obtained from RSM was 800 °C. IR was 1.4 and activation time was 120 minutes (Auta and Hameed, 2011).

2.12 Desorption

Desorption is a phenomenon in which the adsorbed constituent is released from the surface of the adsorbent by using suitable eluents. Desorption is the reverse of adsorption. Desorption is used to regenerate the adsorbent after adsorption. After adsorption, the adsorbent is saturated with the adsorbate and no further adsorption takes place. Replacement with fresh adsorbent is expensive and hence suitable solvents are selected that are used to elute the adsorbate from the surface of the adsorbent. Thus the adsorbent can be reused. The removal efficiency decreases with increase in the adsorption-desorption cycle.

Yuan *et al.* (2009) used 0.01 M NaOH solution for 24 h for desorption of Cr(VI) using diatomite-supported/unsupported magnetite nanoparticles. The adsorption-desorption processes underwent three cycles. After three cycles, most of the Cr(VI) were attached to the active sites permanently. After the first cycle of elution/adsorption, some of the Cr(VI) ions adsorbed by electrostatic attraction were freed from the adsorption sites of both the adsorbents. But after three cycles of elution/adsorption most of the Cr species were fixed to the surface of adsorbents through redox and isomorphic substitution.

Zhou *et al.* (2009) presented the desorption study of copper loaded chitosan coated magnetic nanoparticles coated with α -ketoglutaric acid using Na₂EDTA, acetum solution, HCl and citric acid of various strengths. Na₂EDTA proved to be the best solvent with maximum desorption efficiency. In the work, optimum conditions were determined for adsorption-desorption experiments.

2.13 Characterisation of Adsorbents

The structure and morphology of adsorbents are usually analysed using SEM and XRD. SEM uses a focussed beam of electrons for scanning the surface and produces images of the sample. The interaction of the electron beam with the sample surface generates secondary, back scattered and auger electrons and, at times light. These are collected by detectors in the specimen chamber. Scanning is carried out in different magnification ranges to analyse the morphology of the sample surface. SEM can provide information regarding surface topography, crystalline structure, chemical composition and electrical behaviour of the surface of the sample (Vernon - Parry, 2000).

XRD is used to analyse the atomic or molecular structure of a crystal. The physical properties, crystal structure and chemical composition of sample is measured by X-ray scattering techniques. When the X-ray beam hits a surface, it is scattered, and this scattered intensity is correlated with the properties of the material under study. The average particle size of the sample is also determined from the peaks obtained from the XRD pattern. The peaks are compared with the standard data for analysing the sample.

Energy dispersive X-ray spectroscopy is used for the composition analysis of compounds. X-rays excited from the device interact with the sample and the electromagnetic emission spectrum from the sample is analysed for determining the chemical composition. When a specimen is excited, an electron from its inner shell (low energy) will be excited and move towards the outer shell creating an electron hole. To fill the electron hole, an electron from the outer shell (high energy) will replace its position which will cause the emission of X-rays from the sample. This is measured using an energy dispersive spectrometer.

FTIR spectroscopy is used for analysis of functional groups present in the sample. FTIR is mainly used to identify organic compounds by comparing the functional groups obtained from FTIR spectrum with that of the standard IR data. It can be operated in a wide spectral range for obtaining the infrared spectrum of absorption or emission of a solid, liquid or a gas. It measures how well the sample absorbs the infrared beam of light which in turn is a measure of the functional groups present in the specimen.

FTIR spectroscopy uses infrared light energy by vibrational excitation of molecular bonds. Infrared beam is absorbed by the sample during characterisation. FTIR was used for the identification of yeast collected from human and animals. Potassium bromide based pellets were prepared for sample analysis in the study. Pure potassium bromide was used as blank. The spectra ranging from wave numbers 4000-400 cm^{-1} were recorded using FTIR (Jasco FTIR 6100 Japan) (Taha *et al.*, 2013).

Thermogravimetric analyser measures the change in the properties of a sample with increase in temperature or with change in time isothermally. The test is commonly performed in a nitrogen atmosphere at a constant rate of heating. TGA can provide information of both physical and chemical phenomena regarding the sample. The gain or loss of weight of the specimen with temperature change is determined using TGA. TGA gives information regarding the thermal stability of the substance. TGA is used for material characterisation, degradation mechanisms of the specimen, organic matter determination and inorganic constituent determination. Now-a-days TGA has vast application in polymer technology.

Tensile and compressive strength of materials are tested using universal testing machine. De Silva *et al.* (2013) reported the physico-chemical

characterisation of chitosan/halloysite composite membranes for various weight percentages of halloysite nanotubes. Tensile properties of the composite were obtained from stress-strain curves in the study.

Digital micrometer is incorporated with a calibrated screw gauge. It is also called as a micrometer screw gauge and is used for precise measurement of a specific sample. It carries a spindle and an anvil. The object to be measured is placed between the accurately machined screw and the anvil.

Cavallaro *et al.* (2013) synthesised novel gel beads formed by alginate biopolymer and halloysite nanotubes. The synthesised gel beads were characterised using thermogravimetric analyser, scanning electron microscope and dielectric spectroscopy. Thermogravimetric analysis in the study was used to determine the local composition of halloysite nanotube into the gel beads. SEM image showed that the gel possessed rough surface and pore size was in the micrometer range.

Zinc oxide nanoparticles were synthesised from zinc sulphate and sodium hydroxide using precipitation method (Surabhi *et al.*, 2013). The synthesised particles were characterised using SEM, XRD, EDX and PIXE. Morphological changes of ZnO was studied using SEM. The average crystallite sizes of synthesised particles were determined from the XRD peaks by using Deybe-Scherrer's equation. Composition of synthesised nanoparticles was determined using EDX. PIXE was used for trace elemental analysis of ZnO nanoparticles.

Wilson *et al.* (2014) reported the use of TEM, XRD and magnetometry (VSM) for the characterisation of magnetite and maghemite nanoparticles synthesised using coprecipitation method. JEOL transmission electron microscope, Model 1011 (JEOL, Tokyo, Japan), operated at 110 KV, was used

for testing the nanostructure morphology of synthesised nanoparticles. For crystallographic analysis of magnetite and maghemite, Shimadzu XRD 6000 diffractometer was used. Vibrating sample magnetometer (Lake Shore Model 7300) was used to determine magnetic properties of the sample in the study.

Magnetic hydroxyapatite (HAP) was synthesised from superparamagnetic Fe_3O_4 nanoparticles and HAP (Xianxiang, 2011). The synthesised magnetic materials were characterised by SEM, XRD, FTIR, VSM and N_2 adsorption. The structure and morphology were analysed using SEM, crystal structure was determined using XRD and functional group analysis was carried out in FTIR. The magnetic properties of synthesised materials were determined using VSM.

Lewandowska *et al.* (2014) depicted characterisation of chitosan with various clays. Chitosan/montmorillonite nanocomposite films were synthesised in the study. Nanoclay, both with and without surface modification, was used to form chitosan/nanoclay composite. Three different types of nanoclay after surface modification was used in the work. The morphology of nanocomposite films was analysed using SEM (Leo electron microscopy Ltd, England) at different magnifications. Topographic imaging was performed using a multimode scanning probe with a nanoscope IIIa controller (Digital instruments, Santa Barbara, CA) operating in a tapping mode in air at room temperature. Thermal analysis of the nanoclay/chitosan films were compared using TGA-DTA analyser of TA instruments in the temperature range of 20-650 °C in nitrogen atmosphere. Mechanical properties were measured using tensile tests (Zwick and Roell) at room temperature at a crosshead speed of 5 mm/min in accordance with Polish Norm PN 81/C-8903 4 (ISO527-1 I 527-2).

2.14 Analytical Method

UV-VIS spectrophotometer was used for the analysis of Cr(VI) in the wastewater. UV-VIS spectrophotometer is an absorption spectrophotometer that works in the ultraviolet-visible spectral region. It measures the electronic transitions of atoms and molecules from the ground state to the excited state upon absorption of light in the UV-visible region. This electronic transition of atoms and molecules is a function of the composition of the sample solution. A blank is also used which does not contain the sample. For analysis of Cr(VI) in wastewater, the wastewater after proper dilution is used as the sample. Diphenyl carbazide is used as the indicator and blank is pure water after adding diphenyl carbazide. Analysis of Cr(VI) in UV-VIS spectrophotometer is carried out at 540 nm.

The working of UV-VIS spectrophotometer is based on Beer-Lambert's law which states that the absorbance is directly proportional to concentration of absorbing species and the path length. In this device absorbance is measured which is related to the concentration of the substance under consideration.

Chen *et al.* (2013) used UV-VIS spectrophotometer at 540 nm for the analysis of Cr(VI) in water after adsorption using chitosan/montmorillonite magnetic microspheres. Batch adsorption experiments were performed varying the parameters like pH, time interval, adsorbent dosage, initial concentration and montmorillonite content. After each batch experiment the amount of Cr(VI) remaining in water is tested in spectrophotometer using diphenyl carbazide as the indicator.

The Cr(VI) remaining in water after adsorption using chitosan/organoclay bionanocomposites was measured using UV-VIS spectrophotometer (Pandey and Mishra, 2011).

Shimadzu UV-260 spectrophotometer was used for the analysis of Cr(VI) in aqueous solution after adsorption by diatomite-supported/unsupported magnetite nanoparticles (Yuan *et al.*, 2009). Batch adsorption tests were performed to study the effect of different parameters that affects the Cr(VI) removal and after adsorption the solution was filtered using 0.2 microns cellulose acetate syringe filters and residual concentration was measured in a spectrophotometer.

2.15 Continuous Removal in Packed Bed Adsorption Column

Batch studies will provide elementary information regarding the factors affecting the adsorption. Batch adsorption is applicable for a single contact time and requires large quantity of adsorbent for a given volume of solution. So it is not economic for higher capacity operations (Lim and Aris, 2014). In column operation, the removal of pollutants is achieved continuously and is also favourable from an economic point of view. More control of the process is achieved in continuous operations. The adsorption column can be developed for the treatment of both organic and inorganic pollutants. Attempts must be made for the application of adsorption column to tackle wastewater problems in the commercial level of operations (Imran, 2014).

The time for breakthrough appearance and the shape of breakthrough curve were influenced by various column parameters like initial concentration of the feed solution, bed height, flow rate and pH. Various studies have been conducted previously by conducting continuous experiments in a packed bed adsorption column for removal of toxic heavy metals in wastewater and analysing the factors that influence the column operation.

Heymes *et al.* (2006) conducted a study on hydrodynamics and mass transfer in a packed bed absorption column for removal of toluene from vent

gas using di 2-ethyl hexyl adipate (DEHA). Lim and Aris (2014) modeled an adsorption column for removal of Cd(II) and Pb(II) ions in aqueous solution using dead calcareous ions as adsorbent. The study showed that when bed height was increased, the column exhaustion time also increased, causing an increase in the life span of the column. A continuous bio filter was used for the removal of Cr(VI). In the above work central composite design of RSM was used to design the experiments (Dalcin *et al.*, 2011).

Malkoc and Nuhoglu (2006a) reported the fixed bed study for removal of Cr(VI) from tea factory waste. The effect of liquid flow rate, initial Cr(VI) concentration, pH and bed depth were studied in the above work. Thomas model was applied to the column data in the work. Batch and fixed bed studies were conducted for the removal of methylene blue from aqueous solution using chitosan-clay composite (Auta and Hameed, 2014). Also, comparison was made between modified ball clay (MBC) and chitosan composite (MB-CH) for removal of methylene blue. Adam Bohart model (A-B) and Yoon Nelson model were compared and it was found that the experimental data fitted to A-B model than Yoon Nelson model. MB-CH showed higher desorption efficiency than MBC after 5 regeneration cycles.

Jain *et al.* (2013) conducted adsorption and desorption experiments in fixed bed column for removal of Cd(II) using sunflower waste carbon calcium alginate beads as adsorbent. Bed height, initial Cd(II) concentration and flow rate were the parameters for study. Natural zeolite was packed in the column for removal of lead from aqueous solution by conducting adsorption-desorption experiments (Medvidovic *et al.*, 2006). Kinetic studies were conducted for adsorption of elemental mercury in activated carbon fixed bed reactor (Skodras *et al.*, 2008).

Mohan and Sreelakshmy (2008) reported that low cost raw rice husk and phosphate treated rice husk were used in removing heavy metals like lead, copper, zinc and manganese. The effect of different bed depths on the performance of the column was examined.

Simultaneous biosorption of two different constituents can be carried out in a single packed bed column. Binary biosorption of phenol and Cr(VI) was carried out in a packed bed adsorption column using immobilized activated sludge as the adsorbent (Aksu and Gonen, 2006). The column adsorption capacity was higher for Cr(VI) than for phenol.

Different bioreactors were used for simultaneous Cr(VI) and COD removal from aqueous solution using *Arthrobacter rhombi* RE (MTCC 7048). Aerobic suspended growth system, aerobic attached growth system and anoxic attached growth system were used (Elangovan and Philip, 2009).

2.15.1 Factors Affecting Breakthrough Curves

Break through curve is an indication of the relationship between (C_f/C_0) and time, where C_f is the outlet concentration of solute and C_0 is the inlet solute concentration. It is usually a S shaped curve. The breakthrough point is a point in the breakthrough curve at which the concentration of the adsorbate in the aqueous solution reaches its maximum allowable value. When the concentration of the adsorbate reaches 95% its initial value, the bed is said to be saturated and no further adsorption is possible. At this point the bed needs regeneration or is to be replaced (Medvidovic *et al.*, 2006).

The height of the bed, flow rate through the bed, initial concentration, pH of the influent solution and variation of adsorbent particle sizes are the important parameters that affect the performance of the packed adsorption tower. Column experiments for the removal of lead from aqueous solution

using fixed bed of natural zeolite-clinoptilolite in two beds with variation in adsorbent particle size were performed (Medvidovic *et al.*, 2006). The first bed was of 0.6-0.8 mm zeolite particle size and the second bed contained zeolite adsorbent of 0.1-0.5 mm particle size. When the bed was saturated, the regeneration was conducted by using sodium nitrate as the eluent. In the work, only after the first cycle, the breakthrough curve showed an S shape for both the particle sizes. The time to attain breakthrough point was increased in the second cycle after regeneration for both the particle sizes when the bed was operated at constant initial concentration, pH and bed height. The effect of initial concentration was studied at particle size 0.6-0.8 mm at constant flow rate. The results indicated that when the initial lead concentration was increased, the breakthrough point was attained earlier. When the flow rate was increased for the lead bed, the column was saturated earlier.

Jain *et al.* (2013) reported the fabrication of a fixed bed column of internal diameter 2.5 cm and length 60 cm using sunflower waste carbon-calcium alginate beads for cadmium(II) removal. Continuous experiments were conducted to determine the effect of bed height and initial concentration on the bed adsorption capacity. The results indicated that with increase in bed height the saturation of the column was slowed down when the experiments were conducted by keeping all other parameters constant. Study of Cd(II) column performance showed that at low initial concentration, the breakthrough curves occurred late.

Goel *et al.* (2005) reported a comparative study between batch and continuous removal of lead using treated and untreated granular activated carbon. In the packed column for lead the effect of bed height, hydraulic loading rate and initial feed concentration on breakthrough curves were analysed. The regeneration study was conducted in the work using HNO₃.

The effect of liquid flow rate, initial feed concentration, particle size, solution pH and bed depth on breakthrough data and column adsorption capacity was examined (Malkoc and Nuhoglu, 2006a) for Cr(VI) removal on fixed bed column using tea factory waste as the packing material. The bed capacity was inversely proportional to particle size and flow rate. When the flow rate was less the loading kinetics of the waste tea was slow and long residence time was needed for attaining the equilibrium. The adsorption capacity was found to increase when the initial concentration was increased from 50 to 200 mg/L. At high initial concentration, the adsorbent bed got saturated quickly and hence breakthrough curve shifted towards the left. From the column experimental data obtained from the work, the longest breakthrough time was observed for low pH. pH is an important factor that determines the physico chemical interaction of the ions in the adsorbate solution with that of the active sites of the adsorbent. At low pH the Cr(VI) solution exists in acid chromate form HCrO_4^- and as pH increases the Cr(VI) solution exists as CrO_4^{2-} and $\text{Cr}_2\text{O}_7^{2-}$. With increase in pH, the surface of the adsorbent acquires an overall negative charge and hence adsorption capacity decreases.

From the results obtained by Malkoc and Nuhoglu (2006a), increase in bed height was required for high adsorption capacity and longest breakthrough time. At low bed depth axial dispersion of the adsorbate is more predominant than diffusion into the adsorbent active site. At low bed height, therefore bed was saturated early. With increase in the bed height more volume of solution could be treated since fixation to the active sites is increased with bed height. At larger bed depth, the adsorbent dosage was increased which indicates that greater surface area for adsorption is obtained showing delayed breakthrough curve. The removal of Ni(II) ions from aqueous solution using tea factory waste in fixed bed column was reported by Malkoc and Nuhoglu (2006b).

Bamboo based granular activated carbon was used in fixed bed column for adsorptive removal of C.I. Reactive black (RB5). Experiments were conducted by varying the initial concentration, bed height and flow rate. Maximum bed adsorption capacity was obtained for longest bed height and minimum flow rate. The maximum bed adsorption capacity of 39.02 mg/g was reported for initial dye concentration of 100 mg/L (Ahmad and Hameed, 2010).

Ahamad *et al.* (2010) reported the removal of chromium from industrial wastewater using ChromeBac™ system. Polyaniline synthesised on the surface of jute fibre (PANI-Jute) was packed in continuous column for removal of Cr(VI). With increase in bed depth from 40-60 cm, the Cr(VI) uptake increased from 4.14-4.66 mg/g. The optimum pH for removal was 3.0 (Kumar and Chakraborty, 2009).

The effect of parameters like bed depth, flow rate, influent concentration, influent solution pH was analysed on the performance of packed bed column for Cr(VI) removal using modified corn stalk as the packing adsorbent material. With increase in bed depth, more volume of effluent could be treated in the Cr(VI) column. The exhaustion time increased with decrease of flow rate and decrease of inlet Cr(VI) concentration (Chen *et al.*, 2012).

2.15.2 Mathematical Models of Packed Column

The influence of various parameters and breakthrough performance of the adsorption column were described by mathematical models of the column data. In modeling, first, the model parameters are estimated, and the experimental data are fitted to the various model equations. Thomas model, Yoon Nelson model and Adam Bohart model are used commonly by various researchers to model the experimental column data.

Adam Bohart, Thomas, Clark and Yoon Nelson model were applied to fit the equilibrium column data of biosorption of phenol by immobilized activated sludge in a continuous packed bed column (Aksu and Gonen, 2004). Flow rate and initial phenol concentration were varied to model column and it was found that all models fitted to the column data.

Thomas model is simple and reasonably accurate in predicting the performance of the column. Yoon Nelson model requires only less column data for prediction of breakthrough curves and is mostly applicable for single component systems (Lim and Aris, 2014). Adam Bohart model is applicable only for the initial part of the breakthrough curve.

Malkoc and Nuhoglu (2006a) checked the applicability of Thomas model for adsorption of Cr(VI) onto tea factory waste in a packed column. In the work, Thomas model fitted the experimental data well and the deviation between experimental and predicted breakthrough curves was very less.

Lim and Aris (2014) applied Thomas model, Yoon Nelson model and Adam Bohart model to the experimental column data for adsorption of Cd(II) and Pb(II) using dead calcareous skeletons. The value of correlation coefficients indicated that Thomas model fitted better to Cd(II) column than to Pb(II) column. Yoon Nelson model was applicable for both the columns. Adam Bohart model assessed the saturation state of the column performance.

Chu (2004) developed new mathematical models derived from the existing models for breakthrough curves for heavy metal biosorption in fixed bed column. The models provided fast and accurate analysis of the breakthrough curves using the experimental column data.

Lua and Jia (2009) used activated carbon obtained from oil palm shells for phenol adsorption in a fixed bed column. Linear driving force model based on the

particle phase concentration difference (LDFQ) was used to simulate the column data. The model equation obtained was found to be in well agreement with the experimental column data.

Suskabye *et al.* (2008) reported the removal of Cr(VI) from electroplating wastewater in a fixed bed column. The effect of bed depth and flow rate was investigated in the work. It was shown that the Bed Depth Service Time Model (BDST) fitted well with the experimental data for the initial part of the breakthrough curve. Thomas model was used for the simulation of the whole breakthrough curve using non-linear regression analysis.

Sag and Aktay (2001) used a packed column reactor for the dynamic removal of Cr(VI) by chitin flakes. The effect of flow rate, bed depth, particle size and initial Cr(VI) concentration on the column performance was analysed in the study. The applicability of Adam-Bohart model, Wolborska Model and Clark Model was investigated in the work.

Vijayaraghavan *et al.* (2004) used a crab shell packed up flow adsorption column of internal diameter 2 cm, for removal of nickel(II) ions from aqueous solution. The effect of bed height and flow rate on breakthrough curves was investigated. The Bed Depth Service Time Model (BDST) was used to describe the performance of the column.

2.16 Summary

This chapter contains a detailed literature review on the sources of hexavalent chromium in aqueous solution, impacts of chromium on all forms of life and their remedial measures. Advantages of adsorption when compared to other water treatment methods has been presented. The various adsorbents that are suitable for Cr(VI) removal from aqueous solution, the mechanism of adsorption, kinetics, thermodynamics, equilibrium models and desorption have been depicted.

A review of application of nanoadsorbents in wastewater treatment and their characterisation are presented in this section. Disadvantages of nanomaterials and application of nanocomposite adsorbents have been highlighted.

The various research works involving preparation of nanoadsorbents and nanocomposites have been stated clearly. Batch adsorption of Cr(VI) using nanoadsorbents and nanocomposites are also being discussed. A detailed literature review on the design, fabrication and modeling of continuous fixed bed adsorption column for heavy metal removal has been presented.

From the previous research works on both batch and continuous adsorption, we can summarise that adsorption using nanomaterial is seen to be highly effective in reducing the Cr(VI) concentration from aqueous solution. In order to overcome the difficulty of separation of nanomaterials from aqueous solution they can be made composite with suitable polymeric material and they can be used for heavy metal removal in continuous fixed bed column.

MATERIALS AND METHODS

● Contents ●	3.1 Introduction
	3.2 Preparation of Cr(VI) Stock Solution
	3.3 Preparation of Adsorbents
	3.4 Analytical Method for Cr(VI) Determination
	3.5 Characterisation of Adsorbents
	3.6 Batch Experiments
	3.7 Removal of Cr(VI) in Continuous Fixed Bed Adsorption Column Using Chitosan/Halloysite Clay Nanocomposite Film as Adsorbent
	3.8 Summary of the Chapter

3.1 Introduction

In this chapter the materials used for conducting adsorption tests for Cr(VI) removal for both batch and continuous experiments has been discussed. Detailed presentation of experimental procedures is included in this section. The experiments conducted for adsorption study is divided into two sections. In the first section, batch studies were carried out to select the best adsorbent for Cr(VI) removal. In the batch studies three adsorbents namely, ordinary nanokaolinite, magnetite nanoparticles and chitosan/halloysite clay nanocomposite films were used. In the second part, continuous experiments for Cr(VI) removal were performed in a fixed bed adsorption column using the selected adsorbent and the column was mathematically modeled.

3.2 Preparation of Cr(VI) Stock Solution

Potassium dichromate (99.9%) for preparing Cr(VI) stock solution was purchased from Sigma Aldrich. 1000 ppm of Cr(VI) solution was prepared by

adding 2.83 g potassium dichromate in 1 L ultrapure water and stored. Ultrapure water was produced in situ using Millipore Direct-Q3 UV system device. Various concentrations of Cr(VI) solution was obtained by diluting the stock solution.

3.3 Preparation of Adsorbents

In this section preparation of the adsorbents has been discussed. Nanokaolinite clay was purchased from Sigma Aldrich and used without further purification. Nanomagnetite was synthesised in the laboratory by sol gel method using ferric nitrate nonahydrate and ethylene glycol. 0.02 mol ferric nitrate nonahydrate and 25 mL ethylene glycol was mixed uniformly and stirred using a magnetic stirrer for 3 hours at room temperature. The solution was turned to a brown sol which was heated at 80 °C in a constant temperature bath. Brown gel was obtained and for 1 hour it was aged at room temperature and dried in a muffle furnace. Then finally it was annealed at 400 °C for 8 hours under inert atmosphere. Black magnetite powder was obtained (Cai and Wan, 2007; Cotica *et al.*, 2012). All the chemicals mentioned in the synthesis of magnetite nanoparticles were purchased from Sigma Aldrich. Fig. 3.1 represents the synthesised nanomagnetite.

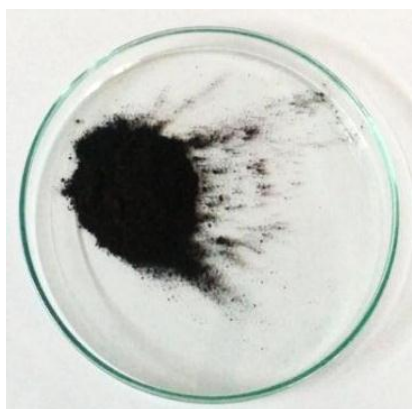


Fig. 3.1 Synthesised magnetite nanoparticles

For the preparation of nanocomposite films, chitosan with degree of deacetylation 0.85, halloysite nanoclay and lactic acid were purchased from Sigma Aldrich and used without further purification. 2.0 g chitosan was dissolved in 100 mL of 1% lactic acid. The mixture was stirred for 10 hours at 500 rpm. To the above mixture, 0.5 g halloysite nanoclay was added. Then the resulting solution was magnetically stirred for 8 hours at 1000 rpm. After stirring, sonication was carried out for 4 hours. After sonication, 40 mL of the above solution was poured into a glass petri dish. The films were dried in an oven at 80 °C for 24 hours. After drying, the films were treated with sodium hydroxide and left for 30 minutes for neutralization of any leftover lactic acid (Casariego *et al.*, 2009; Desilva *et al.*, 2013). Further the films were washed with distilled water to remove sodium hydroxide. The films were then peeled off. The films were cut into equal diameter particles for performing the adsorption experiments. Fig. 3.2 and Fig. 3.3 depicts the synthesised nanocomposite films.

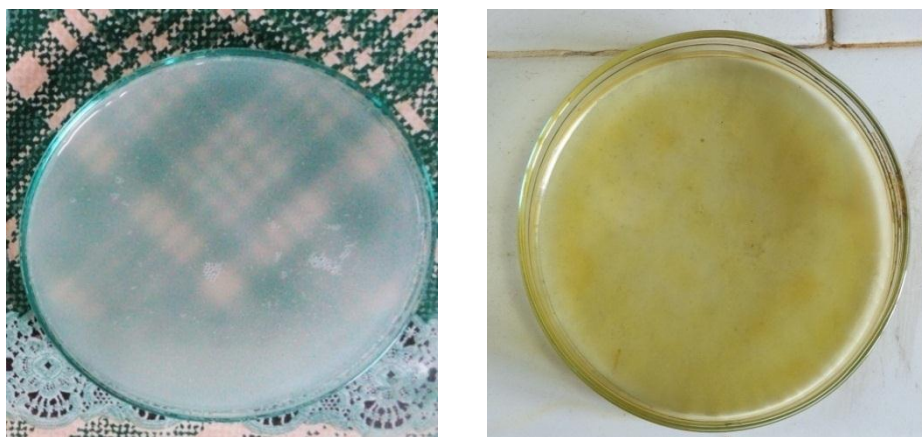


Fig. 3.2 Chitosan/halloysite nanocomposite film before and after drying



Fig. 3.3 Nanocomposite films used for adsorption

3.4 Analytical Method for Cr(VI) Determination

Analysis of Cr(VI) solution was carried out in a UV-VIS spectrophotometer (Hitachi U-2900). 1, 5 Diphenyl carbazide was used for spectrophotometric determination of Cr (VI) at $\lambda_{\max} = 540$ nm. 250 mg 1, 5 diphenyl carbazide was dissolved in 50 mL acetone and stored in a brown bottle. 4 mL of diphenyl carbazide solution was mixed with 1 mL Cr(VI) solution. To this mixture added 10 mL 5% sulphuric acid and made up to 50 mL. This solution was analysed in spectrophotometer. A blank solution containing diphenyl carbazide made up to 50 mL was used as the blank for analysis. Spectrophotometer was first calibrated using Cr(VI) (Standard Methods for the Examination of Water and Wastewater, 1992). Fig. 3.4 shows the sample of chromium solution after adding diphenyl carbazide.



Fig. 3.4 Sample for analysing in UV-spectrophotometer

UV-VIS spectrophotometer was first calibrated using Cr(VI) solution of different known concentrations. Cr(VI) solution of various concentrations were mixed with diphenyl carbazide as per the procedure given above. Blank solution without containing Cr(VI) solution was taken in the cuvette. Both the sample and blank solution was used in UV-VIS spectrophotometer and standard calibration curve was obtained (Rai *et al.*, 2016). This calibration curve was used to measure the concentration of Cr(VI) solution (Annexure I).

3.5 Characterisation of Adsorbents

The surface morphology of nanokaolinite clay, nanomagnetite particles and nanocomposite films were determined using scanning electron microscope (JEOL-JSM-6390). The elemental composition of nanokaolinite and nanomagnetite were estimated using energy dispersive X-ray spectroscopy (EDX). The crystal structure, average particle size and basal spacing of nanokaolinite clay, nanomagnetite and nanocomposite films were obtained from X-ray diffraction pattern (Standard X-ray Diffraction Powder Patterns, 1981). Bruker AXS X-ray powder diffractometer (Cu $K\alpha$ radiation) was used to find

the crystal structure and basal spacing of nanomaterials in the present work. Thermogravimetric analyser and differential thermal analyser was used to determine thermal stability of magnetite nanoparticles and nanocomposite films. STA 6000 Perkin Elmer TGA-DTA system was used for thermal analysis in the present study. Nitrogen gas was used to maintain the inert atmosphere.

Fourier transform infrared spectroscopy was used to analyse the functional group present in chitosan/halloysite clay nanocomposite film. Perkin Elmer FTIR spectrophotometer with 20 scans and resolution 4 was used for analysing the composite film. The average particle size of synthesised nanoparticles was calculated using Deybe-Scherrer's formula (Annexure II) which is given by equation 3.1.

$$D = \frac{K\lambda}{\beta \cos \theta} \quad (3.1)$$

where, D = mean diameter of nanoparticles

β = Full width at half maximum value of XRD diffraction lines in radians

λ = the wavelength of X-ray radiation source

θ = angle of incidence

K = the Scherrer constant with value from 0.9 to 1.

The nanocomposite film thickness was measured using a hand held digital micrometer. Strength of nanocomposite films were analysed using Universal Testing Machine (Shimadzu Autograph AG-I series).

3.6 Batch Experiments

Adsorption experiments were carried out in a temperature controlled incubated shaker (ROTEK Incubated shaker). For all the batch tests, 100 mL of Cr(VI) solution was taken in stoppered flasks and kept for shaking in the incubated shaker. Experiments were designed by Box-Behnken design under response surface methodology of Minitab16. Nanokaolinite clay adsorbents were used only for preliminary experiments. According to the design of experiments of RSM batch experiments were conducted for Cr(VI) removal using magnetite nanoadsorbent and chitosan/halloysite nanocomposite adsorbent. The efficiency of Cr(VI) adsorption and the metal adsorption capacity were determined using the following equations.

$$E = \frac{(C_0 - C_t)}{C_0} \times 100 \quad (3.2)$$

$$q(\text{mg} / \text{g}) = \frac{(C_0 - C_t)}{m} \quad (3.3)$$

where C_0 is the concentration of Cr(VI) in the solution before adsorption in mg/L and C_t is the concentration of Cr(VI) in the solution after adsorption in mg/L and m is the amount of adsorbent in gram in one litre of solution (g/L).

3.6.1 Batch Experiments for Cr(VI) Removal Using Nanokaolinite Clay

Adsorption experiments were conducted by diluting stock solution of Cr(VI) using deionized Millipore water. Constant volume of 100 mL of adsorbate solution was taken in stoppered flasks for the batch tests. After adding definite amount of adsorbent, the flasks were shaken in an incubated shaker at room temperature. After the required time was reached the solution was filtered using Whatman 0.2 μm cellulose nitrate membrane filter paper in

vacuum filtration unit and then centrifuged. The solution was then diluted using diphenyl carbazide and analysed using UV-VIS spectrophotometer. The effect of pH, initial concentration, adsorbent dose and time were studied and efficiency was found out for the batch tests. All the batch tests were conducted at 300 K and 200 rpm shaking speed. pH of the solution was adjusted using either hydrochloric acid or sodium hydroxide (0.1 N). Chemicals for pH adjustment were also purchased from Sigma Aldrich.

3.6.2 Adsorption Using Magnetite Nanoparticles

Adsorption experiments were performed according to the design of experiments given by Box-Behnken design under response surface methodology of Minitab 16. Optimisation of operating parameters for Cr(VI) removal was also carried out using RSM. Response surface methodology gave 27 sets of experimental combinations. The parameters for batch study were initial concentration, adsorbent concentration, time and pH. The effect of these variables were also studied separately at constant temperature and shaking speed. All the batch tests were conducted at 303 K and 200 rpm shaking speed (Yuan *et al.*, 2009). After adjusting initial concentration, adsorbent concentration and pH, the test solution was shaken in the incubated shaker for the specified time. pH was adjusted using 0.1 N HCl and 0.1 N NaOH. After adsorption filtration was carried out using 0.2 μm cellulose nitrate membrane filter paper in a vacuum filtration unit. Magnetic field was also applied for the separation of magnetite nanoparticles. After filtration the concentration of solution was determined using previously calibrated UV-VIS spectrophotometer at 540 nm.

3.6.3 Design of Experiments for Magnetite Nanoadsorbents

Conventional methods of changing one parameter keeping other influencing parameters constant and performing the adsorption experiments is time consuming. The study of interaction between various parameters is not possible using the conventional batch adsorption tests. The variable under study may not be able to give appropriate removal when another influencing variable changes. When more than one variable influences a process, the correct approach is to use factorial approach. Moreover, optimisation of adsorption process can be carried out by using the design of experiments. Design of experiments using Minitab 16 was used to develop the model equation and optimisation of Cr(VI) removal using magnetite nanoadsorbents.

In the present study optimisation of Cr(VI) removal using magnetite nanoparticles was carried out using Box-Behnken (BBD) design under response surface methodology of Minitab 16. RSM consists of a group of empirical techniques devised to generate the relationship between a group of controlled experimental parameters and measured responses (Ghorbani *et al.*, 2008). The advantage of RSM is that it is cost effective, smooth working and accurate for optimisation of output response. Surface plots or contour plots are used to represent the response graphically. Box-Behnken method demands minimum experimental runs and is used for optimisation of three or higher number of variables affecting the process. Design of experiments were carried out first using initial concentration, pH, time and adsorbent dosage. Experiments were conducted secondly. Efficiency was found out and analysed using RSM.

If all the variables are assumed to be measurable, the response surface is given by $Y = f(X_1, X_2, X_3 \dots X_K)$, Y is the efficiency of Cr(VI) removal by

adsorption (response variable), X_i is called variables of action called factors (Aslan and Cebeci, 2007). Our goal in the present study is to maximize Y .

Second order model is assumed in RSM. Mathematical model equation of second order was developed using RSM and optimal set of parameters that maximise the efficiency was found out. The mathematical model equation representing Box- Behnken design is given by

$$Y = \beta_0 + \beta_1 X_1 + \beta_2 X_2 + \beta_3 X_3 + \beta_4 X_4 + \beta_{11} X_1^2 + \beta_{22} X_2^2 + \beta_{33} X_3^2 + \beta_{44} X_4^2 + \beta_{12} X_1 X_2 + \beta_{13} X_1 X_3 + \beta_{14} X_1 X_4 + \beta_{23} X_2 X_3 + \beta_{24} X_2 X_4 + \beta_{34} X_3 X_4 \quad (3.4)$$

The four factors in the present study were designated as initial concentration (X_1), pH (X_2), time (X_3) and adsorbent dosage (X_4). They were prescribed in three levels coded as +1 for high, 0 for intermediate and -1 for low value. β_0 is a constant, $\beta_{12}, \beta_{13}, \beta_{14}, \beta_{23}, \beta_{24}, \beta_{34}$ are called interaction coefficients, $\beta_{11}, \beta_{22}, \beta_{33}, \beta_{44}$ are quadratic coefficients, $\beta_1, \beta_2, \beta_3, \beta_4$ are regression coefficients for linear effects and Y is the response variable under study. In the present work, response surface methodology was also used to study the interaction between variable and ANOVA (Analysis of variance). Linear regression coefficient (R^2) between experimental and predicted value of Y was determined to find the quality of fit of model. Response optimiser of RSM gave the optimum conditions of operating parameters for maximum removal.

3.6.4 Effect of Various Parameters on Adsorption of Cr(VI) Using Chitosan/Halloysite Clay Nanocomposite Films

Nanocomposite films synthesised in the laboratory were used for the removal of Cr(VI) from synthetically prepared wastewater. The effects of various parameters on adsorption was studied at constant temperature of 50 °C and agitation speed of 120 rpm (Chen *et al.*, 2013). First the effect of pH was studied keeping the initial concentration at 25 ppm and adsorbent concentration at 0.06 g/

100 mL adsorbate solution. For the study pH was varied from 2 to 10.8 and the above solution was shaken in a temperature controlled incubated shaker for 1 hr. The effect of temperature on adsorption was studied keeping pH 3.0 and time as 1 hour. The initial concentration and adsorbent concentration were 25 ppm and 0.06 g/100 mL respectively and temperature of adsorption was varied from 30 °C to 123 °C. To study the effect of time, initial concentration was fixed as 25 ppm and pH maintained at 3.0. For adsorbent dosage of 0.06 g/100 mL the batch experiments were conducted for time ranging from 15 minutes to 100 minutes. The effect of adsorbent dosage was studied by conducting the batch adsorption tests at 50 °C at pH 3.0. Adsorbent dosage was varied from 0.02 to 0.25 g/100 mL for an initial concentration of 25 ppm. The solution was shaken for one hour and the adsorbent was filtered using Whatman 0.45 mm filter paper. The resulting filtrate solution was analysed using UV-VIS spectrophotometer. Lastly, the effect of initial concentration was studied by varying the initial concentration from 5.6 ppm to 70 ppm. For the study pH was maintained at 3.0, adsorbent dosage at 0.06 g/100 mL and time of shaking was 1 hour. pH was adjusted by using 0.1 N HCl and 0.1 N NaOH. After conducting batch experiments the efficiency and adsorption capacity were evaluated. Fig. 3.5 gives the colour change of Cr(VI) solution before and after adsorption using nanocomposite films.



Fig. 3.5 Cr(VI) solution after and before adsorption using nanocomposite films

3.6.5 Kinetic Studies Using Nanocomposite films as Adsorbent

For kinetic studies, 25 ppm Cr(VI) solution at pH 3.0 was agitated for time intervals 15 to 100 minutes at 50 °C and 120 rpm. 0.06 g adsorbent was added to the 100 mL of adsorbate solution and mixed thoroughly. After shaking the solutions were analysed in UV-VIS spectrophotometer at 540 nm. The kinetic data was fitted to Lagergren's pseudo first order, pseudo second order, second order and intraparticle diffusion model to test the kinetics of adsorption of Cr(VI) on the surface of nanocomposite films.

Lagergren equation is given by equation (3.5), pseudo second order equation is represented by equation (3.6), the second order equation by equation (3.7) and intraparticle diffusion equation by (3.8).

$$\log(q_e - q_t) = \log q_e - \frac{K}{2.303} t \quad (3.5)$$

$$\frac{t}{q_t} = \frac{1}{K_1 q_e^2} + \frac{t}{q_e} \quad (3.6)$$

$$\frac{1}{q_e - q_t} = \frac{1}{q_e} + K_2 t \quad (3.7)$$

$$q_t = K_d t^{1/2} \quad (3.8)$$

K is the Lagergren constant (min^{-1}), K_1 is the pseudo second order rate constant for adsorption ($\text{g mg}^{-1} \text{min}^{-1}$), K_2 is the second order rate constant ($\text{g mg}^{-1} \text{min}^{-1}$) and K_d ($\text{mg g}^{-1} \text{min}^{-1/2}$) is the rate constant for intraparticle diffusion. q_e is the amount of metal ion adsorbed at equilibrium and q_t is the amount of metal ion adsorbed at time t in mg/g.

3.6.6 Equilibrium Studies for Cr(VI) Removal Using Chitosan/Halloysite Clay Nanocomposite Films

Initial concentrations (5.6ppm to 26 ppm) of 100 mL Cr(VI) solution was taken where 0.06 g nanocomposite was added. Then the flasks were shaken in a temperature controlled incubated shaker at 120 rpm and 50 °C until equilibrium concentration between the adsorbent and adsorbate was attained. Langmuir and Freundlich model represents the equilibrium between Cr(VI) in the adsorbent and adsorbate. Langmuir model represents monolayer adsorption. In Langmuir model adsorbent have finite number of identical sites. Adsorbed molecules are not interactive. In Freundlich model, adsorption takes place in non identical sites of adsorbent. Cr(VI) is adsorbed in a heterogeneous surface of the adsorbent by Freundlich model. The equilibrium data was fitted to Langmuir and Freundlich isotherm equations. The Langmuir and Freundlich equations are given by

$$q_e = \frac{q_m b C_e}{1 + b C_e} \quad (3.9)$$

$$\frac{1}{q_e} = \frac{1}{q_m} + \frac{1}{b q_m C_e} \quad (3.10)$$

$$q_e = K_f C_e^{\frac{1}{n}} \quad (3.11)$$

$$\ln q_e = \ln K_f + \frac{1}{n} \ln C_e \quad (3.12)$$

Equation (3.9) represents Langmuir model and (3.10) represents linearized form of (3.9). Equation (3.11) represents Freundlich model and (3.12) represents linearized form of (3.11). C_e represents the equilibrium concentration of the solution in ppm, q_e is the adsorption capacity in mg/g at equilibrium, q_m is related to the maximum adsorption capacity (mg/g), and b is

the Langmuir adsorption constant and is related to the energy of adsorption (L/mg). q_m and b are respectively the intercepts and slope of the plot between $\frac{1}{q_e}$ vs $\frac{1}{C_e}$. K_f is the Freundlich constant ($\text{mg/g}(\text{mg/L})^n$) (Chen *et al.*, 2013).

3.6.7 Thermodynamic Studies Using Nanocomposite Films

Thermodynamic studies were conducted by conducting batch adsorption experiments by varying the temperature from 30 to 123 degree celsius keeping all other parameters constant. pH was maintained 3.0, adsorbent dosage at 0.6 g/L and shaking speed was 120 rpm. Initial concentration for thermodynamic study was kept constant at 25 ppm. The final concentration was measured after 60 minutes using UV-VIS spectrophotometer at 540 nm. The thermodynamic constants such as Gibbs Free Energy, thermodynamic equilibrium constant, entropy change and enthalpy change was determined.

Thermodynamic equilibrium constant is determined using equation given below (Tirtom *et al.*, 2012).

$$K = C_{AD} / C_e \quad (3.13)$$

C_{AD} and C_e are equilibrium concentration in mg/L of Cr(VI) in the film and solution respectively. Thermodynamic parameters of adsorption like Gibbs free energy change (ΔG) kJ/mol, enthalpy change (ΔH) kJ/mol and entropy change (ΔS) kJ/mol K are determined using equations (3.14), (3.15) and (3.16) respectively.

$$\Delta G = -RT \ln K \quad (3.14)$$

$$\Delta G = \Delta H - T\Delta S \quad (3.15)$$

$$\ln K = \frac{\Delta S}{R} - \frac{\Delta H}{RT} \quad (3.16)$$

R is the universal gas constant in J/mol K, and T is the absolute temperature in K.

3.6.8 Desorption Studies of Nanocomposite Films

Desorption study is important for getting information regarding the reusability of the adsorbent. In the present study, first adsorption experiments were conducted at 120 rpm and 60 °C. For first cycle of adsorption-desorption experiments, 0.17 g/L of nanocomposite films were added and pH of Cr(VI) stock solution was maintained at 3.0. 100 mL of 70 ppm of the above solution was shaken for 70 minutes in a temperature controlled incubated shaker and after adsorption the residual solution was filtered and analysed using UV-VIS spectrophotometer at 540 nm. After adsorption the nanocomposite films were washed with HPLC grade water to remove the residual Cr(VI). The adsorbent films were then dried. 0.17 g/L of the dried adsorbent were taken in stoppered flasks. The stripping solution used was 100 mL of 0.01 M NaOH at pH 3.0. Then the flask was placed in incubated shaker and agitated for 30 minutes at room temperature. Then the solution was filtered and analysed for Cr(VI) in UV-VIS spectrophotometer. Percentage desorption was determined. The adsorbent after first cycle was dried and placed in a flask containing 70 ppm Cr(VI) solution. The same procedure was repeated. Four cycles of adsorption - desorption experiments were conducted and the time of reuse was analysed for chitosan/halloysite nanoclay adsorbent. Fig. 3.6 a) shows the Cr(VI) solution before adsorption in the first cycle and Fig. 3.6 b) shows the Cr(VI) solution after desorption in the first cycle.



Fig. 3.6 a) Stock solution before adsorption; b) Solution after desorption (first cycle)

3.6.9 Response Surface Methodology for Cr(VI) Removal Using Nanocomposite Films

Box-Behnken method under response surface methodology of Minitab 16 was used for optimisation of Cr(VI) removal using chitosan/halloysite nanoclay adsorbent. All the experiments were conducted at 30 °C and 120 rpm shaking speed according to the design of experiments provided by Box Behnken design. A total of 15 experimental runs were conducted batchwise at pH 3.0. pH was adjusted by 0.1 N NaOH and 0.1 N HCl. After 15 sets of batch experiments, the response surface was analysed. Response optimiser gave the optimum values of initial concentration, adsorbent concentration and time for maximum removal. Surface plots showing the combined effect of variables were plotted.

3.7 Removal of Cr(VI) in Continuous Fixed Bed Adsorption Column Using Chitosan/Halloysite Clay Nanocomposite Film as Adsorbent

Continuous removal of Cr(VI) from aqueous solution was accomplished using an adsorption column. A schematic diagram showing the principle of working of packed bed adsorption column is shown in Fig. 3.7.

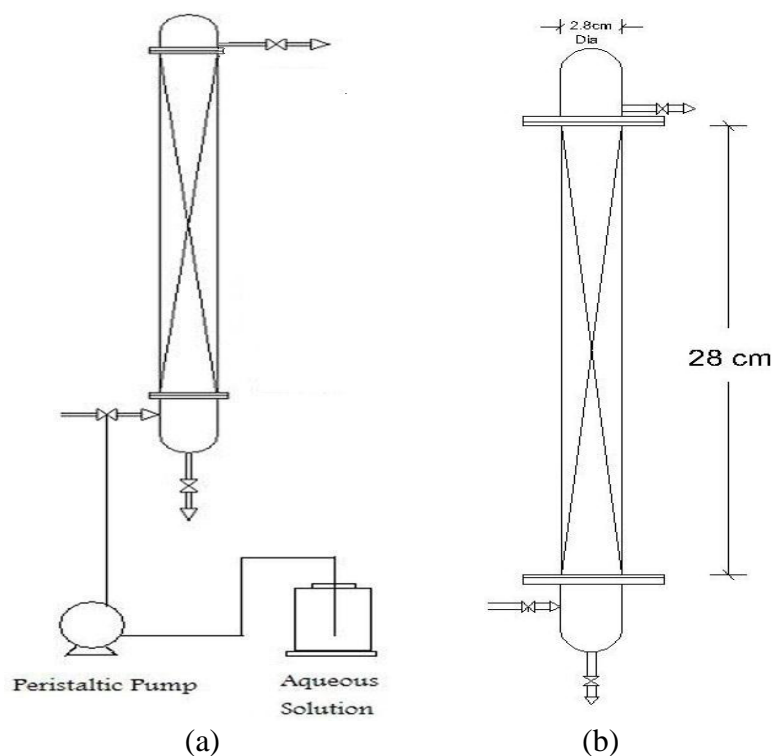


Fig. 3.7 a) Schematic of the experimental set up b) Schematic of the packed bed column with proper dimensions

A perspex column of 28 mm outer diameter, 24 mm inner diameter and 280 mm height was used for column studies (Lim and Aris, 2014). A glass mesh was provided at the bottom of the column to prevent the loss of adsorbent during filtration process. A known weight of adsorbent was mixed uniformly with glass beads as the supporting material and filled into the column. 5 litres of stock solution of Cr(VI) was stored in a glass vessel. A silicon tube of 2 cm diameter and 2 mm thickness was used to connect glass vessel containing the stock solution, peristaltic pump and the glass column. Before the adsorption experiments, the adsorbent packed in the column was wetted with deionized water to remove any trapped air bubbles. The Cr(VI) solution of known initial concentration was pumped to the bottom of the column using the previously calibrated peristaltic pump (Annexure III). The Cr(VI) solution after adsorption

was collected from the top of the column for specified time intervals. The treated Cr(VI) solution was collected until the bed got saturated. The Cr(VI) solution after adsorption was filtered using Whatman 0.45 mm filter paper and analysed for Cr(VI). Fig. 3.8 is the the experimental set up for fixed bed column for Cr(VI) removal. The effect of pH, Initial concentration, bed height and flow rate were studied for continuous experiments. All the experiments were conducted at room temperature of 303K. The adsorbent dosage for the study was 30% of the bed height. The pH of soluton was adjusted using 0.1 N NaOH and 0.1 N HCl. The column parameters were determined mathematically. The breakthrough curve was analysed and the column was mathematically modeled to study the adsorption behaviour.



Fig. 3.8 Cr(VI) fixed bed column using chitosan/halloysite nanocomposite film

The column performance was evaluated by C_f/C_0 , where C_f is the effluent concentration and C_0 is the influent concentration in ppm respectively. Breakthrough curves were obtained by plotting C_f/C_0 against time. Adsorbed metal concentration ($C_0 - C_f$) was also plotted against time to analyse the amount of Cr(VI) adsorbed in each sets of experiments. Volume of effluent collected at any time is given by

$$V_{eff} (mL) = Qt_{total} \quad (3.17)$$

Q represents the volumetric flow rate in mL/min and t_{total} is the total flow time in minutes. The total adsorbed metal ion q_{total} (mg) is obtained by finding the area under the curve $C_0 - C_f$ versus time.

$$q_{total} = \frac{Q}{1000} \int_{t=0}^{t=t_{total}} C_{ad} dt \quad (3.18)$$

$$C_0 - C_f = C_{ad} \quad (3.19)$$

The total amount of metal ions delivered to the column m_{total} in mg is obtained from equation (3.20).

$$m_{total} = \frac{C_0 Q t_{total}}{1000} \quad (3.20)$$

Percentage total removal of Cr(VI) ions is given by equation (3.21).

$$\% \text{ removal} = \frac{q_{total}}{m_{total}} \times 100 \quad (3.21)$$

Equilibrium Cr(VI) uptake also known as column maximum adsorption capacity, q_{eq} in mg/g and unadsorbed metal ion concentration at equilibrium, C_{eq} in mg/L is obtained from equation (3.22) and (3.23) respectively (Lim and Aris, 2014).

$$q_{eq} (mg / g) = \frac{q_{total}}{X} \quad (3.22)$$

$$C_{eq} (mg / L) = \frac{m_{total} - q_{total}}{V_{eff}} \times 1000 \quad (3.23)$$

X is the unit mass of adsorbent packed in the column.

The column was mathematically modeled using Thomas model, Yoon Nelson model and Adam Bohart model. The various models applied to the column data is described below.

3.7.1 Thomas Model

Thomas model developed in 1948 is simple for analysing the performance of packed bed adsorption column. Breakthrough curves of column operation is to be predicted correctly for the successful design of an adsorption column. Thomas model is widely used for the design of adsorption column. Derivation of Thomas model is based on the second order reaction kinetics (Lim and Aris, 2014). Parameters of Thomas model were determined and breakthrough curves were predicted. Thomas model is given by equation (3.24).

$$\ln\left(\frac{C_0}{C_f} - 1\right) = \frac{k_{th}q_0m}{Q} - k_{th}C_0t \quad (3.24)$$

Plot of $\ln\left(\frac{C_0}{C_f} - 1\right)$ versus t (min) will give the Thomas kinetic constant k_{th} (mL/min mg) and maximum solid phase concentration, q_0 (mg/g). m is the mass of adsorbent in the column in g. The experimental column data has been compared with the data predicted by Thomas model and thus the model is validated.

3.7.2 Yoon Nelson Model

Yoon Nelson model contains only very small number of column parameters. It gives the time for 50% adsorbate breakthrough, τ (minute) (Lim and Aris, 2014). The mathematical representation of Yoon Nelson model is shown below in equation (3.25).

$$\ln \frac{C_f}{C_0 - C_f} = k_{YN}t - \tau k_{YN} \quad (3.25)$$

k_{YN} is the Yoon Nelson rate constant (minute⁻¹). In Yoon Nelson model no other physical data is required. A plot of $\ln \frac{C_f}{C_0 - C_f}$ versus time will give the parameters of Yoon Nelson model. The parameters were determined by plotting the experimental data and the breakthrough curves were predicted using the model. The fit of experimental data was checked using the model.

3.7.3 Adam Bohart Model

Adam Bohart model was applied to the column data. Adam Bohart model is based on the theory of surface reaction. It is applicable to the initial part of the column operation that is upto 10-50% of breakthrough (Jain *et al.*, 2013).

$$\ln \frac{C_f}{C_0} = k_{AB}C_0t - \frac{k_{AB}N_0Z}{U_0} \quad (3.26)$$

k_{AB} is the Adam Bohart kinetic constant (L/mg min). N_0 represents the saturation concentration (mg/L) and Z is the bed depth (cm). U_0 is the linear velocity (cm/min) and it was calculated by knowing volumetric flow rate and cross section area of the bed. A plot of $\ln \frac{C_f}{C_0}$ was made with time to give k_{AB} and N_0 . The column data was compared with the data predicted by the model and the linear regression coefficient between experimental data and predicted data was determined (Lim and Aris, 2014).

3.8 Summary of the Chapter

This chapter presented a detailed study on the various materials and methods used in the removal of hexavalent chromium from aqueous solution using nanomaterials. Three nanoadsorbents namely nanokaolinite, nanomagnetite and chitosan/halloysite clay nanocomposite films were used in the study. The synthesis and characterisation of the nanomaterials are being discussed. Due to better performance of nanocomposite films, their use in the fixed bed adsorption column for Cr(VI) removal have also been described. Modeling of the column using Thomas model, Yoon Nelson model and Adam Bohart model and their equations have been depicted clearly in this chapter.

RESULTS AND DISCUSSION

4.1 Introduction
4.2 Batch Adsorption Study for Cr(VI) Removal Using Nanokaolinite Clay
4.3 Batch Adsorption Study of Cr(VI) Removal Using Nanomagnetite
4.4 Batch Adsorption of Cr(VI) Using Chitosan/Halloysite Clay Nanocomposite Films
4.5 Continuous Removal of Cr(VI) in Packed Column Using Nanocomposite Films
4.6 Modeling of Packed Bed Adsorption Column
4.7 Summary

4.1 Introduction

The presence of Cr(VI) in water has a lot of adversities that will affect all sorts of life. Adsorption is one of the effective methods for removing low concentrations of Cr(VI) from wastewater. In the present work adsorption is carried out for separating Cr(VI) from aqueous solution so that the water can be reused. Three materials were selected as adsorbents and adsorption experiments were performed as described in chapter 3. In this chapter, comparison has been made between nanokaolinite clay (unmodified), nanomagnetite and chitosan/halloysite clay nanocomposite films for the adsorptive removal of Cr(VI) from wastewater. Unmodified nanoclay had only small Cr(VI) removal efficiency and adsorption capacity. Nanomagnetite possessed less adsorptive removal efficiency and adsorption capacity when compared to the nanocomposite films. The characterisation has been done for the three adsorbents. Due to the higher adsorption capacity and ease of

separation after adsorption, chitosan/halloysite clay nanocomposite films have been used in the fixed bed column for Cr(VI) removal. In the last section of this chapter, the performance of the nanocomposite adsorbent for Cr(VI) removal has been analysed in continuous experiments and the Cr(VI) column has been modeled mathematically.

4.2 Batch Adsorption Study for Cr(VI) Removal Using Nanokaolinite Clay

The variables that are affecting the adsorption of Cr(VI) on nanokaolinite have been analysed. Batch adsorption experiments were conducted by varying the pH, nanoclay dosage, initial Cr(VI) concentration and time of adsorption. To study the effect of pH on adsorption, pH of the solution was varied from 2 to 10. 7.5 g/L of nanoclay was added to the solution of 10 ppm initial concentration and shaken for 70 minutes in a temperature controlled incubated shaker. The optimum pH obtained was 3.0 and all other experiments were conducted at this pH. To study the effect of nanoclay dosage, the dosage of adsorbent was varied from 5 g/L to 10 g/L keeping all the parameters same as in the pH study. The effect of initial concentration was studied by changing the initial concentration from 10 ppm to 50 ppm with all other conditions kept same as in the previous tests. Batch study for time was conducted by changing the time of shaking from 20 to 140 minutes.

4.2.1 Effect of Various Parameters on Cr(VI) Removal

The effect of various parameters was studied at 300 K and 200 rpm speed. The removal efficiency first increased with pH. At pH 3.0 maximum removal was observed. Further increase in pH caused decrease in adsorption capacity and percentage of Cr(VI) removal. At low pH the adsorption free energy is less. Beyond pH 7.0, the surface of adsorbent become more negatively charged causing repulsion of adsorbent and adsorbate. When adsorbent dosage

increases, there will be greater availability of the exchangeable sites. With increase in the adsorbent dosage, the removal first increased due to increase in the number of active sites for Cr(VI) adsorption. At 7.5 g/L maximum removal of 50% has been observed. Further increase in the adsorbent dosage caused reduction in the active sites due to aggregation of Cr(VI) ions and hence the percentage removal decreased. Fig. 4.1 shows the effect of pH and adsorbent dosage on Cr(VI) removal.

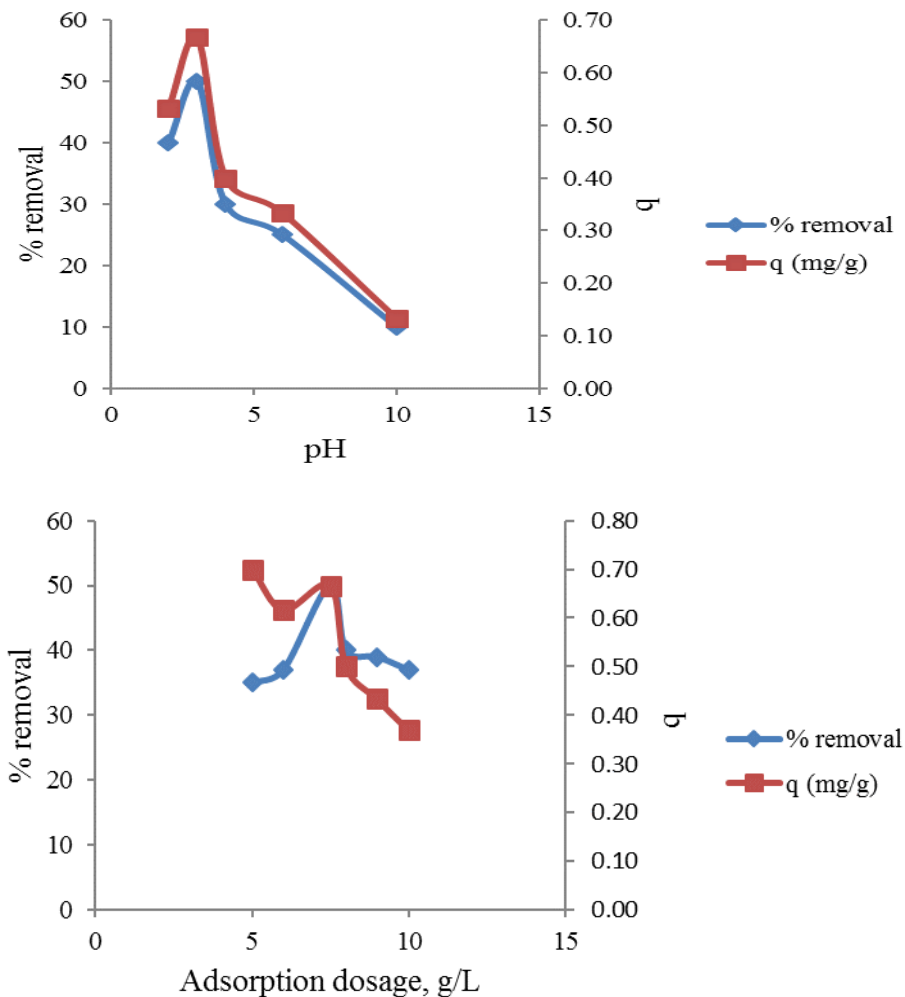


Fig. 4.1 Effect of pH and adsorbent dosage on adsorption efficiency and adsorption capacity of nanokaolinite clay

With increase in initial concentration, the driving force for mass transfer increases. So initially there was increase in the percentage Cr(VI) removal. When the initial concentration was increased beyond 15 ppm, the percentage Cr(VI) removal decreased. This is because there is no change in the no of active sites with increase in the initial concentration. Increase in Cr(VI) concentration causes accumulation near the active sites. With time the removal efficiency increased up to 120 minutes. Further increase in time did not cause any change in the adsorption capacity and percentage Cr(VI) removal because steady state has been achieved. The effect of initial concentration and time on Cr(VI) removal efficiency and adsorption capacity is shown in Fig. 4.2.

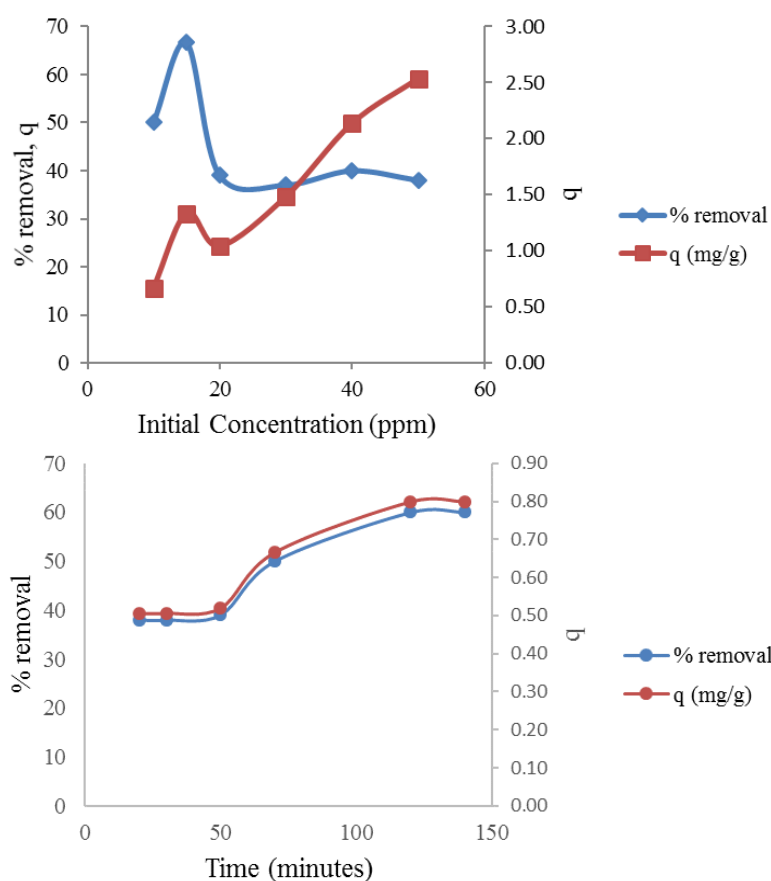


Fig. 4.2 Effect of initial concentration and time on percentage Cr(VI) removal and adsorption capacity of nanokaolinite clay

From the batch study of removal of Cr(VI) using nanokaolinite clay it was observed that the percentage removal was very low and maximum the removal efficiency obtained was 67% which is not desirable for continuous plant operations. Also unmodified nanoclay possessed very low adsorption capacity. Separation of this adsorbent was very difficult from the adsorbate after the process and there was chance of escaping of the adsorbent along with the adsorbate solution. To improve the adsorption capacity and ease of separation, some surface modification has to be carried out. So no further studies has been conducted using this adsorbent.

4.2.2 Characterisation of Nanoclay

Morphological characterisation of nanokaolinite clay was performed using SEM-EDX. XRD was used to analyse the crystal structure of nanokaolinite clay.

4.2.3 Scanning Electron Microscopy Equipped with Energy Dispersive X-ray Spectroscopy

Scanning electron microscopy depicts the surface topography and morphological characteristics of clay. Pure unmodified clay has non uniform surface. SEM image at different magnification range indicated the agglomeration of nanoclay. SEM image shown in the Fig. 4.3 was compared with that of standard image of nanokaolinite clay and showed similarity. Basically kaolinite clay is an aluminium-silicate material which is soft and white. The elemental composition of nanoclay given by EDX (Fig. 4.4) indicated the presence of aluminium and silicate.

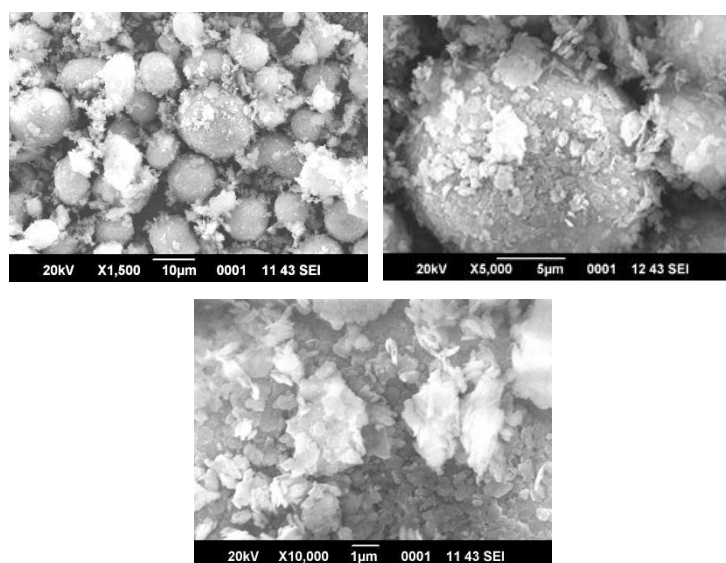


Fig. 4.3 SEM images of nanokaolinite clay at various magnification

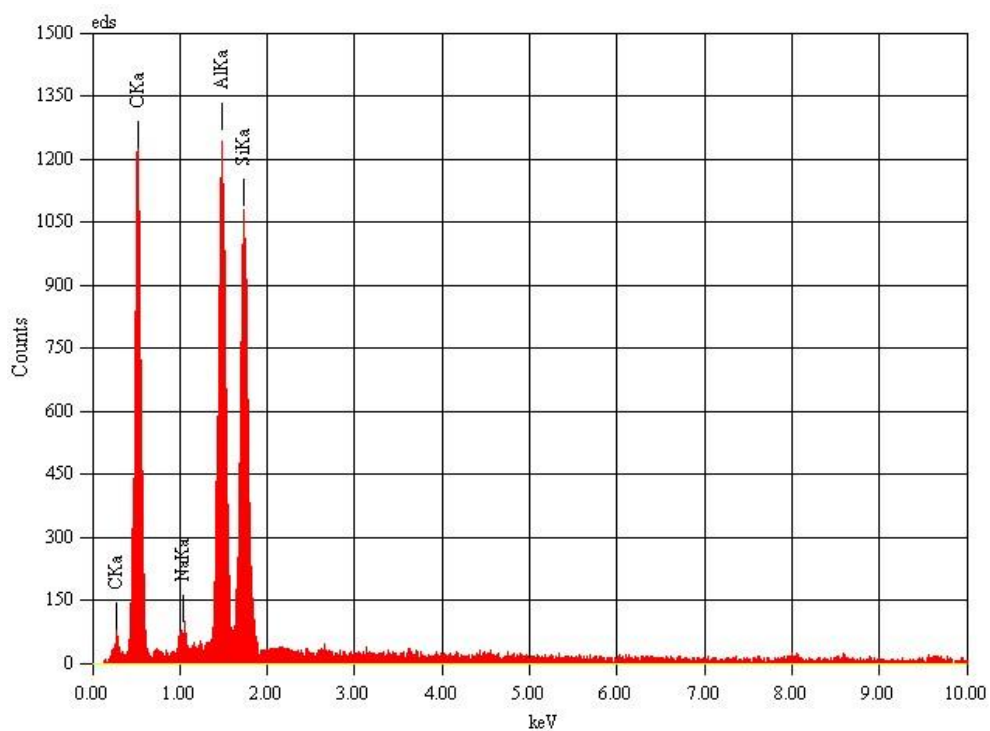


Fig. 4.4 EDX of nanokaolinite clay

Kaolinite clay is a layered silicate mineral with one tetrahedral sheet of silica (SiO_4) linked through oxygen atoms to one octahedral sheet of alumina (AlO_6). Table 4.1 indicates the elemental composition of nanoclay used for adsorption of Cr(VI).

Table 4.1 Elemental composition of unmodified nanokaolinite from EDX

Element	(Kev)	Mass%	Atom%	K
C K	0.277	4.41	7.53	2.6284
O K	0.525	39.05	50.06	1
Na K	1.041	1.42	1.26	0.7506
Al K	1.486	29.45	22.39	0.7564
Si K	1.739	25.68	18.75	0.7676
Total		100	100	

4.2.4 X-ray Diffraction Pattern of Nanokaolinite Clay

Scattering of X-rays by atoms of a crystal produces an interference effect and the diffraction pattern is produced which is an indication of identity of the substance. X-ray diffraction pattern of nanokaolinite showed that the adsorbent contains aluminium oxide, silicon oxide together with small amounts of sodium and carbon. The material was scanned from $3\text{-}80^\circ$ at a wavelength of 1.5406 \AA in a X-ray diffractometer. The characteristic peaks in the XRD spectrum of nanokaolinite clay is due to their regular layered structure. The peaks indicated the d-spacing in the structure of clay. The first basal reflection peak was at 12.607° which correspond to intergallery spacing 7.01 \AA . The significant peaks at 20.175° , 25.13° , 38.6° correspond to 4.3 \AA , 3.54 \AA and 2.32 \AA intergallery spacing respectively. These three peaks correspond to that of silicon oxide (JCPDS data). The other peaks are at 20.631 , 20.901 , 21.058 , 21.505 , 21.631 , 62.511 degree. The peak at 62.511 indicates the presence of sodium aluminium oxide. The peaks in the XRD

curve were compared with that of standard data and are similar. XRD pattern of nanokaolinite clay matched with those presented in previous works (Anjana *et al.*, 2014). This showed that the adsorbent used is nanokaolinite clay. The x-ray diffraction pattern is shown in the Fig. 4.5. The average grain size of particles from XRD calculated using Scherrer's equation is 6.86 nm.

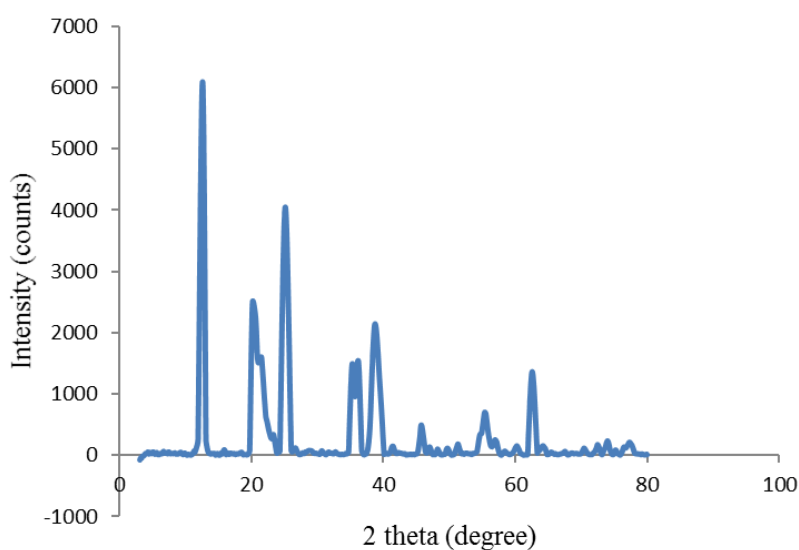


Fig. 4.5 XRD of nanokaolinite clay

4.3 Batch Adsorption Study of Cr(VI) Removal Using Nanomagnetite

To study the effect of the variables affecting adsorption of Cr(VI) using magnetite nanoparticles synthesised in the laboratory, batch experiments were conducted by varying the adsorbent dosage from 5 to 10 g/L by taking all other parameters constant, initial concentration from 10 to 60 ppm, pH from 2-10 which was adjusted using 0.1 M HCl and 0.1 M NaOH. The optimum pH of adsorption was 2.0 and all batch studies were conducted at pH 2.0. Time of shaking was changed from 20 to 120 minutes. Response surface methodology

of Minitab 16 was used to study the combined effect of variables at 30 °C and 200 rpm. The effect of the variables affecting adsorption of Cr(VI) on magnetite nanoparticles has been studied.

4.3.1 Effect of pH

To study the effect of pH on adsorption of Cr(VI), the 0.75 g of nanomagnetite was added in 100 mL of 50 ppm Cr(VI) solution. Then the solution was shaken for 70 minutes in an incubated shaker at 303 K. The pH was varied from 2 to 10. The effect of pH is shown in Fig. 4.6. As pH was increased, the efficiency of adsorption of Cr(VI) decreased. The maximum removal was observed at low pH. As pH was increased from 3.0, the adsorption capacity also decreased. Cr(VI) exists at various forms like CrO_7^{2-} , $HCrO_4^-$, $Cr_3O_{10}^{2-}$, $Cr_4O_{13}^{2-}$ at low pH. At pH 2 and 3, the predominant species is $HCrO_4^-$. It has low free energy of adsorption on the surface of magnetite nanoparticles. Therefore, the efficiency of Cr(VI) removal was high at low pH. At higher pH the surface of magnetite is more negatively charged. As a result, there will be repulsion between negatively charged Cr(VI) anions and the adsorbent. Hence removal decreased. Also, there will be release of adsorbed Cr(VI) from the surface of the adsorbent at high pH. Also, the adsorption capacity of magnetite nanoparticles decreased with increase in pH of Cr(VI) solution. The adsorption mechanism can be described as the electrostatic attraction of negatively charged chromate to the positively charged surface of magnetite nanoparticles followed by reduction of Cr(VI) to Cr(III). Previous literature showed similar result (Yuan *et al.*, 2009).

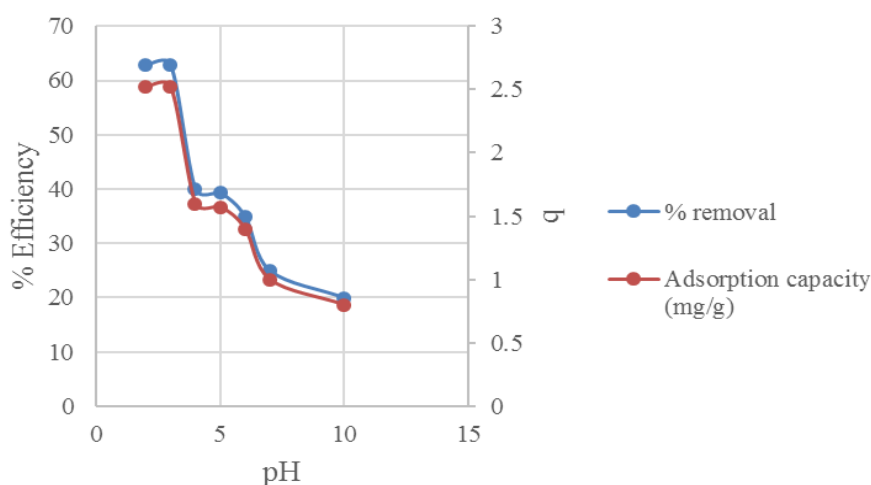


Fig. 4.6 Effect of pH on removal efficiency of Cr(VI) and adsorption capacity of magnetite nanoparticles

4.3.2 Effect of Adsorbent Dosage on Adsorption of Cr(VI)

The effect of adsorbent dosage was studied for an initial Cr(VI) concentration of 50 ppm. The pH of the solution was maintained at 2.0. The required adsorbent was added to the solution and shaking time was 70 minutes at 200 rpm and 303 K. At adsorbent concentration of 5 g/L, the removal efficiency was 60%. As adsorbent concentration was increased, initially there was increase in removal of Cr(VI). After a certain adsorbent concentration, the efficiency decreased instead of increasing. Initially when the adsorbent dosage increases, the active sites for Cr(VI) adsorption also increases. At very high adsorbent dosages, there will be aggregation of Cr(VI) particles near the active sites and less binding sites are available for adsorption. This is because the agitation speed is constant. Also, the adsorption capacity was higher at low adsorbent dosage. At higher adsorbent dosage the solution ion concentration drops to a low value. The adsorbent remains unsaturated at lower values of q . This means that at higher adsorbent dosage, the system reaches equilibrium. Hence maximum adsorption capacity was observed at 5 g/L (Zhou *et al.*, 2009). Effect of adsorbent dosage on adsorption of Cr(VI) using nanomagnetite is shown in Fig. 4.7.

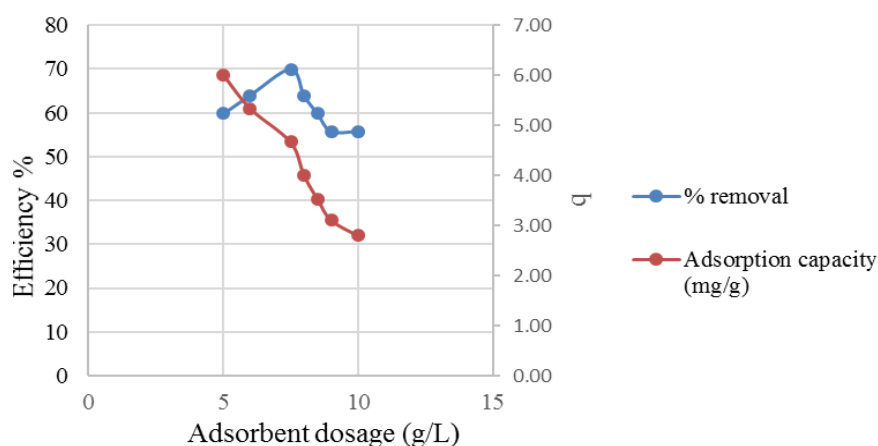


Fig. 4.7 Effect of adsorbent dosage on adsorption of Cr(VI) using nanomagnetite

4.3.3 Effect of Initial Concentration

The effect of initial concentration was studied for Cr(VI) solution at pH 2.0. 7.5 g/L of magnetite nanoparticles was added to 100 mL flask and shaken for 70 minutes. Initial concentration was varied from 10 to 60 ppm. It was observed that with increase initial concentration there was a decrease in removal efficiency initially and thereafter there was a slight increase in removal of Cr(VI). But the change in removal efficiency was only very less. Therefore, we can conclude that initial concentration has no observable effect on the removal of Cr(VI) using magnetite nanoadsorbents. The small change in removal efficiency with initial concentration can be explained as follows. Initially the small decrease in removal efficiency is because the active sites of the adsorbent remain unchanged with change in the initial concentration. Accumulation of Cr(VI) ions occurs near the active sites which results a slight decrease in Cr(VI) removal. At high initial concentration of 50 ppm, the driving force for adsorption is very high due to concentration gradient in the adsorbent and adsorbate. This increases the mass transfer rate. So high removal efficiency was observed. After 50 ppm, the

adsorbent is saturated and desorption takes place and finally equilibrium is attained. The adsorption capacity showed a steady increase from 0.93mg/g to 5.73 mg/g with increase in the initial concentration. Fig. 4.8 represents the effect of initial concentration on Cr(VI) removal efficiency and adsorption capacity of magnetite nanoparticles.

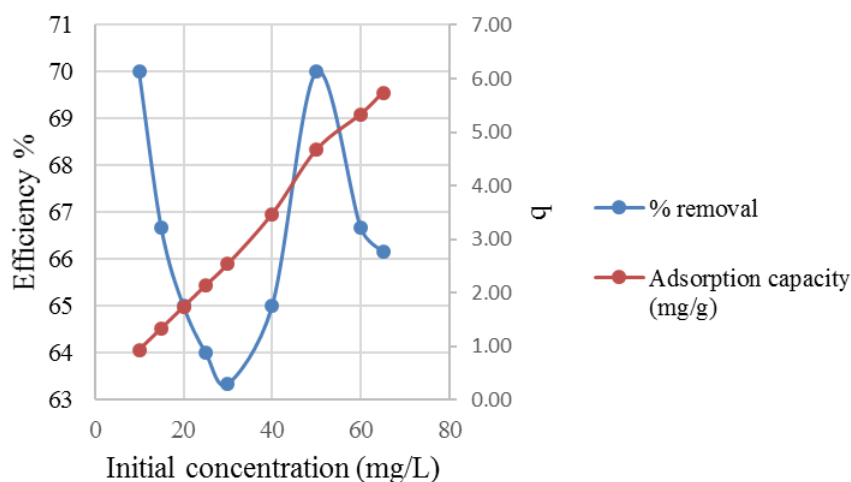


Fig. 4.8 Effect of initial concentration on adsorption using nanomagnetite

4.3.4 Effect of Time

To study the effect of contact time, 50 ppm of Cr(VI) solution of pH 2.0 was taken and 7.5 g/L of magnetite nanoadsorbent was added and shaken for various time ranging from 20 to 120 minutes. The effect of contact time studied at 303 K and 200 rpm shaking speed is shown graphically in Fig. 4.9. Initially as the contact time was increased from 20 to 40 minutes, there was a steady increase in percentage removal and the increase in percentage removal decreased as time elapsed and finally there was no observable change in the removal efficiency. Initial rapid increase in the percentage adsorption is due to the fact that external surface adsorption is predominating. Most of the active

sites are located at the exterior of magnetite nanoparticles which are occupied during the initial time. With time, no further adsorption has been observed and steady state was achieved at 90 minutes. Further increase in contact time had no influence in adsorption as reported in previous work (Yuan *et al.*, 2009). Adsorption capacity did not show remarkable change with time of adsorption eventhough a slight increase was observed with contact time.

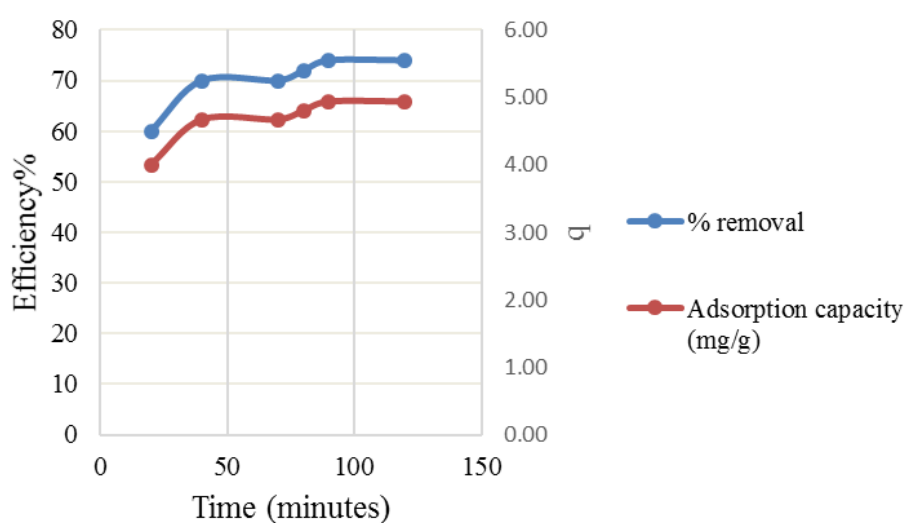


Fig. 4.9 Effect of time on adsorption of Cr(VI) using magnetite nanoparticles

4.3.5 Application of Response Surface Methodology for Cr(VI) Removal Using Magnetite Nanoadsorbents

The relationship between several explanatory variables and one or more response variables is explored using RSM. This method was developed in 1951 by George E.P. Box and K.B. Wilson. To obtain an optimal response a sequence of designed experiments is being used. A second order degree polynomial equation is used in RSM to develop the model equation. The four factors in the present study were designated as initial concentration (x_1), pH (x_2), time (x_3) and adsorbent dosage (x_4). They were prescribed in three levels

coded as +1 for high, 0 for intermediate and -1 for low value. In this study the analysis was carried out in coded units to eliminate statistical errors due to difference in scale of measurements. The range and level of parameters used in the design of experiments were obtained by conducting batch experiments. The range of variables chosen for experimental design of adsorption process is shown in Table 4.2.

Table 4.2 Coded levels of independent variables in Box-Behnken design using nanomagnetite

Variables	Actually coded levels			Δx_j (step change values)
	Low (-1)	Medium (0)	High (+1)	
Initial concentration, ppm (x_1)	10	30	50	20
Adsorbent Concentration, g/L (x_2)	5	7.5	10	2.5
pH (x_3)	2	6	10	4
Time, minutes (x_4)	20	70	120	50

Design of experiments using Box Behnken method under response surface methodology gave 27 combinations of four factors viz. pH, adsorbent dosage, initial concentration and time at temperature 303 K and shaking speed 200 rpm. The 27 sets are shown in the Table 4.3. E represents the calculated efficiency and P represents the efficiency predicted by the model.

Table 4.3 Design of experiments and experimental and predicted efficiency for adsorption of Cr(VI) using nanomagnetite

Sl. no.	Initial concentration, ppm	Adsorbent concentration, g/L	pH	Time, minutes	Final Concentration, ppm	$q = (C_0 - C_t)/m$, mg/g	$E\% = (C_0 - C_t) \times 100 / C_0$	P %
1	30	7.5	6	70	19.5	1.4	35.0	35.0
2	30	5.0	10	70	25.5	0.9	15.0	15.903
3	10	5.0	6	70	7.0	0.6	30.0	30.764
4	50	7.5	2	70	15.0	4.7	70.0	69.722
5	10	7.5	10	70	8.0	0.3	20.0	19.167
6	30	7.5	10	20	24.0	0.8	20.0	19.653
7	30	7.5	2	20	9.5	2.7	68.3	69.375
8	30	7.5	6	70	19.5	1.4	35.0	35.000
9	30	5.0	2	70	10.5	3.9	65.0	63.958
10	50	7.5	6	20	32.5	2.3	35.0	35.347
11	30	10.0	2	70	7.5	2.3	75.0	75.069
12	30	5.0	6	20	20.5	1.9	31.7	30.883
13	50	7.5	6	120	32.5	2.3	35.0	35.625
14	30	7.5	2	120	9.0	2.8	70.0	70.486
15	30	10.0	10	70	24.0	0.6	20.0	22.014
16	30	5.0	6	120	20.5	1.9	31.7	31.111
17	10	10.0	6	70	6.0	0.4	40.0	39.375
18	30	10.0	6	20	18.0	1.2	40.0	39.444
19	30	7.5	10	120	24.0	0.8	20.0	19.097
20	10	7.5	6	20	6.5	0.5	35.0	35.347
21	10	7.5	2	70	3.0	0.9	70.0	69.722
22	10	7.5	6	120	6.5	0.5	35.0	35.625
23	50	7.5	10	70	40.0	1.3	20.0	19.167
24	50	10.0	6	70	30.0	2.0	40.0	39.375
25	50	5.0	6	70	35.0	3.0	30.0	30.764
26	30	7.5	6	70	19.5	1.4	35.0	35.0
27	30	10.0	6	120	18.0	1.2	40.0	39.722

The estimated regression coefficients in uncoded units are shown in the Table 4.4.

Table 4.4 Coefficients of the model equation and t, p, (1-p) values for nanomagnetite

Factor	Regression Coefficients in uncoded units	t value	p value	significance level (1-p), %
β_0	74.11	55.885	0.000	>99
β_1	-0.0208	-0.000	1.000	0
β_2	2.6388	13.750	0.000	>99
β_3	-12.2153	-80.723	0.000	>99
β_4	-0.004166	0.444	0.665	>33
β_{11}	0.00347	0.296	0.773	>22
β_{22}	-0.0111	-0.148	0.885	>11
β_{33}	0.5815	19.811	0.000	>99
β_{44}	0.00013	0.739	0.474	>52
β_{12}	-1.037×10^{-16}	-0.000	1.000	0
β_{13}	2.1778×10^{-17}	0.000	1.000	0
β_{14}	1.187×10^{-19}	0.000	1.000	0
β_{23}	-0.1250	-2.305	0.040	>95
β_{24}	-1.231×10^{-17}	-0.000	1.000	0
β_{34}	-0.002088	-0.768	0.457	>54

The equation (4.1) represents the model equation for efficiency in uncoded terms.

$$\begin{aligned}
 Y = & 74.11 - 0.0208X_1 + 2.6388X_2 - 12.2153X_3 - 0.004166X_4 + 0.00347X_1^2 - 0.0111X_2^2 + 0.5815X_3^2 \\
 & + 0.00013X_4^2 - 1.037 \times 10^{-16} X_1X_2 + 2.1778 \times 10^{-17} X_1X_3 + 1.187 \times 10^{-19} X_1X_4 - 0.1250X_2X_3 \\
 & - 1.231 \times 10^{-17} X_2X_4 - 0.002088X_3X_4
 \end{aligned} \quad (4.1)$$

Here Y is the removal efficiency. From the model equation it is observed that efficiency is mostly influenced by pH (X_3) and adsorbent concentration (X_2), whereas initial concentration (X_1) and time (X_4) are the least influential terms affecting the adsorption of Cr(VI). The quadratic coefficient for pH and adsorbent concentration have a significance level >99%. The interaction of pH and adsorbent dosage as a higher level of significance >95%. Experimental versus predicted efficiency for Cr(VI) removal using magnetite nanoparticles is shown in Fig. 4.10. The predicted and experimental efficiency matched well with linear regression coefficient (R^2) = 0.998. The model is thus validated.

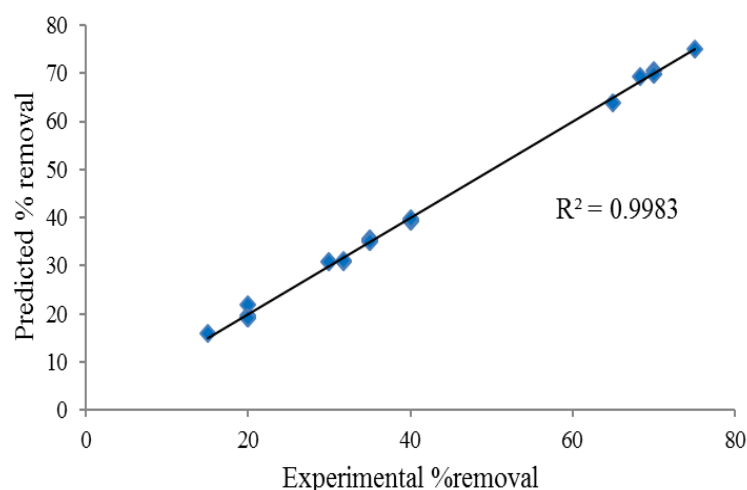


Fig. 4.10 Predicted versus experimental Cr(VI) removal efficiency

Analysis of variance of the models for Cr(VI) removal using magnetite nanoparticles is shown Table 4.5. Analysis of variance gives higher F value for regression coefficient as 513.85 and standard statistical table value is 2.6 which shows that the quadratic model from Box-Behnken design can navigate the design space well.

Table 4.5 Analysis of variance for efficiency of adsorption

Source	degrees of freedom	sum of squares	mean Square	F	P
Regression	14	8465.10	604.65	513.85	0
Linear	4	7890	145.908	1676.36	0
Square	4	567.88	141.969	120.65	0
Interaction	6	6.94	1.157	0.98	0.474
residual error	12	14.12	1.177		
lack of fit	10	14.12	1.412		
pure error	2	0	0		
Total	26				

4.3.6 Optimisation Using Response Surface Methodology

Optimisation was carried out using response optimiser of Minitab 16. Optimisation plot of Cr(VI) removal using magnetite nanoparticles is shown in Fig. 4.11. According to prediction by the model the optimum time for conducting the experiment was 120 minutes starting with an initial Cr(VI) concentration of 50 ppm. 10 g/L of magnetite nanoadsorbent was to be added and the solution pH was to be maintained at 2.0. Then the predicted removal efficiency by the model was 76.11%. Batch experiments were conducted with the conditions predicted by Box- Behnken design and a removal efficiency 73% was obtained. This result did not show much variation from the predicted value.

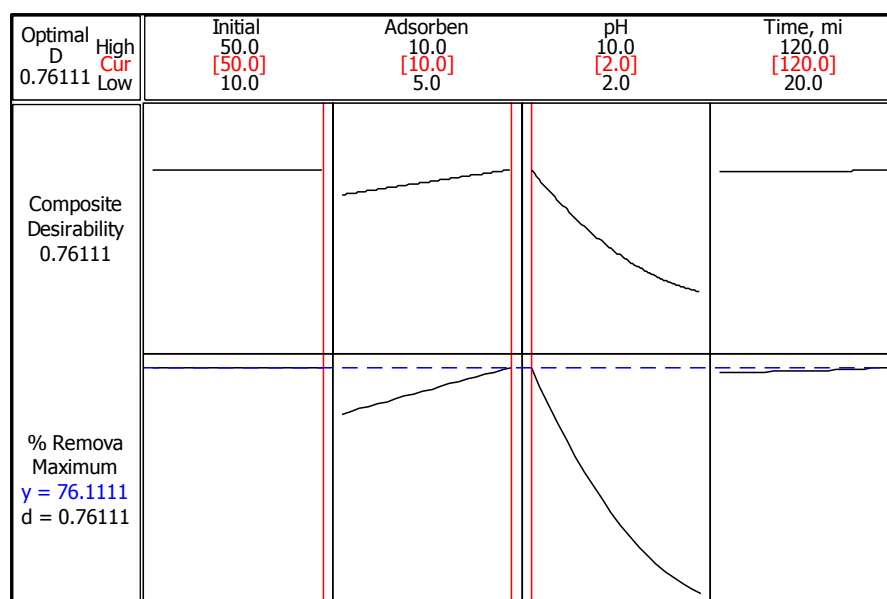
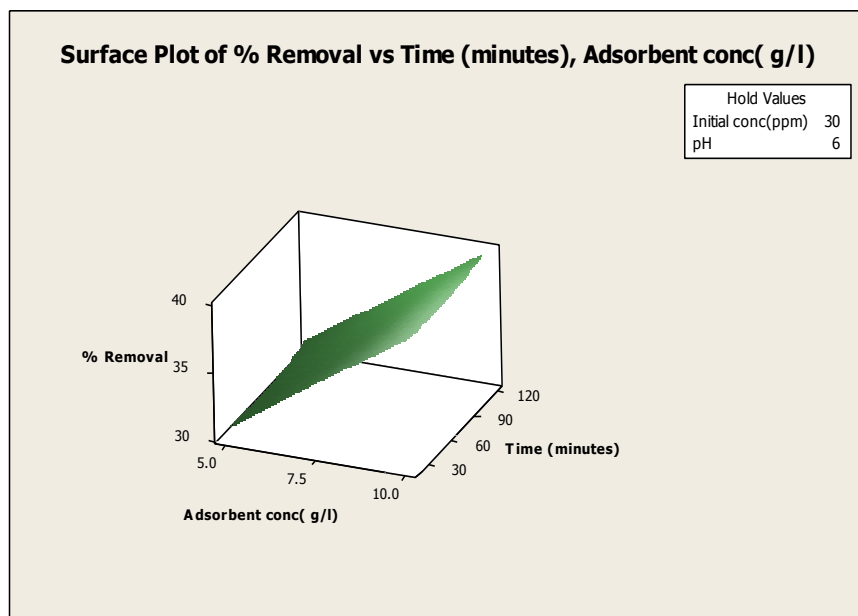
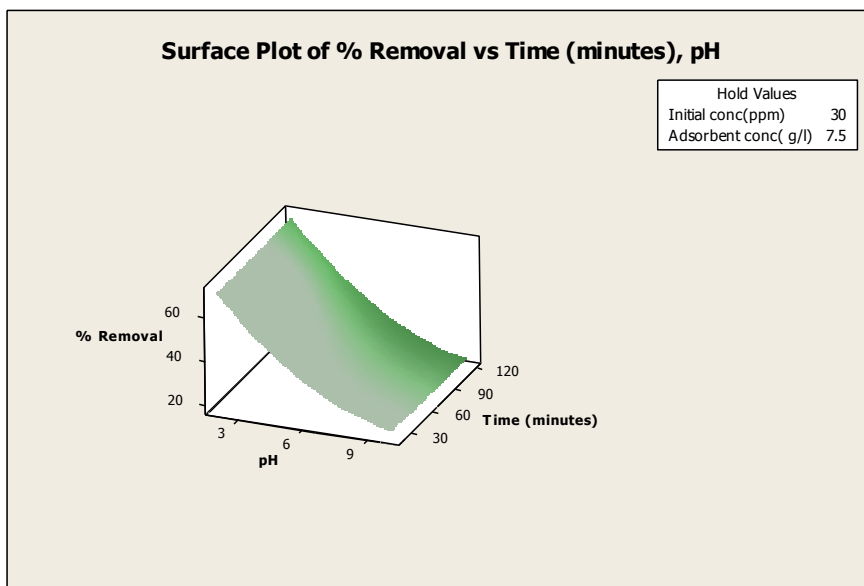


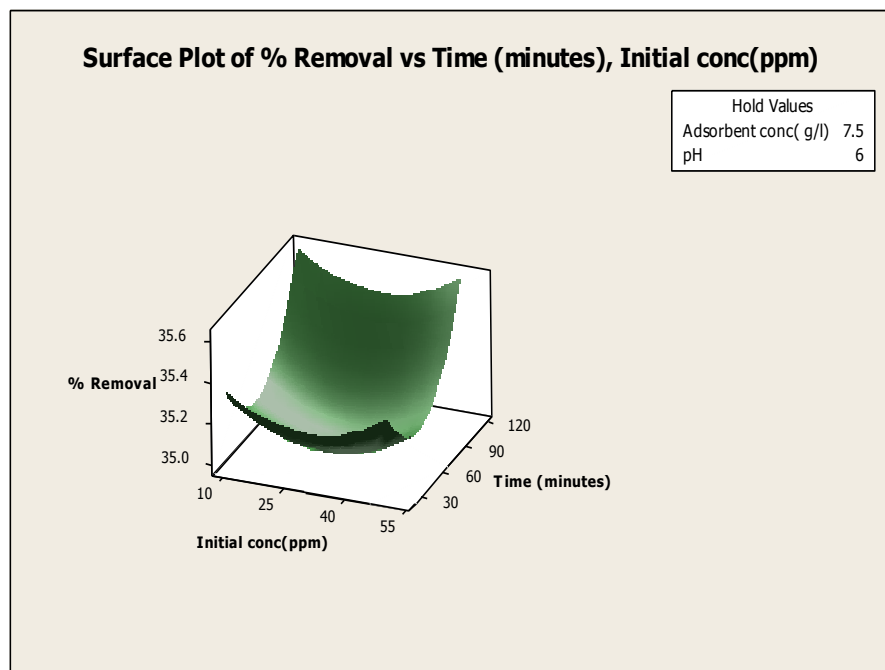
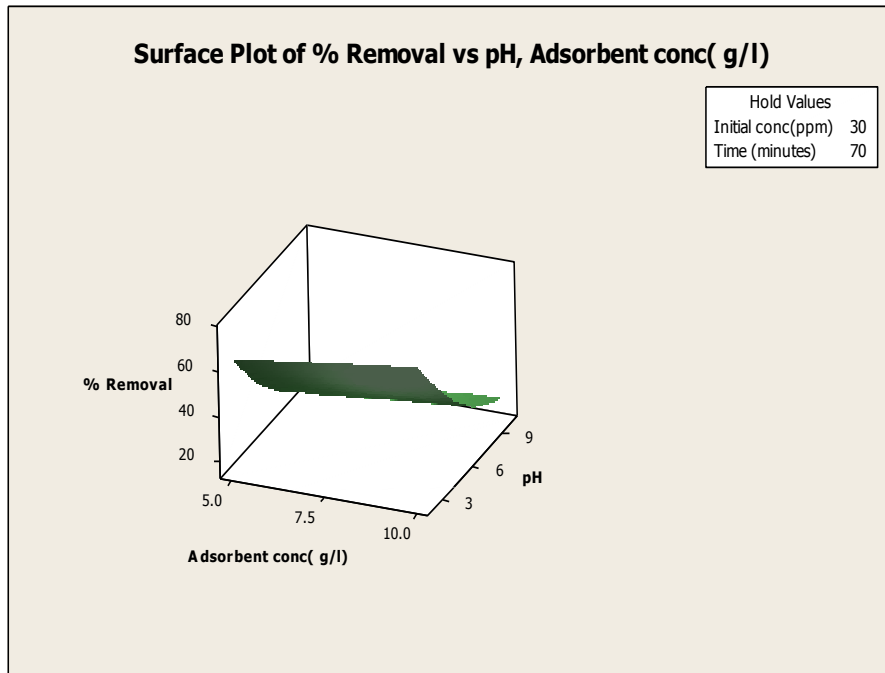
Fig. 4.11 Optimisation plot for Cr(VI) removal using magnetite nanoparticles

4.3.7 Combined Effect of Variables on Adsorption of Cr(VI) Using Magnetite Nanoadsorbents

If a process is influenced by more than one variables, then their combined effect on the process is to be studied. The surface plots of response surface methodology were used to describe the combined effects of the parameters affecting adsorption. The effect of time of shaking and pH represented graphically (Fig. 4.12) shows that adsorption is favourable at low pH. The removal efficiency decreased with increase in the solution pH. The effect of time on removal efficiency was very less according to the model equation. However, the removal at first showed a small increase with time and thereafter the change in percentage removal was less. The system reached steady state after certain time. With increase in adsorbent dosage, the removal of Cr(VI) first increased and attained a maximum and then decreased. With increase in initial concentration the Cr(VI) removal first decreased and then increased.

The combined effect of adsorbent dosage and pH was mostly influencing the percentage removal as given by the model. The combined effect of pH and time was nextly influencing the percentage removal. All other combinations of parameters were leastly affecting the response.





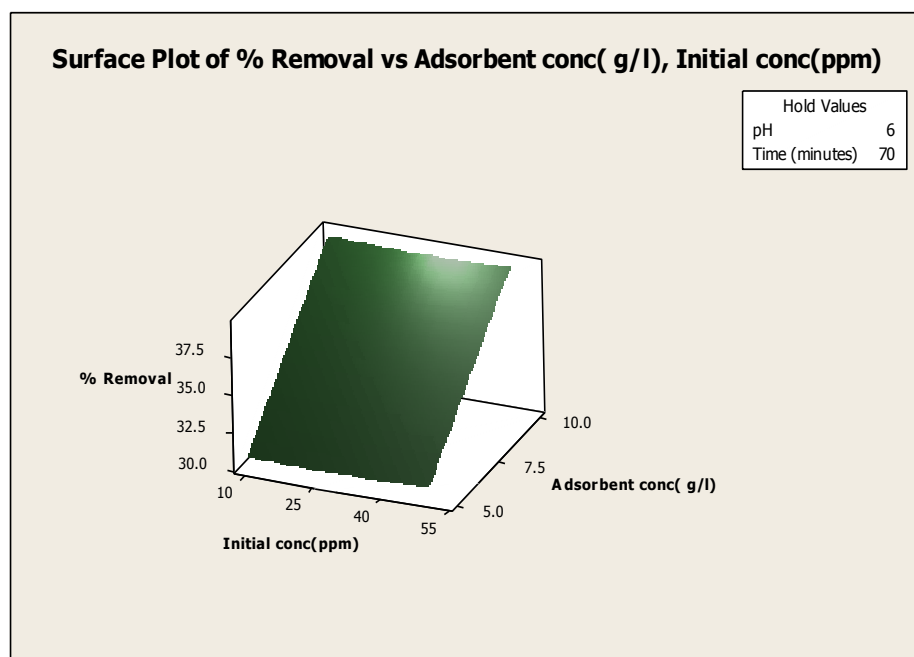
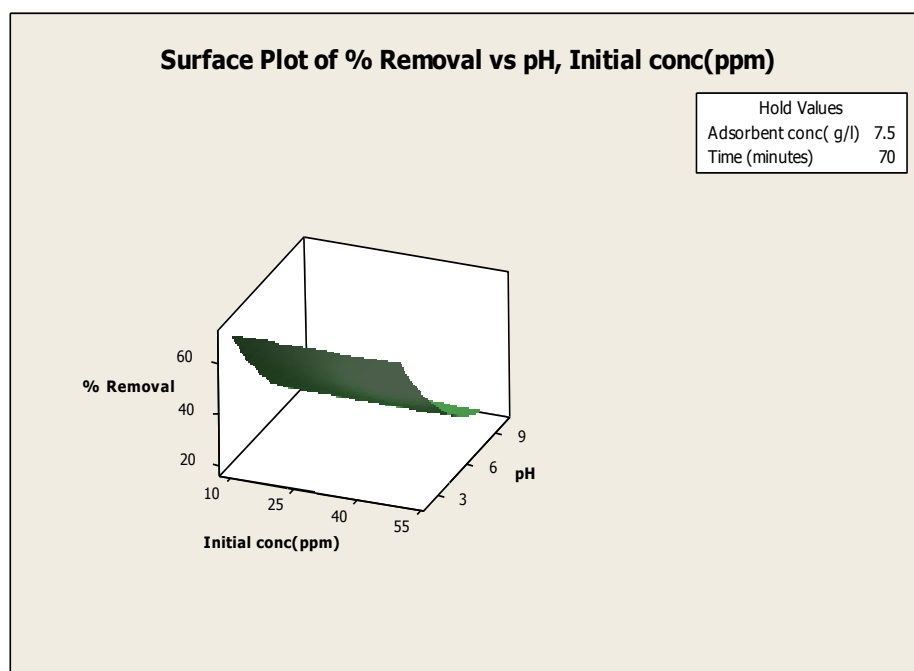


Fig. 4.12 Combined effect of variables on adsorption of Cr(VI) using magnetite nanoparticles

4.3.8 Characterisation of Magnetite Nanoparticles

Scanning electron microscopy equipped with energy dispersive X-ray spectroscopy was used for determining the morphological characteristics and elemental composition of synthesised magnetite nanoparticles. X-ray diffraction pattern gives the average grain size of the synthesised particles. Thermal stability of the synthesised particles were analysed using thermogravimetric analyser.

4.3.9 Scanning Electron Microscopy Equipped with Energy Dispersive X-ray Spectroscopy

SEM image of magnetite nanoparticles at various magnification ranges are shown in the Fig. 4.13. From the SEM image it is clear that the synthesised magnetite nanoparticles were agglomerated in nature. The SEM image of synthesised magnetite nanoparticles matched well to those reported in the previous literature (Giri *et al.*, 2011). Further the particles were of nonuniform size and shape.

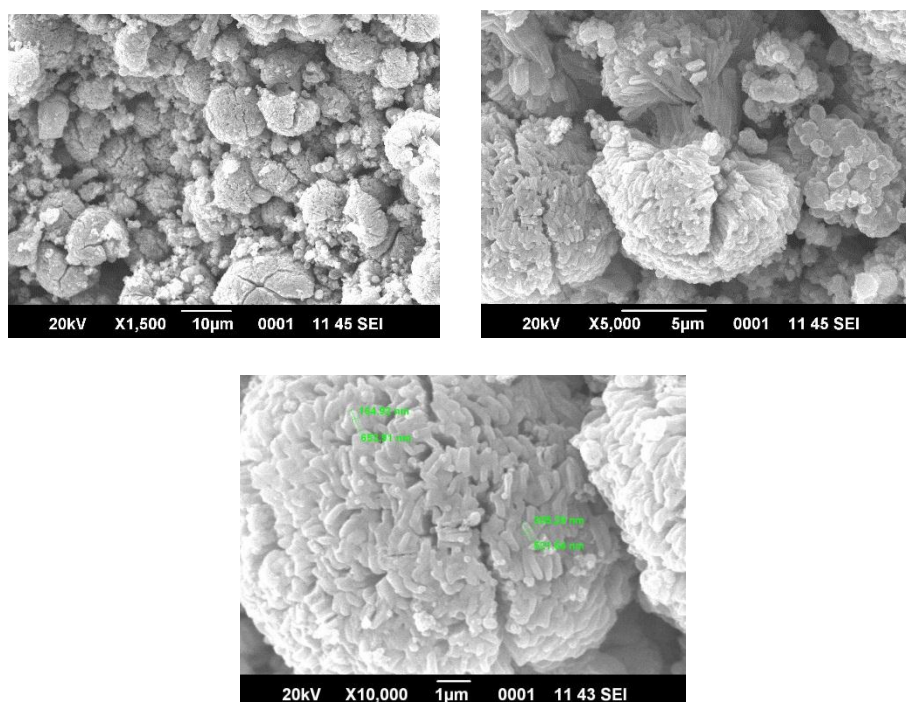


Fig 4.13 SEM of magnetite nanoparticles

EDX showed that the synthesised particles contain only iron and oxygen. The mass fraction of iron in the mixture was 80.62% and that of oxygen was 19.38%. The presence of other impurities was not observed from EDX data. The elemental composition of synthesised magnetite nanoparticles is shown in Table 4.6.

Table 4.6 Elemental composition of magnetite nanoparticles

Element	(keV)	Mass%	Atom%	K
O K	0.525	19.38	45.63	0.4247
Fe K	6.398	80.62	54.37	1
Total		100	100	

EDX of magnetite nanoparticles is shown in Fig. 4.14.

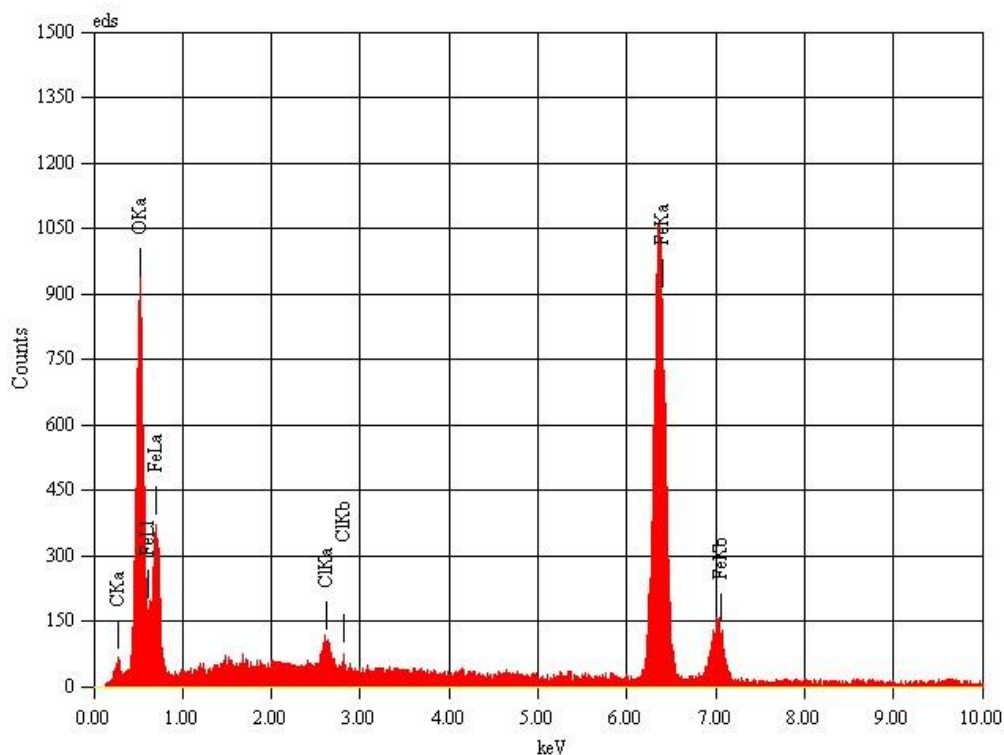


Fig. 4.14 EDX of magnetite nanoparticles

4.3.10 Characterisation Using X-ray Diffraction

The crystal structure of synthesised particles was analysed using X-ray diffraction. Sharp peaks were seen in the X-ray diffraction pattern of prepared magnetite nanoparticles. The d values (\AA) of diffraction peaks were 3.68 (438), 2.69 (1705), 2.5 (1544), 2.20 (452), 1.84 (681), 1.69 (818), 1.48 (576), 1.45 (548), 1.31 (234). Position and intensity of diffraction peaks showed reasonable similarity with the standard data for magnetite (JCPDS-19-0629). The additional peaks found in the X-ray diffraction spectrum is be due to presence of maghemite ($\Upsilon\text{-Fe}_2\text{O}_3$) or alpha iron ($\alpha\text{-Fe}$) which interferes with the results obtained from x-ray diffraction spectrum (Giri *et al.*, 2011). The average particle size of nanoparticles was calculated using Deybe-Scherrer formula. Using Scherrer equation the average grain size of magnetite nanoparticles was calculated corresponding to highest peak in XRD pattern and obtained as 28.26 nm. The d-spacing and 2 theta values of synthesised magnetite nanoparticles is shown in the Table 4.7.

Table 4.7 d spacing and 2 θ values of synthesised magnetite nanoparticles

d-spacing, Angstrom	2 θ , degree
3.68	24.13
2.70	33.14
2.52	35.62
2.20	40.85
1.84	49.44
1.69	54.04
1.60	57.46
1.48	62.4
1.45	63.97
1.31	71.9
1.25	75.46

XRD spectrum of magnetite nanoparticles is shown in Fig. 4.15

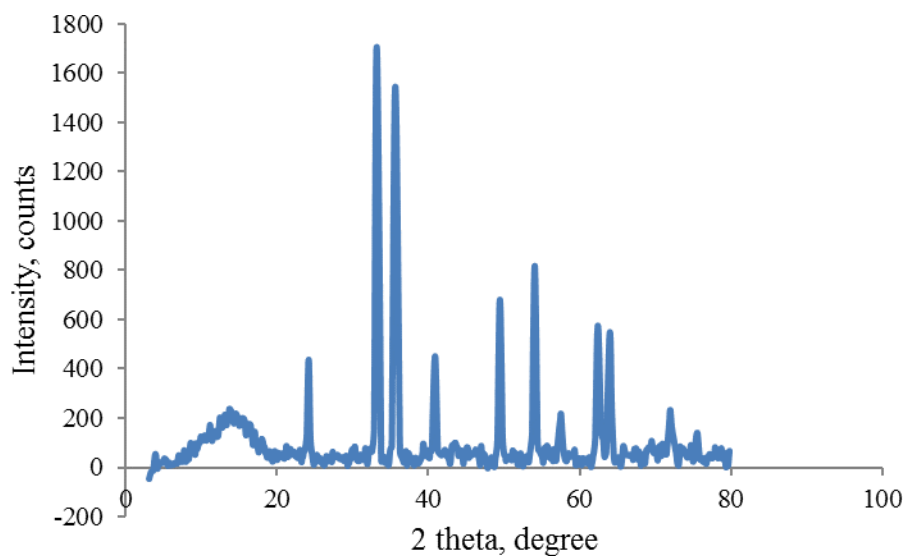


Fig. 4.15 XRD of magnetite nanoparticles

4.3.11 Thermogravimetric Analysis

The thermal stability of synthesised magnetite nanoparticles was analysed using thermogravimetric analyser. Nitrogen atmosphere was maintained for the study. The sample was heated at the rate of 5 ° per minute from room temperature to 600 °C. The temperature and weight were noted. Fig. 4.16 represent the weight loss for a specified temperature range. The weight loss will be negligible for a thermally stable material. The initial weight loss is due to the removal of moisture present in the particles. Weight decreases rapidly after 200 °C. This is because the crystal water is desorbed in the gel. Final weight loss is due to decomposition of gel to form iron oxides at higher temperature. The thermogram is in close resemblance with the that reported in previous literature (Cai and Wan, 2007)

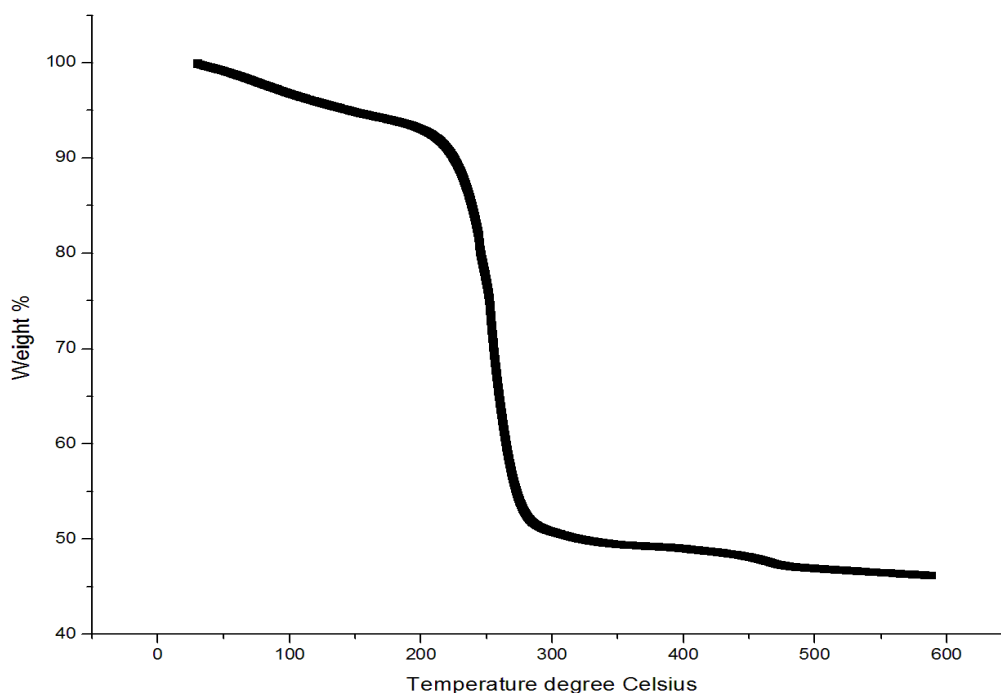


Fig. 4.16 TGA of magnetite nanoadsorbents

4.4 Batch Adsorption of Cr(VI) Using Chitosan/Halloysite Clay Nanocomposite Films

Due to the low removal efficiency and adsorption capacity of nanokaolinite clay and magnetite nanoparticles, chitosan/halloysite clay nanocomposite was developed for removal of Cr(VI) from aqueous solution. The nanocomposite film was prepared as described in chapter 3. The effect of pH, adsorbent dosage, temperature, initial concentration and time of adsorption is discussed in detail in the present section. Kinetics of adsorption, isotherm and thermodynamic studies using novel chitosan/halloysite clay nanocomposite for Cr(VI) adsorption were analysed. Desorption studies were also conducted batch wise. The combined effect of variables was studied using response surface methodology and the optimum conditions were determined for Cr (VI) removal

using the response optimiser of Box-Behnken design. In all the batch experiments, films of constant diameter 6.5 mm and thickness 0.2 mm was used.

4.4.1 Effect of pH on Adsorption

The effect of pH on adsorption between pH 2 to 10.8 is shown in Fig. 4.17. At pH 3.0, the percentage removal was maximum. Adsorption capacity at pH 3.0 was 37.5 mg/g which was also maximum. At pH 2.0 the removal efficiency of Cr(VI) was 72 % and as pH was increased the adsorption efficiency also increased up to pH 3.0 and further percentage removal decreased with increase in pH. The study showed that the optimum pH for adsorption was 3.0 and all other studies were conducted at this pH. At pH 10.8 the removal efficiency reached 14%. pH is an important factor that controls the surface charge of an adsorbent and functional group dissociation of active sites of the adsorbent. The metal speciation is controlled by the pH of the solution. The adsorption capacity is also greatly influenced by the solution pH. Mechanism of adsorption is electrostatic attraction followed by reduction of Cr(VI) to Cr(III) at pH 3.0. Cr(VI) exists as CrO_4^{2-} , $HCrO_4^-$, $Cr_2O_7^{2-}$, $Cr_3O_{10}^{2-}$ etc. in pH range 2-3. So, at this pH adsorption of negatively charged chromate ions on the surface of positively charged surface of adsorbent is maximum. The hydroxyl, amino, carboxylic and carbonyl group present in the nanocomposite films are positively charged at low pH and negatively charged at higher pH. As the solution pH increases formation of hydroxyl (OH^-) groups takes place and adsorption of chromate ions become competitive in this pH range. Also at higher pH metal precipitation occurs. Therefore, adsorption capacity and efficiency of Cr(VI) removal decreases in this pH range.

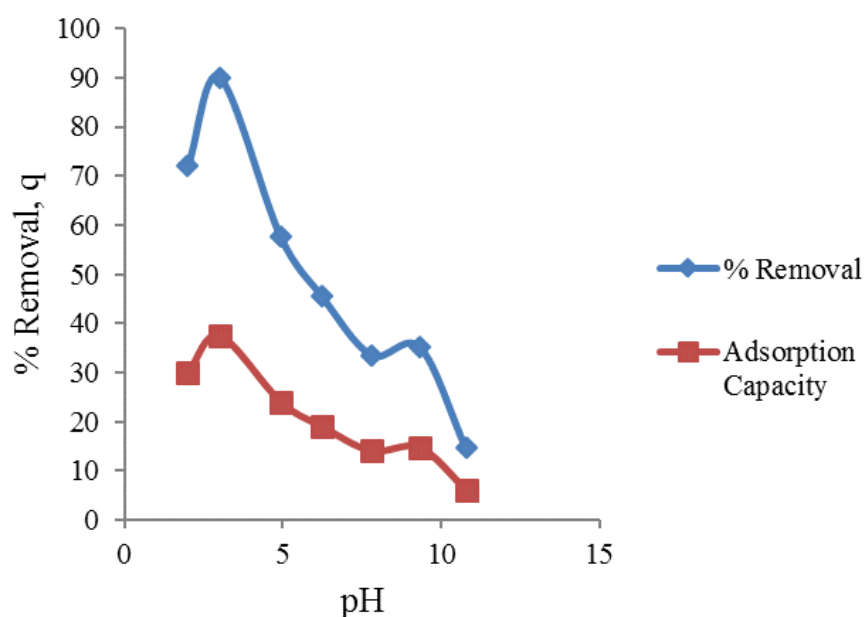


Fig. 4.17 Effect of pH on the adsorption of Cr(VI) using chitosan/halloysite clay nanocomposite adsorbent

4.4.2 Effect of Adsorbent Dosage

The effect of adsorbent weight was studied at pH 3.0. The Cr(VI) removal first increased with increase in adsorbent dosage and reached a maximum of 92% at adsorbent dosage of 1.7 g/L and then decreased. Meanwhile adsorption capacity showed a decreasing trend with increase in adsorbent weight. Maximum adsorbent capacity was 32.725 mg/g at adsorbent dosage of 0.2 g/L. The solution ion concentration drops to a lower value at higher adsorbent dosage and at lower values of q the adsorbent is unsaturated (Zhou *et al.*, 2009). At 2.0 g/L saturation was attained and hence no further removal of Cr(VI) was achieved. As adsorbent dose was increased from 0.2 to 1.7 g/L, there was an increase in the number of active sites available for adsorption and hence removal efficiency was increased. Above 1.7 g/L there was aggregation of adsorbent particles since there was no change in speed of agitation. So, the percentage Cr(VI) removal decreased at adsorbent dosage

higher than 1.7 g/L. When the adsorbent dose was increased to 2.0 g/L, the nanocomposite film was saturated. An equilibrium was attained between adsorbent and adsorbate. The percentage removal of 80% was attained at 2.0 g/L and it remained unchanged when the adsorbent dosage was increased to 2.5 g/L. Presence of halloysite nanoclay in the nanocomposite film enhances the adsorption capacity and removal efficiency of the adsorbent. Fig. 4.18 represents the effect of adsorbent dosage on Cr(VI) removal and adsorption capacity.

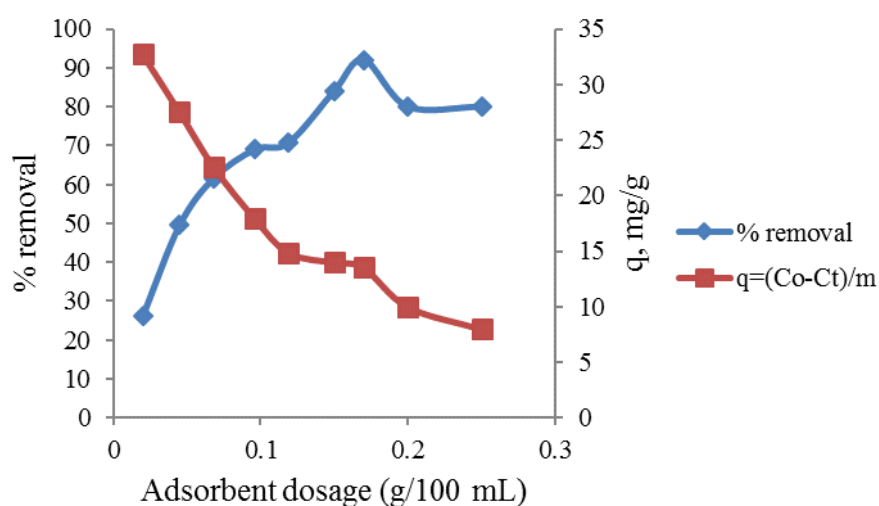


Fig. 4.18 Effect of nanocomposite film dosage on the removal efficiency and adsorption capacity of nanocomposite film

4.4.3 Effect of Temperature on Adsorption of Cr(VI) Using Nanocomposite Films

The effect of temperature on the percentage Cr(VI) uptake and adsorption capacity is shown in Fig. 4.19. The Cr(VI) uptake efficiency and adsorption capacity increased up to 60 °C and reached a maximum and then decreased when the temperature was increased from 30 to 123 °C. The increase in adsorption capacity and removal efficiency with temperature is because the adsorption of Cr(VI) using nanocomposite films is endothermic.

At high temperature desorption of Cr(VI) takes place and as a result efficiency and adsorption capacity decreases at temperature greater than 60 °C.

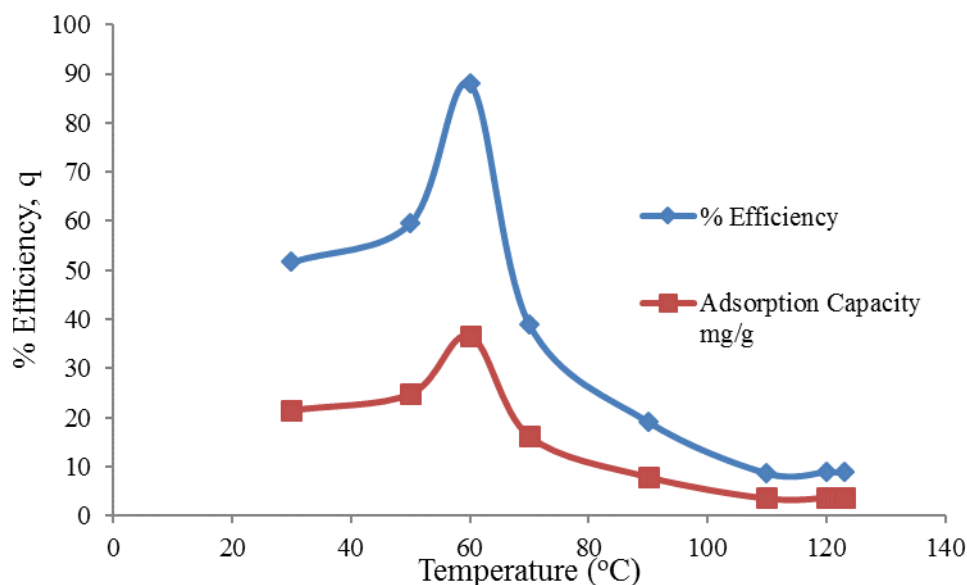


Fig. 4.19 Effect of temperature on adsorption using nanocomposite films

4.4.4 Effect of Initial Concentration on Adsorption

Initial concentration is an important factor that controls the adsorption process. In the present study, initial concentration was varied from 5.6 to 90 ppm keeping all other parameters constant. Initially there was a small decrease in percentage Cr(VI) uptake from 54 to 40% and after 26 ppm the removal efficiency rapidly increased from 40% to 83% and further increase in removal efficiency was less and reached 88.5% at 70 ppm. After 70 ppm there was no appreciable change in Cr(VI) uptake and equilibrium was reached. Adsorption capacity showed a steady increase from 5.1 mg/g to 133.3 mg/g with increase in initial concentration. When the initial concentration increases the concentration gradient within the system increases and hence the driving force increases. As a result the percentage of Cr(VI) uptake increases. After a certain value of initial concentration, the adsorbent is saturated with the adsorbate and adsorption ceases.

Hence removal efficiency shows no further change. Fig. 4.20 depicts the effect of initial concentration on adsorption using nanocomposite films.

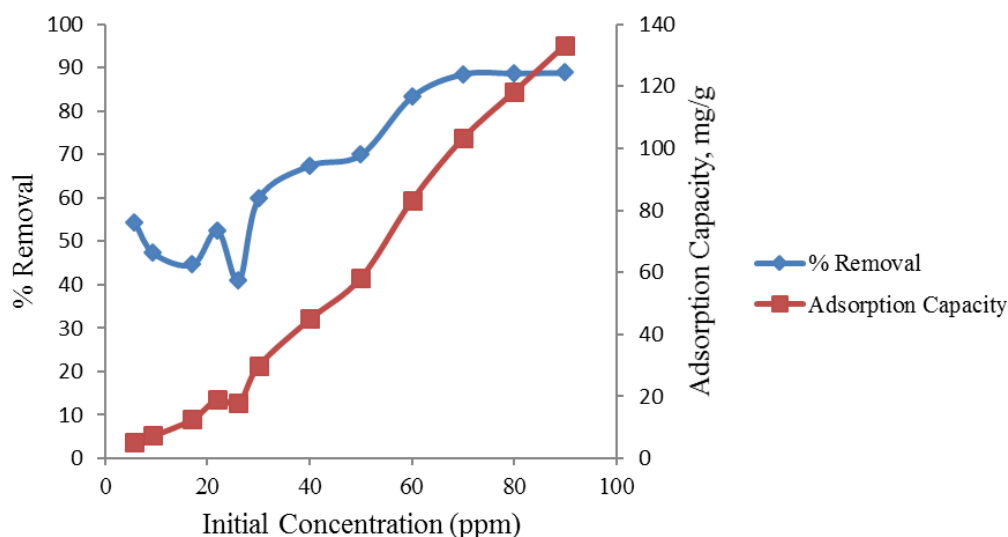


Fig. 4.20 Effect of initial concentration on adsorption of Cr(VI) using nanocomposite films

4.4.5 Effect of Contact Time

The effect of contact time on percentage Cr(VI) uptake and adsorption capacity is shown in Fig. 4.21. For an economical wastewater treatment process contact time is an important operational parameter. The equilibrium contact time was determined by batch experiments by varying the time of adsorption from 15 to 100 minutes keeping all other parameters constant. The percentage removal and adsorption capacity has been determined. Initially the percentage uptake increased between 15 minutes to 70 minutes. At 70 minutes shaking time, 90% removal of Cr(VI) has been observed and the adsorption capacity at this time was 37.5 mg/g. Initially the surface coverage of adsorbent is low and as time elapses the surface coverage increases with more active sites are occupied by adsorbate. As time of adsorption increases the surface of the adsorbent reaches saturation limit (Zhou *et al.*, 2009). As the active sites

are saturated there is no increase in metal uptake with further increase in time beyond 70 minutes. Maximum adsorption capacity is attained at equilibrium time. Thus equilibrium time for batch adsorption for Cr(VI) removal in the present study is 70 minutes.

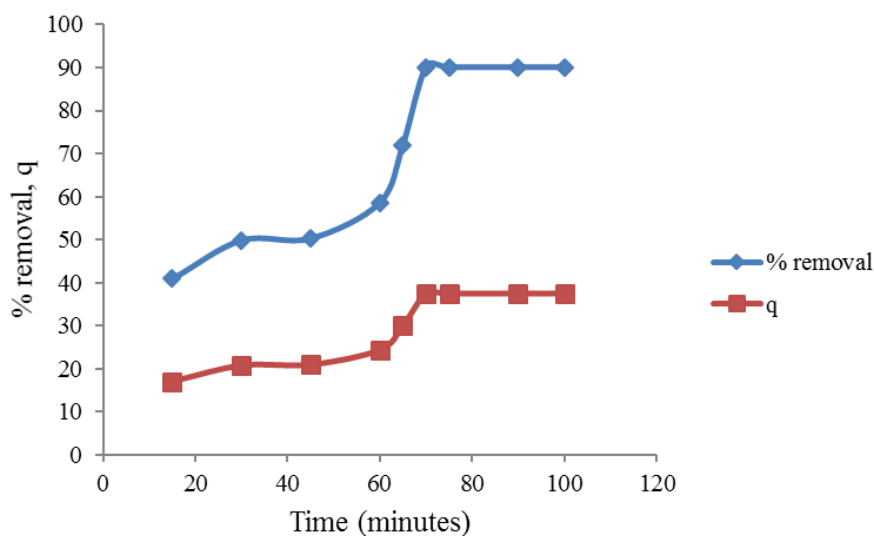


Fig 4.21 Effect of time on adsorption of Cr(VI) onto chitosan/halloysite nanocomposite films

4.4.6 Sorption Kinetics

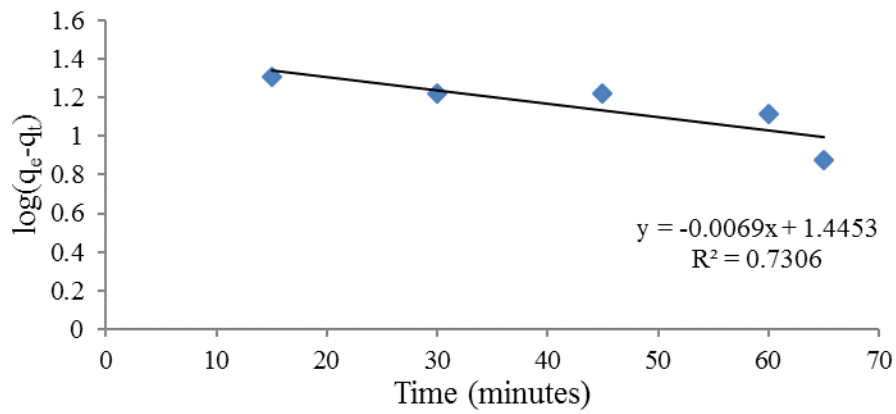
In order to investigate the controlling mechanism of adsorption, kinetic studies were conducted by conducting the adsorption experiments at different time intervals and measuring the final concentration in UV-VIS spectrophotometer at 540 nm (Annexure IV). Four kinetic models namely, Lagergren model (pseudo first order), pseudo second order model, second order and intra particle diffusion model were analysed in the present study which is shown in the Fig. 4.22. The kinetic constants and correlation coefficients for the four models are presented in the Table 4.8. The linear correlation coefficient for pseudo first order, second order and intra particle diffusion model were very low. For pseudo second order kinetic model the

correlation coefficient was 0.882. This indicates that the data fits more to pseudo second order kinetics. Meanwhile, the q_e experimental and q_e calculated values showed large deviation for pseudo first order and second order models which indicated that these two models were poor fit for adsorption of Cr(VI) on the surface of nanocomposite films. The q_e experimental values were almost consistent with q_e calculated values for pseudo second order kinetics. These show that the adsorption of Cr(VI) using nanocomposite films is pseudo second order (Chen *et al.*, 2013). For wastewater treatment by adsorption of pollutants, pseudo second order kinetic models have been used now-a-days. In pseudo second order kinetic model the rate controlling step involved is the chemical sorption involving valence forces through sharing or exchange of electrons between sorbent and sorbate (Ho, 2006; Sonia *et al.*, 2011). The pseudo second order rate constant was obtained as $0.001483 \text{ g mg}^{-1} \text{ min}^{-1}$. The low value of rate constant indicates that the adsorption is slower which is due to heterogeneous surface reaction or intraparticle diffusion (Mandeep *et al.*, 2010).

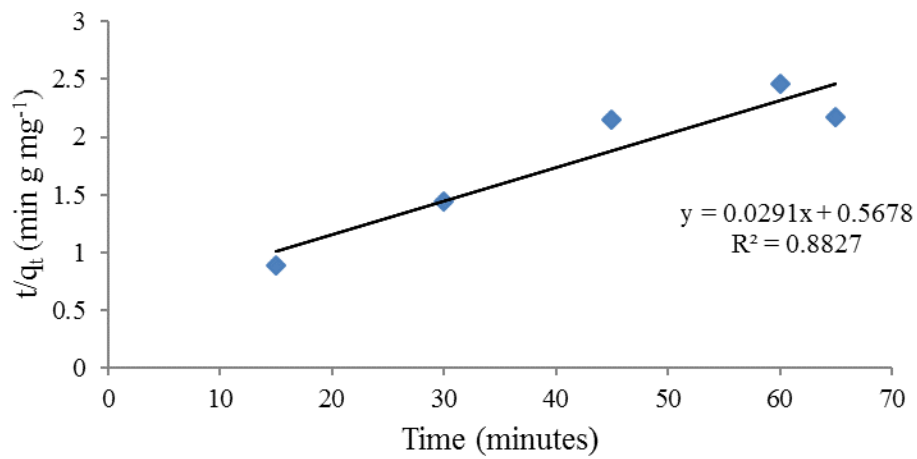
Table 4.8 The kinetic constants and correlation coefficients for adsorption of Cr(VI)

$q_e \text{ exp, mg/g}$	Pseudo first order			Pseudo second order			Second order			Intraparticle diffusion	
	$q_e \text{ cal}$	R^2	$K, \text{ min}^{-1}$	$q_e \text{ cal}$	R^2	$K_1, \text{ g mg}^{-1} \text{ min}^{-1}$	$q_e \text{ cal}$	R^2	$K_2, \text{ g mg}^{-1} \text{ min}^{-1}$	R^2	$K_d, \text{ mg g}^{-1} \text{ min}^{-1/2}$
37.5	4.24	0.73	0.0138	34.48	0.882	0.001483	50	0.622	0.001	0.794	2.515

Pseudo first order



Pseudo second order



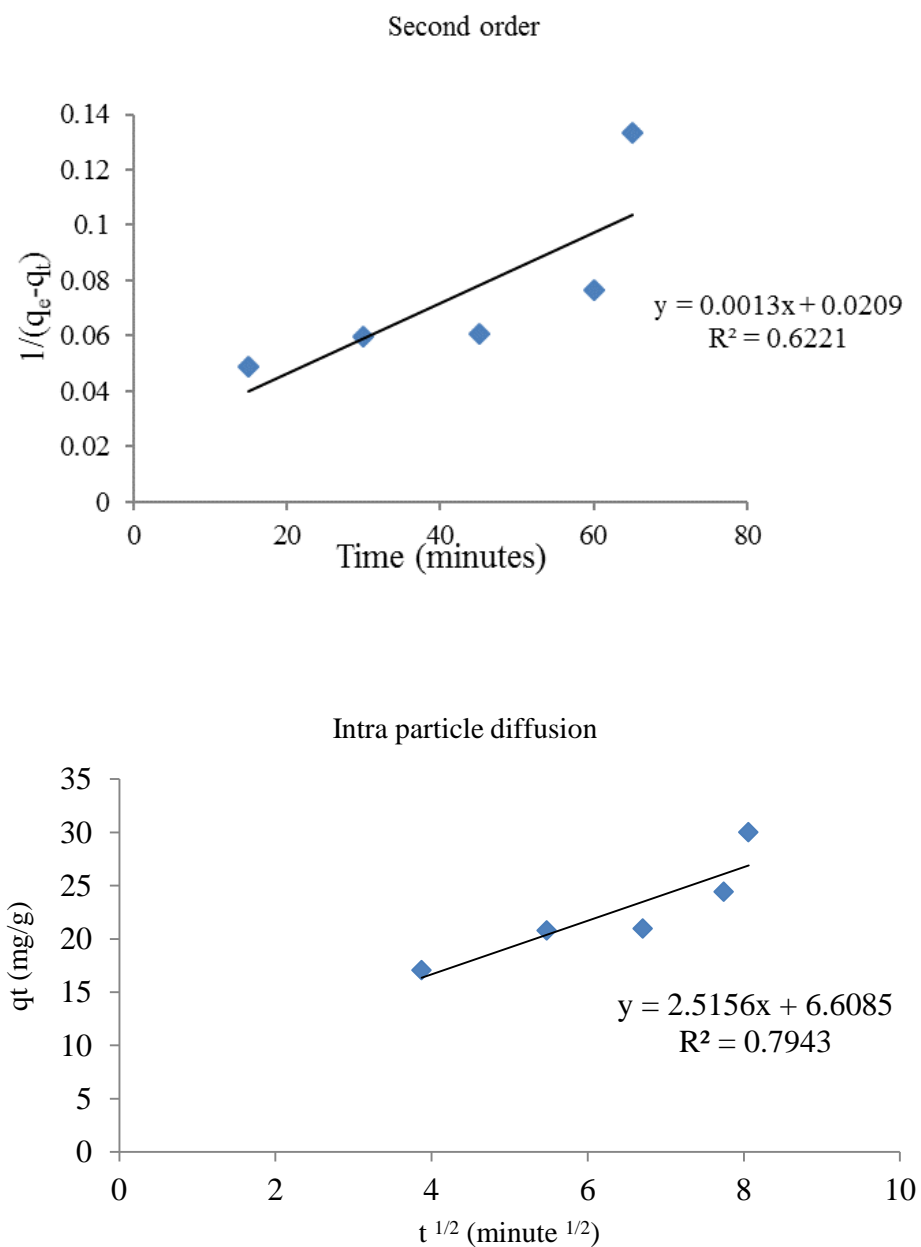


Fig. 4.22 Kinetics of adsorption of Cr(VI) using nanocomposite films- pseudo first order, pseudo second order, second order and Intra particle diffusion

4.4.7 Adsorption Isotherm Studies

Langmuir and Freundlich isotherms were analysed using the equilibrium data for Cr(VI) adsorption using nanocomposite film as adsorbent (Annexure IV). The Freundlich and Langmuir plots are shown in Fig. 4.23. The Langmuir and Freundlich constants are represented in the Table 4.9. Langmuir and Freundlich plots had R^2 as 0.959 and 0.926, respectively. So the equilibrium data was fitted more to Langmuir Isotherm model. This indicates that adsorption occurs in monolayer or at certain fixed localized sites of the adsorbent. When compared to Freundlich model, Langmuir model possess maximum adsorption capacity of 26.178 mg/g which is high when compared to conventional adsorbents reported in previous literature. Aydin and Aksoy (2009) reported that the adsorption of Cr(VI) on chitosan followed Langmuir isotherm and the maximum adsorption capacity was 7.943 mg/g at room temperature and 5.663 mg/g at 50 °C which is less when compared to chitosan/nanofilm adsorbent. Therefore impregnation of halloysite nanoclay on chitosan increases the adsorption capacity and hence is more beneficial for Cr(VI) removal. Rojas *et al.*, (2005) showed that the adsorption of Cr(VI) on crosslinked chitosan followed Langmuir model with an adsorption capacity of 215 mg/g. The high adsorption capacity of nanocomposite film when compared to other adsorbents indicates that the specific surface area, pore volume and average pore width also play a key role on adsorption of Cr(VI) (Mandeep *et al.*, 2010). A dimensionless separation factor R_L indicates whether the adsorption is favourable or not. Value of $R_L < 1$ indicates that adsorption is favourable and $R_L > 1$ indicates unfavourable adsorption (Cho *et al.*, 2012). Here in the present work C_0 taken as 5.693 ppm which was the lowest initial concentration taken for isotherm study, R_L was obtained as 0.54. This indicates that adsorption is favourable. The value of R_L was between 0

and 1 for all initial concentrations in the adsorption study. Eventhough saturation of adsorbent at high Cr(VI) concentration occurs, very low weight of chitosan based nanocomposite films are required for the removal of Cr(VI) from water (Rojas *et al.*, 2005).

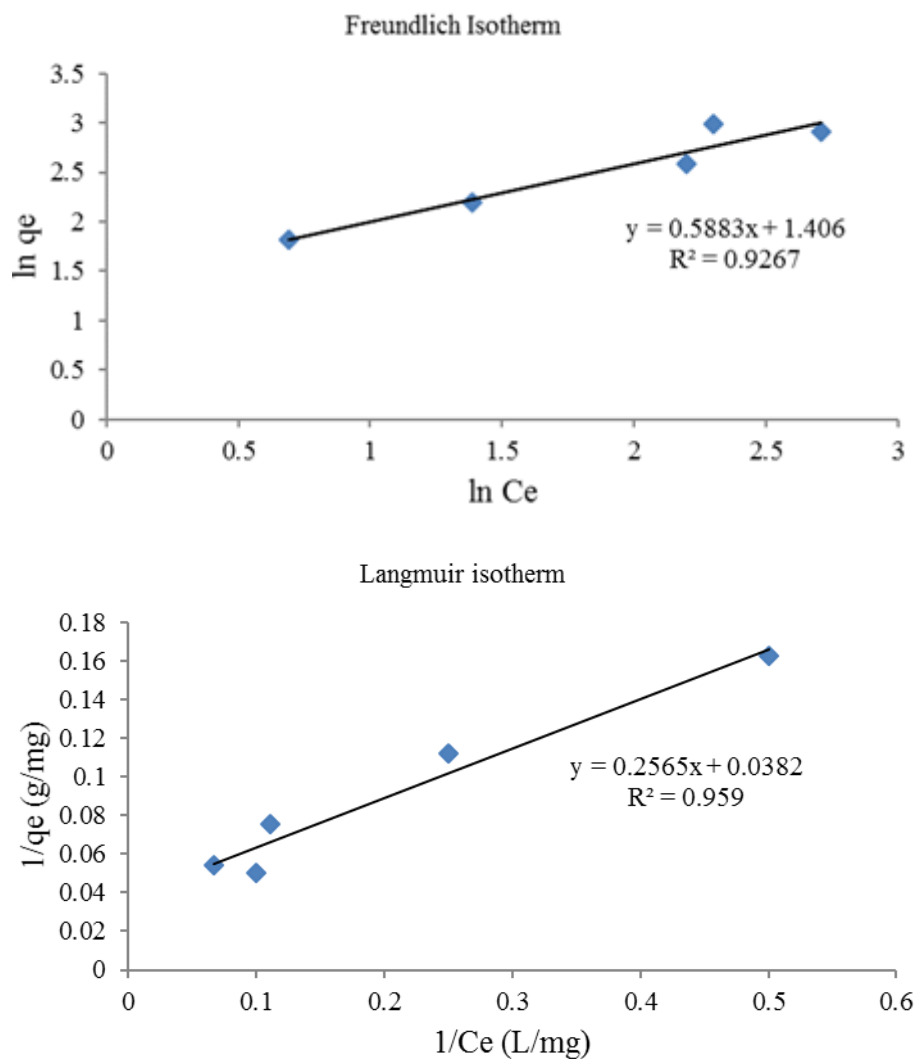


Fig. 4.23 Freundlich and Langmuir isotherm of Cr(VI) adsorption using nanocomposite films

Table 4.9 Equilibrium parameters for adsorption of Cr(VI) on nanocomposite film

Langmuir Isotherm			Freundlich Isotherm		
q_m , mg/g	b , L/mg	R^2	K_f , mg/g(mg/L) ⁿ	n	R^2
26.178	0.148	0.959	4.079	1.7	0.926

4.4.8 Thermodynamics of Adsorption of Cr(VI) Using Nanocomposite Films

From the batch experiments (Annexure IV), thermodynamic parameters were evaluated. The negative values of ΔG indicates that the adsorption process is favourable and this also indicates that the process is spontaneous in nature. The increase in the values of magnitude of Gibbs free energy change shows that there is increase in spontaneity of the adsorption process with temperature. Above 60 °C removal of Cr(VI) was decreased. ΔG becomes positive above 60 °C which indicates that the adsorption is not feasible above this temperature. The enthalpy change and entropy change of the process were determined graphically shown in the Fig. 4.24.

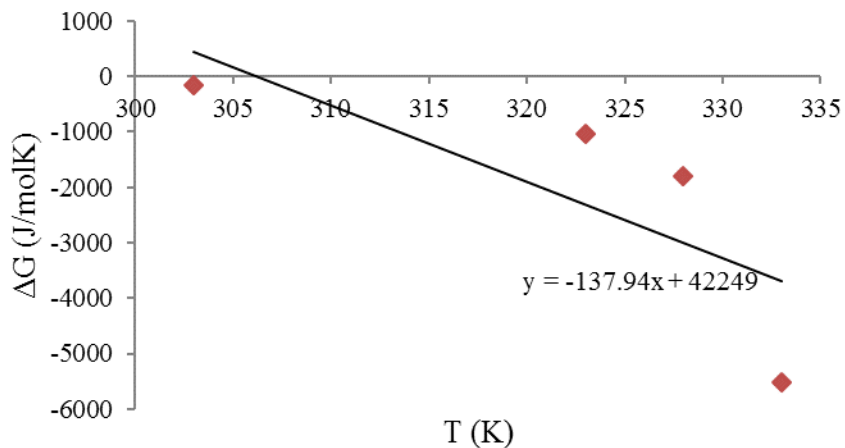


Fig. 4.24 Free energy change of adsorption of Cr(VI) using chitosan/halloysite nanoclay adsorbent versus temperature

The positive value of ΔH shows that the adsorption is endothermic and positive value of ΔS indicates that the metal ion has good affinity towards the adsorbent (Pandey and Mishra, 2011). Also positive value of entropy change suggests the increase in disorder at the solid-solution interface during the binding of metal ion into the active site of the adsorbent. Before adsorption the randomness of Cr(VI) ions near the surface of nanocomposite film is very less and during adsorption the ratio of Cr(VI) interacting to free Cr(VI) ions in the solution will be higher. The distribution of rotational and translational energy among metal ions increase during adsorption. As a result entropy change increase during adsorption. Positive value of entropy change indicates that the adsorption is favourable. Table 4.10 represents the thermodynamic parameters of adsorption.

Table 4.10 Thermodynamic parameters of nanocomposite film

T, K	K	ΔG , J/mole	ΔH , J/mole	ΔS , J/mole K
303	1.067996	-166	42249	137.9
323	1.473778	-1041		
328	1.941176	-1809		
333	7.333333	-5516		

4.4.9 Desorption Studies

For application of adsorbents in wastewater treatment plant, there should be methods for reuse of spent high cost adsorbent. The advantage of nanostructured materials is that its functionality can be retained after multiple use (Chen *et al.*, 2013). In the present work alkali solution has been used for desorption experiments. Desorption study of nanocomposite adsorbents was conducted using 0.01 M sodium hydroxide with solution of initial concentration of 70 ppm (Annexure IV). Adsorption experiments were first conducted at conditions specified in chapter 3. After the first cycle, adsorption efficiency was 91.4%. After adsorption, desorption was conducted using 100 mL NaOH solution and the percentage desorption after the first adsorption - desorption cycle was 93.75. In the second cycle the adsorption efficiency was

decreased to 85.5% and desorption efficiency was 83%. Adsorption efficiency was decreased to 81% followed by desorption efficiency of 78.6% in the third cycle. After the fourth cycle the adsorption and desorption efficiency were 81% and 77% respectively. The adsorption efficiency decreases in successive experiments due to the fact that the concentration gradient of Cr(VI) between the adsorbent and adsorbate decreases. Also some active sites are not available for further adsorption. In the first cycle, fresh adsorbent has been used and therefore higher Cr(VI) uptake. The desorption of chemically bonded Cr(VI) is due to the formation of soluble sodium chromate. The efficiency decreases in successive cycle is due to reduction in activity of adsorbent. This study shows that chitosan/halloysite nanocomposite films can be reused in wastewater treatment plants using sodium hydroxide as eluent. The relation between time for reuse and adsorption-desorption efficiency is shown in Fig. 4.25. Desorption ratio is given by equation (4.2).

$$\text{Desorption ratio} = \frac{\text{Amount of metal ions desorbed}}{\text{Amount of metal ions adsorbed}} \quad (4.2)$$

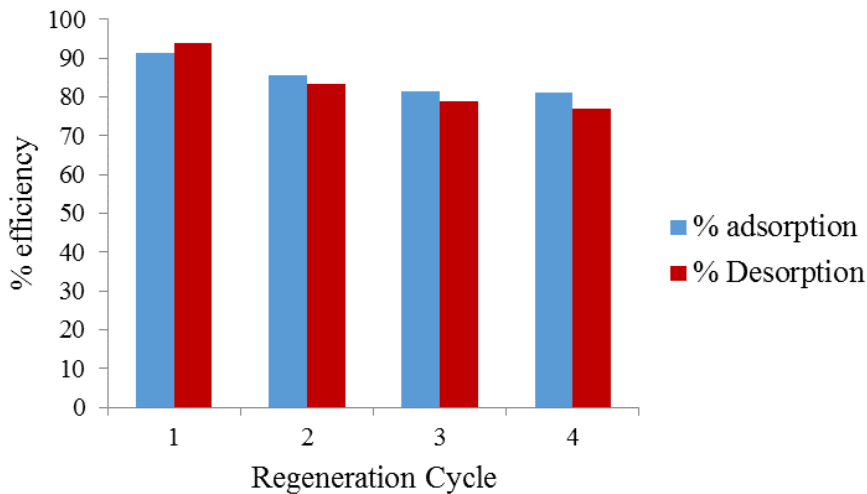


Fig. 4.25 Desorption of nanocomposite films

4.4.10 Response Surface Methodology for Analysis of Cr(VI) Removal Using Chitosan/Halloysite Nanoclay Nanocomposite Films

The optimum conditions for adsorption of Cr(VI) by nanocomposite films were determined by Box Behnken design under response surface methodology. Optimisation studies were conducted at constant pH 3.0. The temperature and speed of shaking respectively were 30 °C and 120 rpm. The three parameters for study in uncoded units were Initial Cr(VI) concentration (X_1), nanocomposite dosage (X_2) and time of adsorption (X_3). The design of experiments gave 15 different combinations of the parameters as shown in the Table 4.11. The analysis was done in coded units. The model equation in uncoded terms is given by equation (4.3).

Table 4.11 Design of experiments for Cr(VI) removal using nanocomposite films

Initial concentration., ppm	Adsorbent dose, g/L	Time, minutes	Final Concentration, ppm	Experimental % removal	Predicted % removal
75	1.1	75	9	88	88
50	1.1	100	8	84	82.125
75	2	50	13	82.7	80.45
100	1.1	100	11	89	84.125
75	1.1	75	9	88	88
75	1.1	75	9	88	88
100	2	75	14	86	86.375
75	0.2	100	7	90.7	92.95
50	2	75	13	74	71.375
75	0.2	50	10	87	82.5
50	0.2	75	10	80	79.625
50	1.1	50	20	60	64.875
100	1.1	50	20	80	81.875
100	0.2	75	19	81	83.625
75	2	100	11	85	89.5

The model equation in uncoded units is obtained from RSM and is given by

$$Y = -51.63 + 2.4X_1 - 10X_2 + 1.1X_3 - 0.013X_1^2 + 0.216X_2^2 - 0.003X_3^2 + 0.12X_1X_2 - 0.006X_1X_3 - 0.016X_2X_3 \quad (4.3)$$

where Y is the percentage removal of Cr(VI) by adsorption. The percentage Cr(VI) removal obtained experimentally and that predicted by the model does not show much deviation with the $R^2=0.856$ (Fig. 4.26). This showed that the model fitted well with the experimental data.

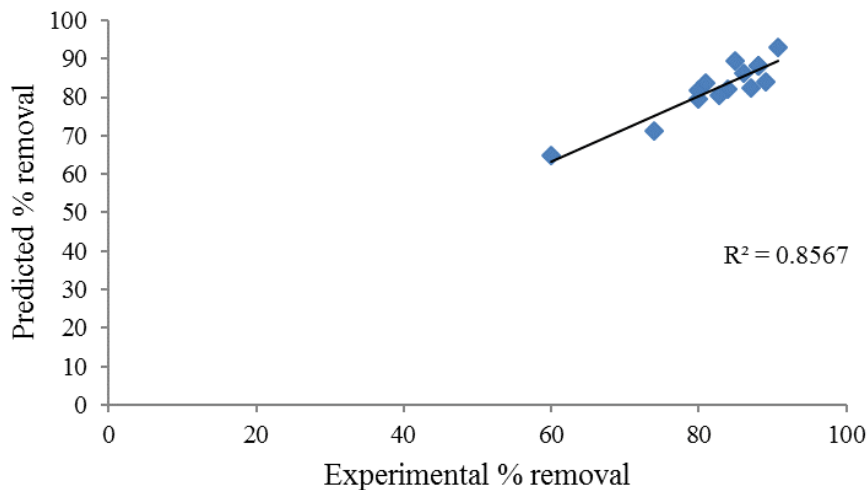


Fig. 4.26 Experimental versus predicted efficiency for nanocomposite films

Response optimiser helps in obtaining optimum values of the parameters affecting the adsorption of Cr(VI). Optimum conditions were obtained by taking top summit points of response surface plots. From the optimisation plot of Minitab 16, 93.04% removal of Cr(VI) was obtained at 72.2 mg/L initial Cr(VI) concentration with 0.2 g/L of nanocomposite film added to the solution. The time of shaking was 100 minutes at pH 3.0. When experiment has been

conducted batch wise under these conditions, 90% Cr(VI) removal was observed. Thus the model was theoretically validated. Optimisation of Cr(VI) removal using nanocomposite films is shown in Fig. 4.27.

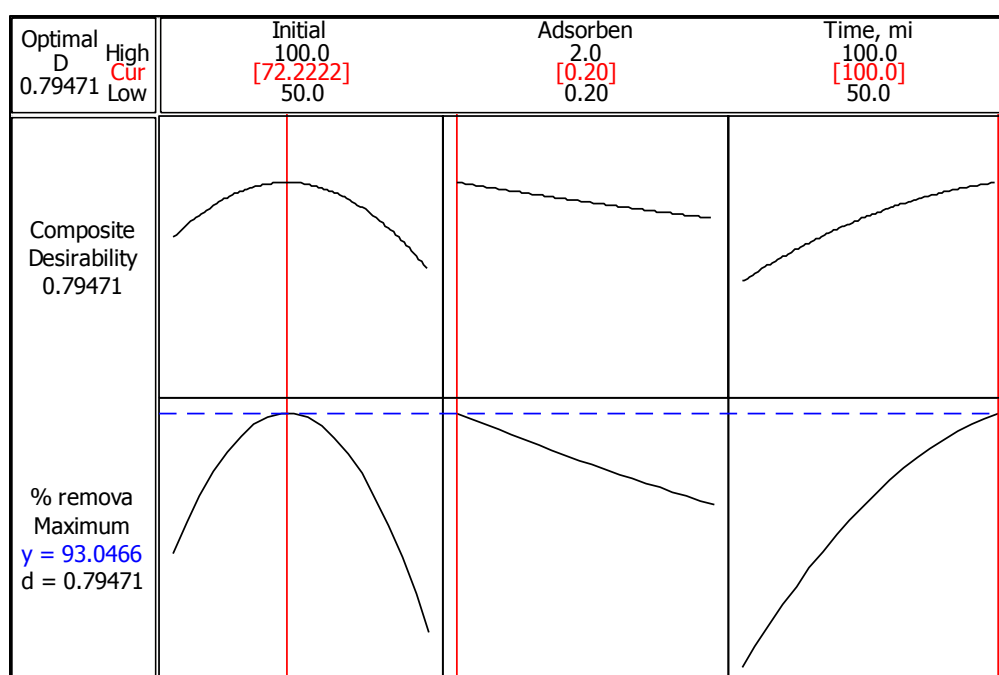
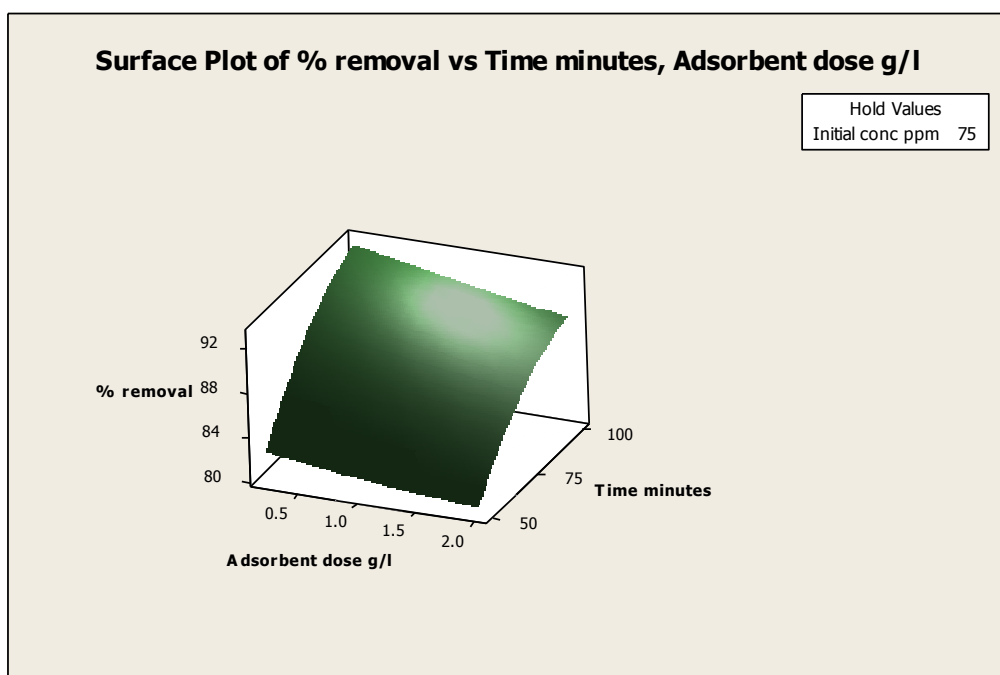


Fig. 4.27 Optimisation of performance of chitosan/halloysite nanocomposite films for Cr(VI) removal

4.4.11 Combined Effect of Variables on Cr(VI) Removal

Combined effect of initial concentration, adsorbent concentration and time at pH 3.0 were analysed using Minitab 16. The adsorption experiments were conducted at 30 °C and 120 rpm shaking speed. With increase in adsorbent dosage since the number of active sites increases, the percentage removal increased up to a certain nanocomposite dosage. After a certain adsorbent dose due to aggregation of Cr(VI) near active sites, the removal decreased since there is no change in the shaking speed. The removal of Cr(VI) first increased with time and finally steady state was achieved. With increase in the initial concentration

the driving force for adsorption was increased. So initially the removal was increased. There is no change in the number of active sites with increase in initial concentration. So due to accumulation of Cr(VI) near the nanofilms, there was a small decrease in the percentage removal and finally equilibrium was attained between the adsorbent and adsorbate. Surface plots for combined effect of initial concentration, adsorbent dosage and time is shown in Fig. 4.28. From the model equation the combined effect of initial concentration and adsorbent dosage was mostly influencing the percentage removal. The combined effect of nanocomposite dosage and time was also influencing the percentage removal of Cr(VI). The Cr(VI) removal efficiency was leastly influenced by the combined effect of initial concentration and time.



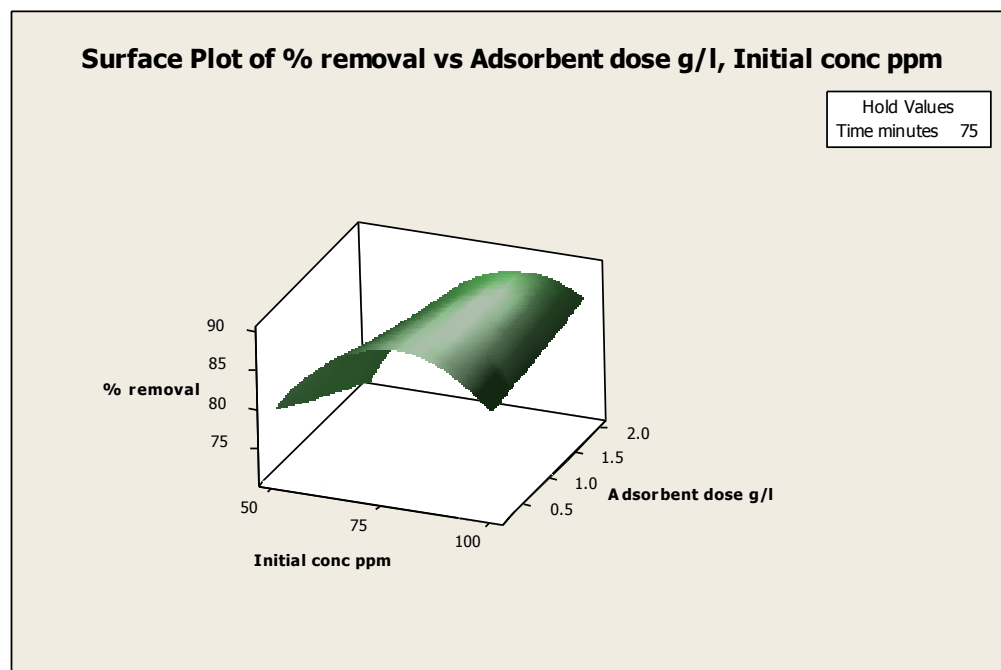
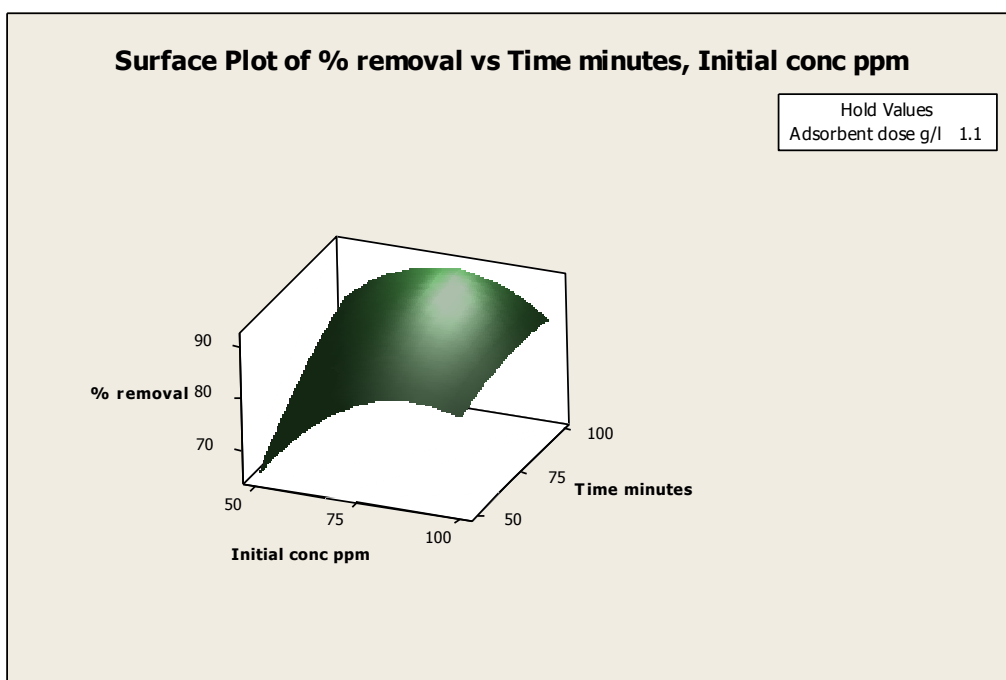


Fig 4.28 Surface plots for combined effect of variables using nanocomposite films

4.4.12 Characterisation of Chitosan/Halloysite Clay Nanocomposite Films

Scanning electron microscopy was used to analyse the morphological structure of nanocomposite films. The basal spacing of nanocomposites was determined using X-ray diffraction. Thermal stability was analysed in a thermogravimetric analyser. The strength of the film was determined in a universal testing machine. The thickness was determined using a hand held digital micrometer. The functional groups present in the nanocomposite films before and after adsorption was measured using FTIR spectroscopy.

4.4.13 Scanning Electron Microscopy

The SEM images of chitosan/halloysite clay nanocomposite shown in Fig. 4.29 at different magnification ranges proved that the nanoclay has been aggregated in the chitosan matrix. The halloysite nanoclay embedded in the chitosan matrix was seen separately in the micrographs. The SEM image assessed the morphological change after nanoclay was embedded in the chitosan matrix. The bulk like agglomerates protruding in the chitosan matrix is an indication of the presence of halloysite nanoclay (Nesic *et al.*, 2012; Casariego *et al.*, 2009). The structure of chitosan was altered completely after nanoclay was added to the matrix. The SEM image showed a heterogeneous surface which means that two different constituents were present in the matrix. The smaller size clay particles were found scattered in the chitosan surface which caused a different property for the chitosan/halloysite nanocomposite.

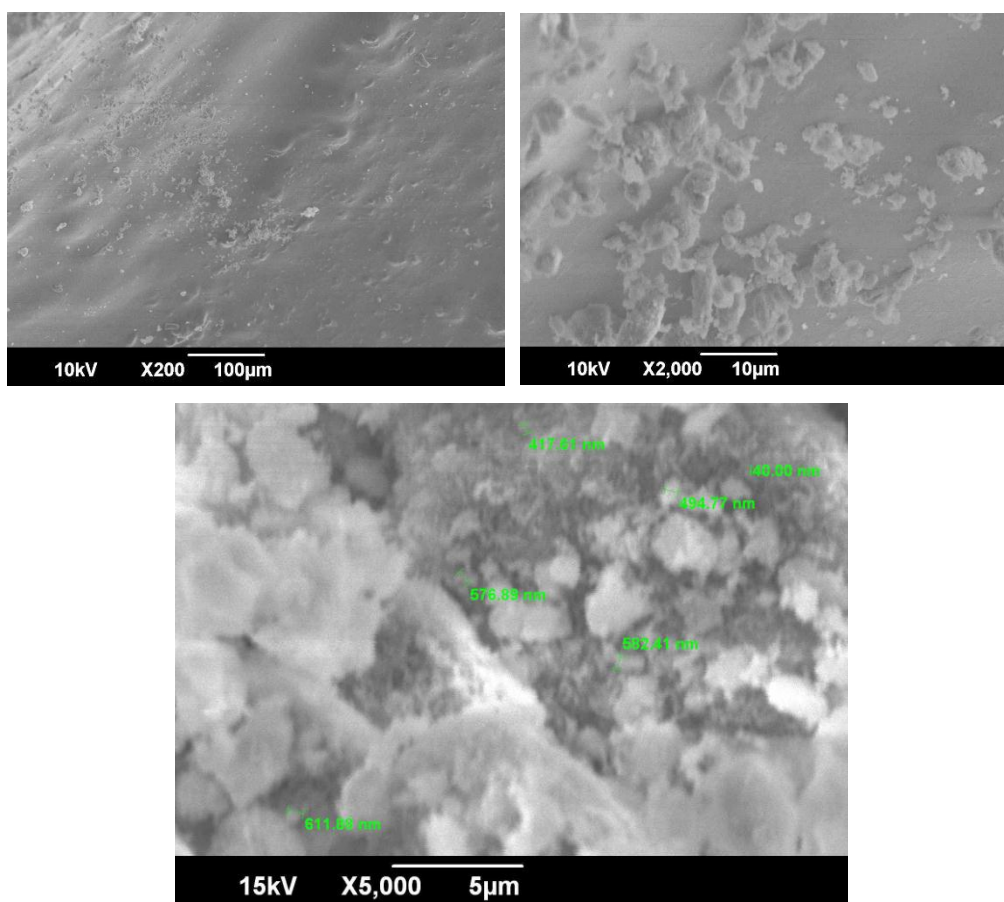


Fig 4.29 SEM of chitosan/ halloysite nanocomposite films before adsorption

4.4.14 X-ray Diffraction

X-ray diffraction is an indication of the variation of crystal structure of chitosan after addition of halloysite nanoclay. From the standard data of chitosan, no appreciable crystalline peaks could be observed indicating that the chitosan is amorphous in nature (Chen *et al.*, 2013). The peaks in the XRD pattern of halloysite nanoclay is an indication of its crystalline structure. On addition of nanoclay to chitosan, there was change in the crystal structure as indicated in the XRD pattern. After adsorption of Cr(VI) there was change in the crystalline peaks and intergallery spacing, which is an indication of Cr(VI)

in the matrix. The characteristic peaks and the d spacing of halloysite nanoclay and nanocomposite are shown in Table 4.12. There was change in d spacing of nanocomposite when compared to nanoclay at same 2θ values. This is because chitosan molecules are intercalated between nanoclay galleries. Thus an intercalated structure is formed. After adsorption the structure of nanocomposite film was altered considerably showing maximum peak at $2\theta = 35.8^\circ$ which was corresponding to an intergallery spacing of 2.5 \AA . Fig. 4.30 shows the XRD pattern of nanoclay, Fig. 4.31 shows the XRD of nanocomposite film before adsorption and Fig. 4.32 shows the XRD of nanocomposite film after adsorption. Using Deybe-Scherrer formula the average particle crystallite size of halloysite nanoclay powder was determined as 14.03 nm.

Table 4.12 The characteristic peaks and intergallery spacing of halloysite nanoclay powder and nanocomposite film

Halloysite nanoclay powder		Chitosan/ halloysite nanocomposite (before adsorption)	
2 theta, degree	d spacing, \AA°	2 theta, degree	d spacing, \AA°
12.030	7.35	11.997	7.37
18.424	4.81	20.104	4.41
20.139	4.40	24.406	3.64
24.89	3.57	38.323	2.34
26.607	3.347		
35.070	2.56		
37.991	2.366		
54.586	1.67		
62.475	1.48		

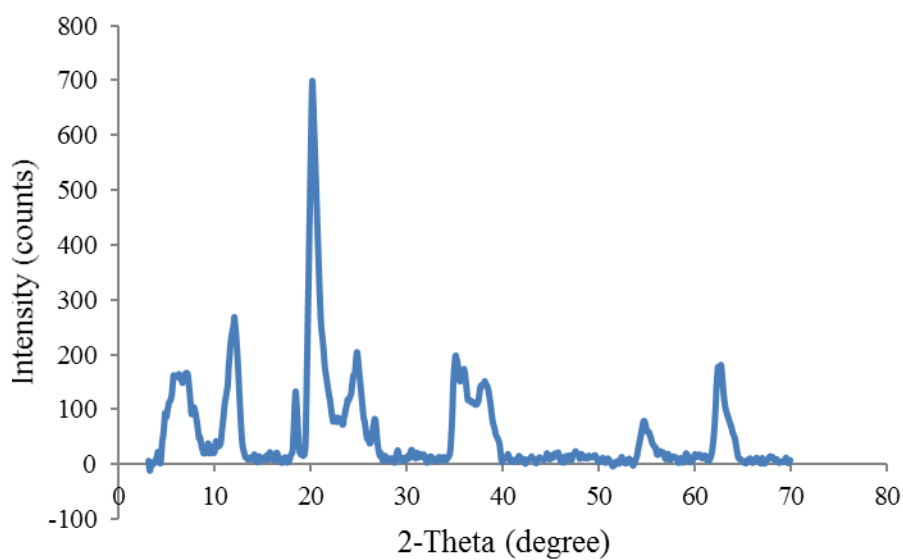


Fig. 4.30 XRD of halloysite nanoclay powder

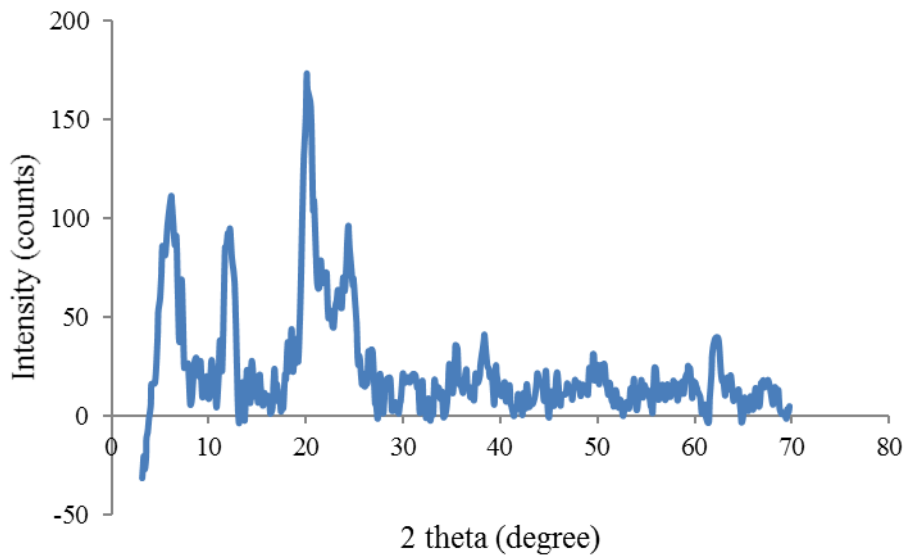


Fig. 4.31 XRD of nanocomposite films before adsorption

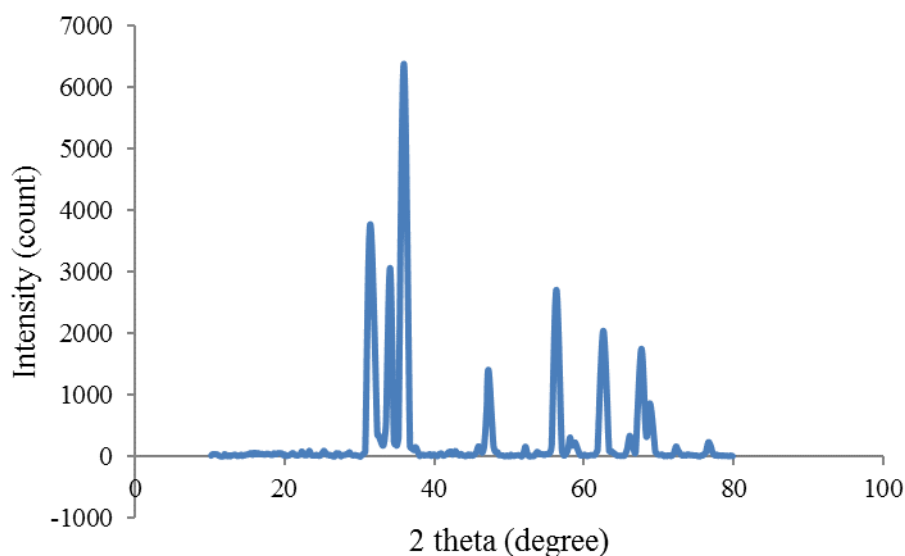


Fig. 4.32 XRD of nanocomposite films after adsorption

4.4.15 Thermogravimetric Analysis

The nanofilm was heated from room temperature to 895 °C at the rate of 5 ° per minute and weight loss was noted. The addition of halloysite nanoclay caused a significant delay in the weight loss (Wang *et al.*, 2005) and increased the thermal stability of chitosan. The weight loss was very small initially. The initial weight loss is due to the moisture loss. After 200 °C the weight loss was rapid, and this is due to the degradation and deacetylation of nanofilm. When the temperature reached 450 °C, only 5% of the material was remaining. Thermogravimetric degradation of pure chitosan starts at 60 °C where moisture removal takes place. Around 220 °C rapid degradation of chitosan takes place and reaches maximum at 240 °C (De Silva *et al.*, 2013). Enhancement of thermal stability of chitosan by the addition of halloysite nanoclay occur due to the formation of char as barrier which reduces the loss of volatile matter from the film. The weight loss with change in temperature for chitosan/halloysite nanocomposite films is shown in Fig. 4.33.

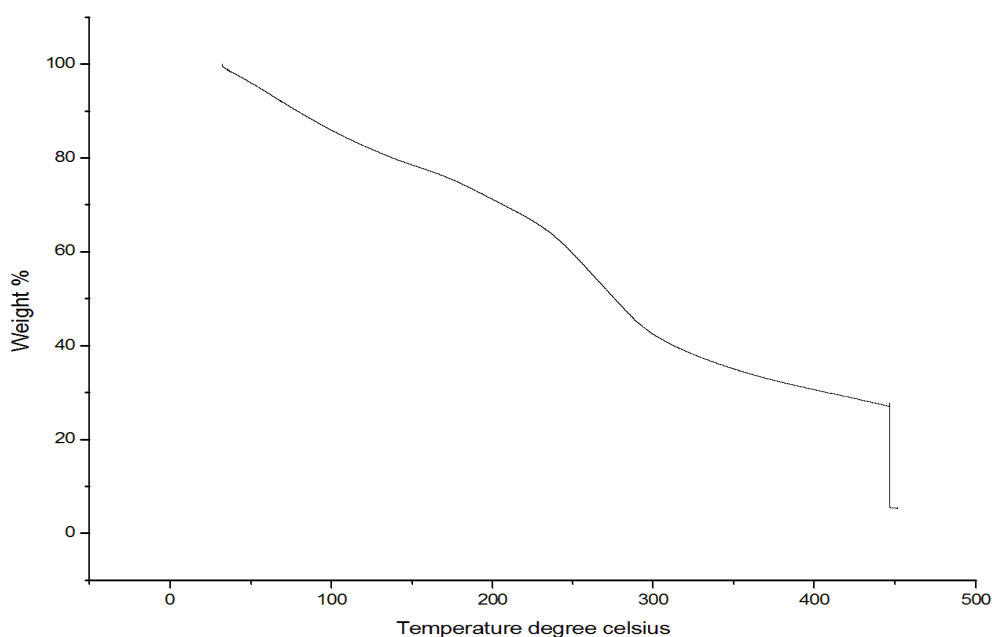


Fig. 4.33 Thermogravimetric analysis of nanocomposite films

4.4.16 Fourier Transform Infrared Spectroscopy

The functional groups present in the nanocomposite film were analysed using FTIR spectra. The functional groups present were compared with standard IR charts. FTIR spectra of films before and after adsorption are shown in the Fig. 4.34 and Fig. 4.35 respectively. The characteristic bands present in the film were 3252.36 cm^{-1} due to vibration of O-H bonds, 2977.7 and 2925 cm^{-1} due to C-H stretch, 2103.31 cm^{-1} due to C=C stretch and 1719.91 cm^{-1} due to C=O stretch. -H bending caused band at 1454.86 cm^{-1} . Peaks at 1029.72 cm^{-1} and 1067.65 cm^{-1} were due to C-N stretching. The characteristic bands present in the spectrum of pure chitosan were also present in the chitosan/halloysite nanocomposite film. Pure chitosan shows IR bands at 2880 cm^{-1} due to C-H (-CH₃) stretching, 1375.95 cm^{-1} due to vibration of methylene groups, 1590 cm^{-1} due to N-H bending (C=O-NHR), 1150 and 1025.51 cm^{-1} due to C—O stretching and 3353 cm^{-1} and 3297 cm^{-1} due to

vibration of OH groups. These are shown in the spectra of nanocomposite films (De Silva *et al.*, 2013).

Additional peaks in the FTIR spectrum of composite film was due the presence of halloysite nanoclay in the chitosan matrix. The peaks of pure halloysite nanoclay were present in the films (De Silva *et al.*, 2013). The band at 926.72 cm^{-1} in the film was due to OH deformation of the inner hydroxyl groups. The bands at 1119.06 and 1151.25 cm^{-1} corresponded to Si-O stretching. Peak at 897.17 cm^{-1} was due to Al-OH vibrations and at 926.72 cm^{-1} was due to Al-OH. The bands at 673.00 cm^{-1} and 666.21 cm^{-1} indicated the presence of Al-OH. After adsorption, there was considerable change in the spectrum of nanocomposite membrane. The peak corresponding to O-H stretching was shifted to 3338.62 cm^{-1} after adsorption. Intensity of Si-O stretching was reduced, and C-O stretching vibration was reduced significantly. The disappearance of various bands after binding of Cr(VI) is attributed to interaction of Cr(VI) with the film. All these confirm that Cr(VI) was bound to chitosan/clay film.

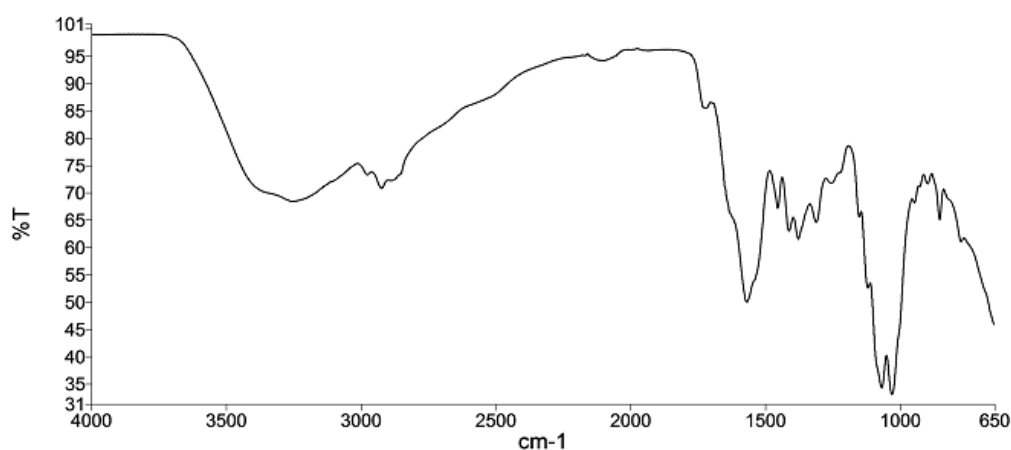


Fig. 4.34 FTIR of chitosan/halloysite nanoclay films before adsorption

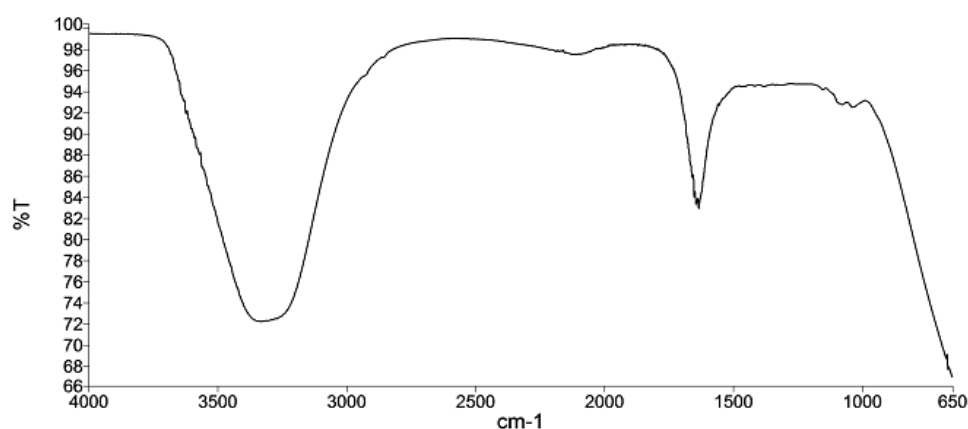


Fig. 4.35 FTIR of chitosan/halloysite nanoclay nanocomposite films after adsorption

4.4.17 Tensile Strength of Films and Film Thickness Measurement

Tensile strength were evaluated using Shimadzu Autograph AG-I series Universal Testing Machine with a load cell capacity of 10 kN. Films were made dumbbell specimens with length 100 mm and thickness 0.2 mm for testing the strength. The results obtained for tensile strength is shown graphically (Fig. 4.36). The tensile strength of chitosan increases with the addition of halloysite nanoclay (Desilva *et al.*, 2013). From UTM experiments the tensile strength was 12.29 N/mm^2 and maximum strain was 17.77%.

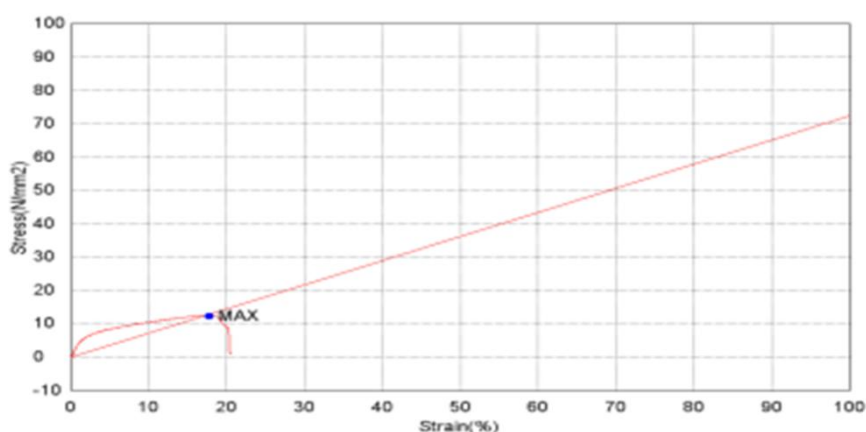


Fig 4.36 Tensile strength of nanocomposite films

The film thickness was measured using hand held digital micrometer. All the adsorption experiments were conducted with nanocomposite film of constant thickness 0.2 mm.

4.5 Continuous Removal of Cr(VI) in Packed Column Using Nanocomposite Films

The performance of continuous packed bed adsorption column was studied by plotting the breakthrough curves. The breakthrough curve is a plot of the ratio of effluent Cr(VI) concentration to the Cr(VI) inlet concentration (C_f/C_0) against time (Lim and Aris, 2014). The column was operated under various conditions to study the effect of various parameters on the breakthrough performance of the column (Annexure IV). The parameters under study were initial concentration, pH, bed height and flow rate of Cr(VI) solution. The amount of adsorbent taken was 30% of bed height.

4.5.1 Effect of Initial Concentration

The effect of initial concentration on the performance of packed adsorption column at a constant flow rate of 6 mL/min and constant bed height of 10 cm was studied. The pH of the stock solution was kept at 4.0. The study was conducted for three different initial concentrations 50 ppm, 70 ppm and 100 ppm. The break through curve was plotted between C_f/C_0 and time (Fig. 4.37).

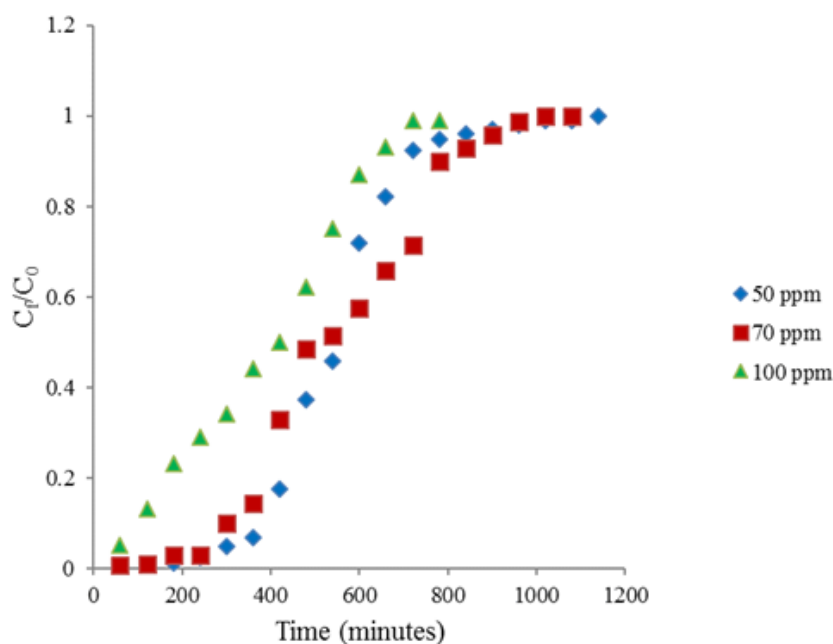


Fig. 4.37 Effect of initial concentration of Cr(VI) on breakthrough curves in continuous packed bed column

The breakthrough curves were compared for the three different initial concentrations. From the study it was clear that breakthrough occurred faster with increase in initial concentration. Low initial concentration delayed the exhaustion time of the adsorbent. At low initial concentration more volume of effluent could be treated in the column. As initial concentration was increased the breakthrough curve occurred early. From the plot the 50 ppm Cr(VI) solution did not suffer exhaustion at 1080 minutes but other two concentration suffered exhaustion at this time. At low initial concentration the driving force for adsorption is less. So the rate of diffusion is low and hence adsorption is slow. At higher initial concentration the active sites are saturated quickly and the beds gets saturated faster (Jain *et al.*, 2013). A plot of adsorbed Cr(VI) concentration versus time is shown in the Fig. 4.38. The equilibrium uptake of Cr(VI) was increased with increase in initial concentration.

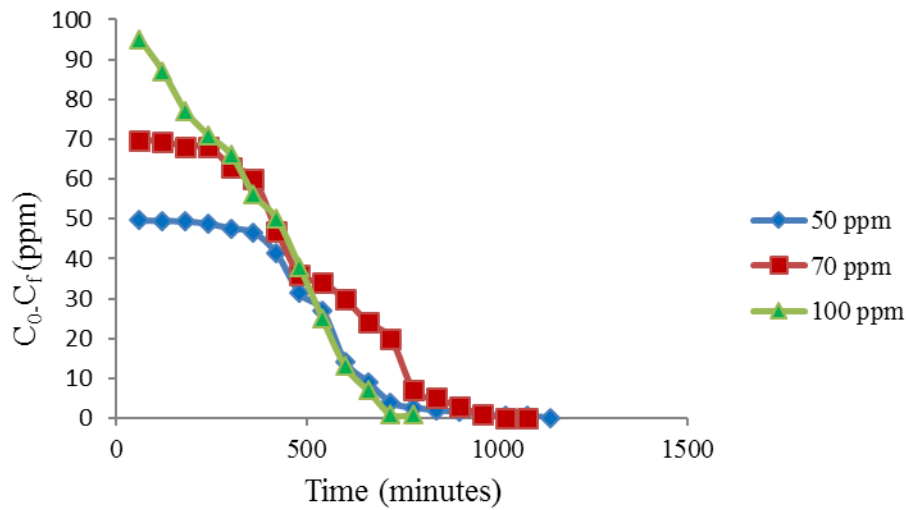


Fig. 4.38 Adsorbed concentration versus time for various initial concentration in packed bed column

4.5.2 Effect of pH

The effect of pH on the performance of breakthrough curve was evaluated for three pH 4, 6.5 and 9.0. The bed height was maintained 10 cm and initial concentration was 50 ppm. The adsorbent weight was 3 g and flow rate was maintained at 6 mL/min. The results of the continuous experimental data is shown graphically in the Fig. 4.39. As pH was increased the treated volume in the bed decreased. Low pH possessed maximum adsorption efficiency. Breakthrough time was higher at pH 4.0 and decreased with increase in pH. At low pH Cr(VI) takes the form CrO_4^{2-} and $Cr_2O_7^{2-}$. So at this pH adsorption of negatively charged chromate and dichromate ions onto positively charged adsorbent surface by electrostatic attraction is maximum. The hydroxyl, amino, carboxylic and carbonyl group present in the nanocomposite films are positively charged at low pH and negatively charged at higher pH. At pH less than 4.0, Cr(VI) is reduced to Cr(III). As the solution pH increases formation of hydroxyl (OH⁻) groups takes place and adsorption of chromate ions become competitive in this pH range. Also at higher pH metal

precipitation occurs. Therefore, adsorption capacity and efficiency of Cr(VI) removal decreases with increase in solution pH (Malkoc and Nuhoglu, 2006a).

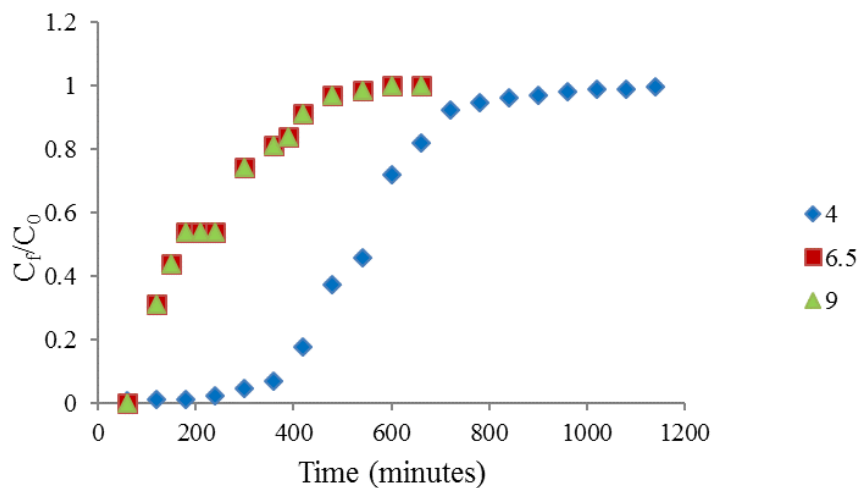


Fig. 4.39 Effect of pH on the breakthrough curves of Cr(VI) column

The amount of Cr(VI) adsorbed was also high at pH 4.0 and decreased with increase in pH. A plot of adsorbed concentration versus time for varying pH is shown in Fig. 4.40.

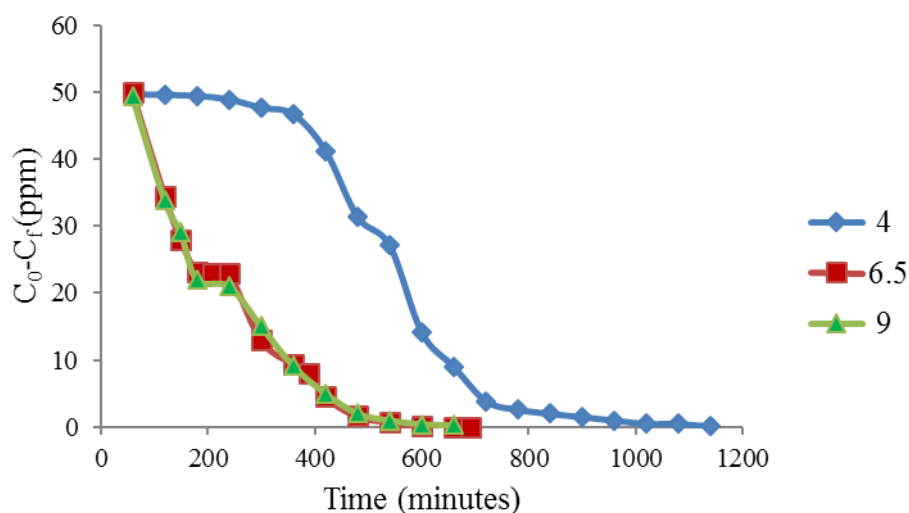


Fig 4.40 Adsorbed concentration of Cr(VI) versus time for various pH of Cr(VI) solution

4.5.3 Effect of Bed Height on Breakthrough Curves

The effect bed height was studied for continuous removal of Cr(VI) in packed bed adsorption column for three different bed heights 10 cm, 20 cm and 25 cm. The flow rate of 50 ppm Cr(VI) solution was maintained at 6 mL/min and pH of stock solution was 4.0. When bed height changes consequently there will be change in the nanocomposite adsorbent weight in the column. From the plot it is clear that the amount of Cr(VI) adsorbed increased with increase in bed height. More volume of effluent can be treated when we increase the bed height. When the bed height of the column was increased, the breakthrough curve shifted from left to right. The breakthrough occurred slowly for 25 cm bed than for 10 and 20 cm beds. Axial dispersion predominates for low bed height systems. As a result the metal ions do not get enough time for diffusion onto the surface of the adsorbent. Also the adsorption capacity was increased with bed depth. This is due to the fact that with increase in bed height, the amount of adsorbent also increases and as a result specific surface area of the adsorbent increases. So more Cr(VI) ions can be fixed on the active site of the nanocomposite film. This results in a delayed breakthrough curve for higher depths and hence exhaustion time of adsorbent was increased (Auta and Hameed, 2014). Breakthrough curves for various bed height and plot of amount of Cr(VI) adsorbed versus time is shown in Fig. 4.41 and Fig. 4.42 respectively.

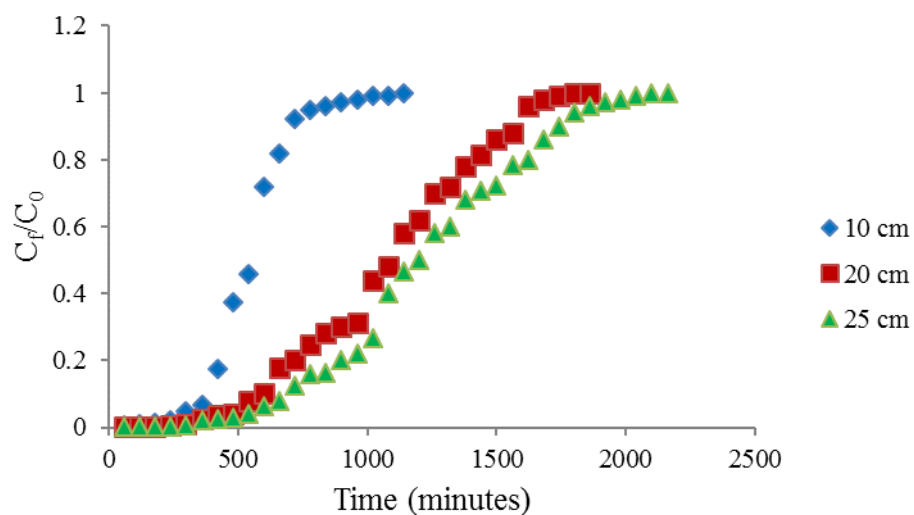


Fig. 4.41 Effect of bed height on breakthrough curves

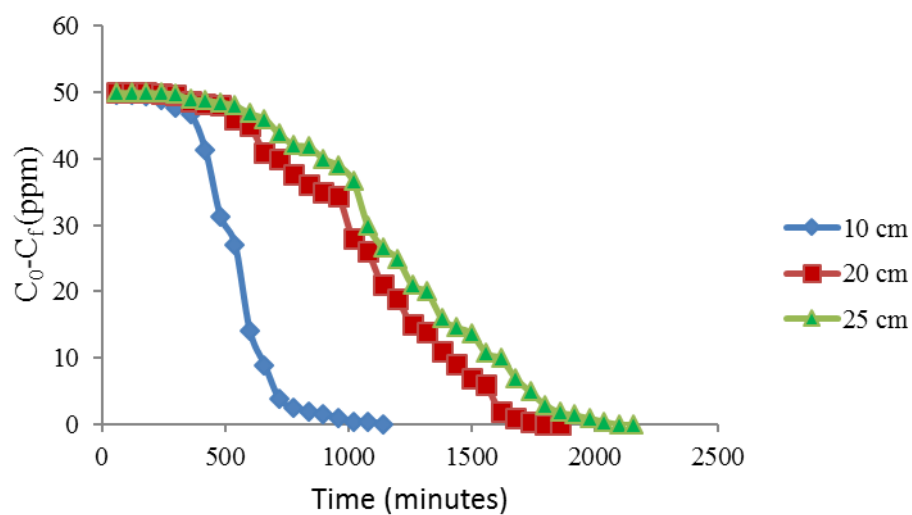


Fig. 4.42 Effect of bed height on adsorbed concentration in continuous packed bed Cr(VI) column

4.5.4 Effect of Flow Rate on the Performance of Packed Column

The flow rate for the study was varied keeping the bed height at 10 cm, pH at 4.0 and initial concentration 50 ppm. The influent flow rate was varied from 6 mL/min to 15 mL/min. As flow rate was increased the saturation of bed occurred faster. The amount of Cr(VI) adsorbed in a given time was decreased with increase in flow rate. This is because with increase in flow rate the residence time of the heavy metal ions decreases and there is no sufficient time for diffusion into the active site of chitosan/halloysite nanocomposite. At lower flow rate the Cr(VI) ions get sufficient time for diffusion. At higher flow rate the heavy metal solution leaves the column before equilibrium is reached. As a result the amount adsorbed was decreased and increase in breakthrough was observed with increase in flow rate of feed Cr(VI) solution. Breakthrough curve shifted from right to left as flow rate was increased. As flow rate was increased the adsorption capacity of bed was increased. As the flow rate of adsorbate was increased, the total amount of metal ions delivered to the column at steady state was also increased. Mass loading and total adsorbed metal ion concentration and hence percentage Cr(VI) removal at steady state was increased with increase in flow rate. From the study it is clear that due to faster exhaustion of the bed, higher residence time and lower flow rate are required for the best performance of the column (Jain *et al.*, 2013). Plots of breakthrough curve (Fig. 4.43) and amount adsorbed at various times (Fig. 4.44) are depicted below.

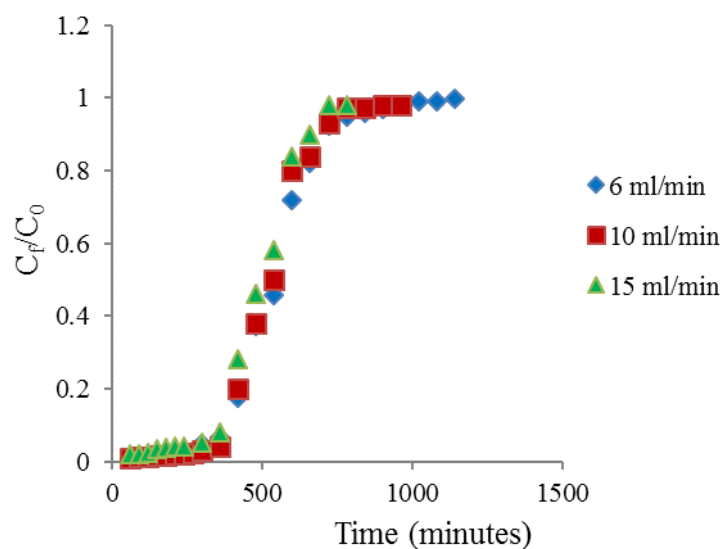


Fig. 4.43 Effect of flow rate on breakthrough curves

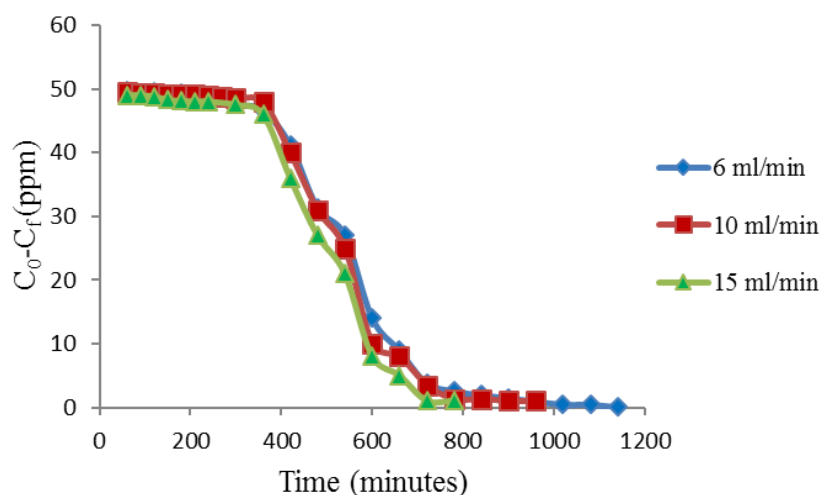


Fig. 4.44 Effect of flow rate on adsorbed concentration

From the continuous study of Cr(VI) removal in fixed bed adsorption column using chitosan/halloysite clay nanocomposite films we can summarise that low pH, low initial concentration, small flow rate and large bed depth is favourable for treating higher volume of the aqueous solution. Mathematical description of column parameters for various experimental conditions are shown in Table 4.13.

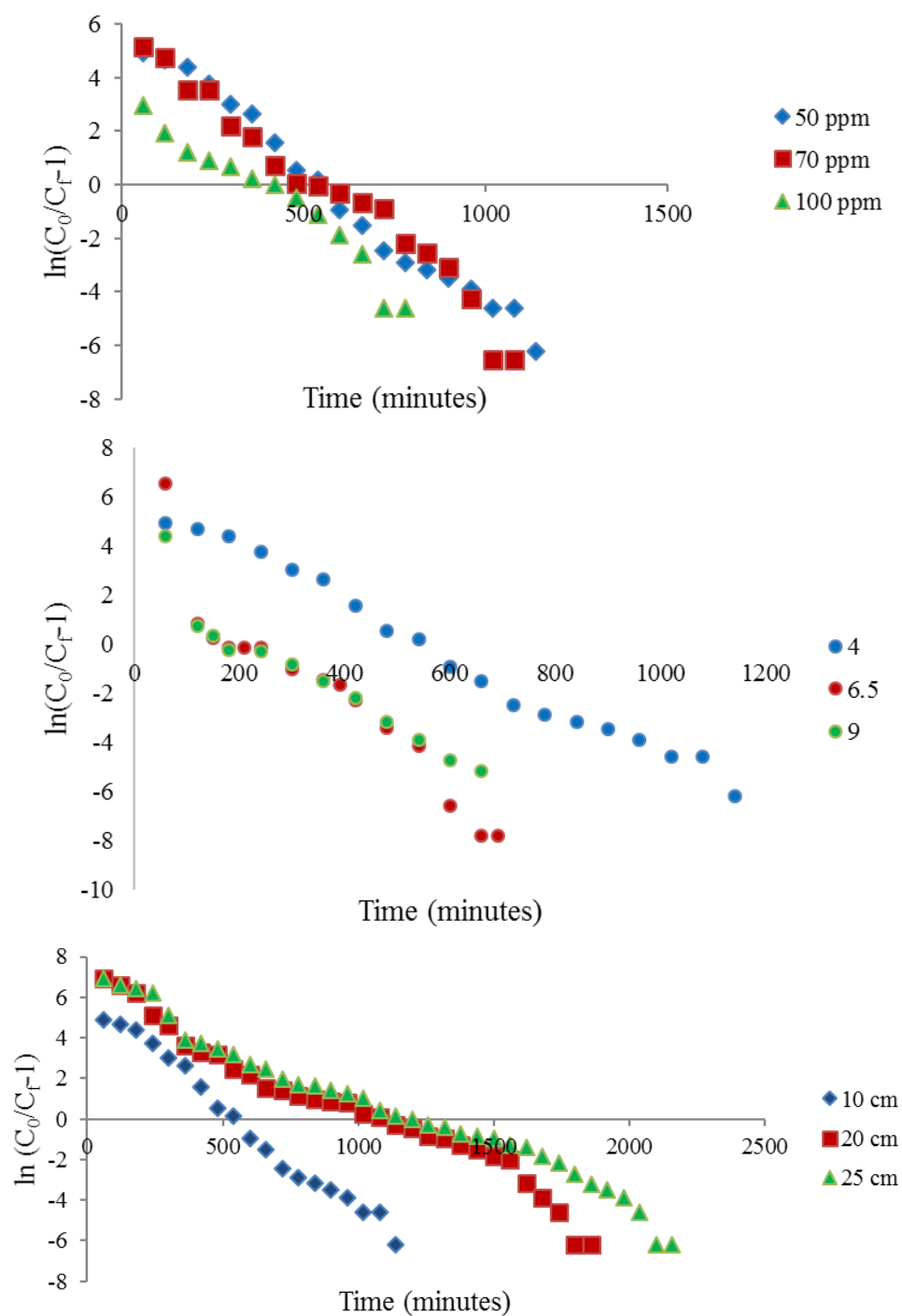
Table 4.13 Mathematical description of fixed bed Cr(VI) column parameters

C_0 , mg/L	Q, mL/min	pH	Bed Height, cm	Mass of adsorbent, mg	t_{total} , minute	V_{eff} , mL	Area	q_{total} , mg	m_{total} , mg	% Total removal	q_{eq} , mg/g	C_{eq} , mg/L
50	6	4	10	3	1140	6840	24100	144.6	342	42.3	48.2	28.86
70	6	4	10	3	1080	6480	34209	205.3	453.6	45.3	68.4	38.33
100	6	4	10	3	780	4680	32340	194.0	468	41.5	64.7	58.54
50	6	4	10	3	1140	6840	24100	144.6	342	42.3	48.2	28.86
50	6	6.5	10	3	1080	6480	8106	48.6	324	15.0	16.2	42.49
50	6	9	10	3	660	3960	8083	48.5	198	24.5	16.2	37.75
50	6	4	10	3	1140	6840	24100	144.6	342	42.3	48.2	28.86
50	6	4	20	6	1860	11160	50631	303.8	558	54.4	50.6	22.78
50	6	4	25	7.5	2160	12960	57761	346.6	648	53.5	46.2	23.26
50	6	4	10	3	1140	6840	24100	144.6	342	42.3	48.2	28.86
50	10	4	10	3	960	9600	23417	234.2	480	48.8	78.1	25.61
50	15	4	10	3	780	11700	21681	325.2	585	55.6	108.4	22.20

4.6 Modeling of Packed Bed Adsorption Column

4.6.1 Thomas Model

Thomas model was applied to the column data by varying the initial concentration, pH, bed height and flow rate. Thomas kinetic coefficient k_{th} (mL/min mg) and maximum solid phase concentration q_0 (mg/g) were determined from the experimental data for all the experimental sets by plotting $\ln(C_0/C_f - 1)$ versus time. Plots for determining k_{th} and q_0 for varying initial concentration, pH, bed height and flow rate is shown in Fig. 4.45.



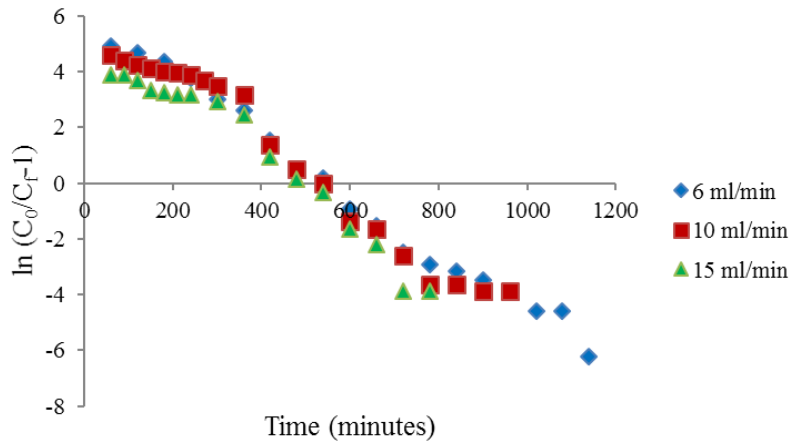
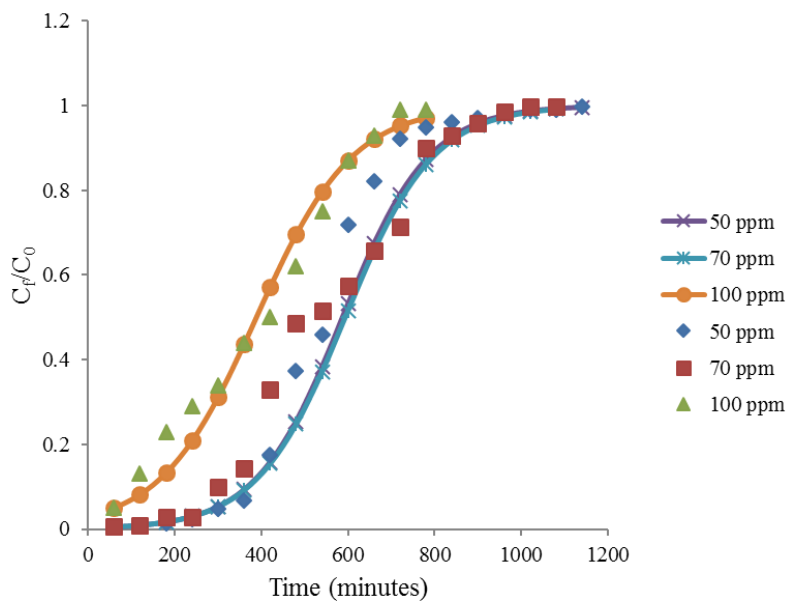


Fig. 4.45 Plot for determining Thomas kinetic coefficient k_{th} (mL/min mg) and maximum solid phase concentration q_0 (mg/g) for varying initial concentration, pH, bed height and flow rate

Breakthrough curves predicted by Thomas model were compared with the experimental breakthrough curves. Separate plots are shown for determination of the effect of initial concentration, pH, bed height and flow rate on breakthrough curve. Comparison between experimental breakthrough curves and that predicted by Thomas model for varying initial concentration, pH, bed height and flow rate is shown in Fig. 4.46.



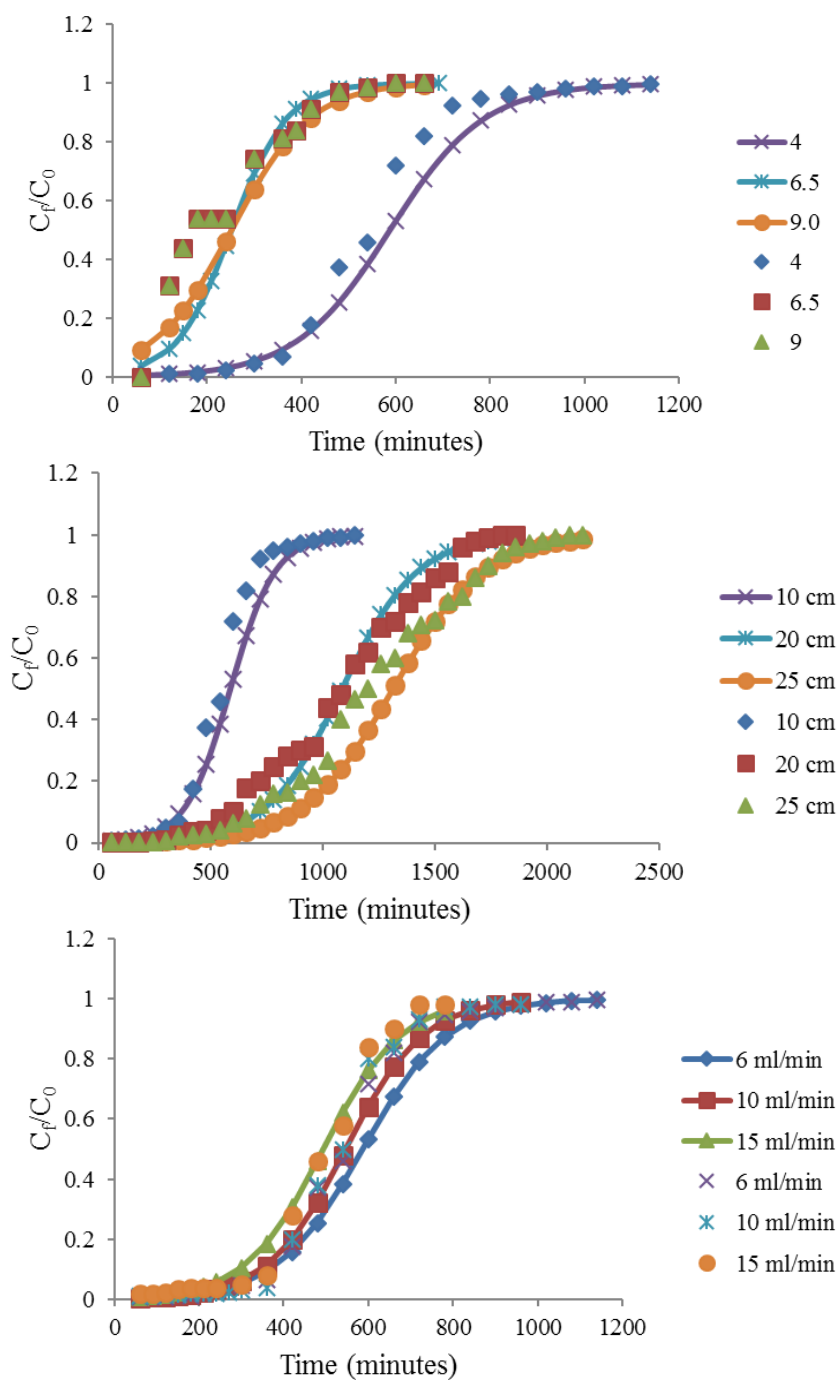


Fig. 4.46 Comparison of experimental and theoretical breakthrough curves predicted by Thomas model for varying initial concentration, pH, bed height and flow rate

Thomas Model is simple and accurate for breakthrough performance of fixed bed adsorption column (Malkoc and Nuhoglu, 2006a). The smooth curve represents the prediction by Thomas model. The experimental and theoretical breakthrough curves predicted by Thomas model were superimposed which clearly indicates that there is fit between experimental and predicted values of C_f/C_0 . The bed capacities showed slight variation between the experimental and predicted values. The correlation coefficients in the determination of coefficients of Thomas model lay between 0.892 and 0.985 for all experimental parameters. With increase in initial concentration, k_{th} was decreased and q_0 first increased and then decreased. This is because the driving force increases with initial concentration. The adsorption capacity of the bed q_0 was increased by 41% when the initial concentration was increased from 50 to 70 ppm. When the initial concentration was increased from 70 to 100 ppm the bed adsorption capacity was slightly decreased by 6.7%. The same results were also obtained for experimental data. This is due to the saturation of active sites at high initial concentration. With increase in pH, k_{th} first increased and then showed a slight decrease whereas q_0 had a decreasing trend with increase in pH. Similarly for experimental data for pH, the maximum solid phase concentration decreased with increase in pH. This shows that low pH is favourable for adsorption of Cr(VI) on nanocomposite films in packed adsorption column. For increasing bed depth, k_{th} did not show much change. When the bed depth was increased from 10 cm to 25 cm, q_0 showed a decreasing trend, but the percentage decrease was less. The regression coefficients for changing bed depth were in the range 0.95 - 0.985 which showed that the parameters of Thomas model were determined without much error. When the flow rate was increased from 6 - 15 mL/min, both the experimental and calculated q_0 showed a steady increase whereas Thomas

kinetic coefficient remained constant. The parameters predicted by Thomas model for different experimental conditions in fixed bed adsorption column is shown in Table 4.14.

Table 4.14 Parameters predicted by Thomas model at different initial Cr(VI) concentration, pH, bed height and flow rates

C_0 , mg/L	pH	Q, mL/min	Mass of adsorbent (m), g	k_{th} , mL/min mg	q_0 , mg/g	R^2
50	4	6	3	0.2	58.75	0.985
70	4	6	3	0.14	83.1	0.969
100	4	6	3	0.09	77.53	0.944
50	4	6	3	0.2	58.75	0.985
50	6.5	6	3	0.34	25.25	0.892
50	9	6	3	0.24	25.23	0.914
50	4	6	3	0.2	58.75	0.985
50	4	6	6	0.12	54.24	0.959
50	4	6	7.5	0.1	52.448	0.971
50	4	6	3	0.2	58.75	0.985
50	4	10	3	0.22	91.242	0.967
50	4	15	3	0.22	123.6	0.953

4.6.2 Yoon Nelson Model

Yoon Nelson Model is simple and requires very less column parameters. This model gives the Yoon Nelson rate constant and time for 50% of adsorbate breakthrough. In the present work, the fit of experimental data was checked for the packed bed Cr(VI) adsorption column. k_{YN} and τ are determined graphically by plotting $\ln \frac{C_f}{C_0 - C_f}$ versus time. Breakthrough curves predicted by this model were analysed graphically for change in various parameters. Fig. 4.47 represents the Yoon Nelson parameter determination for varying initial concentration.

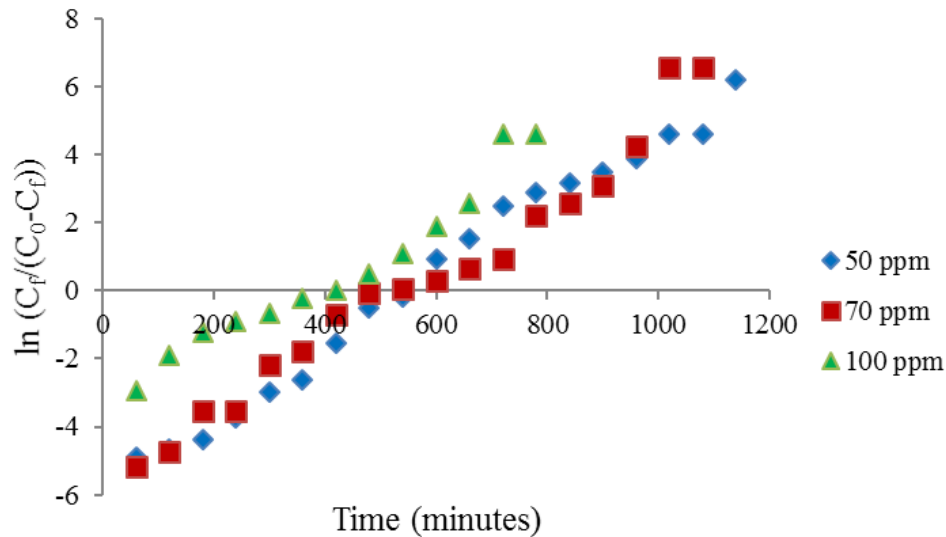


Fig. 4.47 Determination of Yoon Nelson parameters for varying initial concentration

For initial concentration of 50 ppm, the time for 50% breakthrough predicted by Yoon Nelson model was 587.5 minutes. The experimental data for $C_0 = 50$ ppm gave 50% breakthrough time 580 minutes. For $C_0 = 70$ ppm, 50% breakthrough time by experimental and Yoon Nelson model were respectively, 510 minutes and 581 minutes. For 100 ppm initial concentration the 50% breakthrough time were 387.6 and 420 minutes by Yoon Nelson Model and experimental data respectively. These results showed that Yoon Nelson model did not show much deviation from experimental results for change in initial concentration. The correlation coefficients for determining the parameters of Yoon Nelson model lie between 0.944 - 0.985 for varying initial concentration.

Plot for determining Yoon Nelson coefficient for varying pH is depicted in Fig. 4.48. From the experimental and theoretical values of time for 50% adsorbate breakthrough indicated only a slight variation for pH 6.5 and 9.0. For pH 4.0, the $\tau_{\text{theoretical}}$ value was 587.5 minutes and $\tau_{\text{experimental}}$ was 580

minutes. For pH 6.5, $\tau_{\text{theoretical}}$ was 252.6 minutes and $\tau_{\text{experimental}}$ was 200 minutes which was only slightly different. For pH 9.0, theoretical and experimental values of 50% breakthrough time respectively were 251 minutes and 170 minutes respectively.

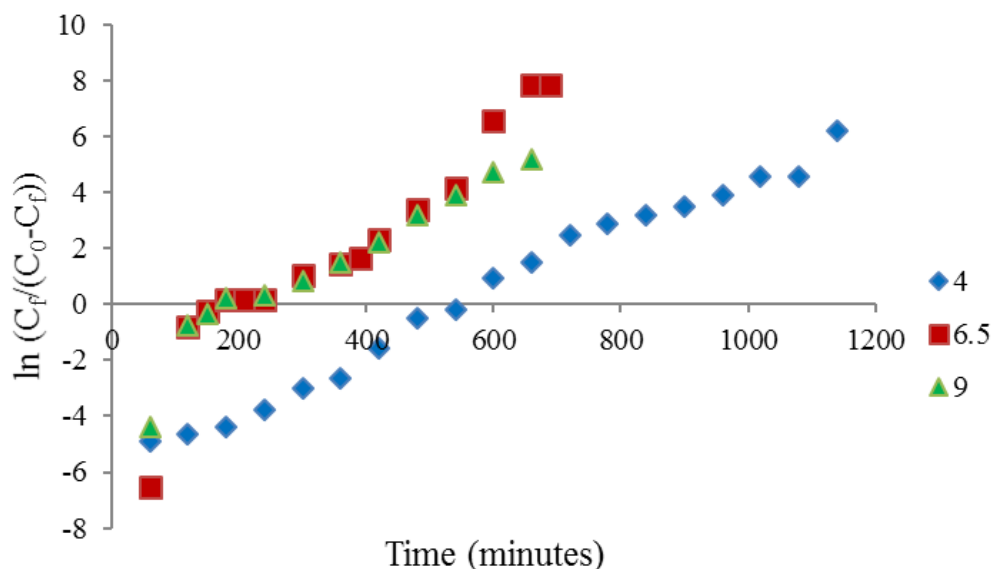


Fig. 4.48 Determination of Yoon Nelson coefficients for varying pH

The Yoon Nelson parameters for changing bed depth were determined from the graph. For bed height of 10 cm, the 50% breakthrough time was 587.5 minutes which was close to experimental results. For 20 cm bed height, the 50% breakthrough time was 1082 minutes and theoretical value was 1084 minutes which showed that Yoon Nelson model fitted best to the experimental data for longer beds. For 25 cm bed depth the 50% breakthrough time was 1311 minutes which was very close to experimental results. The correlation coefficients range from 0.985 - 0.971 for varying bed depth. Determination of Yoon Nelson parameters for changing bed depth is shown in Fig. 4.49.

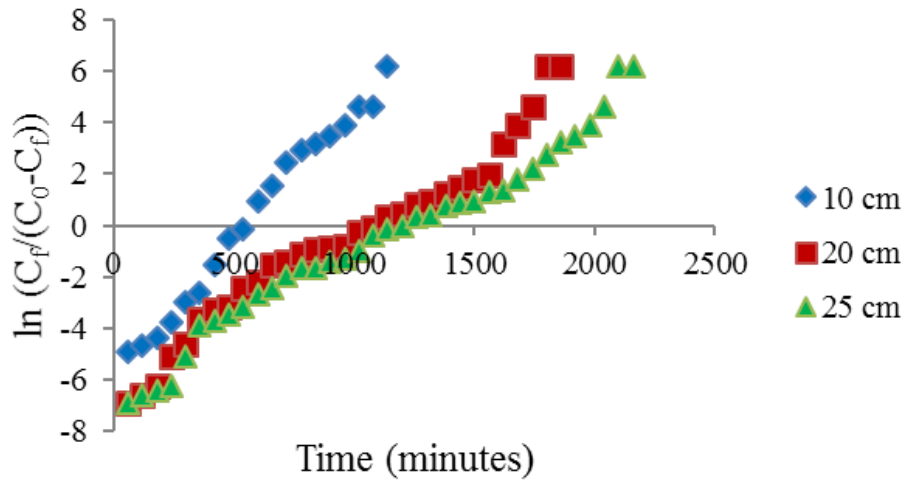
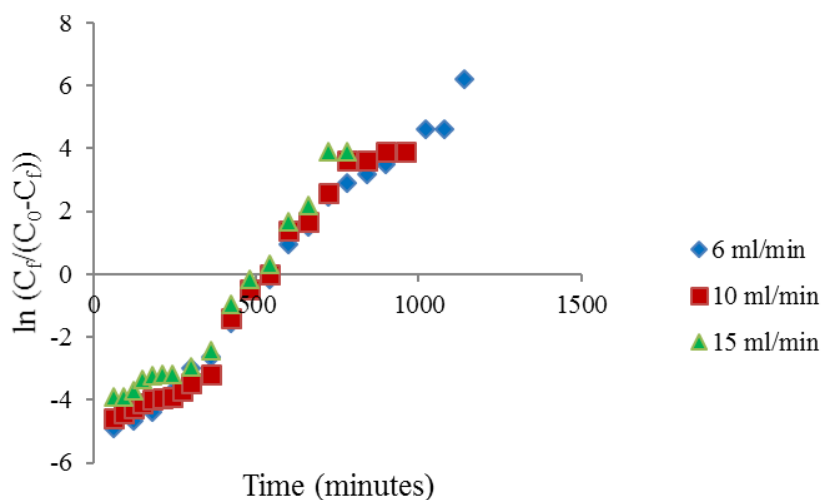


Fig. 4.49 Yoon Nelson parameters determination for varying bed height

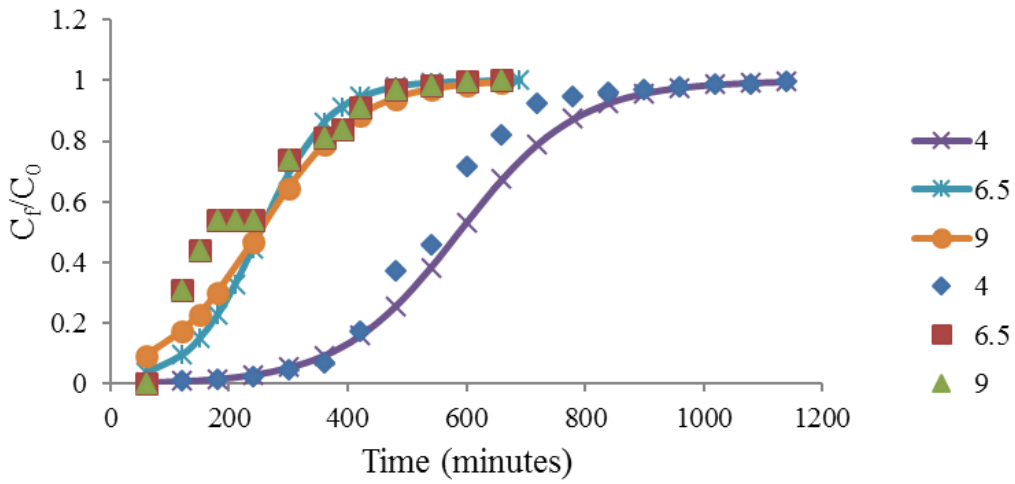
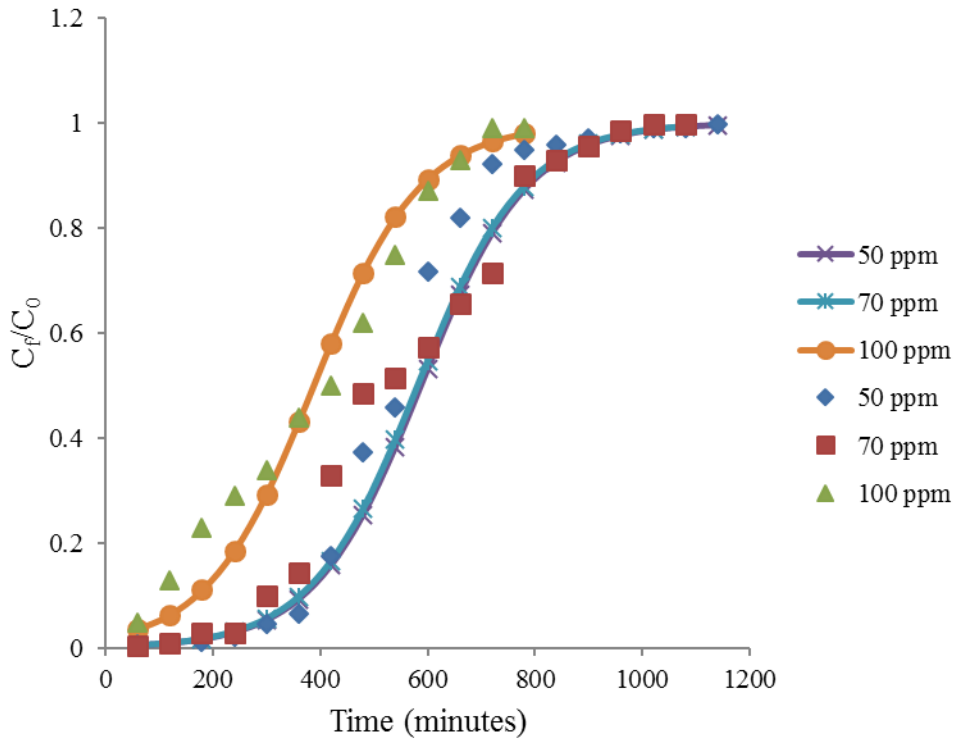
From Yoon Nelson model time required for 50% adsorbate breakthrough for flow rate of 6 mL/min was 587.5 minutes which was very close to experimental results of 549.6 minutes, with a regression coefficient of 0.985. for 10 mL/min, $\tau_{\text{theoretical}}$ was 547.5 minutes whereas $\tau_{\text{experimental}}$ was 540 minutes. Linear regression coefficient for 10 mL/min was 0.967. For 15 mL/min, $\tau_{\text{theoretical}}$ was 494.5 minutes and $\tau_{\text{experimental}}$ was 490 minutes with $R^2 = 0.953$. This study proved that Yoon Nelson model is an excellent method for determining the 50% breakthrough time for Cr(VI) column for varying flow rate. The plot for determining of τ and k_{YN} for flow rates of 6 mL/min, 10 mL/min and 15 mL/min is shown graphically (Fig.4.50). Table 4.15 represents the parameters of Yoon Nelson model for changing initial concentration, pH, bed height and flow rate.

Table 4.15 Parameters predicted by Yoon Nelson model for varying initial concentration, pH, bed height and flow rate

C_0 , mg/L	pH	Q, mL/min	mass of adsorbent (m), g	k_{YN} , minute^{-1}	τ , minute	R^2
50	4	6	3	0.01	587.5	0.985
70	4	6	3	0.01	581.4	0.969
100	4	6	3	0.009	387.6	0.944
50	4	6	3	0.01	587.5	0.985
50	6.5	6	3	0.017	252.6	0.892
50	9	6	3	0.012	251	0.914
50	4	6	3	0.01	587.5	0.985
50	4	6	6	0.006	1084.3	0.959
50	4	6	7.5	0.005	1311	0.971
50	4	6	3	0.01	587.5	0.985
50	4	10	3	0.011	547.5	0.967
50	4	15	3	0.011	494.54	0.953

**Fig. 4.50** Determination of coefficients in the Yoon Nelson model for varying flow rate

Breakthrough curves predicted by Yoon Nelson model for varying initial concentration, pH, bed height and flow rate was compared with the experimental breakthrough curves as shown in Fig. 4.51. The solid lines represent the prediction by the model.



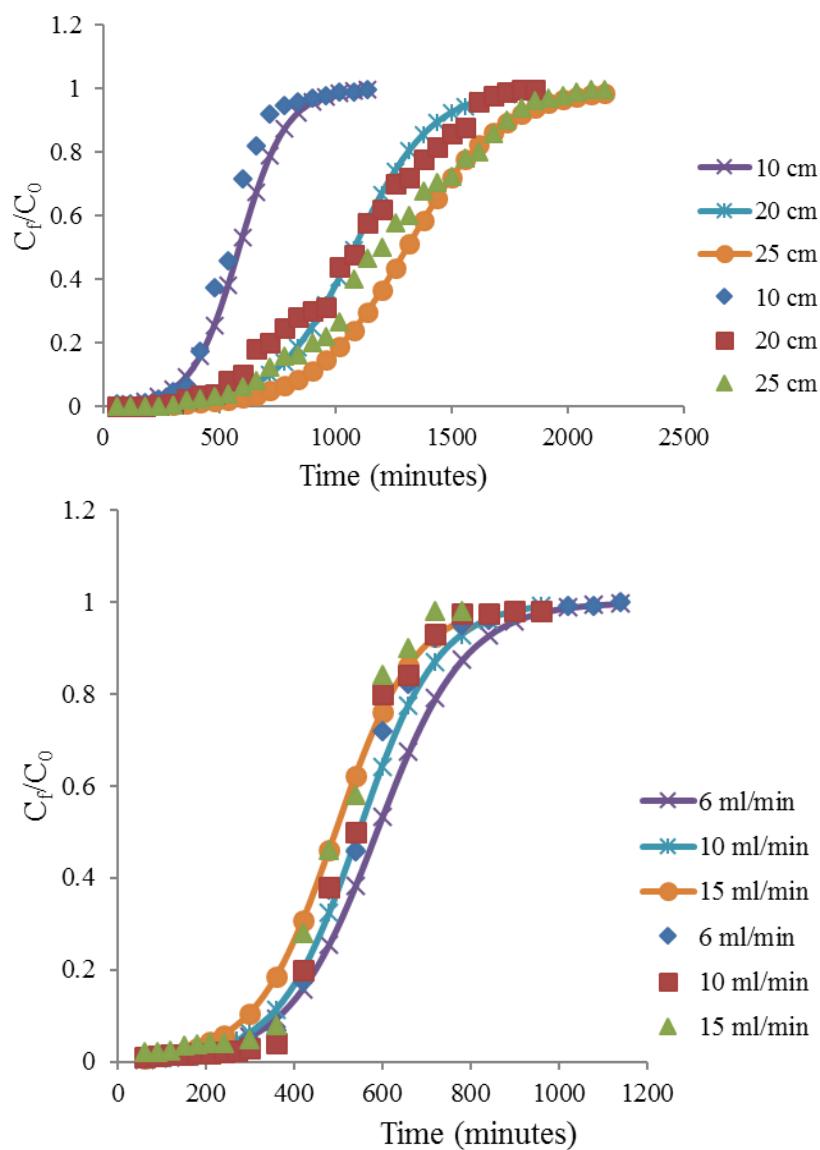


Fig. 4.51 Comparison of experimental and theoretical breakthrough curves by Yoon Nelson model

4.6.3 Adam Bohart Model

Adam Bohart model is used for interpretation of upto 50% of breakthrough time ie, initial state of operation. Adam Bohart kinetic constant k_{AB} and saturation concentration N_0 were determined for the present work on adsorption of Cr(VI) on chitosan/halloysite clay nanocomposite film in a packed adsorption column. The

breakthrough curves predicted by this model were compared with the experimental curves. For change in initial concentration the Adam Bohart parameters has been determined from plot of $\ln C_f/C_0$ vs time. The model's saturation concentration N_0 increased with initial concentration, whereas k_{AB} decreased when C_0 was increased. The decrease in mass transfer coefficient with increase in initial concentration is due to the fact that the external mass transfer processes come into play during the initial part of the column operation (Auta and Hameed, 2014). The saturation concentration increased with initial concentration because as the initial concentration was high the bed adsorbent achieved exhaustion. The linear regression coefficient was in the range 0.8 - 0.86 for all the three initial concentrations (Fig. 4.52). From the plot of breakthrough curves for the three concentrations (Fig. 4.53), it can be observed that the curves were overlapping in the initial part of the column operation, but showed considerable change at the right end. Thus this model can be used for designing a column for Cr(VI) removal using nanocomposite films for different initial concentrations using the determined Adam Bohart parameters without conducting further experiments.

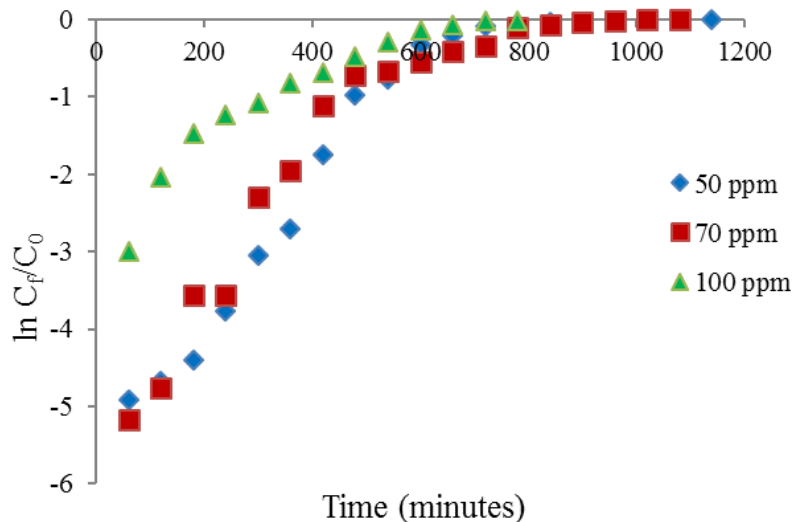


Fig. 4.52 Determination of Adam Bohart model parameters for $C_0 = 50$ ppm, $C_0 = 70$ ppm and $C_0 = 100$ ppm

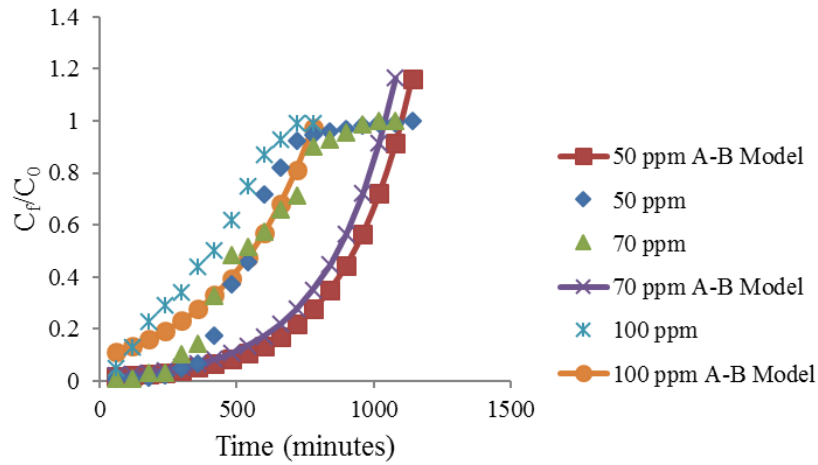


Fig. 4.53 Breakthrough curves by Adam Bohart Model for different C_0

Adam Bohart model when applied to column data for varying pH of the Cr(VI) solution did not show variation in k_{AB} values whereas N_0 decreased with increase in pH. This showed that at low pH adsorption is favourable than at high pH. As pH value was increased the saturation of column occurred at a faster rate. Consequently less volume was treated at higher pH. The regression coefficient in determining parameters of Adam Bohart model value was less at high pH. The parameters of Adam Bohart model was determined from the plot shown below (Fig. 4.54).

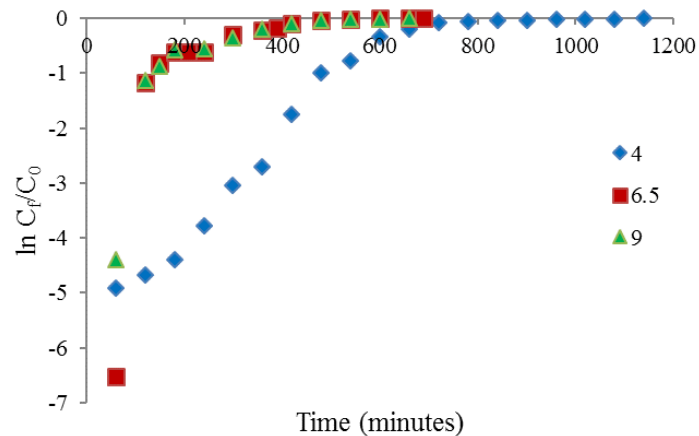


Fig. 4.54 Determination of Adam Bohart model parameters for pH = 4, 6.5 and 9

The breakthrough curves predicted by Adam Bohart model is depicted in Fig. 4.55. From the breakthrough curves it was seen that the curves are overlapping for lower part of the column operation for pH = 4 and show considerable difference towards the right end. For pH 6.5 and 9.0 the extent of fit of the model with experimental data was very less.

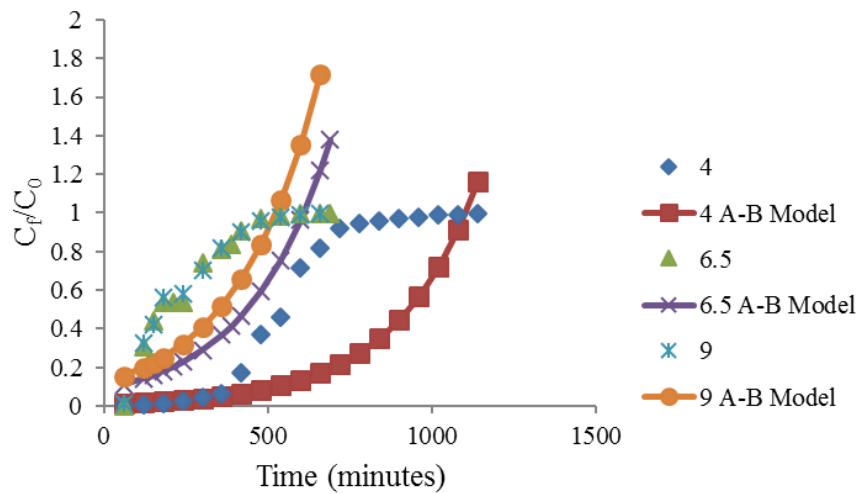


Fig. 4.55 Breakthrough curves by Adam Bohart Model for varying pH

Adam Bohart parameters for varying bed height were determined using the plot shown below (Fig. 4.56). k_{AB} value at first decreased when the bed height was increased from 10 cm to 20 cm and further when bed height was increased from 20 cm to 25 cm, no change in Adam Bohart rate constant was observed. N_0 showed a decreasing trend with increase in bed height. This is due to the fact that when bed height increases, the number of active sites available for adsorption also increases due to increase in adsorbent weight (Lim and Aris, 2014). The linear regression coefficient for determining A - B parameters lay in the range 0.81 - 0.82.

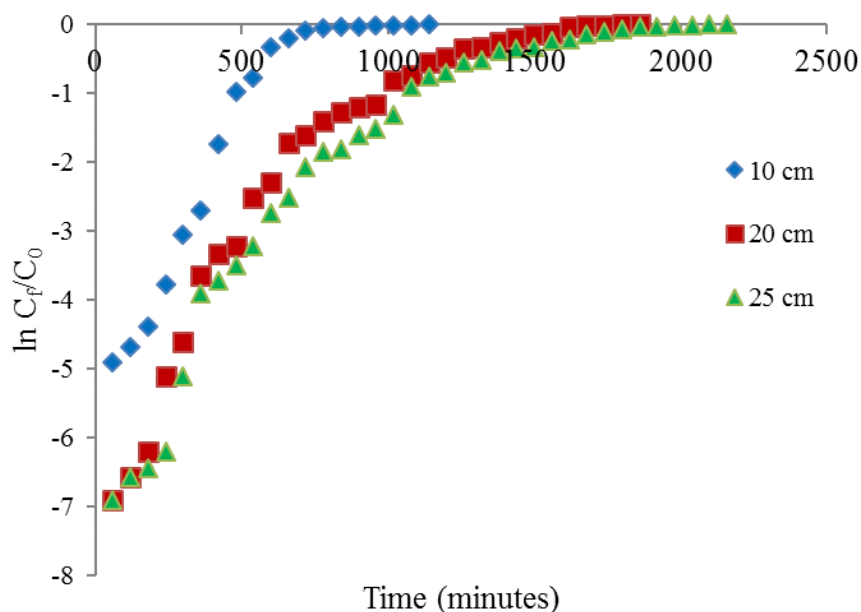


Fig. 4.56 Determination of Adam Bohart model parameters for bed height = 10 cm, 20 cm and 25 cm

Cr(VI) removal predicted by Adam Bohart model for changing bed height are shown in Fig. 4.57. Adam Bohart model was satisfying for the initial time for the three different bed heights. In the initial part the breakthrough curves were overlapping. As time proceeds the difference between breakthrough curves were also increasing for the three different bed heights. For bed height of 10 cm, upto 360 minutes the difference between experimental and predicted values did not show much variation but after 360 minutes there was significant difference in the values of C_t/C_0 . For bed height of 20 cm, the C_t/C_0 values showed considerable variation after 540 minutes whereas for 25 cm bed height the variation started at 660 minutes. This shows that Adam Bohart model can be applied to analyse the performance of Cr(VI) column using chitosan/halloysite nanocomposite adsorbent.

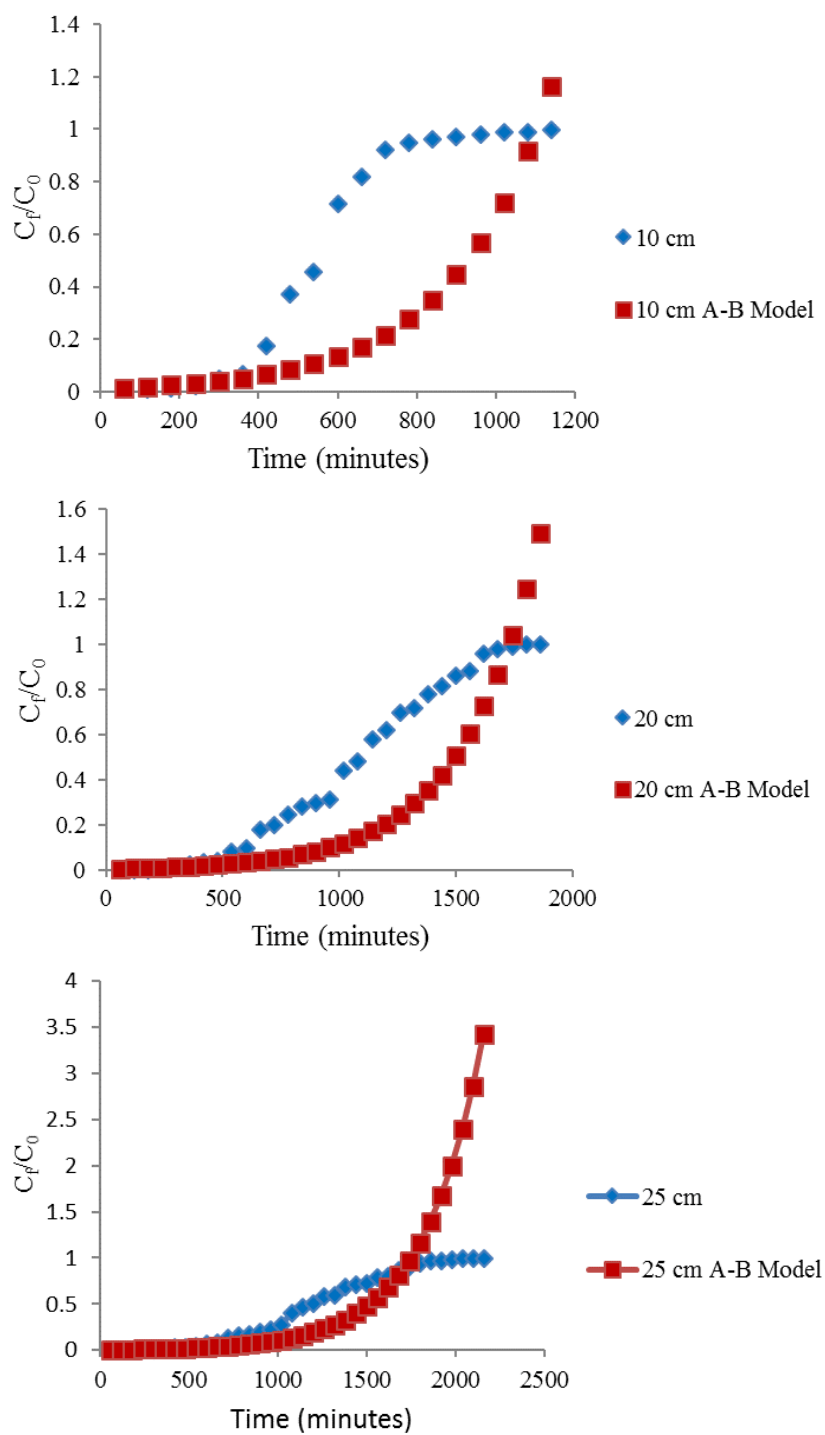


Fig. 4.57 Breakthrough curves by Adam Bohart Model for bed height = 10 cm, 20 cm and 25 cm

Plot for determining Adam Bohart coefficients for varying flow rate is shown in Fig. 4.58. When flow rate was increased the values of k_{AB} and N_0 increased. The linear regression coefficient for determining Adam Bohart parameters for the three flow rates lie between 0.82-949.

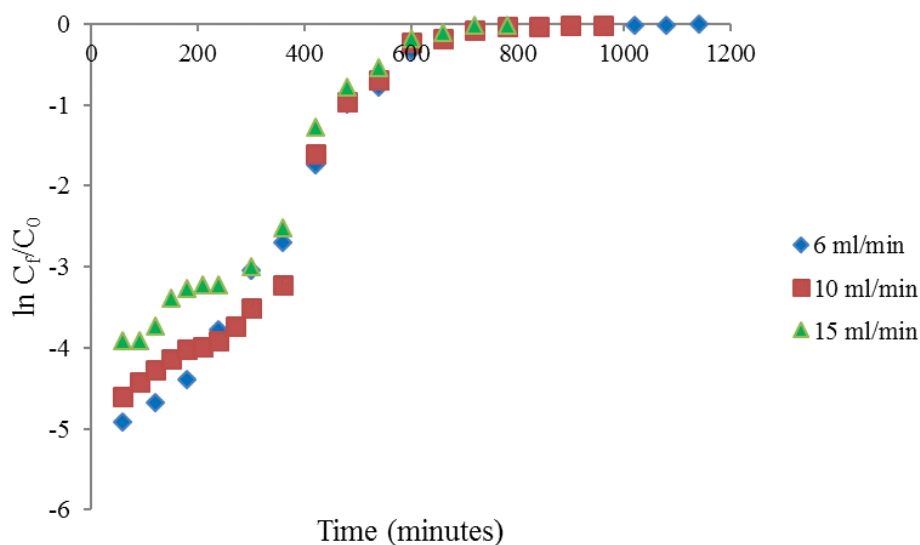


Fig. 4.58 Determination of Adam Bohart model parameters varying flow rate

The comparison between experimental and theoretical breakthrough curves for three different flow rates by Adam Bohart model is shown in Fig. 4.59. With increase in the flow rate the bed saturation occurred faster. This is because more adsorbate enters the active site of the adsorbent when the flow rate is increased. For flow rate of 6 mL/min, the experimental and predicted C_t/C_0 were almost same upto 360 minutes. After 360 minutes, the experimental value increased more rapidly than the theoretical C_t/C_0 . For flow rate 10 mL/min, experimental and predicted curves overlapped upto 360 minutes, ie initial part of column operation. For flow rate of 15 mL/min, upto 240 minutes the breakthrough curves overlapped and after 300 minutes there was considerable difference between the experimental and predicted values. This model can be applied to predict the Cr(VI) removal in the proposed column for varying flow rates.

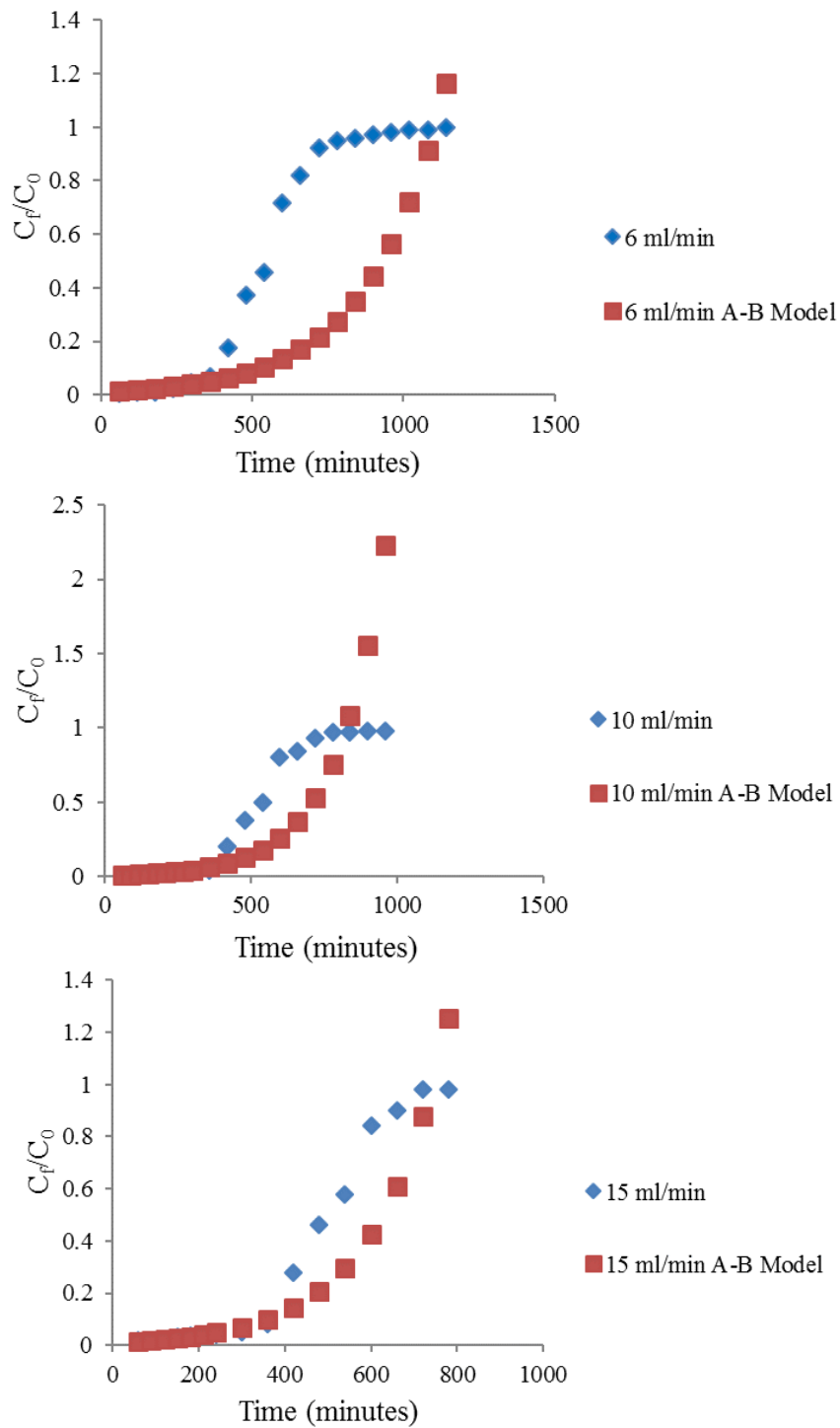


Fig. 4.59 Breakthrough curves by Adam Bohart Model for varying flow rate

Adam Bohart parameters for varying initial concentration, pH, bed height and flow rate is shown in Table 4.16.

Table 4.16 Parameters predicted by Adam Bohart model for varying initial concentration, pH, bed height and flow rate

C_0 , mg/L	pH	Q, mL/min	Z, cm	U_0 , cm/min	k_{AB} , L/mgmin	N_0 , mg/L	R^2
50	4	6	10	1.326964	0.00008	7313.23	0.82
70	4	6	10	1.326964	0.00005	9678.875	0.804
100	4	6	10	1.326964	0.00003	10469.75	0.864
50	4	6	10	1.326964	0.00008	7313.23	0.82
50	6.5	6	10	1.326964	0.00008	4045.6	0.336
50	9	6	10	1.326964	0.00008	3478.304	0.45
50	4	6	10	1.326964	0.00008	7313.23	0.82
50	4	6	20	1.326964	0.00006	5728.06	0.815
50	4	6	25	1.326964	0.00006	4642.6	0.816
50	4	6	10	1.326964	0.00008	7313.23	0.82
50	4	10	10	2.211607	0.00012	9141.3	0.904
50	4	15	10	3.31741	0.00012	12310.35	0.949

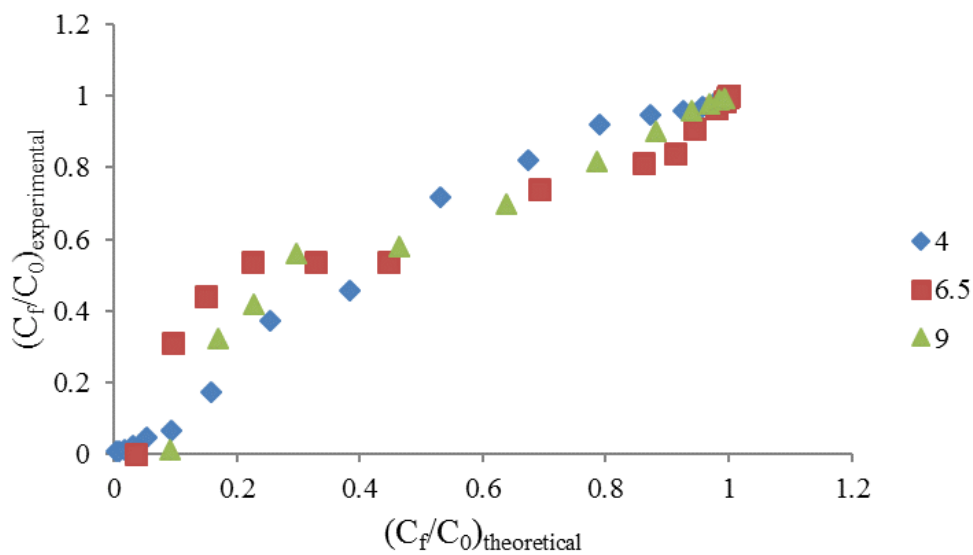
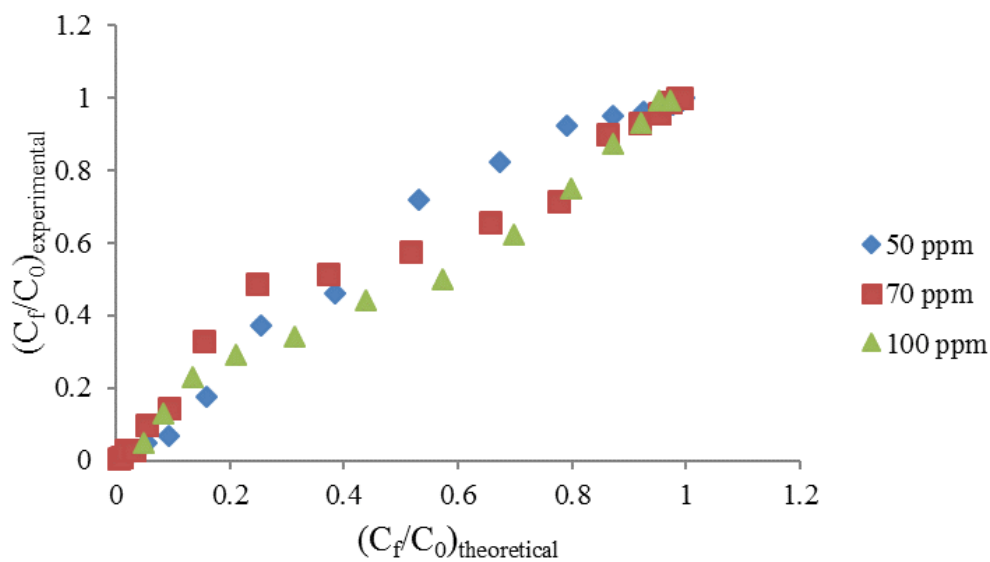
4.6.4 Comparison of Thomas Model, Yoon Nelson Model and Adam Bohart Model

The correlation between experimental and theoretical data of column operation was compared for the three models. Thomas model and Yoon Nelson model was fitted to the experimental data well. Adam Bohart correlation coefficients were low and this model fitted best to the initial part of the column operation for varying initial concentration, bed height and flow rate. Adam Bohart model was fitted more to the low pH influent solution than to the high pH Cr(VI) solutions. Correlation coefficients for experimental versus theoretical C_t/C_0 by Thomas model, Yoon Nelson model and Adam Bohart model for various experimental conditions is shown in Table 4.17.

Table 4.17 Correlation coefficients for Thomas model, Yoon Nelson model and Adam Bohart model for various experimental conditions

C_0 , mg/L	pH	Q, mL/min	Z, cm	R^2 (Thomas model)	R^2 (Yoon Nelson model)	R^2 (Adam Bohart Model)
50	4	6	10	0.979	0.979	0.550
70	4	6	10	0.968	0.970	0.685
100	4	6	10	0.979	0.974	0.901
50	4	6	10	0.979	0.979	0.550
50	6.5	6	10	0.918	0.913	0.585
50	9	6	10	0.928	0.929	0.628
50	4	6	10	0.979	0.979	0.550
50	4	6	20	0.987	0.987	0.716
50	4	6	25	0.983	0.983	0.619
50	4	6	10	0.979	0.979	0.550
50	4	10	10	0.990	0.990	0.598
50	4	15	10	0.989	0.989	0.816

Comparison of $(C_f/C_0)_{\text{theoretical}}$ and $(C_f/C_0)_{\text{experimental}}$ data for varying initial concentration, pH, bed height and flow rate by Thomas model is shown in Fig. 4.60. The verification of $(C_f/C_0)_{\text{theoretical}}$ and $(C_f/C_0)_{\text{experimental}}$ by Yoon Nelson model is given in Fig. 4.61 and the experimental and theoretical data validation by Adam Bohart model is given by Fig. 4.62.



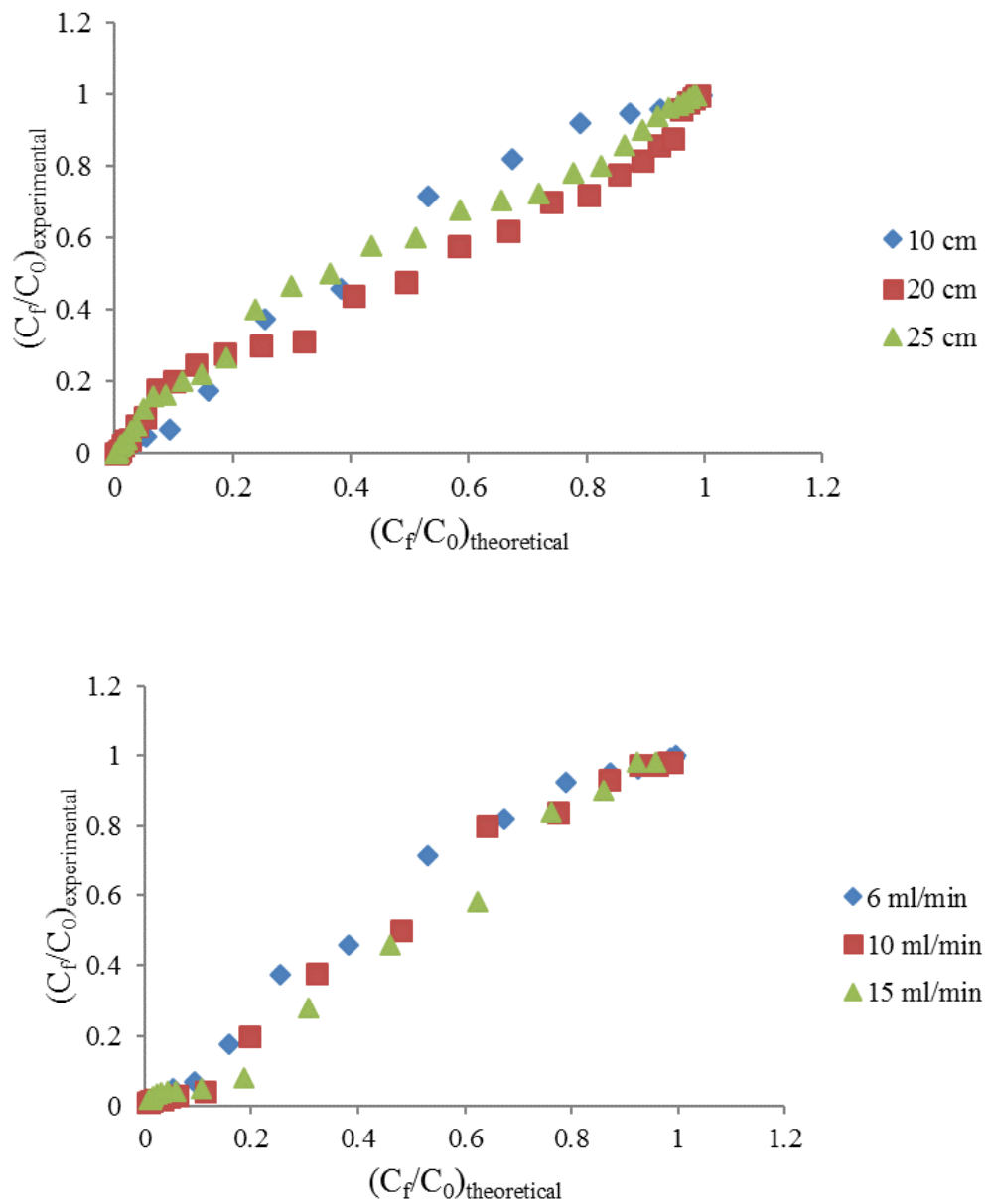
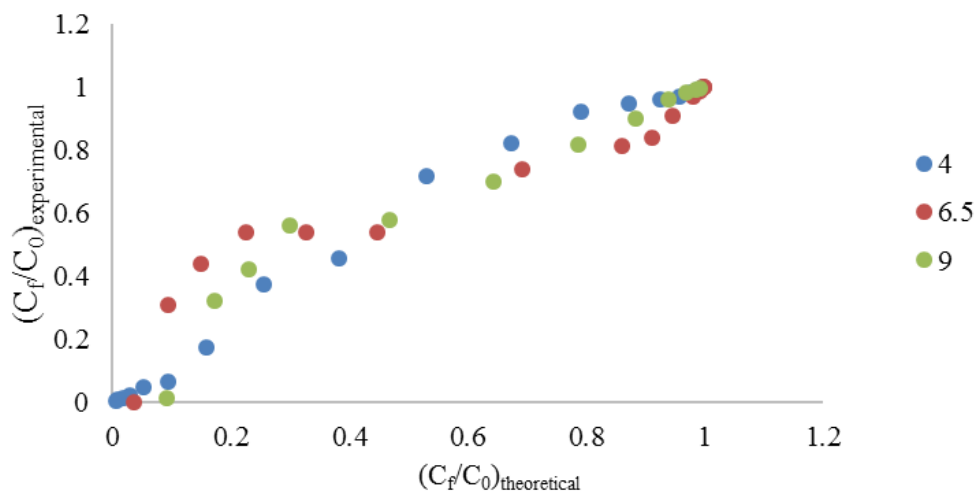
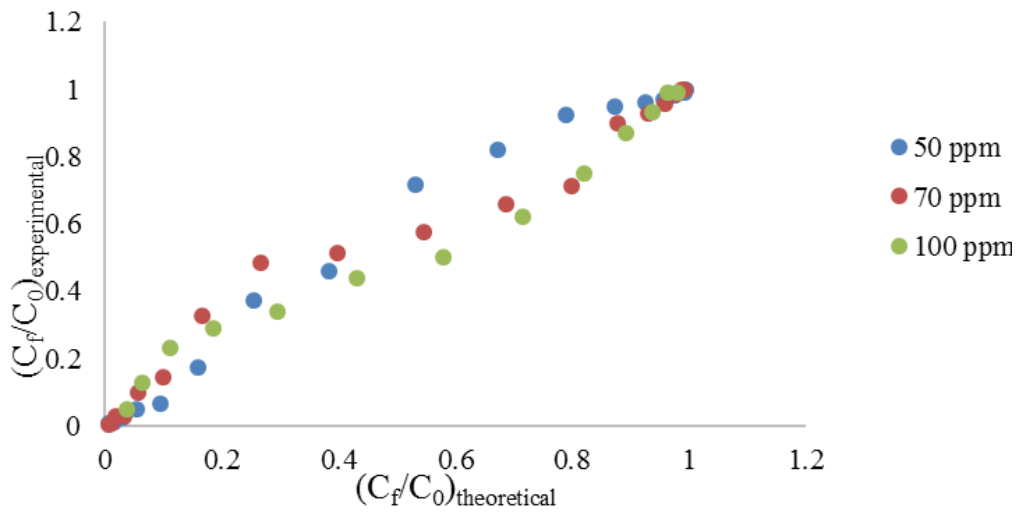


Fig. 4.60 Comparison of $(C_f/C_0)_{\text{experimental}}$ and $(C_f/C_0)_{\text{theoretical}}$ by Thomas model for varying initial concentration, pH, bed height and flow rate



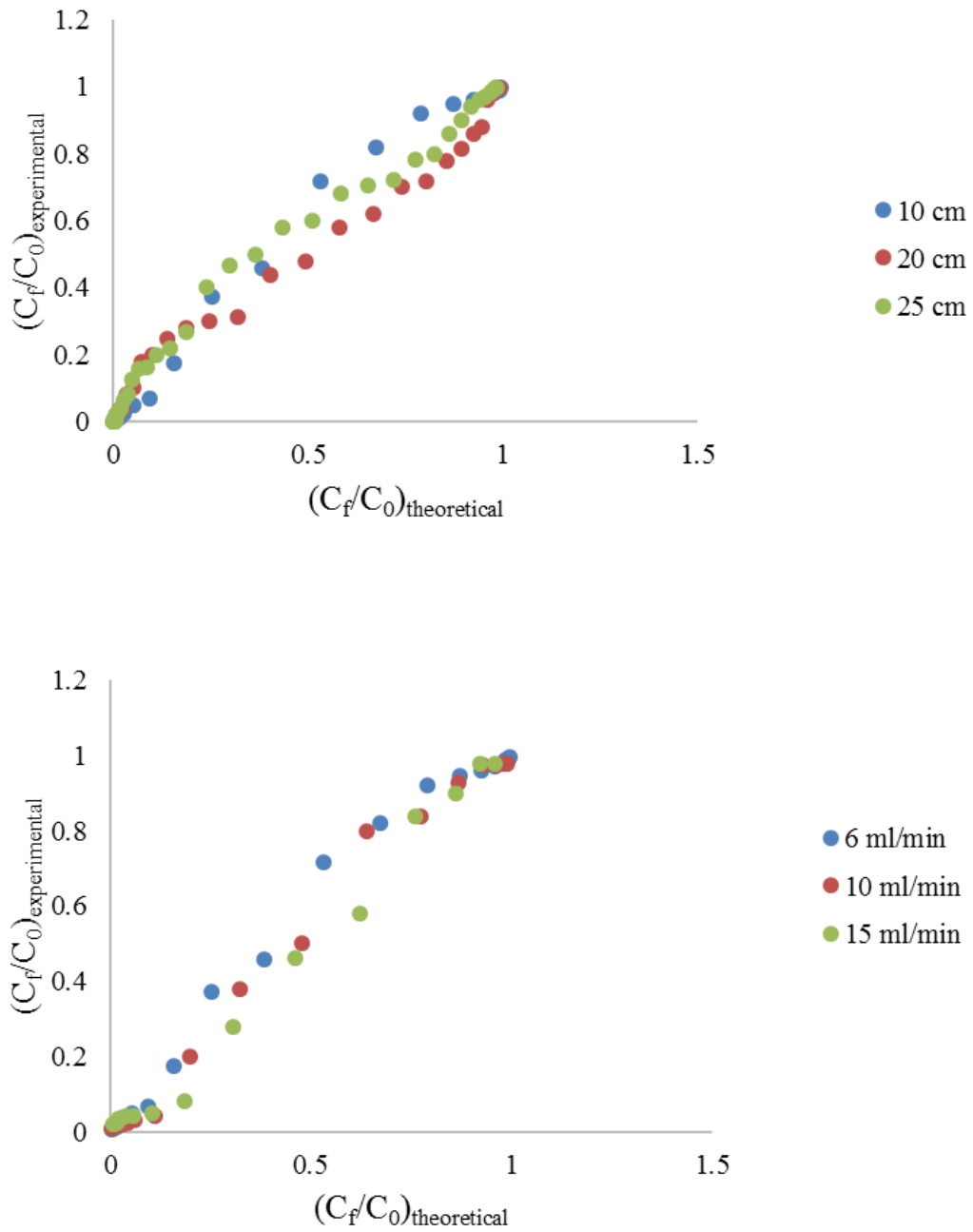
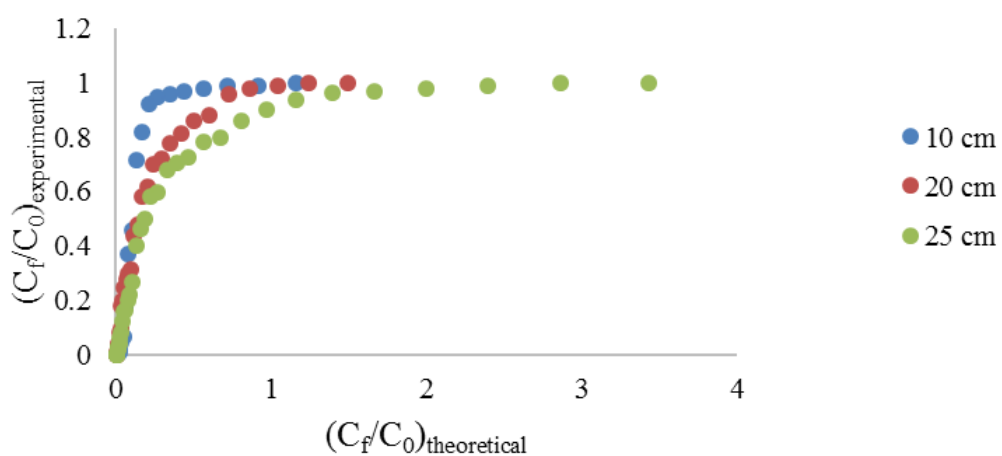
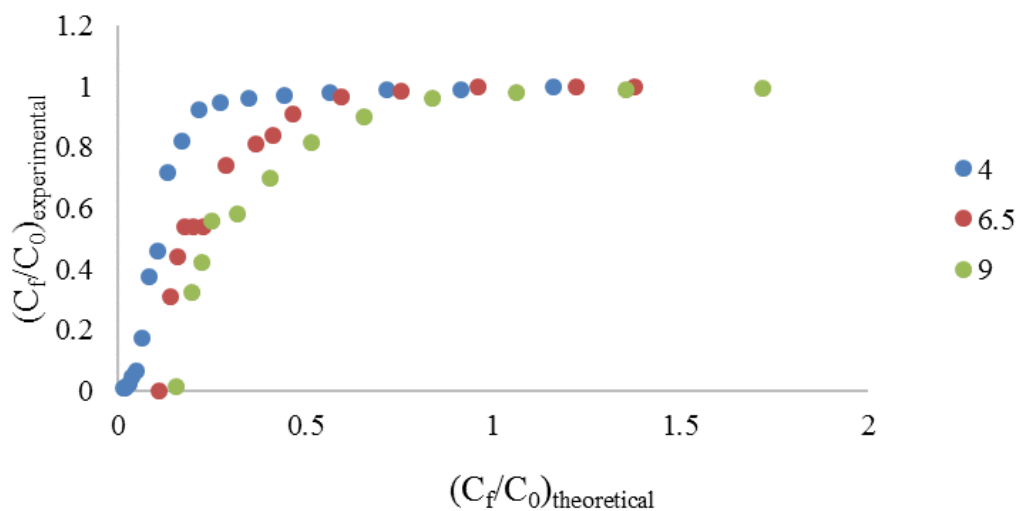
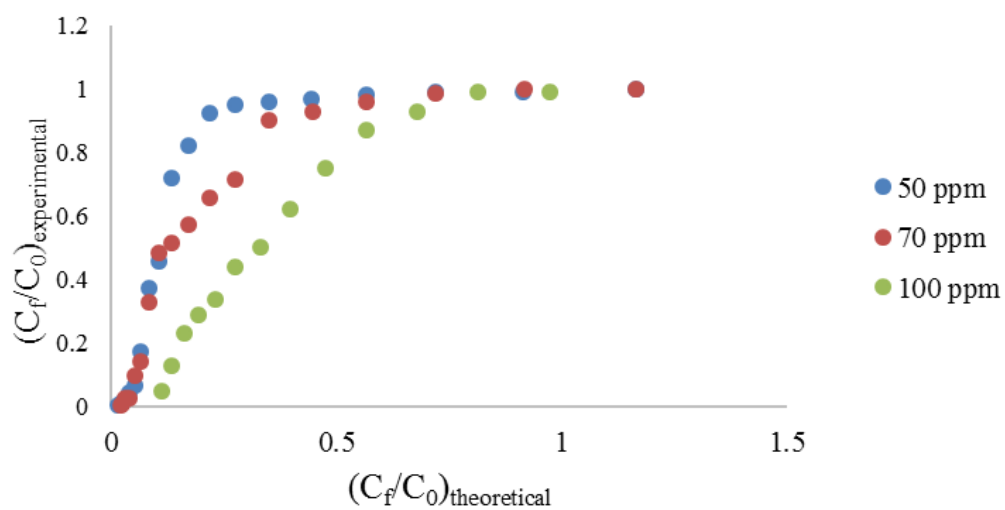


Fig. 4.61 Comparison of $(C_f/C_0)_{\text{experimental}}$ and $(C_f/C_0)_{\text{theoretical}}$ by Yoon Nelson model for varying initial concentration, pH, bed height and flow rate



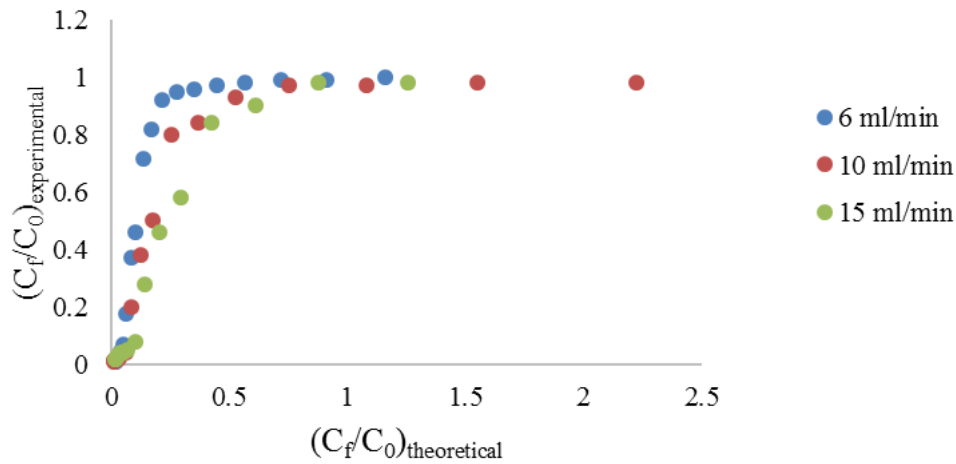


Fig. 4.62 Comparison of $(C_f/C_0)_{\text{experimental}}$ and $(C_f/C_0)_{\text{theoretical}}$ by Adam Bohart model for varying initial concentration, pH, bed height and flow rate.

4.7 Summary

In this chapter the adsorptive removal of Cr(VI) using nanoadsorbents has been investigated in detail. The adsorption efficiency and adsorption capacity of three adsorbents namely nanokaolinite clay, nanomagnetite and chitosan/halloysite clay nanocomposite film have been compared. Nanokaolinite clay possessed only very less adsorption efficiency and it also possessed difficulty in separation after adsorption. Hence detailed investigation using this adsorbent was not conducted. Nanomagnetite possessed higher adsorption capacity and percentage Cr(VI) removal efficiency than nanoclay. Optimisation of Cr(VI) adsorption using nanomagnetite was conducted using RSM. Model equation of second order was developed and it was validated. Chitosan/halloysite clay nanocomposite films possessed ease of separation after adsorption. Batch studies were conducted for adsorptive removal of Cr(VI) from aqueous solution and it possessed very high adsorption efficiency and adsorption capacity when compared to other two adsorbents. Model equation for Cr(VI) removal using nanocomposite films by adsorption was developed using

Box-Behnken design of RSM. Optimisation using response optimiser was carried out and it was validated. Fixed bed Cr(VI) column was fabricated using chitosan/halloysite clay nanocomposite film as adsorbent and the effect of various experimental conditions in the column performance were analysed. The modeling of the column was performed using Thomas model, Yoon Nelson model and Adam Bohart model. Cr(VI) removal was successfully accomplished in the fixed bed adsorption column using chitosan/halloysite nanocomposite films.

SUMMARY AND CONCLUSIONS**Contents**

- 5.1 Summary
- 5.2 Conclusions of Batch Study
- 5.3 Conclusions of Fixed Bed Study
- 5.4 Scope for Future Research

5.1 Summary

Water bodies are the ultimate sink for the metallic pollutants. Hexavalent chromium is one such heavy metal that is toxic to all forms of life. Chromium exists in both insoluble Cr(III) at high pH and soluble Cr(VI) forms. Cr(VI) introduces a variety of adverse effects in biological systems which enters the ground water and surface waters by soil leaching. Cr(VI) is classified as a carcinogen possessing both mutagenic and teratogenic properties. The main cause of occurrence of Cr(VI) is rapid industrialisation and various anthropogenic activities. Even though there are various methods for removing Cr(VI) from aqueous solutions like chemical precipitation, ion exchange, membrane filtration, electrochemical methods, photocatalysis, coagulation and flocculation, all these methods pose certain drawbacks in one form or another.

Adsorption is a commonly used method due to its simplicity and suitability for higher capacity processes. During adsorption the species of interest is deposited on a surface. The surface on which adsorption takes place is called adsorbent and the deposited species is called adsorbate. This process requires selection of a suitable adsorbent which poses high adsorption capacity and removal efficiency. To conduct preliminary studies batch adsorption test is

to be conducted in the laboratory. Batch adsorption study can be used to study the effect of various parameters on adsorption.

Various types of adsorbents are available for Cr(VI) removal. The specific surface area and pore size distribution are the important characteristics that govern the properties of a good adsorbent. Due to large surface area and pore size distribution, nanomaterial poses higher removal efficiency of adsorption. This work aims at developing a suitable nanomaterial based adsorbent for the removal of low concentration of Cr(VI) from aqueous solution.

Sol gel method was used in the laboratory for the synthesis of magnetite nanoparticles for use as adsorbent for Cr(VI) removal. Nanokaolinite clay was used as another adsorbent for Cr(VI) removal batch wise in the present work. One of the drawback the nanomaterials are facing for use as adsorbent is their difficulty in separating the adsorbent after adsorption. Nanomaterials can be made as a composite with suitable matrix and the composite can be used as adsorbent for heavy metal removal. Chitosan has been used as adsorbent for Cr(VI) removal. It is compatible with halloysite nanoclay and hence chitosan/halloysite clay nanocomposite films were used for adsorption of hexavalent chromium in batch and packed bed column in the study.

The analysis of Cr(VI) before and after adsorption was done using UV-VIS spectrophotometer. The selected nanomaterials and nanocomposite were characterised using SEM-EDX, XRD, TGA, FTIR and digital micrometer. The optimisation of batch adsorption was carried out using design of experiments under Response Surface Methodology of Minitab 16.

Desorption is the reverse process of adsorption where the adsorbed substance is released from the surface. This unit operation is necessary for the reuse of the adsorbent. This also reduces the problem of disposal of the spent adsorbent. Sodium hydroxide solution was used for the regeneration of chitosan/halloysite clay nanoadsorbents.

Batch adsorption is not practical for large scale operations. So fixed bed continuous packed bed Cr(VI) column was fabricated using nanocomposite films and experiments were performed. The breakthrough curves were analysed for various experimental conditions and the column was modeled using Thomas model, Yoon Nelson model and Adam Bohart model.

5.2 Conclusions of Batch Study

- Nanokaolinite clay was used for batch adsorption of Cr(VI) from synthetically prepared Cr(VI) containing aqueous solution. The effect of pH of Cr(VI) solution, nanoclay dosage, initial Cr(VI) concentration, time of shaking was analysed at 200 rpm and 300 K. With pH the adsorption efficiency first increased, reached a maximum at pH 3.0 and then decreased with increase in the solution pH. At 7.5 g/L of nanoclay dosage, maximum removal of 50% was observed. Initially there was increase in Cr(VI) removal with initial concentration but beyond 15 ppm, the removal efficiency showed a decreasing trend. After 120 minutes of shaking time, the adsorption reached a steady state.
- Nanomagnetite was synthesised in the laboratory using sol gel method for use as adsorbent for Cr(VI) from wastewater. Maximum removal was obtained at low pH of 2. All the other batch experiments were performed at pH 2. With increase in adsorption dosage, removal first increased, attained a maximum value and then decreased. Even though

there was a slight change in the removal efficiency with change in initial Cr(VI) concentration, the magnitude was very less. The adsorption capacity showed a steady increase from 0.93-5.73 mg/g with increase in initial concentration from 10-65 ppm. Percentage adsorption of Cr(VI) first increased with time and after certain time the adsorption reached a steady state.

- The optimisation of adsorption of Cr(VI) using magnetite nanoadsorbents by RSM showed that 76.11% removal was obtained at initial concentration of 50 ppm by providing 120 minutes adsorption time. The adsorbent dosage was 10 g/L at a pH of 2.0. This model was validated by conducting the batch experiments by maintaining the prescribed conditions and 73 % removal of Cr(VI) was obtained.
- Chitosan/halloysite clay nanocomposite films of thickness 0.2 mm, diameter 6.5 mm were synthesised in the laboratory. The results of batch experiments showed that at low pH the adsorption was favourable and all the other batch studies were carried out at pH 3.0. With the increase in nanocomposite film dosage the adsorption efficiency also increased and then after a maximum of 92% at an adsorption dosage of 1.7 g/L, the adsorption efficiency decreased. The adsorption capacity and efficiency decreased beyond 60 °C. The removal efficiency of Cr(VI) using nanocomposite film was maximum at 70 ppm initial concentration and the equilibrium time for the study was 70 minutes.
- The experimental batch adsorption data using nanocomposite film fitted more to pseudo second order kinetics and the equilibrium adsorption data fitted more to Langmuir isotherm model.

- Thermodynamic study using chitosan/halloysite nanocomposite film showed that ΔG was negative upto 60 °C which indicated that the adsorption was favourable upto that temperature. Positive value of ΔH showed the endothermicity of the process and positive value of ΔS meant that the process was feasible.
- The desorption study of nanocomposite film after Cr(VI) adsorption showed that 0.01 M NaOH could be used as a desorbent and the desorption efficiency decreased with increase in adsorption-desorption cycle.
- RSM was used for modeling the adsorption process and optimum values of parameters that affects the adsorption were determined using response optimiser. 93.04% removal of Cr(VI) was obtained at 72.2 mg/L initial Cr(VI) concentration with 0.2 g/L of nanocomposite film added to the solution. The optimum time of adsorption was 100 minutes at pH 3.0. The model was experimentally validated.
- The adsorption capacity of nanokaolinite clay was very less when compared to the other two adsorbents. Nanocomposite films possessed higher adsorption capacity when compared to nanomagnetite for the removal of Cr(VI).
- Characterisation of nanoadsorbents were conducted using SEM-EDX, XRD, TGA, UTM, micrometer and FTIR.

5.2.1 Limitations of Batch Study

- Synthetic wastewater was used in the whole work. No real wastewater samples containing Cr(VI) were taken from any industry for the experiments.

- Thermal stability of nanoclay was not investigated.
- Effect of temperature and agitation speed were not studied for nanoclay and nanomagnetite.
- Kinetics, isotherm and thermodynamic studies were performed only for nanocomposite films.
- Effect of shaking speed on percentage removal of Cr(VI) using nanocomposite films were not included in the work.
- Desorption study was conducted only for nanocomposite film adsorbent using NaOH. The desorbent used was of only 0.01 M strength.

5.3 Conclusions of Fixed Bed Study

- A perspex column of diameter 28 mm outer diameter, 24 mm inner diameter and 280 mm height was used for continuous removal of Cr(VI) from aqueous solution using chitosan/halloysite nanocomposite films as adsorbent.
- The effect of initial concentration at constant pH of the influent solution was analysed graphically and showed that at low initial concentration more volume of Cr(VI) solution could be treated and breakthrough curve occurred slowly at low initial concentration.
- The effect of pH at constant bed height, influent flow rate and bed height was analysed by plotting C_t/C_0 versus time. At low pH the breakthrough curve occurred slowly which indicated that the bed got saturated slowly.

- At bed heights of 10 cm, 20 cm and 25 cm, the breakthrough curves were analysed and showed that higher the bed height more volume of water could be treated before saturation. The breakthrough time was higher for 25 cm bed than for 10 and 20 cm beds.
- The bed was operated at 6 mL/min, 10 mL/min, 15 mL/min to study the effect of flow rate on breakthrough curve appearance. From the experimental results the breakthrough curve shifted from right to left as the flow rate was increased at pH 4.0, initial concentration 50 ppm and bed height 10 cm. Low flow rate was favourable for treating higher volume of feed in a fixed bed packed adsorption column.
- Mathematical modeling of the column was carried out using Thomas model, Yoon Nelson model and Adam Bohart model. From the model equations, it showed that Thomas model and Yoon Nelson model fitted well to the experimental data. Adam Bohart model fitted best to the initial part of the column operation except for high pH of influent solution.

5.3.1 Limitations of Fixed Bed Study

- Continuous study was conducted using only one adsorbent.
- The effect of temperature on the working of Cr(VI) column using chitosan/halloysite clay nanocomposite adsorbent was not included in the work.
- Modeling of fixed bed operation using suitable software's was not performed.
- Empty Bed Contact Time (EBCT) was not considered in the operation of fixed bed column.

5.4 Scope for Future Research

- Surface modification of synthesised magnetite nanoparticles and nanokaolinite particles could be carried out for getting higher removal efficiency and adsorption capacity.
- The effect of thickness of chitosan/halloysite nanocomposite films on Cr(VI) adsorption could be conducted.
- The effect of chitosan to halloysite nanoclay weight ratio in the synthesis of nanocomposite films and hence in adsorption efficiency could be assessed on both batch and fixed bed operation.
- Studies could be conducted using actual industrial wastewaters for the removal of hexavalent chromium and other heavy metals.
- Hydrodynamic study of fixed bed Cr(VI) column using nanocomposite films could be conducted.

REFERENCES

1. **Abdeen, Z., S.G. Mohammad, and M.S. Mahmoud** (2015) Adsorption of Mn(II) ion on polyvinyl alcohol/chitosan dry blending from aqueous solution. *Environmental Nanotechnology, Monitoring and Management*, **3**, 1 - 9.
2. **Ahamad, W.A., Z.A. Zakaria, A.R. Khasim, M.A. Alias, and S.M.H.S. Ismail** (2010) Pilot scale removal of chromium from industrial wastewater using the ChromeBac™ system. *Bioresource Technology*, **101**, 4371 - 4378.
3. **Ahmad, A.A. and B.H. Hameed** (2010), Fixed bed adsorption of reactive azo dye onto granular activated carbon prepared from waste. *Journal of Hazardous Materials*, **175**, 298 - 303.
4. **Ajmal, M., R.A.K. Rao, S. Anwar, J. Ahmad, and R. Ahmad** (2003) Adsorption studies on Rice Husk: Removal and recovery of Cd(II) from wastewater. *Bioresource Technology*, **86**, 147 - 149.
5. **Aksu, Z. and F. Gonen** (2004) Biosorption of phenol by immobilised activated sludge in a continuous packed bed: prediction of breakthrough curves. *Process Biochemistry*, **39**, 599 - 613.
6. **Aksu, Z. and F. Gonen** (2006) Binary Biosorption of phenol and chromium(VI) onto immobilized activated sludge in a packed bed: prediction of kinetic parameters and breakthrough curves. *Separation and Purification Technology*, **49**, 205 - 216.
7. **Anjana, R., K.K. Asha, S.G. Tresa, and K.E. George** (2014) Design of experiments for thermo mechanical behaviour of polypropylene/high-density polyethylene/nanokaolinite clay composites. *Polymer Bulletin*, **71**, 315 - 335.

8. **Aslan, N. and Y. Cebeci** (2007) Application of Box-Behnken design and application of response surface methodology for modeling of some Turkish Coal. *Fuel*, **86**, 90 - 97.
9. **Auta, M. and B.H. Hameed** (2011) Optimised waste tea activated carbon for adsorption of methylene blue and acid blue 29 dyes using response surface methodology. *Chemical Engineering Journal*, **175**, 233 - 243.
10. **Auta, M. and B.H. Hameed** (2014) Chitosan-clay composite as highly effective and low-cost adsorbent for batch and fixed bed adsorption of methylene blue. *Chemical Engineering Journal*, **237**, 352 - 361.
11. **Awwad, A.M. and N.M. Salem** (2012) A green and facial approach for synthesis of magnetite nanoparticles. *Nanoscience and Nanotechnology*, **2**, 208 - 213.
12. **Ayari, F., E. Srasra, and M. Trabelsi Ayadi** (2005) Characterisation of bentonitic clays and their use as adsorbent. *Desalination*, **185**, 391 - 397.
13. **Aydin, Y.A. and N.D. Aksoy** (2009) Adsorption of chromium on chitosan: Optimisation, kinetics and thermodynamics. *Chemical Engineering Journal*, **151**, 188 - 194.
14. **Azizian, S.** (2004) Kinetic models of sorption: a theoretical analysis. *Journal of Colloid and Interface Science*, **276**, 47 - 52.
15. **Babel, S. and T.A. Kurniavans** (2003) Low cost adsorbents for heavy metals uptake from contaminated water: A Review. *Journal of Hazardous Materials*, **97**, 219 - 243.

16. **Bai, S.R. and T.E. Abraham** (2001) Biosorption of Cr(VI) from aqueous solution by *Rhizopus nigricans*. *Bioresource Technology*, **79**, 73 - 81.
17. **Barakat, M.A.** (2011) New trends in removing heavy metals from wastewater. *Arabian Journal of Chemistry*, **4**, 361 - 377.
18. **Barnhart, J** (1997) Occurrences, uses and properties of chromium. *Regulatory Toxicology and Pharmacology*, **26**, S3 - S7.
19. **Casariello, A., B.W.S. Souza, M.A. Cerqueira, J.A. Teixeira, L. Cruz, R. Diaz, and A.A. Vicente** (2009) Chitosan/clay films properties as affected by biopolymer and clay micro nanoparticles concentrations. *Food Hydrocolloids*, **23**, 1895 - 1902.
20. **Bhatnagar, A., and M. Sillanpaa** (2009) Application of chitin and chitosan derivatives for the detoxification of water and wastewater- a short review. *Advances in Colloid and Interface science*, **152**, 26 - 38.
21. **Brown, P.A., S.A. Gill, and S.J. Allen** (2000) Metal Removal from wastewater using peat. *Water Research*, **34**, 3907 - 3916.
22. **Cai, W. and J. Wan** (2007) Facile synthesis of superparamagnetic magnetite nanoparticles in liquid polyols. *Journal of Colloid and Interface Science*, **305**, 366 - 370.
23. **Cavallaro, G., A. Gianguzza, G. Lazzara, S. Milioto, and D. Piazzese** (2013) Alginate gel beads filled with halloysite nanotubes. *Applied Clay Science*, **72**, 132 - 137.
24. **Chang, Q. and G. Wang** (2007) Study on the macromolecular coagulant PEX which traps heavy metals. *Chemical Engineering Science*, **62**, 4636 - 4643.

25. **Chauhan, D. and N. Sankararamakrishnan** (2011) Modeling and evaluation on removal of hexavalent chromium from aqueous systems using fixed bed column. *Journal of Hazardous Materials*, **185**, 55 - 62.
26. **Chen, D., W. Li, Y. Wu, Q. Zhu, Z. Lu, and G. Du** (2013) Preparation and characterisation of chitosan/montmorillonite magnetic microspheres and its application for the removal of Cr(VI). *Chemical Engineering Journal*, **221**, 8 - 15.
27. **Chen, J.M. and O.J. Hao** (1996) Environmental factors and modeling in microbial chromium(VI) reduction. *Water Environment Research*, **68**, 1156 - 1164.
28. **Chen, S., Q. Yue, B. Gao, Q. Li, X. Xu, and K. Fu** (2012) Adsorption of hexavalent chromium from aqueous solution by modified corn stalk, a fixed bed column study. *Bioresource Technology*, **113**, 114 - 120.
29. **Cho, D.W., B.H. Jeon, C.M. Chon, Y. Kim, F.W. Schwartz, E.S. Lee, and H. Song** (2012) A novel Chitosan/ Clay/magnetite composite for adsorption of Cu(II) and As(V). *Chemical Engineering Journal*, **200**, 654 - 662.
30. **Chowdhury, S., R. Mishra, P. Saha, and P. Kushwaha** (2011) Adsorption thermodynamics, kinetics and isosteric heat of adsorption of malachite green onto chemically modified rice husk. *Desalination*, **265**, 159 - 168.
31. **Chu, K.H.** (2004) Improved fixed bed models for metal Biosorption. *Chemical Engineering Journal*, **97**, 233 - 237.

32. **Cimen, A.** (2015) Removal of chromium from wastewater by reverse osmosis. *Russian Journal of Physical Chemistry A*, **89**, 1238 - 1243.
33. **Cotica, L.F., V.F. Freitas, G.S. Dias, I.A. Santos, S.C. Vendrame, N.M. Khalil, R.M. Mainardes, M. Staruch, and M. Jain** (2012) Simple and facile approach to synthesis magnetite nanoparticles and assessment of their effects on blood cells. *Journal of Magnetism and Magnetic Materials*, **324**, 559 - 563.
34. **Dalcin, M.G., M.M. Pirete, D.A. Lemos, E.J. Ribeiro, V.L. Cardoso, and M.M. de Resende** (2011) Evaluation of hexavalent chromium removal in a continuous biological filter with the use of central composite design (CCD). *Journal of Environmental Management*, **92**, 1165 - 1173.
35. **Das, A.P. and S. Mishra** (2008) Hexavalent Chromium(VI): Environment Pollutant and Health Hazard. *Journal of Environmental Research and Development*, **2**, 386 - 392.
36. **Davis, T.A., B. Volesky, and A. Mucci** (2003) A Review of the biochemistry of heavy metal biosorption by brown algae. *Water Research*, **37**, 4311 - 4330.
37. **Dawodu, F.A. and K.G. Akpomie** (2014) Simultaneous adsorption of Ni (II) and Mn (II) ions from aqueous solution onto a Nigerian kaolinite clay. *J. Mater Res. Technol.*, **3**, 129 - 141.
38. **De Silva, R.T., P. Pasbakhsh, K.L. Goh, S.P. Chai, and H. Ismail** (2013) Physio-chemical characterisation of chitosan/halloysite composite membranes. *Polymer Testing*, **32**, 265 - 271.

39. **Demirbas, A.** (2008) Heavy metal adsorption onto agro based waste materials: a review. *Journal of Hazardous Materials*, **157**, 220 - 229.
40. **Dharnaik, A.S. and P.K. Ghosh** (2014) Hexavalent chromium (Cr(VI)) removal by electrochemical-ion exchange process. *Environmental Technology*, **35**, 2272 - 2279.
41. **Dhermendra, K.T., J. Behari, and S. Prasenjit** (2008) Applications of nanoparticles in waste water treatment. *World Applied Science Journal*, **3**, 417 - 433.
42. **Dr. Kotaiah, B. and P. Chiranjeev** (1998) Performance of alum coagulation and flocculation in Cr(VI) removal from water. *International Journal of Environmental Studies*, **32**, 33 - 39.
43. **Elangovan, R. and L. Philip** (2009) Performance evaluation of various bioreactors for the removal of Cr(VI) and organic matters from industrial effluent. *Biochemical Engineering Journal*, **44**, 174 - 186.
44. **Foo, K.Y. and B.H. Hameed** (2010) Insights into the modeling of adsorption isotherm systems. *Chemical Engineering Journal*, **156**, 2 - 10.
45. **Fu, F. and Q. Wang** (2011) Removal of heavy metal ions from wastewaters: A review. *Journal of Environmental Management*, **92**, 407 - 418.
46. **Ghasemi, J. and S. Asadpour** (2007) Thermodynamics study of the adsorption process of methylene blue on activated carbon at different ionic strengths. *The Journal of Chemical Thermodynamics*, **39**, 967 - 971.
47. **Ghorbani, F., H. Younesi, S.M. Ghasempouri, A.A. Zinatizadeh, M. Amini, and A. Daneshi** (2008) Application of response surface methodology for optimisation of cadmium biosorption in an aqueous solution by *Saccharomyces cerevisiae*. *Chemical Engineering Journal*, **145**, 267 - 275.

48. **Ghosh, P.K.** (2009) Hexavalent chromium Cr(VI) removal by acid modified activated waste carbons. *Journal of Hazardous Materials*, **171**, 116 - 122.
49. **Giri, S.K., N.N. Das, and G.C. Pradhan** (2011) Synthesis and characterisation of magnetite nanoparticles using waste iron ore tailings for adsorptive removal of dyes from aqueous solution. *Colloids and surfaces A: Physicochemical and Engineering Aspects*, **389**, 43 - 49.
50. **Goel, J., K. Kadirvelu, C. Rajagopal, and V.K. Garg** (2005) Removal of lead(II) by adsorption using treated granular activated carbon: batch and column studies, *Journal of Hazardous Materials*, **125**, 211 - 220.
51. **Gordon, M., M.S. Otterburn, and A.A. Jamal** (1987) Intraparticle diffusion process occurring during the adsorption of dye stuffs. *Water, Air and Soil Pollution*, **36**, 381 - 390.
52. **Guibal, E.** (2004) Interactions of metal ions with chitosan based sorbents: a review. *Separation and Purification Technology*, **38**, 43 - 74.
53. **Heymes, F., P. Manno-Demoustier, F. Charbit, J.L. Fanlo, and P. Moulin** (2006) Hydrodynamics and mass transfer in a packed column: Case of toluene absorption with a viscous absorbent. *Chemical Engineering Science*, **61**, 5094 - 5106.
54. **Ho, Y.S.** (2006) Review of second order models for adsorption systems. *Journal of Hazardous Materials*, **136**, 681 - 689.
55. **Hsu, H.T., S.S. Chen, and Y.S. Chen** (2011) Removal of Cr(VI) and naphthalene sulfonate from textile wastewater by photocatalysis combining ionic exchange membrane processes. *Separation and Purification Technology*, **80**, 663 - 669.

56. **Ihsanullah, F.A. Al-Khaldi, B. Abusharkh, A.M. Abulkibash, M.I. Qureshi, T. Laoui, and M.A. Atieh** (2016) The effect of acid modification on adsorption of hexavalent chromium (Cr(VI)) from aqueous solution by activated carbon and carbon nanotubes. *Desalination and Water treatment*, **57**, 7232 - 7244.
57. **Imran, A.** (2014) Water treatment by adsorption columns: Evaluation at ground level. *Seprn & Purfn. Rev.*, **43**, 175 - 205.
58. **Imran, A., M. Asim, and A.K. Tabrez** (2012) Low cost adsorbents for the removal of organic pollutants from wastewater. *Journal of Environmental Management*, **113**, 170 - 183.
59. **Inyinbor, A.A., F.A. Adekola, and G.A. Olatunji** (2016) Kinetics, isotherm and thermodynamic modeling of liquid phase adsorption of Rhodamine B dye onto *Raphia hookerie* fruit epicarp. *Water Resources and Industry*, **15**, 14 - 27.
60. **Jain, M., V.K. Garg, and K. Kadirvelu** (2009) Chromium (VI) removal from aqueous system using *Helianthus annuus* (sunflower) stem waste. *Journal of Hazardous Materials*, **162**, 365 - 372.
61. **Jain, M., V.K. Garg, and K. Kadirvelu** (2013) Cadmium(II) sorption and desorption in a fixed bed column using sunflower waste calcium alginate beads. *Bioresource Technology*, **129**, 242 - 248.
62. **Johnson, J., L. Shewel, and T.E. Graedel** (2006) The contemporary anthropogenic chromium cycle. *Environ. Sci. Technology*, **40**, 7060 - 7069.

63. **Kannan, N. and M.M. Sundaram** (2001) Kinetics and mechanism of removal of methylene blue by adsorption on various carbons-A comparative study. *Dyes and Pigments*, **51**, 25 - 40.
64. **Karagozoglul, B., M. Tasdemir, E. Demirbas, and M. Kobya** (2007) The adsorption of basic dye (Astrazon blue FGRL) from aqueous solutions onto sepiolite, fly ash and apricot shell activated carbon: Kinetic and equilibrium studies. *Journal of Hazardous Materials*, **147**, 297 - 306.
65. **Klein, C. and C.S. Hurlbut** *Manual of Mineralogy* (20th edn.). Wiley, New York, 1985.
66. **Kobya, M.** (2004) Removal of Cr(VI) from aqueous solutions by adsorption onto hazelnut shell activated carbon: kinetic and equilibrium studies. *Bioresource Technology*, **91**, 317 - 321.
67. **Kralik, M.** (2014) Adsorption, chemisorption and catalysis. *Chemical Papers*, **68**, 1625 - 1638.
68. **Krzysztof, K. and A. Swiatkowski** (2016) The influence of different agitation techniques on the adsorption kinetics of 4-chlorophenol on granular activated carbon. *Reaction kinetics, Mechanisms and Catalysis*, **116**, 261 - 271.
69. **Kumar, U. and M. Bandyopadhyay** (2006) Sorption of cadmium from aqueous solution using pre-treated rice husk. *Bioresource Technology*, **97**, 104 - 109.
70. **Kumar, P.A. and Chakraborty** (2009) Fixed bed column study for hexavalent chromium removal and recovery by short chain poly aniline synthesised on jute fibre. *Journal of Hazardous Materials*, **162**, 1086 - 1098.

71. **Kundu, S. and A.K. Gupta** (2006) Arsenic adsorption onto iron oxide-coated cement IOCC: regression analysis of equilibrium data with several isotherm models and their optimisation. *Chemical Engineering Journal*, **122**, 93 - 106.
72. **Kyzas, G.Z., M. Kostoglou, and N.K. Lazaridis** (2009) Copper and chromium (VI) removal by chitosan derivatives- equilibrium and kinetic studies. *Chemical Engineering Journal*, **152**, 440 - 448.
73. **Largitte, L and R. Pasquier** (2016) A review of kinetics adsorption models and their application to the adsorption of lead by an activated carbon. *Chemical Engineering Research and Design*, **109**, 495 - 504.
74. **Lee, C.K., K.S. Low, and K.L Kek** (1995) Removal of chromium from aqueous solution. *Bioresource Technology*, **54**, 183 - 189.
75. **Lemine, O.M., K. Omri, B. Zhang, L. El Mir, M. Sajieddine, A. Alyamani, and M. Bououdina** (2012) Sol gel synthesis of 8 nm magnetite (Fe₃O₄) nanoparticles and their magnetic properties. *Superlattices and Microstructures*, **52**, 793 - 799.
76. **Lewandowska, K., A. Sionkowska, B. Kaczmarek, and G. Furtos** (2014) Characterisation of chitosan composites with various clays, *International Journal of Biological Macromolecules*, **65**, 534 - 541.
77. **Li, W., H. Muhr, and E. Plasari** (2012) Use of different rapid mixing devices for controlling the properties of magnetite nanoparticles produced by precipitation. *Journal of Crystal Growth*, **342**, 21 - 27.
78. **Lim, A.P. and A.Z. Aris** (2014) Continuous fixed-bed column study and adsorption modeling: Removal of cadmium(II) and lead(II) ions in

- aqueous solution by dead calcareous skeletons. *Biochemical Engineering Journal*, **87**, 50 - 61.
79. **Lingyun, C., L. Zhen, Z. Chenglan, Z. Yiyang, Z. Yang, and P. Hui** (2011) Direct Synthesis and characterisation of mesoporous Fe₃O₄ through pyrolysis of Ferric Nitrate-Ethylene Glycol Gel. *Journal of Alloys and Compounds*, **509**, L1 - L5.
80. **Lua, A.C. and Q. Jia** (2009) Adsorption of phenol by oil palm shell activated carbons in a fixed bed. *Chemical Engineering Journal*, **150**, 455 - 461.
81. **Maclver, D.S. and H.H. Tobin** (1960) Physical adsorption on chemisorbed films. *Journal of Physical Chemistry*, **64**, 683 - 686.
82. **Malkoc, E., and Y. Nuhoglu** (2006a) Fixed bed studies for the sorption of chromium (VI) onto tea factory waste. *Chemical Engineering Science*, **61**, 4363 - 4372.
83. **Malkoc, E., and Y. Nuhoglu** (2006b), Removal of Ni(II) ions from aqueous solutions using waste of tea factory: Adsorption on a fixed bed column. *Journal of Hazardous Materials*, **135**, 328 - 336.
84. **Mandeep, S., N.T. Dong, U. Pavel, S. Nina, and S. Frantisek** (2010) Synthesis, characterisation and study of arsenate adsorption from aqueous solution by α and δ phase manganese dioxide nanoadsorbents. *Journal of Solid State Chemistry*, **183**, 2979 - 2986.
85. **Medvidovic, N.V., J. Peric, and M. Trgo** (2006) Column performance in lead removal from aqueous solutions by fixed bed of natural zeolite-clinoptilolite. *Separation and Purification Technology*, **49**, 237 - 244.

86. **Mirbagheri, S.A. and S.N. Hossieni** (2005) Pilot plant investigation on petrochemical wastewater treatment for the removal of copper and chromium with the objective of reuse. *Desalination*, **171**, 85 - 93.
87. **Miretzky, P.A. and F. Cirelli** (2009) Hg (II) removal from water by Chitosan and Chitosan derivatives: A review. *Journal of Hazardous Materials*, **167**, 10 - 23.
88. **Mohan, S and G. Sreelakshmy** (2008) Fixed bed column study for heavy metal removal using phosphate treated rice husk. *Journal of Hazardous Materials*, **153**, 75 - 82.
89. **Mukherjee, S., S. Kumar, A.K. Misra, and M. Fan** (2007) Removal of phenols from water environment by activated carbon, bagasse ash and wood charcoal. *Chemical Engineering Journal*, **129**, 133 - 142.
90. **Mustafa, Y., G. Fethiye, P. Erol, O. Sema, and C.S. Yogesh** (2008) An economic removal of Cu^{2+} and Cr^{3+} on the new adsorbents: Pumice and polyacrylonitrile/pumice composite. *Chemical Engineering Journal*, **137**, 453 - 461.
91. **Nataraj, S.K., K.M. Hosamani, and T.M. Aminabhavi** (2007) Potential application of an electro dialysis pilot plant containing ion exchange membranes in chromium removal. *Desalination*, **217**, 181 - 190.
92. **Nesic, A.R., S.J. Velickovic, and D.G. Antonovic** (2012) Characterisation of chitosan/montmorillonite membranes as adsorbents for Bezactiv Orange V-3R dye. *Journal of Hazardous Materials*, **209-210**, 256 - 263.

93. **Nora, S. and S.D. Mamadou** (2005) Nanomaterials and water purification: opportunities and challenges. *Journal of Nanoparticle Research*, **7**, 331 - 342.
94. **Owlad, M., M.K. Aroua, W.A.W. Daud, and S. Baroutian** (2009) Removal of hexavalent chromium-contaminated water and wastewater: a review. *Water, Air and Soil Pollution*, **200**, 59 - 77.
95. **Pan, B. and B. Xing** (2008) Adsorption mechanisms of organic chemicals on carbon nanotubes. *Environ Sci. Technol.*, **42**, 9005 - 9013.
96. **Pandey, S and S.B. Mishra** (2011) Organic-inorganic hybrid of chitosan/organoclay bionanocomposites for hexavalent chromium uptake. *Journal of colloid and interface Science*, **361**, 509 - 520.
97. **Parsons, J.G., M.L. Lopez, J.R. Peralta-Videa, and J.L. Gardea-Torresdey** (2009) Determination of arsenic(III) and arsenic(V) binding to microwave assisted hydrothermal synthetically prepared Fe_3O_4 , Mn_3O_4 and MnFe_2O_4 nanoadsorbents. *Microchemical Journal*, **91**, 100 - 106.
98. **Pasbakhsh, P., J. Churchman, and J.L. Keeling** (2013) Characterisation of properties of various halloysites relevant to use as nanotubes and microfiber fillers, *Applied Clay Science*, **74**, 47 - 57.
99. **Ponder, S. M., J.G. Darab, and T.E. Mallouk** (2000) Remediation of Cr(IV) and Pb (II) aqueous solutions using supported nanoscale zerovalent iron. *Environ. Sci. Technol.*, **34**, 2564 - 2569.

100. **Rai, M.K., G. Shahi, V. Meena, R. Meena, S. Chakraborty, R.S. Singh, and B.S. Rai** (2016) Removal of hexavalent chromium Cr(VI) using activated carbon prepared from Mango Kernel activated with H_3PO_4 . *Resource Efficient Technologies*, **2**, S63 - S70.
101. **Raji, C. and T.S. Anirudhan** (1998) Batch Cr(VI) removal by polyacrylamide-grafted sawdust: Kinetics and thermodynamics, *Water Res.*, **32**, 3772 - 3780.
102. **Rengaraj, S., K.H. Yeon, and S.H. Moon** (2001) Removal of chromium from water and wastewater by ion exchange resins. *Journal of Hazardous Materials*, **87**, 273 - 287.
103. **Rojas, G., J. Silva, J.A. Flores, A. Rodriguez, M. Ly, and H. Maldonado** (2005) Adsorption of chromium onto crosslinked chitosan. *Separation and Purification Technology*, **44**, 31 - 36.
104. **Rongzhi, C., Z. Chunyi, Y. Huang, B. Yoshio, Z. Zhenya, S. Norio, and G. Dmitri** (2011) Arsenic(V) adsorption on Fe_3O_4 nanoparticles-coated born nitride nanotubes. *Journal of colloid and interface science*, **359**, 261 - 268.
105. **Roy, A. and J. Bhattacharya** (2012) Removal of Cu(II), Zn(II) and Pb(II) from water using microwave assisted synthesised maghemite nanotubes. *Chemical Engineering Journal*, **211-212**, 493 - 500.
106. **Ruthven, D.M.** *Principles of adsorption and adsorption processes*. Wiley, New York, 1984.
107. **Sadhukhan, B., N.K. Mondal, and S. Chatteraj** (2016) Optimisation using central composite design (CCD) and the desirability function for sorption of methylene blue from aqueous solution onto Lemna major. *Karbala International Journal of Modern Science*, **2**, 145 - 155.

108. **Sag, Y. and Y. Aktay** (2001) Application of equilibrium and mass transfer models to dynamic removal of Cr(VI) ions by Chitin in packed column reactor. *Process Biochemistry*, **36**, 1187 - 1197.
109. **Sahu, S.K., P. Meshram, B.D. Pandey, and T.R. Mankhand** (2009) Removal of chromium(III) by cation exchange resin, Indion 790 for tannery waste treatment. *Hydrometallurgy*, **99**, 170 - 174.
110. **Sarkar, S., E. Guibal, F. Quignard, and A.K. Sengupta** (2012) Polymer supported metals and metal oxide nanoparticles synthesis, characterisation and application. *Journal of Nanopart Res.*, **14**, 715.
111. **Sheng, H.L., T.S. Ching, and M.C. Sun** (1998) Saline wastewater treatment by electrochemical method. *Water Research*, **32**, 1059 - 1066.
112. **El- Safty, S.A., A. Shahat, and M.R. Awual** (2011) Efficient adsorbents of nanoporous aluminosilicate monoliths for organic dyes from aqueous solution. *Journal of Colloid and Interface Science*, **359**, 9 - 18.
113. **Skodras, G., I. Diamantopoulou, G. Pantaleontos, and G.P. Sakellariopoulos** (2008) Kinetic studies of elemental mercury adsorption in activated carbon fixed bed reactor. *Journal of Hazardous Materials*, **158**, 1 - 13.
114. **Soloman, P.A., C. Ahmed Basha, M. Velan, N. Balasubramanian, and P. Marimuthu** (2009) Augmentation of biodegradability of pulp and paper industry wastewater by electrochemical pre-treatment and optimisation by RSM. *Separation and Purification Technology*, **69**, 109 - 117.

115. **Sonia, R., G. Ana, G. Edgar, C. Eudald, P. Victor, S. Antoni, and F. Xavier** (2011) Use of CeO₂, TiO₂ and Fe₃O₄ nanoparticles for the removal of lead from water toxicity of nanoparticles and derived compounds. *Desalination*, **277**, 213 - 220.
116. Standard Methods for the Examination of Water and Wastewater, American Public Health Association, American Water Works Association, Water Environment Federation, 1992.
117. Standard X-ray Diffraction Powder Patterns, US Department of Commerce, National Bureau of Standards, Section **18**, 1981.
118. **Steven, L., B. Nathan, K. Jisoo, and J.G. Parsons** (2012) Removal of arsenic from aqueous solution: A study of the effects of pH and interfering ions using iron oxide nanomaterials. *Microchemical Journal*, **101**, 30 - 36.
119. **Sudha Bai, R. and A. Emilia** (2003) Studies on chromium (VI) adsorption –desorption using immobilized fungal biomass. *Bioresource Technology*, **87**, 17 - 26.
120. **Suksabye, P., P. Thiravetyan, and W. Nakbanpote** (2008) Column study of chromium(VI) adsorption from electroplating industry by coconut coir pith. *Journal of Hazardous Materials*, **160**, 56 - 62.
121. **Surabhi, S., V. Putcha, R.R. Vanka, and N.R. Gollapalli** (2013) Synthesis, Characterisation and optical properties of Zinc oxide nanoparticles. *International Nanoletters*, **3**, 30.
122. **Taha, M., M. Hassan, S. Essa, and Y. Tartor** (2013) Use of Fourier transform infrared spectroscopy (FTIR) for rapid and accurate identification of Yeasts isolated from human and animals. *International Journal of Veterinary Science and Medicine*, **1**, 15 - 20.

123. **Tchobanoglous, G., F.L. Burton, and H.D. Stensel** *Wastewater Engineering, Treatment and Reuse*. McGraw Hill, 2003.
124. **Tirtom, V.N., A. Dincer, S. Becerik, T. Aydemir, and A. Celik** (2012) Comparative adsorption of Ni(II) and Cd(II) ions on Epichlorohydrin crosslinked chitosan-clay composite beads in aqueous solution. *Chemical Engineering Journal*, **197**, 379 - 386.
125. **Vasanth Kumar, K.** (2006) Linear and nonlinear regression analysis for the sorption kinetics of methylene blue onto activated carbon. *Journal of Hazardous Materials*, **B137**, 1538 - 1544.
126. **Vashchenko, L.A., V.V. Katalnikova, and V.V. Serpinskii** (1993) Effect of temperature on the adsorption equilibrium in the H₂-Ne-zeolite NaA system. *Russian Chemical Bulletin*, **42**, 579 - 581.
127. **Vernon-Parry, K.D.** (2000) Scanning Electron Microscopy-an introduction. *III-Vs Review*, **13**, 40 - 44.
128. **Vijayaraghavan, K., J. Jegan, K. Palanivelu, and M. Velan** (2004) Removal of nickel(II) ions from aqueous solution using crab shell particles in a packed bed upflow column. *Journal of Hazardous Materials*, **113**, 223 - 230.
129. **Wang, J. and C. Chen** (2006) Biosorption of heavy metals by *saccharomyces cerevisiae*: A review. *Biotechnol. Adv.*, **24**, 427 - 451.
130. **Wang, L. and A. Wang** (2007) Adsorption characteristics of Congo red onto Chitosan/ Montmorillonite nanocomposite. *Journal of Hazardous Materials*, **147**, 979 - 985.

131. **Wang, S.F., L. Shen, Y.J. Tong, L. Chen, I.Y. Phang, P.Q. Lim, and T.X. Liu** (2005) Biopolymer/Chitosan/montmorillonite nanocomposites: Preparation and characterisation. *Polymer Degradation and Stability*, **90**, 123 - 131.
132. **Wang, X.H., Y.A. Zheng, and A.Q. Wang** (2009) Fast removal of copper ions from aqueous solution by chitosan-g-poly (acrylic acid)/attapulgite composites. *Journal of Hazardous Materials*, **168**, 970 - 977.
133. **Wassana, Y., L.W. Cynthia, S. Thanapon, R. Shane Addleman, G.C. Timothy, J.W. Robert, E.F. Glen, T. Charles, and M.G. Warner** (2007) Removal of heavy metals from aqueous systems with thiol functionalized superparamagnetic nanoparticles. *Environ. Sci. Technol.*, **41**, 5114 - 5119.
134. **Wenjun, J., P. Miguel, D.D. Dionysios, H.E. Mohammad, T. Dimitra, and O.S. Kevin** (2013) Chromium (VI) removal by maghemite nanoparticles. *Chemical Engineering Journal*, **222**, 527 - 533.
135. **Wilson, S.P., M.F. Victoria, L.F. Maria, R.D.S. Jaqueline, C.S. Renata, M.L. Carolina, and B.D.A. Ricardo** (2014) Experimental investigation of the co-precipitation method: An approach to obtain magnetite and maghemite nanoparticles with improved properties. *Journal of Nanomaterials*, **2014**, doi: 10.1155/2014/682985.
136. **Xianxiang, W.** (2011) Preparation of magnetic hydroxyapatite and their use as recyclable adsorbent for phenol in wastewater. *Clean-Soil, Air, Water*, **39**, 13 - 20.

137. **Yang, J.K. and S.M. Lee** (2006) Removal of Cr(VI) and humic acid by using TiO₂ photocatalysis. *Chemosphere*, **63**, 1677 - 1684.
138. **Yang, L. and P. Chen** (2008) Biosorption of hexavalent chromium onto raw and chemically modified Sargassam sp. *Bioresource Technology*, **99**, 297 - 307.
139. **Yavuz, M., F. Gode, E. Pehlivan, S. Ozmert, and Y.C. Sharma** (2008) An economic removal of Cu²⁺, Cr³⁺ on the new adsorbents: Pumice and polyacrylonitrile/pumice composite. *Chemical Engineering Journal*, **137**, 453 - 461.
140. **Yuan, P., D. Liu, M. Fan, D. Yang, R. Zhu, F. Ge, J.X. Zhu, and H. He** (2009) Removal of Hexavalent chromium [Cr(VI)] from aqueous solutions by the diatomite- supported/unsupported magnetite nanoparticles. *Journal of Hazardous Materials*, **173**, 614 - 21.
141. **Zhao, Y., E. Abdullayev, A. Vasiliev, and Y. Lvov** (2013) Halloysite nanotubule clay for efficient water purification. *Journal of Colloid and Interface Science*, **406**, 121 - 129.
142. **Zheng, Y. and A. Wang** (2009) Enhanced adsorption of ammonium using hydrogel composites based on chitosan and halloysite. *Journal of Macromolecular Science, Part A: Pure and Applied Chemistry*, **47**, 33 - 38.
143. **Zhitkovich, A.** (2017) Chromium in drinking water: Sources, Metabolism and Cancer Risks. *Chem Res. Toxicology*, **24**, 1617 - 1629.
144. **Zhou, Y.T., H.L. Nie, C. Branford-White, Z.Y. He, and L.M. Zhu** (2009) Removal of Cu²⁺ from aqueous solution by chitosan coated magnetic nanoparticles modified with α - ketoglutaric acid. *Journal of Colloid and Interface Science*, **330**, 29 - 37.

- 145. Zongo, I., J.P. Leclerc, A.H. Maiga, J. Wethe, and F. Lopicque** (2009) Removal of hexavalent chromium from industrial wastewater by electrocoagulation: A comprehensive comparison of aluminium and iron electrodes. *Separation and Purification Technology*, **66**, 159 - 166.

ANNEXURES

Annexure I (section 3.4)

Calibration of UV-VIS spectrophotometer

Equipment used- Hitachi U-2900

Method- Calibration curve was plotted by taking 0, 5, 10, 15, 20, 30, 40, 50, 60, 70, 80, 90 and 100 ppm Cr(VI) solution and noting the absorbance for each concentration at 540 nm. From the standard calibration (Fig. A1) the concentration of Cr(VI) solution can be measured.

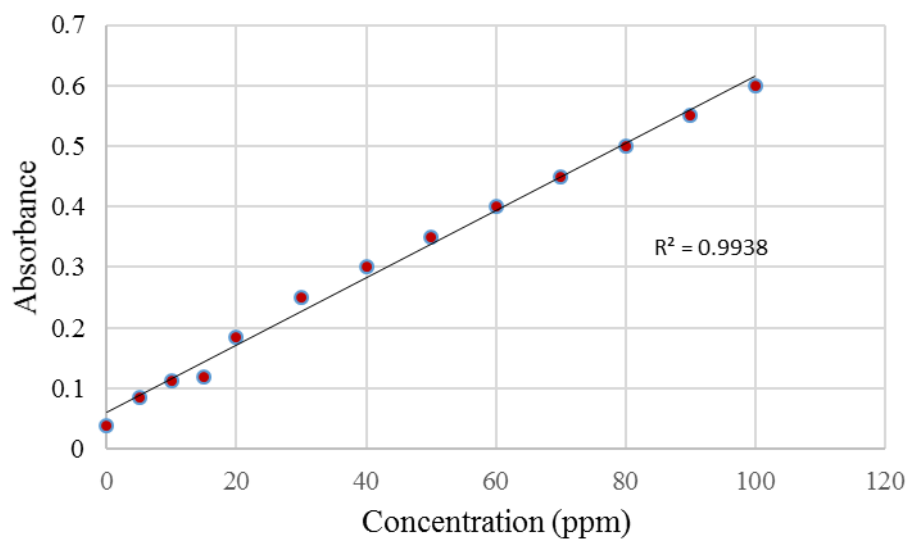


Fig. A1 Standard calibration curve of UV-VIS spectrophotometer

Annexure II (section 3.5)

Determination of average grain size of nanoadsorbents

The average grain size of nanoparticles used for adsorption was calculated using Debye Scherrer equation using the data obtained from XRD spectrum. Table A.1 represents the determination of average crystallite size of halloysite nanoclay.

Debye Scherrer equation is given by $D = \frac{K\lambda}{\beta \cos \theta}$

D = mean diameter of nanoparticles

β = The full width at half maximum value of XRD diffraction lines in radians (FWHM)

λ = the wavelength of X-ray radiation source = 1.5406 Å

θ = angle of incidence in radians

K = the Scherrer constant with value from 0.9 to 1.

Table A.1 Determination of average crystallite size of halloysite nanoclay

Peak position 2θ °	FWHM °	D, nm	D average, nm
12.058	1.221	6.54	
18.435	0.344	23.40	
20.15	0.834	9.67	14.03
62.652	1.155	8.05	
26.644	0.363	22.49	

For $2\theta=12.058$, FWHM (°) = 1.221

$$D_p = \frac{0.9 \times 1.5406}{\text{radians}(1.221) \times \cos(\text{radians}(\frac{12.058}{2}))} = 6.54 \text{ nm}$$

Annexure III (section: 3.7)**Calibration Details of Peristaltic Pump**

Peristaltic Pump used: Ravel (Make); RHP 100L-200 (Model)

The calibration of peristaltic pump was performed by setting various rpm and measuring the flow rate using a stop watch. Table A.2 represents the calibration data of peristaltic pump used in the operation of packed bed adsorption column for Cr(VI) removal. Calibration curve was plotted between rpm and flow rate (Fig. A2).

Table A.2 Calibration data of peristaltic pump

rpm	Flow rate, mL/min
0.5	6
0.8	10
1	12
1.2	14
1.5	17
1.8	20.5
2	22
2.3	25
2.5	27
3	31
5	50

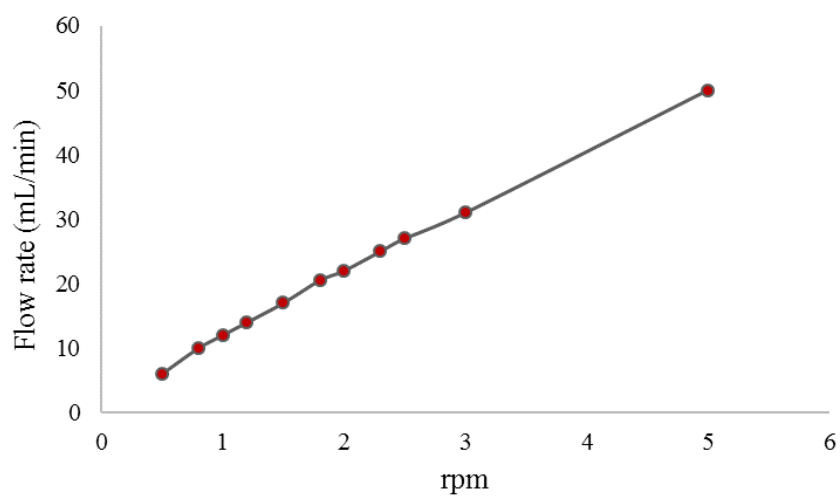


Fig. A2 Calibration curve of peristaltic pump used in the continuous experiment

Annexure IV
Experimental Data

Table A.3 Sorption kinetics (section 4.4.6)

Time, minutes	Initial concentration, ppm	Final concentration, ppm
15	25	14.8
30	25	12.5
45	25	12.4
60	25	10.3
65	25	7
70	25	2.5
75	25	2.5
90	25	2.5
100	25	2.5

Table A.4 Adsorption isotherm (section 4.4.7)

Initial concentration, ppm	Equilibrium concentration, ppm
5.6	2
9.4	4
17.0	9
22	10
26.1	15

Table A.5 Thermodynamic experimental data (section 4.4.8)

Temperature, °C	Temperature, K	Final concentration, ppm
30	303	12.1
50	323	10.1
55	328	8.5
60	333	3
70	343	15.2
90	363	20.2
110	383	22.8
120	393	22.8
123	396	22.8

Table A.6 Desorption data (section 4.4.9)

Cycle	Initial solution concentration, ppm	Final solution concentration, ppm	Initial adsorbent concentration, ppm	Final eluent concentration, ppm
1	70	6	64	4
2	59	8.5	50	8.5
3	40	7.5	30	6.4
4	20	3.8	15	3.4

Table A.7 Effect of initial concentration on the performance of fixed bed column (section 4.5.1)

C ₀ , ppm	C _f , ppm	Time, hour	C ₀ , ppm	C _f , ppm	Time, hour	C ₀ , ppm	C _f , ppm	Time, hour
50	0.4	1	70	0.4	1	100	5	1
50	0.5	2	70	0.6	2	100	13	2
50	0.6	3	70	2	3	100	23	3
50	1.1	4	70	2	4	100	29	4
50	2.4	5	70	7	5	100	34	5
50	3.4	6	70	10	6	100	44	6
50	8.8	7	70	23	7	100	50	7
50	18.7	8	70	34	8	100	62	8
50	22.9	9	70	36	9	100	75	9
50	35.9	10	70	40.2	10	100	87	10
50	41	11	70	46	11	100	93	11
50	46.1	12	70	50	12	100	99	12
50	47.4	13	70	63	13	100	99	13
50	48	14	70	65	14			
50	48.5	15	70	67	15			
50	49	16	70	69	16			
50	49.5	17	70	69.9	17			
50	49.5	18	70	69.9	18			
50	49.9	19						

Table A.8 Effect of pH on the performance of fixed bed column
(section: 4.5.2)

pH	C _t , ppm	Time, hour	pH	C _t , ppm	Time, hour	pH	C _t , ppm	Time, hour
4	0.4	1	6.5	0.1	1	9	0.6	1
4	0.5	2	6.5	15.5	2	9	16.2	2
4	0.6	3	6.5	22	2.5	9	21	2.5
4	1.1	4	6.5	26.9	3	9	28	3
4	2.4	5	6.5	27.0	3.5	9	29	4
4	3.4	6	6.5	27.0	4	9	35	5
4	8.8	7	6.5	37.0	5	9	40.9	6
4	18.7	8	6.5	40.6	6	9	45	7
4	22.9	9	6.5	42	6.5	9	48	8
4	35.9	10	6.5	45.5	7	9	49	9
4	41	11	6.5	48.4	8	9	49.6	10
4	46.1	12	6.5	49.2	9	9	49.7	11
4	47.4	13	6.5	49.9	10			
4	48	14	6.5	50.0	11			
4	48.5	15	6.5	50.0	11.5			
4	49	16						
4	49.5	17						
4	49.5	18						
4	49.9	19						

Table A.9 Effect of bed height on the working of fixed bed column (section 4.5.3)

Bed Height, cm	C _t , ppm	Time, hour	Bed Height, cm	C _t , ppm	Time, hour	Bed Height, cm	C _t , ppm	Time, hour
10	0.4	1	20	0.05	1	25	0.05	1
10	0.5	2	20	0.07	2	25	0.07	2
10	0.6	3	20	0.1	3	25	0.08	3
10	1.1	4	20	0.3	4	25	0.1	4
10	2.4	5	20	0.5	5	25	0.3	5
10	3.4	6	20	1.3	6	25	1	6
10	8.8	7	20	1.8	7	25	1.2	7
10	18.7	8	20	2	8	25	1.5	8
10	22.9	9	20	4	9	25	2	9
10	35.9	10	20	5	10	25	3.2	10
10	41	11	20	9	11	25	4	11
10	46.1	12	20	10	12	25	6.3	12
10	47.4	13	20	12.3	13	25	7.9	13
10	48	14	20	14	14	25	8.2	14
10	48.5	15	20	15	15	25	10	15
10	49	16	20	15.6	16	25	11	16
10	49.5	17	20	22	17	25	13.4	17
10	49.5	18	20	24	18	25	20.1	18
10	49.9	19	20	29	19	25	23.3	19
			20	31	20	25	25	20
			20	35	21	25	29	21
			20	36	22	25	30	22
			20	39	23	25	34	23
			20	40.8	24	25	35.3	24
			20	43	25	25	36.2	25
			20	44	26	25	39.2	26
			20	48	27	25	40	27
			20	49	28	25	43	28
			20	49.5	29	25	45	29
			20	49.9	30	25	47	30
			20	49.9	31	25	48.1	31
						25	48.5	32
						25	49	33
						25	49.5	34
						25	49.9	35
						25	49.9	36

Table A.10 Effect of flow rate on the working of fixed bed column (section 4.5.4)

Flow rate, mL/min	C _f , ppm	Time, hour	Flow rate, mL/min	C _f , ppm	Time, hour	Flow rate, mL/min	C _f , ppm	Time, hour
6	0.4	1	10	0.5	1	15	1	1
6	0.5	2	10	0.6	1.5	15	1	1.5
6	0.6	3	10	0.7	2	15	1.2	2
6	1.1	4	10	0.8	2.5	15	1.7	2.5
6	2.4	5	10	0.9	3	15	1.9	3
6	3.4	6	10	0.9	3.5	15	2	3.5
6	8.8	7	10	1	4	15	2	4
6	18.7	8	10	1.2	4.5	15	2.5	5
6	22.9	9	10	1.5	5	15	4	6
6	35.9	10	10	2	6	15	14	7
6	41	11	10	10	7	15	23	8
6	46.1	12	10	19	8	15	29	9
6	47.4	13	10	25	9	15	42	10
6	48	14	10	40	10	15	45	11
6	48.5	15	10	42	11	15	49	12
6	49	16	10	46.5	12	15	49	13
6	49.5	17	10	48.7	13			
6	49.5	18	10	48.7	14			
6	49.9	19	10	49	15			
			10	49	16			

LIST OF PAPERS SUBMITTED ON THE BASIS OF THIS THESIS

REFEREED JOURNALS

- **K.S. Padmavathy, G. Madhu, and Dipak Kumar Sahoo** (2017) Use of response surface methodology for optimisation of performance of magnetite nanoadsorbents for removal of hexavalent chromium from wastewater. *Int. J. Environment and Waste Management*, **20**, 49 - 65.
- **K.S. Padmavathy, M. Amith, G. Madhu, and Dipak Kumar Sahoo** (2017) Adsorption of hexavalent chromium (Cr(VI)) from wastewater using novel chitosan/halloysite clay nanocomposite films. *Indian Journal of Chemical Technology*, **24**, 593 - 600.

PRESENTATIONS IN CONFERENCES

- **K.S. Padmavathy**. Studies on nanoadsorbents for the selective removal of heavy metals from waste water - A review. *NATCON*, Govt. Engg. College, Thrissur, Kerala, 9 - 10 February, 2012.
- **K.S. Padmavathy**. Review on applicability of magnetic nanoadsorbents, polymeric nanoadsorbents and carbon nanoparticles for the removal of heavy metals from waste water. *NAMESAP 2012*, Govt. Engg. College, Thrissur, Kerala, 5 - 7 September, 2012.
- **K.S. Padmavathy, P.V. Haseena, and G. Madhu**. Studies on pH, initial concentration, adsorbent dosage and time for the removal of hexavalent chromium from wastewater using nanokaolinite clay and optimisation using response surface methodology. *International Conference on advances in applied mathematics, materials science and nanotechnology for engineering and industrial applications (IC-AMMN-2K16)*, Federal Institute of Science and Technology, Hormis Nagar, Angamaly, Kerala, 7 - 9 January, 2016.
- **K.S. Padmavathy, P.V. Haseena, and G. Madhu** (2016) A study on effects of pH, adsorbent dosage, time, initial concentration and adsorbent concentration for the removal of hexavalent chromium from wastewater by magnetite nanoparticles. *Elsevier Procedia*, **24**, 585 -594.

CURRICULUM VITAE

Name : PADMAVATHY K.S.

Date of Birth : 15-09-1980

EDUCATIONAL QUALIFICATIONS

- November 1998- June 2002
B.Tech in Chemical Engineering
Government Engineering College, Thrissur, Kerala, India
- December 2002- February 2006
M.Tech in Process Control (Chemical)
Government Engineering College, Thrissur, Kerala, India
- November 2011- Present
Doctor of Philosophy
Faculty of Engineering, SOE
Cochin University of Science and Technology
Reg. Date : 23-11-2011

EXPERIENCE

- June 2004- May 2017
Assistant Professor in Chemical Engineering,
Government Engineering College, Thrissur, Kerala, India
- May 2017- Till Date
Assistant Professor in Chemical Engineering,
Government Engineering College, Kozhikode, Kerala, India

